CHARACTERIZATION AND CYTOTOXICITY OF NEW COPPER(II) SILVER(II) AND GOLD(III) TETRA ALKYL PHENOXY PORPHYRIN DERIVATIVES

BY

TOSSAPON PHROMSATIT

A DISSERTATION SUBMITTED IN PARTIAL FULFILLMENT
OF THE REQUIREMENTS FOR THE DEGREE OF
DOCTOR OF PHILOSOPHY (CHEMISTRY)
DEPARTMENT OF CHEMISTRY
FACULTY OF SCIENCE AND TECHNOLOGY
THAMMASAT UNIVERSITY
ACADEMIC YEAR 2021

CHARACTERIZATION AND CYTOTOXICITY OF NEW COPPER(II) SILVER(II) AND GOLD(III) TETRA ALKYL PHENOXY PORPHYRIN DERIVATIVES

BY

TOSSAPON PHROMSATIT

A DISSERTATION SUBMITTED IN PARTIAL FULFILLMENT
OF THE REQUIREMENTS FOR THE DEGREE OF
DOCTOR OF PHILOSOPHY (CHEMISTRY)
DEPARTMENT OF CHEMISTRY
FACULTY OF SCIENCE AND TECHNOLOGY
THAMMASAT UNIVERSITY
ACADEMIC YEAR 2021

THAMMASAT UNIVERSITY
FACULTY OF SCIENCE AND THEHNOLOGY

THESIS

BY

MR TOSSAPON PHROMSATIT

ENTITLED

CHARACTERIZATION AND CYTOTOXICITY OF NEW COPPER(II) SILVER(II) AND GOLD(III) TETRA ALKYL PHENOXY PORPHYRIN DERIVATIVES

was approved as partial fulfillment of the requirements for
the degree of Doctor of Philosophy (Chemistry)

on June 29 2021

Chairman _____
(Assistant Professor Soraya Pornsuwan, Ph.D.)

Member and Advisor _____
(Associate Professor Supakorn Boonyuen, Ph.D.)

Member and Co-adviser _____
(Assistant Professor Kittipong Chainok, Ph.D.)

Member _____
(Assistant Professor Nanthawat Wannarit, Ph.D.)

Member _____
(Thapong Teerawatananond, Ph.D.)

Dean _____
(Associate Professor Nuttanont Hongwarittorrn, Ph.D.)

*His Majesty King Bhumibol Adulyadej trained himself physically and mentally in accordance with the **five Dhammic Strengths of Buddhism**, which he ascertained from a sermon during the time of his monkhood in 1956. He continued to study and practice Dhamma, often discussing religion with venerable monks, especially on his trip to the Northeast.*

*The Five Dhammic Strengths are **Saddhā** or right confidence, to develop a strong, firm, and focused mide; **Viriya** of brevity, to fight against obstacles without discouragement; **Sati** or mindfulness, to promote memorization, prevent forgetfulness and mental defilement; **Samādhi** or mental concentration, to support a focused mind; and **Paññā** or wisdom, to illuminate the mind, to clearly understand cause and effect, what is worthy and unworthy, beneficial and useless. His Majesty practiced these in all his activities, carried out for the happiness of his subjects.*

Dissertation Title	Characterization and cytotoxicity of new copper(II) silver(II) and gold(III) tetra alkyl phenoxy porphyrin derivatives
Author	Tossapon Phromsatit
Degree	Doctor of Philosophy
Major Field/Faculty/University	Chemistry Science and Technology Thammasat University
Dissertation Advisor	Associate Professor Supakorn Boonyuen, Ph.D.
Dissertation Co-Advisor	Assistant Professor Kittipong Chainok, Ph.D
Academic Year	2021

ABSTRACT

Porphyrins play a vital role in biological systems. Porphyrins and their metal complexes are used in many applications such as catalyst, dye-sensitized solar cell, photodynamic therapy, medicinal application, etc. due to their outstanding properties such as high chemical and thermal stability, strong absorption in the visible region, and flexible architectural modification. So, the development and modification of porphyrin have been dramatically studies. The series of tetraphenylporphyrin contain different *meso*-substituent groups (phenyl, methoxyphenyl, butyloxtphenyl, octyloxyphenyl, and dectyloxyphenyl), and their copper, silver, and gold porphyrin complexes have been successfully synthesized. Mass spectrometry, ^{1}H NMR and ^{13}C NMR spectroscopy, infrared spectroscopy and CHN elemental analysis were used to confirm the structure of all synthesized compounds. All free-base porphyrin and metalloporphyrin have been characterized using UV-visible, and fluorescence spectroscopy, electron paramagnetic resonance spectroscopy, cyclicvotammetry, and DFT calculation. The electronic absorption band showed a red-shift when the number of carbon atoms in the alkyl long-chain was increased. The thermal stability of synthesized compounds was studied by thermal gravimetric analysis (TGA). All of the synthesized compounds were found to be highly thermally stable over 400°C. Free-base porphyrin and their copper and silver complexes were also tested for antibacterial

activity using disc diffusion technique. Their synthesized compounds were found to be effective for the inhibition of bacterial growth. In addition, the *In vitro* anticancer activity on breast cancer cell (SKBR3 and MCF7) of copper and gold porphyrin complexes have been investigated. Both gold and copper porphyrin complexes exhibited cytotoxicity on MCF7 cell lines. The gold(III) porphyrin complexes show better potential than copper(II) porphyrin complexes. Especially for both AuTPP and AuTOMPP show the cytotoxicity with the IC_{50} values of 4.30 ± 1.30 μM and 25.35 ± 7.14 μM, respectively. Moreover, the cytotoxicity of all metalloporphyrin complexes has investigated the cytotoxicity on Rhesus Monkey Kidney Epithelial Cells (LLC-MK2) representative of the human normal cells. The result shows that all metalloporphyrin complexes exhibited non-cytotoxic on LLC-MK2 cells. In the case of AuTPP shows non-cytotoxic at a concentration lower than 5 μM.

Keywords: Porphyrin, Metalloporphyrin, Anticancer activity

ACKNOWLEDGEMENTS

First and foremost, I would like to express my gratitude to my supervisor, Associate Professor Dr.Supakorn Boonyuen for his continued support, guidance, polish, and encouragement during the research study and the preparation of this thesis.

For their generous assistance in this research, I would like to thank Dr.Thapong Teerawatananond, Associate Professor Dr.Korbtham Sathirakul, Mr.Thitianan Kulsirirat and Department of Pharmacy, Faculty of Pharmacy, Mahidol University for preliminary anticancer activity test of porphyrin compounds. Associate Professor Dr.Premjit Arponmaeklong, and Associate Professor Dr.Yuki Shirosaki for the great opportunity to study the cytotoxicity on cancer cell at Kyushu Institute of Technology. Assistant Professor Dr.Jundee Rabablert and Department of Biology, Faculty of Science, Silpakorn University for studied cytotoxicity of porphyrin complexes on normal cells. Assistant Professor Dr.Ming-Li Tsai from National Sun Yat-sen University and Associate Professor Dr.Yosito Ando from Kyushu Institute of Technology for the EPR spectroscopy studied. Dr.Supawadee Namuangruk, Mr.Chirawat Chitpakdee and National Nanotechnology Center for DFT calculation. Assistant professor Dr.Pariya Na Nakron for the antibacterial activity studied. Assistant Professor Dr.Kittipong Chainok, Assistant Professor Dr.Nanthawat Wannarit, and Assistant Professor Dr.Soraya Pornsuwan for suggestion along with the support from technical staffs of Thammasat Universities. My thanks also to my scholarship, science achievement scholarship of Thailand (SAST) for financial support, and Faculty of Science and Technology, Thammasat University supports for all experiments. I appreciated in support from “Japan Student Services Organization (JASSO)” for a scholarship to internship in Kyushu Institute of Technology, Kitakyushu, Japan.

I wish to thank all of my friends, all of my research group in room C404, and Dr.Nanthawat’s lab members for their help take care of and encouraging me during the preparation of this thesis. Miss Somchintana Puttamat staff of Department of chemistry for the suggestion, taking care of me and supported me since I start my Ph.D. I would be thankful to my parents for their love, support, and stand by me every time. I couldn't have done it without all of you “THANK YOU”.

Mr.Tossapon Phromsatit

TABLE OF CONTENTS

LIST OF TABLES

LIST OF FIGURES

LIST OF FIGURES (CONT.)

LIST OF FIGURES (CONT.)

LIST OF FIGURES (CONT.)

LIST OF FIGURES (CONT.)

LIST OF SCHEME

LIST OF ABBREVIATIONS

Symbols/Abbreviations	Terms
°C	Degree Celsius
^{13}C NMR	Carbon Nuclear Magnetic Resonance Spectroscopy
^{1}H NMR	Proton Nuclear Magnetic Resonance Spectroscopy
AgTOBPP	Tetrakis(4-butyloxyphenyl)porphyrinatosilver(II)
AgTODPP	Tetrakis(4-dectyloxyphenyl)porphyrinatosilver(II)
AgTOMPP	Tetrakis(4-methoxyphenyl)porphyrinatosilver(II)
AgTOOPP	Tetrakis(4-octyloxyphenyl)porphyrinatosilver(II)
AgTPP	Tetraphenylporphyrinatosilver(II)
AuTOBPP	Tetrakis(4-butyloxyphenyl)porphyrinatogold(III) chloride
AuTODPP	Tetrakis(4-dectyloxyphenyl)porphyrinatogold(III) chloride
AuTOMPP	Tetrakis(4-methoxyphenyl)porphyrinatogold(III) chloride
AuTOOPP	Tetrakis(4-butyloxyphenyl)porphyrinatogold(III) chloride
AuTPP	Tetraphenylporphyrinatogold(III) chloride
Cal.	Calculation
CuTOBPP	Tetrakis(4-butyloxyphenyl)porphyrinatocopper(II)
CuTODPP	Tetrakis(4-dectyloxyphenyl)porphyrinatocopper(II)
CuTOMPP	Tetrakis(4-methoxyphenyl)porphyrinatocopper(II)
CuTOOPP	Tetrakis(4-octyloxyphenyl)porphyrinatocopper(II)
CuTPP	Tetraphenylporphyrinatocopper(II)
DFT	Density functional theory
DMSO	Dimethyl Sulfoxide
Egap	Energy gap
EPR	Electron paramagnetic resonance
HOMO	Highest occupied molecular orbital
IC_{50}	Half-maximal inhibitory concentration
IR	Infrared
K	Kelvin

LLC-MK2	Rhesus Monkey Kidney Epithelial Cells
LUMO	Lowest unoccupied molecular orbital
MBC	Minimum bactericidal concentration
MCF7	Michigan Cancer Foundation-7
MIC	Minimum inhibitory concentration
MTT	3-(4,5-Dimethylthiazol-2-yl)-2,5-Diphenyltetrazolium Bromide
TGA	Thermal gravimetric analysis
TOBPP	Tetrakis(4-butyloxyphenyl)porphyrin
TODPP	Tetrakis(4-dectyloxyphenyl)porphyrin
TOMPP	Tetrakis(4-methoxyphenyl)porphyrin
TOOPP	Tetrakis(4-octyloxyphenyl)porphyrin
TPP	Tetraphenylporphyrin

CHAPTER 1
INTRODUCTION

1.1 Overview of porphyrin and metalloporphyrin

Porphyrin is a group of the heterocyclic macrocyclic organic compound. The basic unit of porphyrin compound composed of four modified pyrrole (five-membered ring contain a nitrogen atom) subunits interconnected at their carbon atom via methane bridges (=CH-). The basic porphyrin is called porphin. The structure of porphin and the substituted porphins is call porphyrin (**Figure 1**). In 1912, Kuster first proposes the correct structure of porphyrin and confirmed by Hans Fischer, the father of modern porphyrin chemistry, when he successfully synthesize the first porphyrin protoheme [1]. The origin of the word "porphyrin" comes from the Greek word "porphuros" (πορφύρα), which means the purple color [2]. Generally, porphyrin compound is a dark purple solid and dissolved in non-polar solvent.

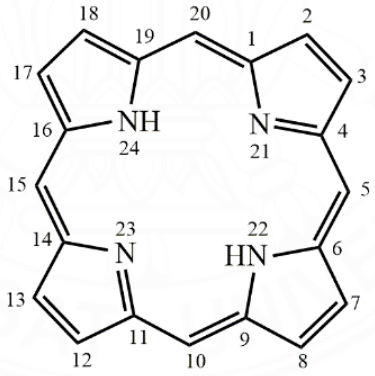

α-positions (1, 4, 6, 9, 11, 14, 16, 19)

β-positions (2, 3, 7, 8, 12, 13, 17. 18)

meso-positions (5, 10, 15, 20)

Figure 1 Structure of porphyrin and the IUPAC numbering system [3]

Porphyrin basically is a cyclic tetrapyrrole derivatives with a highly delocalized planar π-framework having a core system, and in agree with Huckel's Rule [4n + 2]. The porphyrin macrocycle containing 22-π conjugated electron. There are 18-

π electrons of which are in the delocalized pathway. It shows as a result of the extended conjugation (**Figure 2**). The high conjugation π system is the origin of the strong color of the porphyrin compounds, and causes for their characteristic electronic and redox properties. Besides many synthetic and naturally occurring ones with core structure. There are also several porphyrin-like structures which are shown in **Figure 3**.

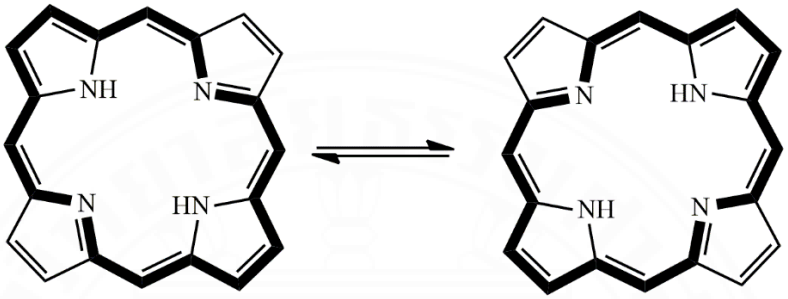

Figure 2 Delocalized 18 π-electron conjugation pathways of the porphyrin ring system

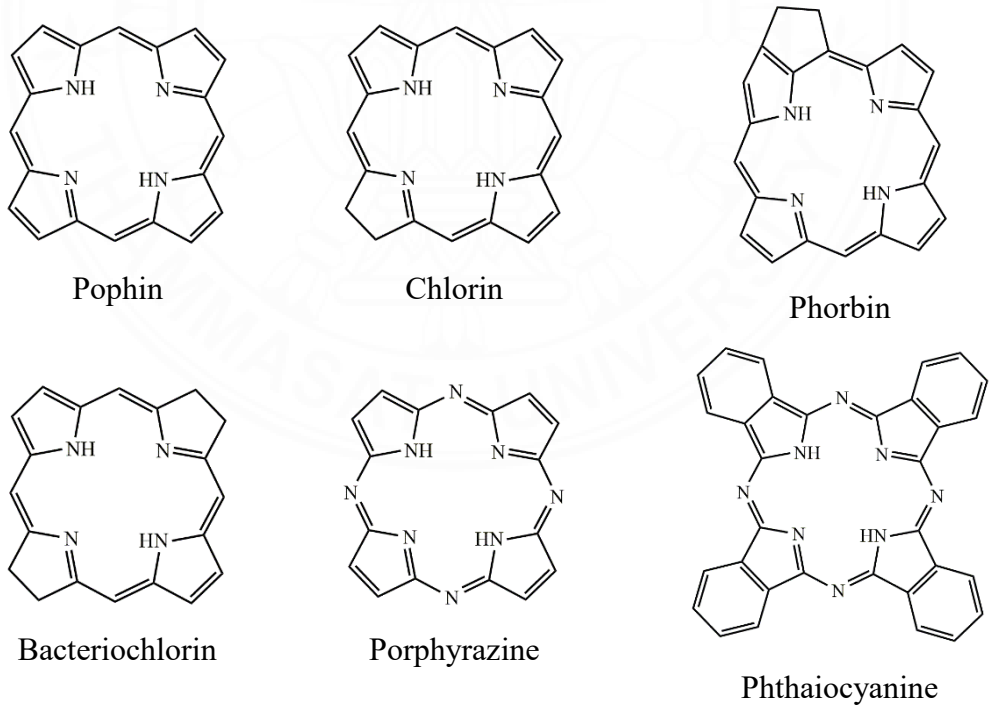

Figure 3 The porphyrin-like structures

Porphyrin is one of the vital chemical units essential for several life processes. Porphyrin plays a vital role in the biological system, and their synthesis arouses containing the interest in biological, material, and inorganic chemistry [4]. The one advantage of porphyrin is it can undergo chemical reactions without loss of its aromaticity because the porphyrin contains 22 conjugated π-electrons, but there are 18 of these are required for its aromatic network. For this reason, the porphyrin compound can be produced in various functionalized to find multiple applications in biology, medicine, and materials science. The structure of a porphyrin exhibits two major points for functionalized, four *meso*-positions and eight *β*-positions (**Figure 1**). The most reactive position is *meso*-position. The synthetic *meso*-substituted porphyrin offers a great advantage to study the physical and chemical properties of the substituents that may be attached to the periphery. The substituents at *meso*-positions can be readily adjusted utilizing alkyl, aryl, the heterocyclic, or organometallic group as other porphyrins. On the other hand, the *β*-pyrrolic positions are the most sterically accessible and can also undergo the same type of reactions [5]. Therefore, the porphyrin compounds can be classified into two main major categories on the pattern of substituents attached to macrocycle namely: *meso*-substituted porphyrins and *β*-substituted porphyrins.

Porphyrin ring provides a vacant site at its center, the acidic character has been processed at the NH protons inside the ring of porphyrin and hence can get deprotonated to give porphyrinato ion. These dianions are able to coordinate may result in the distortion of the planar macrocyclic in order to maximize the binding strength towards the metal fragment. With very few exceptions the porphyrinato dianion act as a tetradentate ligand with a metal ion. Thus the minimum coordination number of the metal ion possible in metalloporphyrin is four. The normal coordination geometry around the metal ion would be square planar. The nature of bonding between a metal center and the porphyrin ligand is found to be originating essentially from the following two types of primary interaction: σ-coordination of nitrogen lone pairs directed towards the metal atom and π-interaction of metal pπ or dπ orbital with nitrogen-based π orbitals (**Figure 4**) [6].

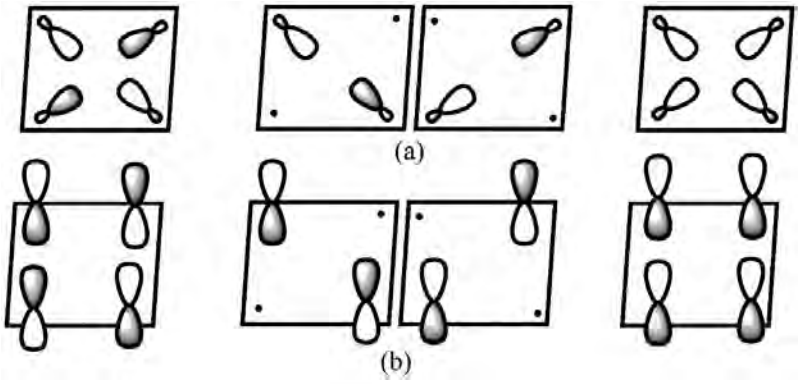

Figure 4 The symmetry adapted linear combinations of porphyrin-ligand orbitals involved in the bonding with metal orbitals are suitable (a) for σ-interactions and (b) for π-interactions

1.2 Porphyrin in life process

A large number of natural metalloporphyrin play a vital role in the biological system including heme, chlorophyll, vitamin B12, and enzyme etc. There are the most important in biological processes such as respiration, photosynthesis, ion transfer, and other applications in the living system.

Heme is a cofactor consisting of a ferrous ion (Fe^{2+}) contained in the center of a porphyrin ring. Many living organisms ranging from bacteria to humans synthesize and use heme. Hemes are most commonly recognized as components of hemoglobin, the red pigment in blood, but are also found in a number of other biologically important hemoproteins such as myoglobin and cytochrome. The heme is an asymmetric molecule and consists of a porphyrin ring and iron atom in the central hole (**Figure 5**). Heme groups contain iron(II) ion molecules, which can reversibly bind to an oxygen molecule and transport them to various areas of the body. Hemoglobin and myoglobin are high molecular weight protein systems containing iron(II) porphyrin four-unit. They are responsible for oxygen transport and storage in the higher animals [7 - 8].

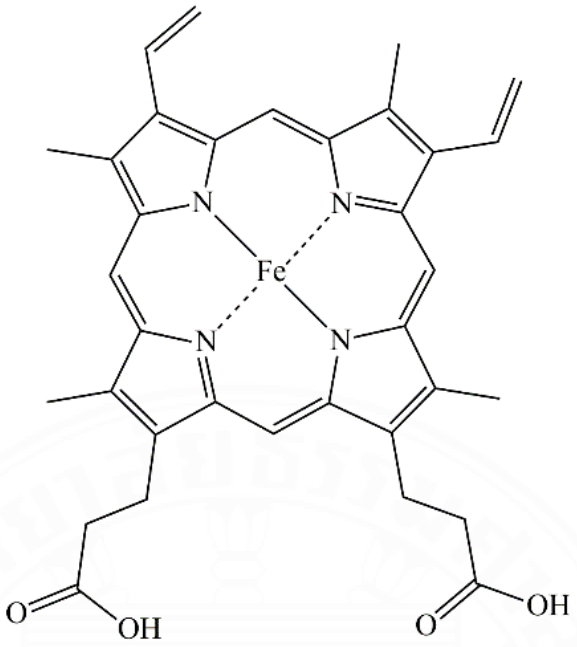

Figure 5 Structure of heme

Chlorophyll is the green coloring matter of leaves and green stems, and its presence is essential for photosynthesis. The word "chlorophyll" comes from two Greek words, ‘chloros’ represent the green color, and ‘phyllon’ represent leaf. Chlorophyll is an extremely important biomolecule critical in photosynthesis, which allows plants to absorb energy from light energy. Chlorophyll is a magnesium derivative of porphyrin (**Figure 6**). The magnesium-containing porphyrin is a square planar structure. Attached to the porphyrin is a long-chain hydrocarbon, insoluble which interacts with the protein of thylakoids and serves to hold the molecule in the internal membranes of the chloroplast. All of the chlorophylls absorb light very intensely, particularly at relatively long-wavelength regions. The light energy absorbed by a chlorophyll molecule becomes delocalized and spread throughout the entire electronic structure of the excited molecule [9 - 10].

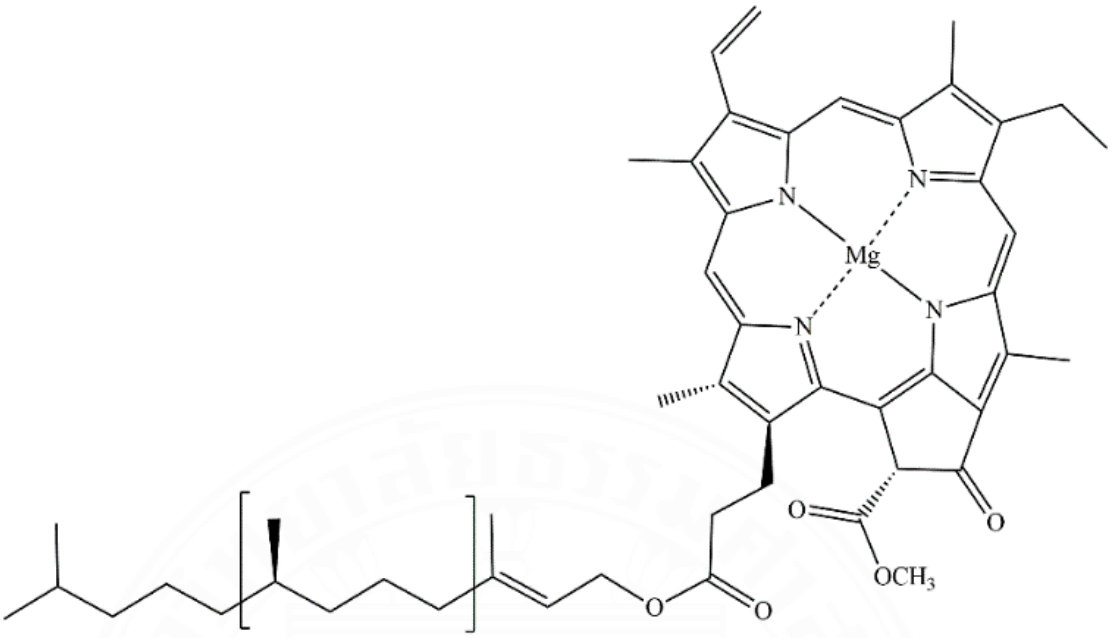

Figure 6 Structure of chlorophyll

Vitamin B12 or cobalamin is a water-soluble vitamin with a key role in the normal functioning of the brain and nervous system, and for the formation of blood. The structure of Vitamin B12 consists of four pyrroles joined on methane bridges from three of these likes and with the two of the pyrrole joined directly. It is similar to a porphyrin, but with one of the bridging methylene groups removed. The structure of vitamin B12 presents a corrin ring with cobalt, positioned right in the center of the structure (**Figure 7**). Biosynthesis of the basic structure of this vitamin is accomplished only by bacteria and Achaea, but conversion between different forms of the vitamin can be accomplished in the human body [11 - 12].

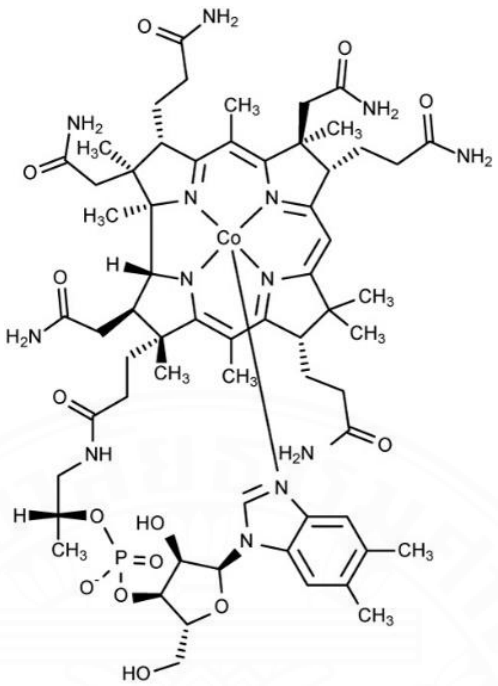

Figure 7 Structure of Vitamin B12

An enzyme is a biological catalyst that governs, initiates, and controls biological reactivity important for the life process. Enzymes are proteins that act as biological catalysts. All known enzymes are proteins, and some contain non-protein moieties termed prosthetic groups that are essential for the main infestation of catalytic activities. Such as the iron-porphyrin complexes, including hemoglobin, myoglobin, and the heme enzyme peroxidase, catalase, cytochrome, and coenzyme. For example, Coenzyme F430 is the prosthetic group of the enzyme methyl coenzyme reductase. It is found only in methanogenic Archaea. This enzyme catalyzes the release of methane in the final step of methanogenesis. F430 is the most reduced tetrapyrrole in nature with only five double bonds. This particular tetrapyrrole derivative is called a corphin. It is also the only tetrapyrrole derivative found in nature to contain nickel. Ni(II) ion is too small for the four nitrogen atom binding site of the corphin, which causes the macrocycle to adopt a ruffled structure. F430 occurs in particularly high concentrations of bacteria. Organisms that promote this remarkable reaction contain 7% by weight nickel protein [13]. Cytochrome P-450 is found in the microsomes of a liver cell [14]. Cytochromes P450 (CYPs) are a superfamily of enzymes containing heme as a cofactor

that function as monooxygenases. CYPs are, in general, the terminal oxidase enzymes in electron transfer chains, broadly categorized as P450-containing systems. Most CYPs require a protein partner to deliver one or more electrons to reduce the iron (and eventually molecular oxygen).

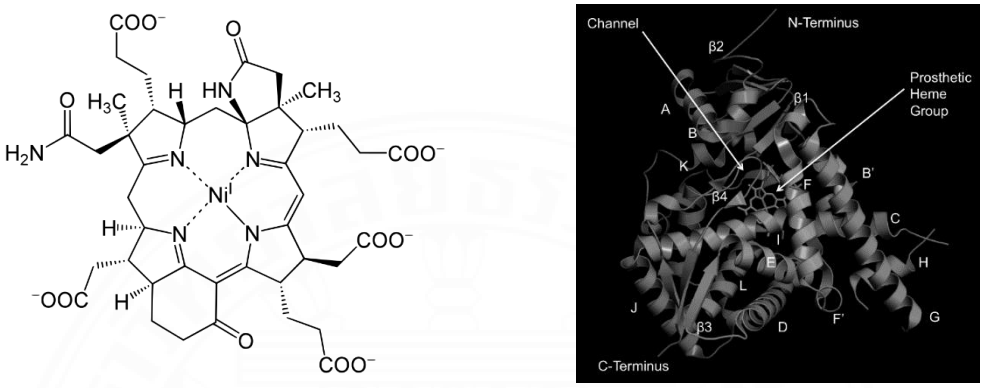

(a) (b)

Figure 8 Structure of (a) Coenzyme F430 and (b) Cytochromes P450 (CYPs)

1.3 Porphyrin synthesis

In the earlier part of this century, synthetic studies of porphyrin have been dramatically developed and modified within the synthesis of a large class of pyrrole. The initial works of synthesis porphyrin began in 1935 when Rotemund first developed a method for the synthesis of *meso*-tetramethylporphyrin from heating acetaldehyde and pyrrole in methanol at 95°C [15]. At present, there are several routes that can be followed to get the *meso*-substituted porphyrin. Since Rothmund reported his work, a series of both symmetric and asymmetric porphyrin has been dramatically studied. Symmetrical porphyrins are more easily synthesized than asymmetrical porphyrins. Their synthesis is based on the condensation of pyrrole and aldehyde with various reaction conditions. The variety of functionalized porphyrin, that continue to find multiple application. The *meso*-position is the most electronically reactive position of porphyrin and generally preferential sites for substitution and addition [21]. The *meso*-substituted porphyrins have been more interested because it have wide applications such as catalysis, electron transfer, photodynamic therapy, and molecular recognition,

dye-sensitized solar cell, antimicrobial agent, anticancer agent, etc. Although, *meso*-substituted porphyrin is not a naturally occurring compound they have to provide chemists and other scientists with a multitude of applications and fundamental studies.

Table 1

The summarize condition for synthesized porphyrin

Condition	Rothemund [16]	Adler-Longo [17]	Lindsey [18]	MacDonald type [2+2] [19]	MacDonald type [3+1] [20]
Reactants	Pyrrole + Benzaldehyde	Pyrrole + benzaldehyde	Pyrrole + benzaldehyde	Dipyrromethanes + N-tosyl imines	Dialdehyde + tripyrrane
Solvent	Pyridine	Propionic acid	CH_2Cl_2 Chloroform	CH_2Cl_2 DDQ	THF, CH_2Cl_2 Et_3N, DDQ
Temperature	150-220 ºC	140 ºC	25 ºC	25 ºC	-
Catalyst	-	-	TFA BF_3-etherate Clays, other acids	-	-
Reaction time	24 hours	30 minite	1hours	1.5 hours	1 hours
Yield	<10%	~20%	~ 30%	~ 40%	~ 60%

1.4 Application of porphyrin compounds

In the past decade, porphyrin has attracted great research attention as a versatile synthetic base for various materials due to its spectroscopy, electrochemical luminescence properties, and biological activity. The synthesis of porphyrins and their metalloporphyrin complexes has received much attention. Porphyrin can undergo

additional reactions without loss of the aromatic properties and it is conformational flexible and usually exhibit strong absorption in UV and Visible regions with high absorption coefficients. So this is a good advantage for using porphyrin and metalloporphyrin in various applications. The potential use of porphyrin and metalloporphyrin for biological, and material has been discussed. Porphyrin and its metal complexes were used in many applications, such as catalysis, dye-sensitized solar cell (DSSC), molecular sensor, anticancer, antimicrobial agent, and photodynamic therapy (PDT), etc. Dye-sensitized solar cells (DSSC) have been recognized as a key technology for the conversion of solar energy into electricity [22]. Porphyrins are one type of dye for cost-effective DSSC. The porphyrin compounds have been intensively studied as artificial light-harvesting systems over the years because they usually exhibit strong absorption in UV and Visible regions with high absorption coefficients. The photophysical properties were affected when the molecular orbital has been disturbed by substitution with electron-withdrawing or electron-donating group at *meso*- or *β*-position of the porphyrin ring. The use of porphyrin as a light harvester in DSSC is particularly attractive [23 - 25]. The modern electronic nose (e-nose) is based on an array of chemo resistive gas sensors that change their conductance when exposed to the volatile substance, generating an analytical signal [26]. For a part few years, porphyrin compounds have been a growing interest in the development of gas sensors with high sensitivity and selectivity [27]. Porphyrin and metalloporphyrin are interesting as gas sensors because their highly conjugated π-electron system yields significant changes in their UV-visible absorption spectrum during exposure to the various compound [28]. The electrical and optical properties of porphyrin and metalloporphyrin can vary widely depending on the electron donor and electron acceptors within the molecule [29]. The porphyrin film base sensor can be considered an excellent gas sensing device at ambient temperature since the change of electrical conductivity take place rapidly as a result of the interaction between the surface of porphyrin complexes and the gas molecule detected [30]. Moreover, the porphyrin compounds have been interesting in biological applications. The novel development of the porphyrin and metalloporphyrin complexes for biological activity has been attracted much [31 - 33]. Due to their ability to act as photosensitizers when irradiated by visible light. Because porphyrin analogous can take cytotoxic singlet oxygen directly in tumor cells causing cell death when irradiate,

photosensitization can represent a useful approach to kill microbial. Several porphyrins and related compounds have displayed phototoxicity against bacteria [34 - 36].

1.5 Porphyrin in cancer treatment application

Cancer is a group of diseases characterized by the uncontrolled growth and spread of abnormal cells. When this cell grows uncontrollably, the cancer cell can spread to other organs in the body it calls metastasizing and it is a major cause of death from cancer. The first recorded cancer case is breast cancer from ancient Egypt in 1500 BC and there was no treatment for the patient, only palliative treatment [37]. The World Health Organization (WHO) reported that cancer is the second leading cause of death globally. Lung, prostate, colorectal, stomach, and liver cancer are the most cancer type of cancer in men, while breast, colorectal, lung, cervical, and thyroid are common among women [38]. The change of normal cells to cancer cells is the result of the interaction between a person's genetic and the external agents including physical carcinogens such as UV and ionizing radiation, chemical carcinogens such as asbestos, smoke, aflatoxin, and arsenic, biological carcinogens such as infection from bacteria or viruses. In Thailand, cancer is the third leading cause of death among the Thai population. National Cancer Institute report that Liver and bile duct cancer is the first common cancer type of male and Breast cancer is the first common cancer type of female in Thailand. **Figure 9** shows the number of new cancer patients by age and group [39]. Cancer can affect almost any part of the body and has many anatomic and molecular subtypes that each requiring specific management strategies [40].

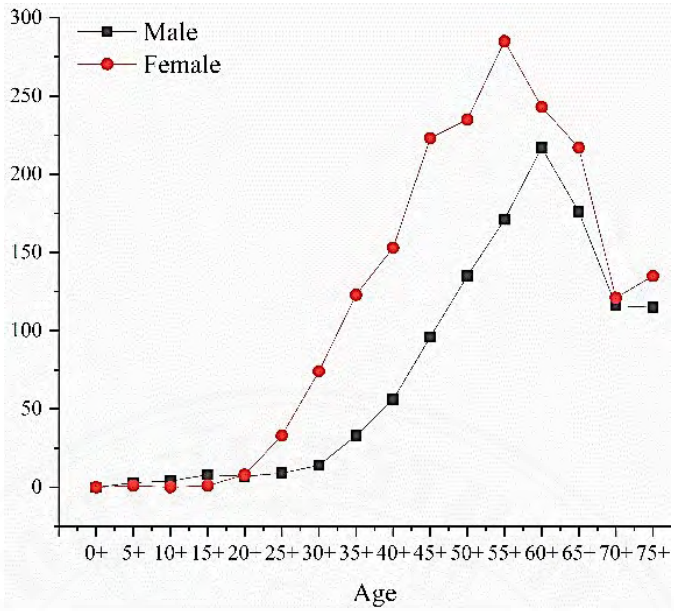

Figure 9 The number of new cancer patients by age and group

There are many types of cancer treatments such as surgery, chemotherapy, radiation therapy, Immunotherapy, Targeted therapy, stem cell therapy, and precision medicine. The type of treatment that you have will depend on the type of cancer. Most people have a combination of treatments to treat cancer. During the first half of the 20th-century surgery and radiotherapy dominated cancer treatment [41 – 42]. Nowadays, one of the most popular cancer treatments is chemotherapy. Chemotherapy, as a viable alternative, was first considered in the 1940s when nitrogen mustards were used against lymphomas [43]. Chemotherapy or chemo usually refers to the user of medicines or drugs to treat cancer. The chemotherapy drug target cell at different phases of the process of forming new cells (cell cycle). The cancer cell tends to form new cells more quickly than normal cells and this makes it a better target for chemotherapy drugs [44]. The most well know chemotherapy drug is cisplatin or *cis*-diamminedichloroplatinum (II) [45]. This compound was first described by Michele Peyrone in 1845 [46]. Since the serendipitous discovery that cisplatin can arrest cell division of *E. coli*, platinum coordination complexes have been widely investigated as anticancer agents [47]. However, the success of cisplatin as an anticancer metal-pharmaceutical drug has simulated the use of metal including gold in anticancer medicine [48]. Due to the gold(III) complex are isoelectronic ($5d^8$) and isostructure (square-planar) with platinum(II) and so have attracted interest as a potential anticancer

agent. The medical properties of gold have been explored throughout the history of civilization. Since gold is one of the oldest metals used in medicine and gold-coordinating complexes are the most extensively investigated metal complexes [49 - 50]. In the previous report, the promising gold(III) candidates are the porphyrinato derivatives developed by Che and Sun, which include the complex $[Au(TPP)]^+$ (**Figure 10**). This compound has received special attention as a promising candidate for a new anticancer drug [51].

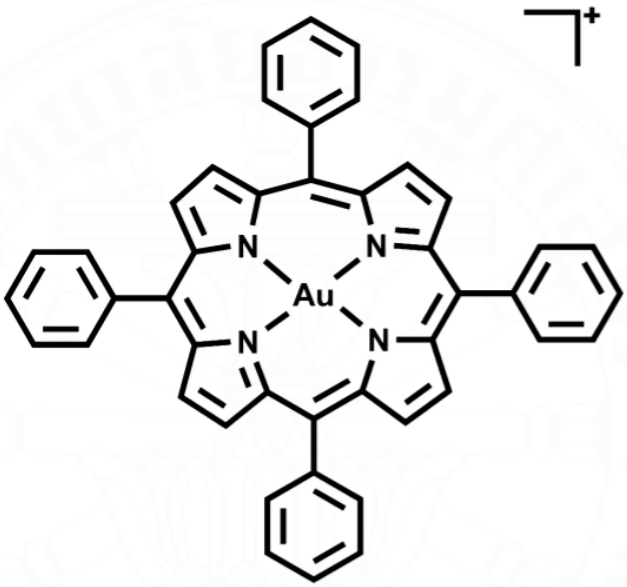

Figure 10 Structure of $[Au(TPP)]^+$ complex

1.6 Research objective

1. To synthesize and characterize aldehyde with different *para*-substituted alkyl long-chain groups
2. To synthesize and characterize free-base porphyrin with different *meso*-substituted groups including phenyl, methoxyphenyl, buthyloxyphenyl, octhyloxyphenyl, and dectyloxyphenyl.
3. To synthesize and characterize metalloporphyrin by adding copper ion (Cu^{2+}), silver ion (Ag^{2+}) and gold ion (Au^{3+}) in to center of the porphyrin ring derivative.

4. To study and compare the chemical, and physical properties of free-base porphyrin, metalloporphyrin, and their derivative which various techniques.
5. To study the anticancer activity of gold(III) porphyrin complexes

1.7 Scope and limitation

1. The various aldehyde was prepared by refluxing a mixture of *4*-hydroxybenzaldehyde with alkyl bromides such as *1*-bromobutane, *1*-bromooctane, and *1*-bromodecane.
2. The long-chain porphyrin and its derivatives with different peripheral substitutions ligands by refluxing pyrrole with the various aldehyde such as *p*-anisaldehyde, butyloxybenzaldehyde, octyloxybenzaldehyde, and decyloxy-benzaldehyde were synthesized by a modified Adler-Longo method due to its easy procedure with medium yields.
3. The metalloporphyrin with various porphyrin was prepared by adding copper ion (Cu^{2+}) silver ion (Ag^{2+}) and gold ion (Au^{3+}) in long-chain free-base porphyrin.
4. The NMR, IR, EPR spectroscopy, mass spectrometry, elemental analysis technique and powder X-ray diffraction or single-crystal X-ray diffraction were applied to confirm the synthesized structure.
5. The effects of macrocyclic structures with different peripheral substitutions, a group of long-chain porphyrins and metalloporphyrins, were characterized by UV-Vis, fluorescence spectroscopy.
6. The porphyrins properties were studied by the thermal gravimetric analysis (TGA), cyclic voltammetry and computational study.
7. The biological activity of all compounds was tested by using the disc diffusion technique.
8. The anticancer activity of gold(III) porphyrin complexes has been studied using MTT assay.

1.8 Expected result

1. All aldehyde, free-base porphyrin, and metalloporphyrin were successfully synthesized and characterized
2. Porphyrins and metalloporphyrins (copper, silver, and gold porphyrin complexes) can be compared by using UV-Vis spectroscopy, fluorescence spectroscopy, thermal gravimetric analysis, cyclic voltammetry, electron paramagnetic resonance spectroscopy and computational study.
3. Gold(III) porphyrin complexes were used to apply in the anticancer application.

CHAPTER 2
REVIEW OF LITERATURE

2.1 Synthesis of free-base porphyrin

In 1936, Rothemund P. reported the first synthesis of *meso*-tetraphenylporphyrins (TPP). The TPP was synthesized by refluxing benzaldehyde and pyrrole under acidic condition with high temperature and high concentration for 24 hours (**Figure 11**). Various aldehydes like propionaldehyde, n-butyraldehyde, and α-furaldehyde with pyrrole were utilized to obtain porphyrin by using this method. However, this method was obtained low yields [16].

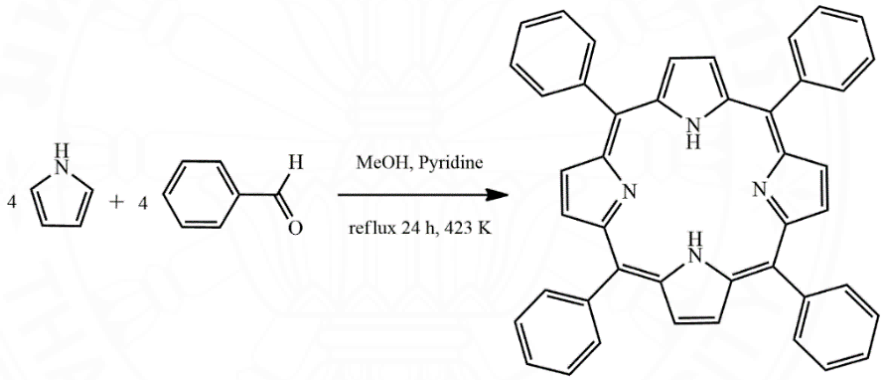

Figure 11 Synthesis of TPP using Rothemund's method

In 1960, Alder A. et al. modified the synthesized method for *meso*-substituted porphyrin synthesis. The conditions of this method is reflux pyrrole and benzaldehyde in propionic acid for 30 minutes under open an atmosphere (**Figure 12**). This reaction conditions were relatively mild, which afforded higher yield and gave faster reaction rate, when the current condition was compared with Rothemund conditions [17].

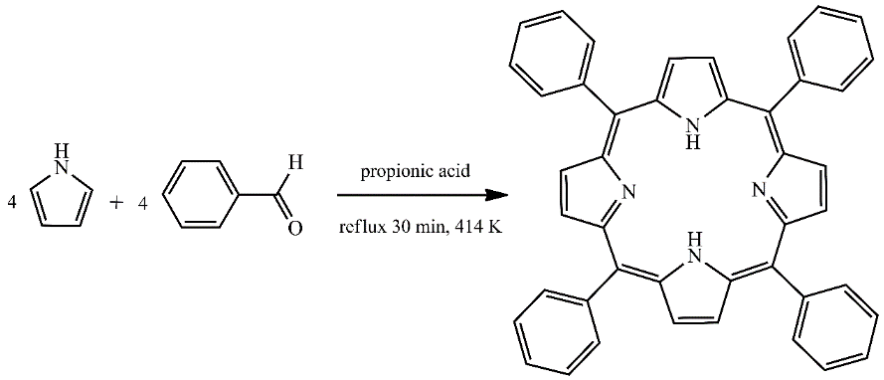

Figure 12 Synthesis of TPP using Alder-Longo's method

In 1980, Lindsey J. et al. report a new synthetic method that set the standard for *meso*-aryl substituted porphyrin. This method involved a condensation between benzaldehyde and pyrrole. Under this method the synthesis product was obtained after two-step reactions, first step is deal with acid-catalyzed (BF_3-Et_2O or TFA) condensation to form the intermediate porphyrinogent, followed by the second step, which is the addition of an external oxidant (DDQ or chlorinal) to form the porphyrin (**Figure 13**). This method is producible with a typical yield in rang 30 – 40% [18].

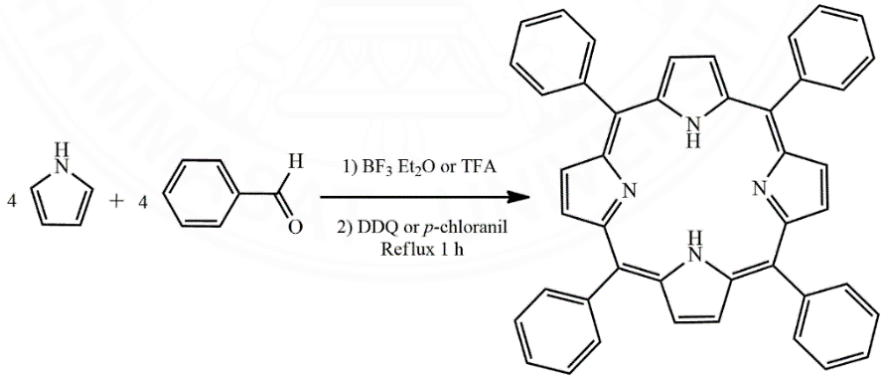

Figure 13 Synthesis of TPP using Lindsey's method

In 1960, Macdonal S.F. et al. presented the MacDonal [2+2] condensation method for symmetrical *meso*-substituted porphyrins synthesis. The condensation

reaction of dipyrromethane or dipyrromethene and aldehyde in acid catalyst to receive the *meso*-substituted porphyrins [19].

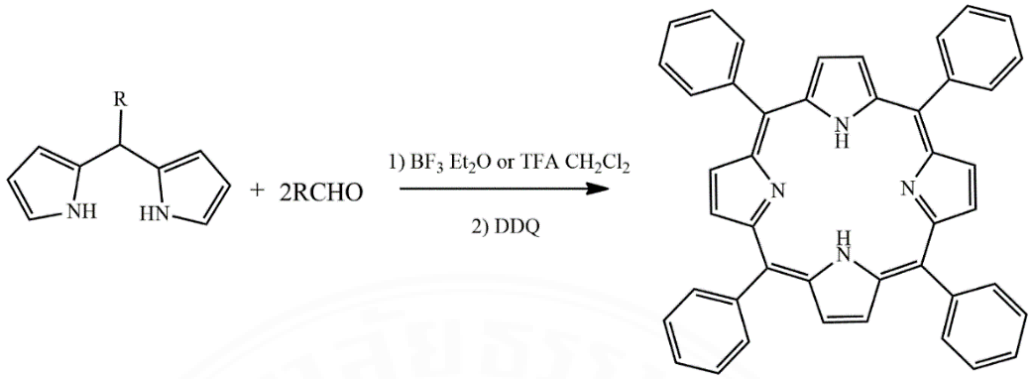

Figure 14 Synthesis of TPP using MacDonald [2+2] condensation

In 1994, Arezki B. et al. presented the new method for porphyrin synthesis. This reaction is the condensation between tripyrrsne that carries out carboxylic acid substituents in their α-positions and 2,5-diformylpyrrole. This method is call '3+1' type condensation. The successes of this method could be extended to the preparation of *meso*-unsubstituted porphyrins [20].

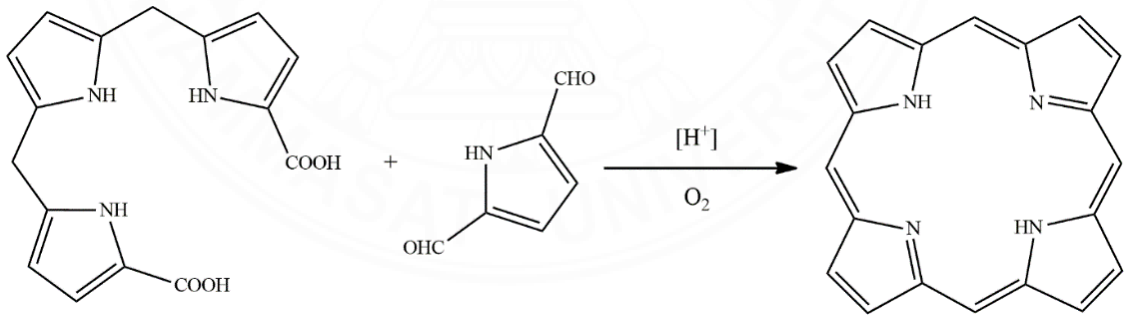

Figure 15 Synthesis of TPP using MacDonald [3+1] condensation

In 2009, Baris T. et al. reported the new synthetic route for porphyrin synthesis. The 5,10,15,20-tetraphenyl porphyrins (TPP) have been prepared by developing the reaction between 5-substituted dipyrrolemethane and N-tosyl imine in presence of metal triflate catalyst. The TPP was formed in two-step under Linsey's condition. First, the porphyrinogen intermediates have been synthesized by

condensation of 5-phenyldipyrromethane and N-benzylidene-4-methylbenzene-sulfonamide. The second step is the oxidation of the porphyrinogen to porphyrin (**Figure 16**). Then the optimum condition of this reaction has been investigated. The result indicated that the best condition for porphyrin synthesis is the condensation of 10 mM of dipyrromethane and N-tosyl imine with 10 mol % $Cu(OTf)_2$ in dichloromethane for 1.5 hours and then oxidation with DDQ at room temperature. Furthermore, this reaction has been used to prepare the tran-A_2B_2-tetraarylporphyrins compound. The porphyrin derivatives were obtained in 18 – 30 %yield. The convenient availability of these intermediates makes it possible to extend this methodology also to the synthesis of tetraphenylporphyrin with a different aryl group [52].

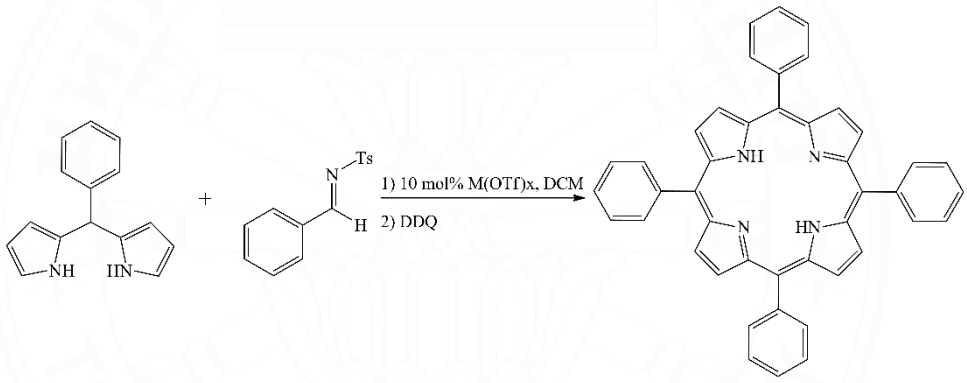

Figure 16 The synthetic route of 5,10,15,20-tetraphenyl porphyrins synthesis

2.2 Synthesis of porphyrins substituent and metalloporphyrin complexes

In 2001, Ming-Cheng W. et al. reported the X-ray structure of mercury(II) porphyrin complexes (**Figure 17**). The Hg(ρ-$(N)_4$tpp and Hg(N-Me-tpp)Cl were synthesized by modification of Alder-Longo method. Both complexes exhibited spec group P1 and triclinic crystal system. The crystal of Hg(ρ-$(N)_4$tpp and Hg(N-Me-tpp)Cl were grown by diffused ether vapor into CH_2Cl_2 solution and layer method between $CHCl_3$ and methanol, respectively [53].

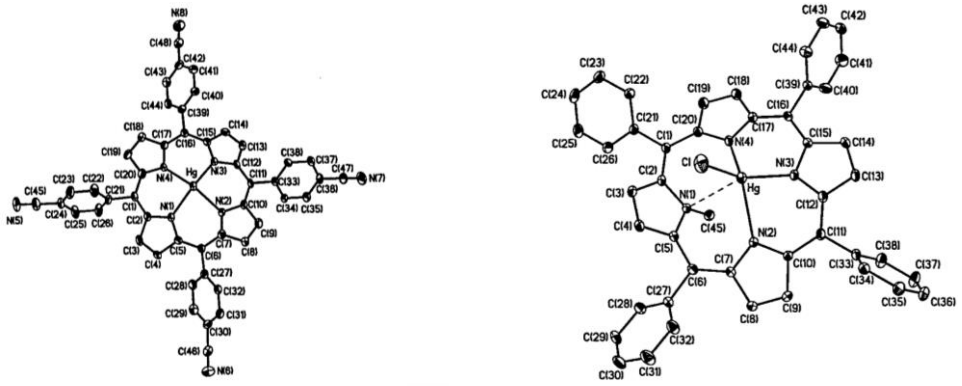

Hg(ρ-(N)$_4$tpp Hg(N-Me-tpp)Cl

Figure 17 The X-ray structure of Hg(ρ-(N)$_4$tpp and Hg(N-Me-tpp)Cl

In 2003, Yu-Yi L. et al. prepared the new thallium complexes acetato-[*meso*-tetra(p-chlorophenyl)porphyrinato]thallium(III), and two new indium complexes acetato-[*meso*-tetra(p-chlorophenyl)porphyrinato]indium(III), and acetato-[*meso*-tetra(p-bromo phenyl)porphyrinato]indium(III). All porphyrins have been synthesized by refluxing porphyrin ligand with metal salt ($Tl(OAc)_2$ and In_2O_3), and the products was obtained in 87%, 84%, and 66% yield, respectively. The purple crystal of all complexes were obtained by layered with MeOH. The porphyrin complexes were characterized by ^1H NMR, ^{13}C NMR, IR, and mass spectroscopy. Furthermore, the X-ray structure of all compounds was determined and exhibited P1 spec group. The coordination sphere around Tl^{3+} ion is six-coordinate distorted square-based pyramid in which the apical site is occupied by a chelating bidentate OAc^- group, whereas the In^{3+} ion is a five-coordinate regular square-based pyramid in which the unidentate OAc^- ligand [54].

In 2004, Ana M. et al. prepared the hydroxynitrophenylporphyrins (tetrakis(2-hydroxy-5-nitrophenyl)porphyrin) compound through Alder's method. This compound has been synthesized by refluxing pryyole and 2-hydroxy-5-nitrobenzaldehyde in propionic acid at 141°C. After purification by silica gel chromatography, the product was obtained 72% yield. This compound exhibited absorption and emission in visible region. The photosensitizer properties have been observed. The results obtained demonstrate that these hydroxyl nitrophenyl porphyrins can be considered promising photosensitizers in PDT [55].

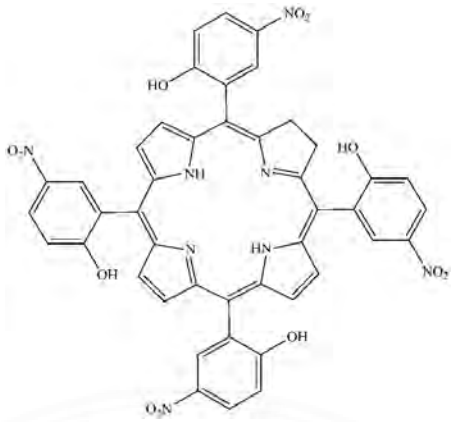

Figure 18 Structure of tetrakis(2-hydroxy-5-nitrophenyl)porphyrin

In 2007, Amrita G. et al. studied the controlled aggregation of tetrakis-(4-(hexadecyl oxy)-phenyl) porphyrin and its copper(II) complex in mix-solvent. This porphyrin synthesized was started by changing cetyl alcohol to cetyl chloride by reacting with $SOCl_2$. Then the long-chain aldehyde has been prepared from the reaction of cetyl chloride and p-hydroxybenzaldehyde in presence of K_2CO_3. The porphyrin was obtained after the long-chain aldehyde reacts with pyrrole through Alder's method. Finally, the copper(II) porphyrin complex has been synthesized by reacting with copper(II) acetate. Furthermore, the aggregation of porphyrin and its copper complexes were studied. The structure of the aggregates was characterized by SEM, TEM, P-XRD, and UV-visible spectroscopy. The different solvent ratios have an effect on the structure of their agitation [56].

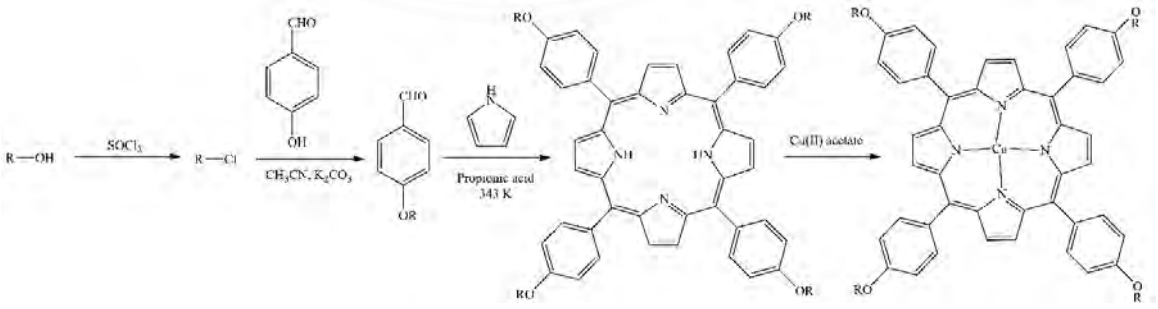

Figure 19 Synthetic route of tetrakis-[4-(hexadecyloxy)phenyl]porphyrin and it copper(II) complex

In 2007, Ioannis D.K. et al. reported the synthesis and catalytic properties of the water-soluble palladium porphyrin complexes. The functionalized benzaldehyde was obtained from alkylation of 4-hydroxybenzaldehyde and 4-bromobutyrate in the presence of K_2CO_3 in DMF. The free-base porphyrin was synthesized following Alder's method. The palladium porphyrin complexes were prepared by refluxing porphyrin with palladium chloride in benzonitrile. The water-soluble palladium porphyrin complexes have been prepared by saponification reaction with excess KOH in THF/MeOH. The final product was obtained as dark red solid in 97% yield (**Figure 20**). All synthesized compounds have been characterized by ^{1}H NMR, ^{13}C NMR, and mass spectroscopy. These complexes can be used as a catalyst precursor for the Susuki-Miyaura cross-coupling of aryl bromide under mind conditions and leading to yields of coupling products in the range of 80-100%. This catalyst can be recycled, but loses inactivity [57].

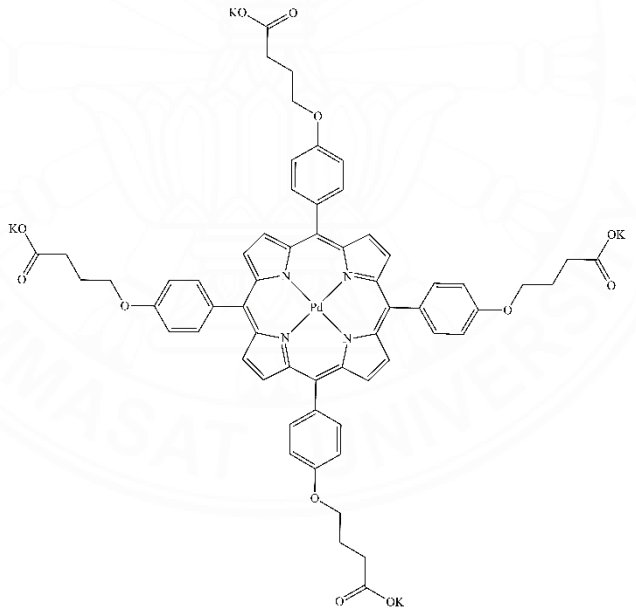

Figure 20 Structure of the water-soluble palladium porphyrin complexes

In 2009, Chen W. et al. prepared the two new series of novel *meso*-substituted porphyrin and their metal complexes. The two type of functionalized benzaldehyde were obtained by reaction between 3-pheoxypropyl with 4-hydroxybenzaldehyde or 2-hydroxybenzaldehyde. The free-base porphyrin 5,10,15,20-

tetra[4-(3-phenoxy)-propoxy]phenyl porphyrin, and 5,10,15,20-tetra[2-(3-phenoxy)-propoxy]phenyl porphyrin have been prepared follow by Lindsay method. Moreover, the Co(II) Cu(II) and Zn(II) complexes were synthesized. The free-base porphyrins provided a low yield. Nevertheless, the metalloporphyrin were all synthesized with yields of around 90%. The CHN elemental analysis, FT-IR, ^{1}H NMR, mass, and UV-visible spectroscopy have been used to characterize the structure of all compounds. Furthermore, their molecular structure was proposed based on DFT calculation. The photocatalytic activities in the degradation of *4*-nitrophenol were investigated using polycrystalline TiO_2 impregnated with the porphyrins and metalloporphyrins. The copper complexes exhibited the highest effective sensitizer than other metal complexes as well as the free-base porphyrin [58].

In 2009, Er-Jun S. et al. reported the liquid crystal behavior of the series of long-chain substituted porphyrin derivative and their Zn complexes. The meso-tetra (4-alkylamidophenyl) -porphyrin ligands (alkyl = 8, 10, 12, 14, 16, 18) were prepared by acylation of the amino group of 5,10,15,20-tetra(4-aminophenyl)porphyrin by alkyl chloride in $CHCl_3$. After purification, their zinc complexes have been prepared by refluxing each free-base porphyrin with zinc chloride in a mixed solvent of $CHCl_3$ and DMF under the protection of a nitrogen stream. All compounds have been characterized by using elemental analysis, cyclic voltammetry, ^{1}H-NMR, IR, UV-vis, and fluorescence spectroscopy. Mesomorphism was investigated by DSC, polarized optical microscopy (POM), and X-ray diffraction (XRD). The results indicated that only porphyrin ligands that contain long-chain carbon (more than 12 atoms) are liquid crystals, while Zinc complexes are not. The studied of photophysical and electrochemical properties of the compounds, which indicated that the structure and properties of the porphyrin have been changes due to the alkylamido-group linking to the porphyrin molecule [59].

In 2011, Jun-Xu L. et al. report the crystal structure and their crystal data of *meso*-tetrakis[p-(heptyloxy)phenyl]porphyrinato}silver(II) (**Figure 21**). This compound has been synthesized by refluxing *meso*-tetrakis[p-(heptyloxy)-phenyl]porphyrin and $AgNO_3$ in chloroform for 6 hours. The product was obtained in a 23 %yield. This compound has characterized by a single X-ray diffraction technic.

The single-crystal was obtained from recrystallization from dichloromethane at room temperature [60].

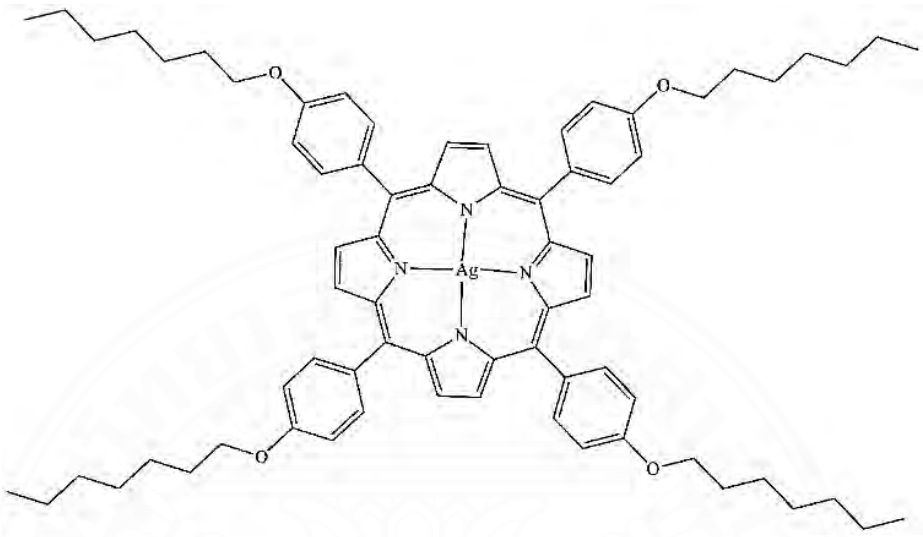

Figure 21 The structures of the silver porphyrin complex

In 2012, Julien T. et al. reported the synthesis of 2,6-dimethyl-4-(triflyloxyphenyl)porphyrin, their derivative, and zinc complexes. The *meso*-tetrakisarylporphyrin prefunctionalized with triflate group was prepared via Linsey method from 2,6-dimethyl-4-(triflyloxy)benzaldehyde and pyrrole. Furthermore, the porphyrin derivative with 3-pyridyl group has been prepared by Suzuki cross-coupling reaction in yield over 85%. The resulted porphyrin was metallated with zinc(II) ion and characterized by X-ray crystallography [61].

In 2013, Yu J.Z. et al. prepared three novel 5,10,15,20- tetra[n-C_nH_{2n+1}-alkyl (n=12,14,16) Carbazole] porphyrin and their lanthanide (Dy, Hs, Er, and Gd) complexes. The free-base porphyrin has been synthesized by the reaction between pyrrole and N-bromotetradecanedcarbaldehyde in xylene. The final product was purified by silica gel column chromatography (petroleum ether: $CHCl_3$ 1:3.5 v/v). All compound were characterized by UV-vis, IR, ^1H NMR, TGA-DTA, and molar conductance. The result showed that a longer alkyl group enhancing the conjugated capability of porphyrin ring and increasing the quantum yield. The redox potential

exhibited that the lanthanide prohpyrin complexes have two redox peaks while the ligand has four redox peak [62].

In 2013, Victor H.A.P. et al. reported the thermal decomposition of Mn(III) *meso*-tetrakis(N-ethylpyridinium-2-yl)porphyrin chloride ($MnTE\text{-}2\text{-}PyPCl_5 \cdot 11H_2O$) **Figure 22**. The thermal stability of $MnTE\text{-}2\text{-}PyPCl_5$ was investigated by TG/DTG/DTA, under dynamic air. All residue were analyzed by TLC and UV-vis spectroscopy. For the thermal stability studied three thermal processes were observed. The first step is dehydration in the 26 – 134 °C range, second step is dealkylation , in the 134 – 279 °C, and the final step is porphyrin ring decomposition in the 279 – 901 °C [63].

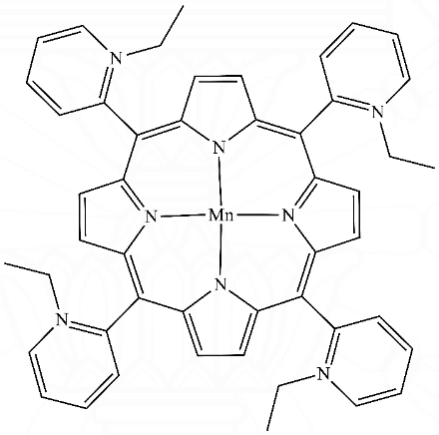

Figure 22 Mn(III) *meso*-tetrakis(N-ethylpyridinium-2-yl)porphyrin

In 2014, Goutam N. et al reported the synthesis of 4-chlorobenzoato-(5,10,15,20-mesotetratolylporphyrinato)-oxo-tungsten(V) [$W^{V}O(TTP)(4\text{-}ClBz)$] by thermal reaction. The tungsten(V) porphyrin complex has been synthesized in high yield using *p*-chlorobenzoic acid as the solid matrix and $[W(NO)_2(py)_2(Cl)_2]$ as the tungsten metal source. The synthesized compound is characterized by elemental analysis, UV-vis, FT-IR, ^{1}H NMR, cyclic voltammetry, DFT calculation, ESR, and ESI mass spectroscopy. The oxo-tungsten(V) *meso*-tetratolylporphyrin complex was purified by alumina column. The tungsten(V) porphyrin complex is hydrolyzed in the presence of traces of moisture present in the eluting solvent mixture. The hydroxo-(5,10,15,20-*meso*-tetratolylporphyrinato)-oxo-tungsten(V) [$W^{V}O(TTP)\ (OH)$] and Methoxo-(5,10,15,20-

*meso*tetratolylporphyrinato)-oxo-tungsten(V) [$W^{V}O$(TTP) (OMe)] have been obtained when used DCM/ethyl acetate and DCM/methanol used as the eluting solvent, respectively. The structure of oxo-hydroxo and oxo-methoxo complexes were studied by single x-ray diffraction. Both compounds exhibited monoclinic crystal system and $P2_1/n$ spec group [64].

In 2014, Zhijie X. et al. synthesis a novel porphyrin-napthalimide pentamer and their metal (Zn^{2+}, Cu^{2+}, Mn^{2+}, Fe^{3+}, Co^{2+}) complexes. The porphyrin-napthalimide ($TNPPH_2$) have been prepared by reaction between 5,10,15,20-tetrakis(4-hydroxyphenyl)-porphyrin and 4-phenyloxy-N-(4-(octyloxy)phenyl)-1,8-naphthalimide. The four light-harvesting napthalimide units have been linked to a porphyrin via ether bridges and obtain in 61% yield. The corresponding metal complexes of $TNPPH_2$ have been prepared. The structure at all compounds was characterized by ^{1}H, and ^{13}C NMR, FTIR, MALDI-TOF-Mass, and elemental analysis. UV-Vis and Fluorescence spectroscopy have been used to investigate the photophysical properties. The result shows that the excitation energy transfer occurs from the napthalimide unit to porphyrin core. Moreover, the electrochemical properties of all compounds were studied by cyclic voltammetry. All compounds show a similar ring oxidation and reduction behavior [65].

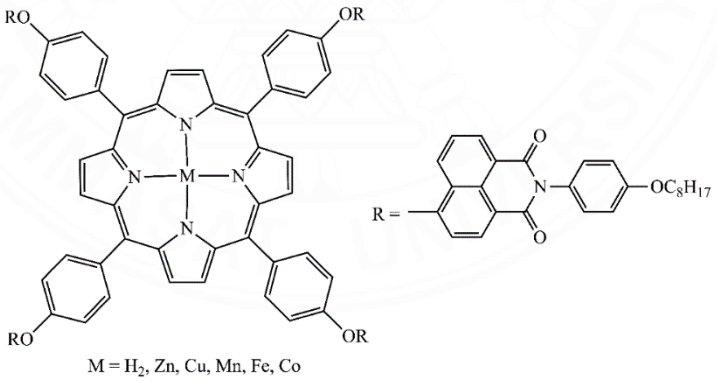

Figure 23 Structure of $TNPPH_2$ and their metal complexes

In 2015, Zhijic X. et al. studied the energy transfer and photophysical properties of the porphyrin-napthalimide ($TANPH_2$) and its zinc and copper complexes (TANPZn and TANPCu). The free-base porphyrin has been synthesized by combination of Sonogashira coupling and Gonsalves and Pereira nitrobenzene reaction, and the corresponding metal (Zn^{2+} and Cu^{2+}) complexes TANPZn and TANPCu were

synthesized. The ^{1}H and ^{13}C NMR spectroscopy, FT-IR, MALDI-TOF-MS and elemental analysis have been used to characterized the structure of all synthesized compounds. The photophysical properties were investigated by UV-vis and fluorescence spectroscopy. The result show that the excitation energy transfer occurred from the napthalimide units to the porphyrin core. The introduction of ethynyl bridges, TANPH2 and TANPZn can emit intense red light with high fluorescence quantum yield [23].

In 2015, Rajneesh M. et al. synthesis the 5,10,15,20-tetrakis(4-ferrocenylethynylphenyl)porphyrin (P1) and 5,10,15,20-tetrakis(3-ferrocenylethynyl-phenyl) porphyrin (P2) and zinc complex (ZnP2). Both porphyrin were synthesized by Lindsey method. After being purified by silica gel column chromatography and crystallization the free-base porphyrin was obtained in 19% and 21% yield respectively. Then the ZnP2 complexes have been prepared. The photophysical properties and thermal stability have been studied. The result shows substantial donor-acceptor interaction. The electrochemical studies reflect the donor nature of the ferrocenyl group and the acceptor character of the porphyrin core. The P1 porphyrin shows a lower HOMO-LUMO gap than P2 because the *para*-linked of the ferrocenyl unit in porphyrin P1 provides better π-conjugation compared to *meta*-linkage in porphyrin P2 confirmed by the computational study. The *meta*-linked of the ferrocenyl group in porphyrin P2 and ZnP2 results in increased thermal stability and better solubility [66].

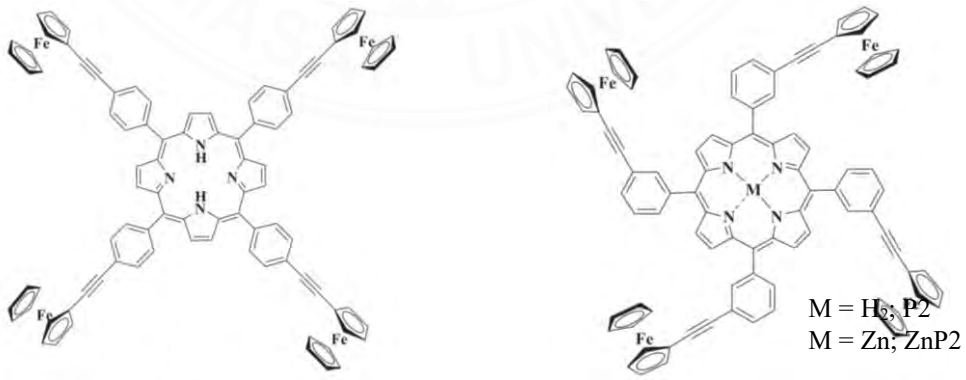

a b

Figure 24 The structure of porphyrin (a) P1 and (b) P2 and ZnP2

In 2004, Raymond L. et al. developed the method for electrophilic nitration reaction of the phenyl group of 5,10,15,20-*meso*-tetraphenylporphyrin (TPP). The nitro-substituted porphyrin was prepared by reaction between TPP and sodium nitrite ($NaNO_2$) in TFA. The equivalent amount of $NaNO_2$ and reaction time have been used to control the degree of nitration. High yields of nitrated benzene and substituted have been reported under these conditions. The corresponding aminoporphyrin derivative has been prepared by reduction of nitro-porphyrin with tin(II) chloride. ^{1}H NMR, UV-Vis spectroscopy, elemental analyst, and mass spectrometry were used for confirmed the structure of all porphyrin products. Furthermore, the structure of mono-aminoporphyrin and di-aminoporphyrin were confirmed by X-ray crystallography [67].

In 2013, Yu-hong W. et al prepared the series of novel *meso*-tetra (Schiff-base substituted phenyl) porphyrins and their corresponding zinc complexes. The Schiff-base porphyrin were synthesized from condensation of *meso*-tetra (*p*-aminophenyl) porphyrin (H_2TAPP) with different substituted benzaldehydes. The ZnTAPP has been successfully synthesized. The zinc complexes of corresponding *meso*-tetra (Schiff base substituted phenyl) porphyrin ligand were also prepared with the similar condition of free ligands. ^{1}H NMR, IR, UV-visible, fluorescence, and EPR spectroscopy and elemental analysis were used to characterize all synthesized compounds. The second substituents in Schiff-base groups provide weakly electronic effects on the π-electron system. These weak electronic effects are also observed in the electronic spectra of their zinc complex [68].

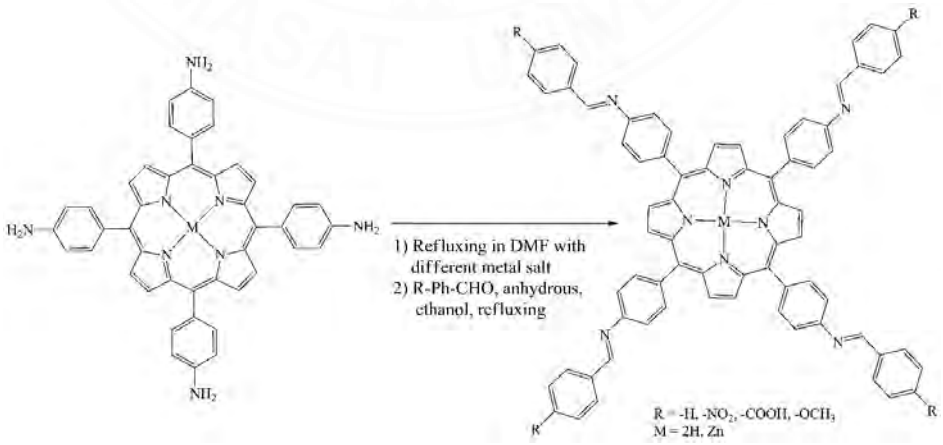

Figure 25 Preparations of tetra-(Schiff-base substituted phenyl) porphyrins and their zinc complexes

In 2007, Fedulova I.N. et al synthesized the symmetrical *meso*-arylsubstituted porphyrin with long-chain hydrophobic substituents in phenyl ring. The lipoporphyrin were synthesized in two pathway. One is the use of dipyrrolemethane, and other one base on the monopyrrole condensation under Lindsey's condition. The structure of all synthesized compounds was characterized by ^{1}H NMR, IR, MS, and CHN elemental analysis. Furthermore, the lipoporphyrins can be used to design supramolecular lipid ensembles of nanometer size [69].

In 2008, Jianzhong L. et al. synthesized the novel *meso*-tetra[4-(3,4,5-trialkoxybenzoate) phenyl porphyrin and their metal (Zn and Ni) complexes. Three different alkyl long-chain group of 3,4,5-trialkoxybenzoyl chloride were synthesized. Then the (4-hydroxyphenyl)porphyrin has been prepared by Alder's method. The porphyrin derivative was prepared through the esterification of (4-hydroxyphenyl)porphyrin and 3,4,5-trialkoxybenzoyl chloride using triethylamine as catalyst (**Figure 26**). Moreover, the metal complexes (Zn and Ni) were obtained from free porphyrin with carbon 12 atom alkyl chain and zinc/nickel acetate. Their molecular structures were confirmed by ^{1}H NMR, FT-IR spectroscopy and elemental analysis. The DSC, X-ray diffraction and polarizing optical microscope have been used to investigate the mesomorphic behavior of the porphyrin derivatives. The mesomorphic properties of the compounds indicate the wanly potential usage in photoelectronic fields [70].

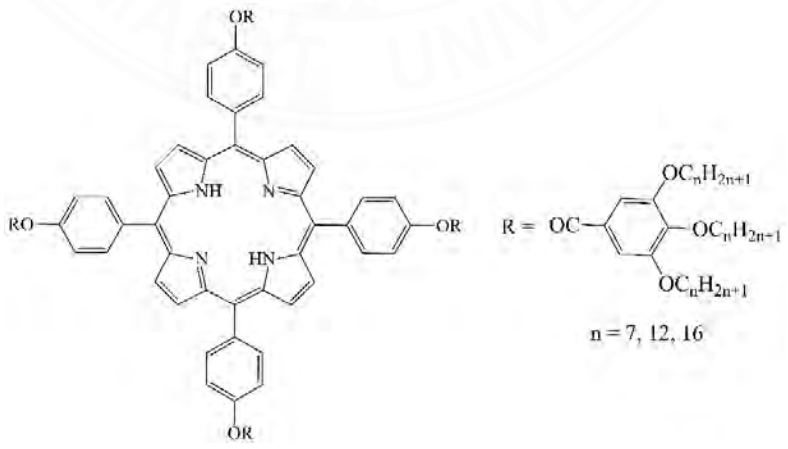

Figure 26 The structure of the porphyrin derivatives

2.3 Application of porphyrins and metalloporphyrin complexes

In 2015, Zengqi Z. et al. reported the catalytic activity of zinc and copper complexes of the novel porphyrin 5,10,15,20-tetra(4-(4-acetateethyl)phenoxy)-phenylporphyrin (H_2Pp). All compound were characterized by spectroscopic techniques. The structure of metalloporphyrin complexes has been investigated by single X-ray diffraction (**Figure 27**). The zinc complex crystallizes in monoclinic system with $P2_1/c$ while, the copper complex is P-1 spec group with triclinic crystal system. Both complexes have five-coordinated pyramid geometry with 4 nitrogen atoms of porphyrin ring and oxygen atom from DMF. The zinc and copper complexes display 3D supramolecular structure constructed by $\pi\cdots\pi$ interaction of porphyrin ring and C-H···O hydrogen bond. Then, both of these complexes exhibit highly selectivity to acetophenone(>99%) with the conversion of 23% and 76%, respectively to act as catalyst in the ethylbenzene oxidation process [71].

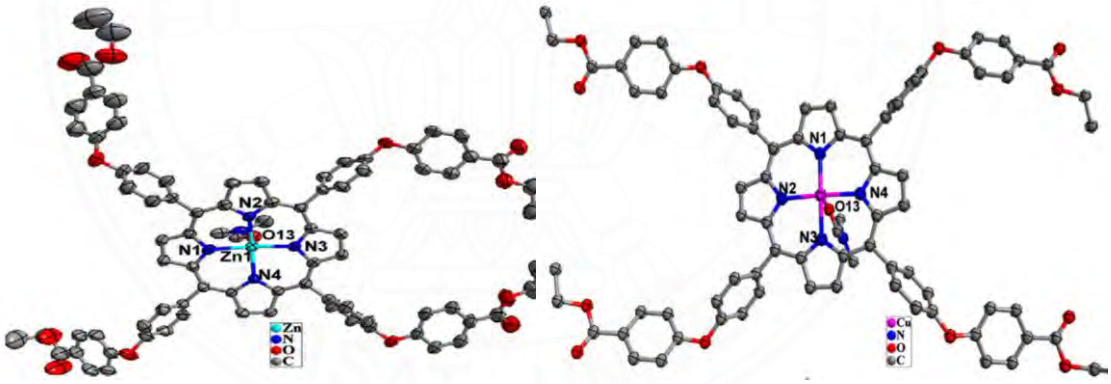

a B

Figure 27 The coordination environment and structure conformation of (a) Zn(II) porphyrin and (b) Cu(II) porphyrin complexes

In 2015, Guan H. et al. reported the catalytic activity properties of tetrakis(pentafluo-rophenyl)porphyrin iron chloride (Fe(TPFPP)) supported onto zinc oxide. This catalyst has been prepared by stirring the Fe(TPFPP) with zinc sulfate heptahydrate at pH = 8. The catalyst Fe(TPFPP)/ZnO was characterized by UV-Vis and FT-IR spectroscopy, XRD, TGA, TEM, FE-SEM, and SSA techniques. The oxidation

reaction of cyclohexane has been used to investigate the catalytic activity of Fe(TPFPP) and Fe(TPFPP)/ZnO. The result show ZnO increased the catalytic activity of Fe(TPFPP) for cyclohexane oxidation. The catalyst Fe(TPFPP) 0.1 μmol in supported ZnO can be reused 10 times at optimized condition 150°C and 0.7 MPa [72].

In 2011, Hongshan H. et al reported the photovoltaic performance of 2-(1-acetyl-2-oxopropyl)-5,10,15,20-tetraphenylporphyrin (H_2TPP-AOP) and its transition metal complexes (MTPP-AOP, M = Cu^{2+} and Zn^{2+}). The 1-acetyl-2-oxopropyl group (AOP) is attached to β-pyrrolic position via substitution reaction of CuTPP-NO_2 with acetylacetone in DMSO. After demetaled with conc. H_2SO_4 the H_2TPP-AOP was obtained and the ZnTPP-AOP has been prepared. The single-crystal X-ray diffraction has been used to analyst the structure of synthesized compounds. The result shows that the (AOP) group is attached to a β-pyrrolic position through the methylene group. The DFT calculation and photophysical properties indicate that these porphyrins are suitable for the normal operation of DSCs. However, the energy conversion efficiencies of three porphyrin sensitized solar cells are lower than reference dye ZnTPP-COOH and N719 due to the AOP prevent their binding to TiO_2 nanotubes [22].

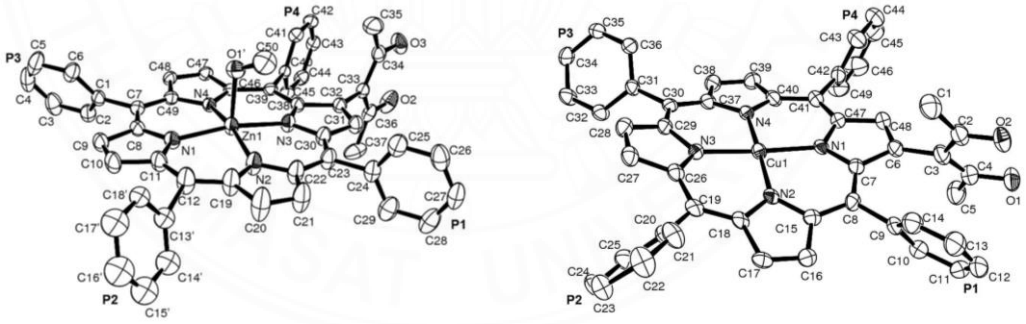

a b

Figure 28 ORTEP diagram of (a) ZnTPP-AOP ·0.36CH_3OH·0.64H_2O and (b) CuTPP-AOP·CH_2Cl_2 with thermal ellipsoids drawn at the 50% probability level

In 2013, Qinglong T. et al. prepared two donor-π-spacer-acceptor porphyrin for use in dye-sensitizer solar cells. The 5-[p-(4-Carboxyl benzyl idene amino)] phenyl-10,15,20-tris (3,4,5-trimethoxy-lphenyl)porphyrin zine (PZn-BIA-COOH) and 5-(4-

Carboxyl) phenyl-10,15,20-tris (3,4,5-trimethoxylphenyl)porphyrin (PZn-COOH) have been synthesized and characterized by ^{1}H NMR, IR, MOLDI-TOF-MS, and elemental analysis. TiO_2 photoelectrode was prepared by screen-printing methods. Then the photoelectrode was dipped into the dye solution after annealing the dye was adsorbed onto the TiO_2 films. Each of the dyes displayed different adsorption behavior and coverage on the TiO_2 surface. The two complexes exhibit maximum power of conversion efficiency for 1.75% and 1.06%, respectively [24].

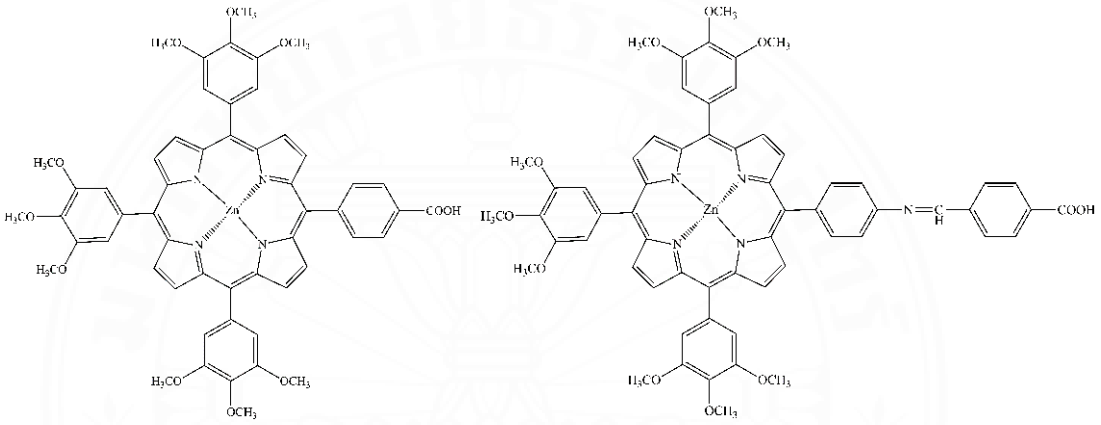

PZn-COOH PZn-BIA-COOH

Figure 29 Molecular structures of PZn-COOH and PZn-BIA-COOH

In 2015, Fasalu R.K. et al. reported the antimicrobial properties of 5,10,15,20-tetrakis(4′-trifluoromethylphenyl)porphyrin and its metal complexes (Fe(II), Ni(II), Cu(II), Zn(II), and Pt(II)) **Figure 30**. The porphyrin ligand was synthesized follow by Lindsey conditions. The metalloporphyrin has been prepared. All synthesized compounds were characterized by UV-vis, fluorescence and ^{1}H-NMR spectroscopy, and mass spectrometry. The free-base porphyrin and the nickel, copper, and zinc complexes were successfully characterized by single-crystal X-ray diffraction analysis. The crystal was grown at room temperature by the vapor diffusion method, and THF was used as a solvent. The free ligand and copper complex crystallized in the triclinic system whereas, nickel and zinc complexes are the monoclinic systems. Furthermore, the antimicrobial activity of all synthesized compounds was studied using a well diffusion method at different concentrations (50, 75, and 100 μg/ml) on *S.*

aureus, *B. subtillis*, *E. coli*, *P. aeruginosa*, and *C.albicans*. The result shows that the free ligand was showed highly effective compared to its metal complex [73].

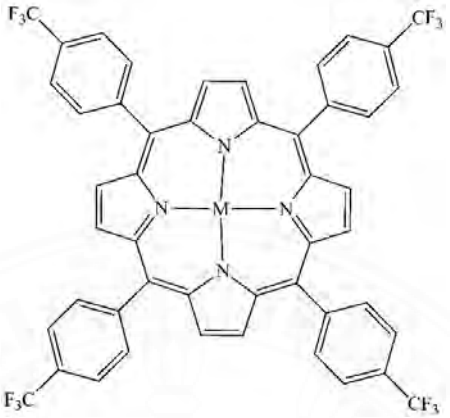

M = 2H, Fe(II), Ni(II), Cu(II), Zn(II), Pt(II)

Figure 30 Structure of fluorinated porphyrin and its metal complexes

In 2008, Xu X. et al. reported the antibacterial effect of Mn(II) ion, tetraphenylporphyrin (TPP), ebselen-porphyrin, and its manganese complexes (**Figure 31**). The stop-flow microcalorimetry has been used to study the antibacterial properties of all compounds on *S. sureus*. The result shows that the manganese(II) ebselen-porphyrin complex exhibited the highest antibacterial activity on *S. aureus* than other compounds with IC_{50} values 100 μg/ml. The sequence of the antibacterial activities of these compounds tested was 2 > 1 > Mn(II) > TPP, respectively [74].

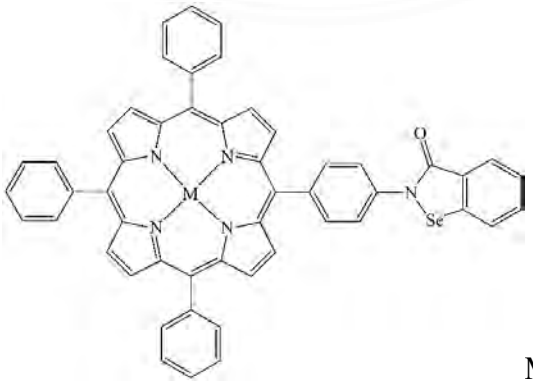

M = H_2 and Mn

Figure 31 Structures of ebselen–porphyrin conjugates and its manganese complexes

In 2016, Feifei S. et al. reported the gas sensing activity of the highly ordered nanotubes of 5, 10, 15, 20-tetrakis(4-aminophenyl)porphyrin zinc (ZnTAP). The ZnTAP nanotube was fabricated by using nanoporous anodized aluminum oxide (AAO) membrane as the template. This porphyrin nanotube was characterized by. Electronic absorption spectra, fluorescence spectra, transmission electron microscope (TEM), scanning electronic microscopy (SEM), low-angle X-ray diffraction (XRD). The ZnTAP nanotube shows good conductivity and presents an efficient gas sensor platform for the ultrasensitive detection of NO_2 at room temperature. This sensor exhibited high sensitivity, fast response and recovery behavior, and good reproducibility to NO_2 gas. Moreover, the ZnTAP nanotube [30].

In 2012, Sumana K. et al. proposed the method for alcohol detection by using magnesium 5,10,15,20-tetraphenyl porphyrin (MgTPP) thin film as an optical sensor. The MgTPP thin film has been prepared by spin-coating the MgTPP solution in chloroform (5 mg/ml) onto a clean glass substrate at 500, 1000, and 1500 rpm at room temperature. This film was subjected to thermal annulling at 280°C under an argon atmosphere. This film was characterized by UV-visible spectroscopy and atomic force microscopy (AFM). Methanol, ethanol, and propanol have been used to investigate the sensing properties of MgTPP thin film. The gas sensing response of MgTPP thin film was analyzed from the change in its optical property by using an electronic nose (e-nose). The result indicates that the MgTPP thin film presents a significant response with methanol compared with ethanol and isopropanol, based on the dynamic flow of alcohol vapors at the same mol% of alcohol concentration. Furthermore, Density functional theory (DFT) calculations were performed to model the underlying mechanism of this selectivity [27].

In 2016, Lizhi Z. et al. prepare the optical sensor membrane for sorption and detection of cadmium in an aqueous solution. These optical sensor have been fabricated by immobilized 5,10,15,20-tetrakis(4-N-methylpyridyl) porphyrin *p*-toluenesulfonate (TMPyP) onto the poly(sodium 4-styrenesulfonate) grafted on chloromethylated polysulfone (PSF-PNaSS). FESEM has been used to characterize the PNaSS-grafted membrane. The prepared membrane exhibit a fast response to Cd(II) including apparent spectral and color change. The optical sensor membrane exhibited

good stability and reusability which made it efficient for various sorption removal and detection application [75].

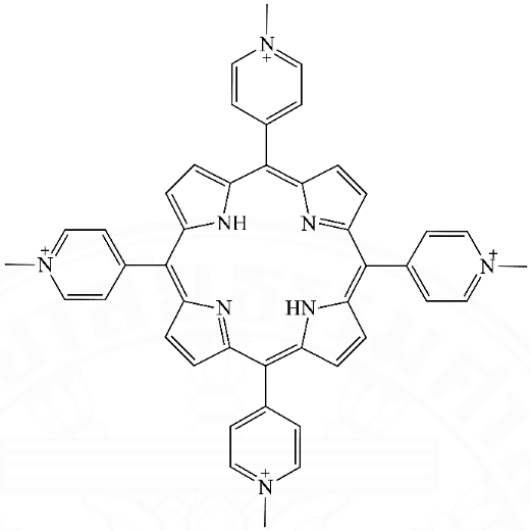

Figure 32 5,10,15,20-tetrakis(4-N-methylpyridyl) porphyrin p-toluenesulfonate (TMPyP)

2.4 Application of Gold porphyrin complex

In 1969, Ererly B.F. et al. reported the synthesis of the gold porphyrin. The 5,10,15,20- tetraphenylporphyrinatogold(III) complexes have been synthesized by refluxing tetraphenylporphyrin (TPP) in glacial acetic acid with an excess $KAuCl_4$. This compound was identified as $[Au(III)TPP][AuCl_4]\cdot 5H_2O$ by CHN elemental analysis, Infrared spectroscopy, and single-crystal X-ray diffraction. Moreover, the gold porphyrin complex was studied by UV-visible spectroscopy compared with AgTPP and CuTPP in several solvents. The result showed the λ_{max} blue shift of AuTPP due to the trivalent ion of the gold complex compared to the silver and copper divalent ion and also a result of the greater stability of the gold tetraphenylporphyrin [76].

In 2004 Elvis N. *et al.* report the effect of aqueous gold(III) and palladium(II) and their metalloporphyrin complexes on *Trypanosoma brucei brucei* growth *In vitro*. Tetrakis(1-methylpyridinium-4-yl)porphyrin ($H_2(TMPyP)^{4+}$) and their gold(III) and palladium(II) were synthesized. The trypanocidal effects of all

compounds on *T. b. brucei* growth in culture have been studied using an Alamar Blue indicator assay. All test compounds exhibited more toxicity on *T. b. brucei* growth. The palladium(II) porphyrin showed toxicity on the parasite's growth than the aqueous palladium(II) ion. In contrast the aqueous gold(III) ion was more toxic to these parasites than gold(III) porphyrin complexes due to the free radical generation in the presence of gold(III) ion which increased the toxicity of gold(III) to the parasite compared its gold(III) porphyrin complex [77].

In 2003 Chi-Ming C. et al. studied the cytotoxicity of gold(III) porphyrin complexes (**Figure 33**) on various human cervix epitheloid cancer cells by using MTT assay. All gold(III) porphyrin complexes show significant cytotoxicity against human cancer cells including drug-resistant variants and cisplatin-resistant with IC_{50} 0.1 – 1.5 μM. Especially, compound A exhibits the most prominent activity with IC_{50} 0.1 – 0.8 μM. Moreover, the cytotoxicity of compound A on normal cells has been studied. This result confirmed that compound A show more toxic to cancer cells than to normal cells [78].

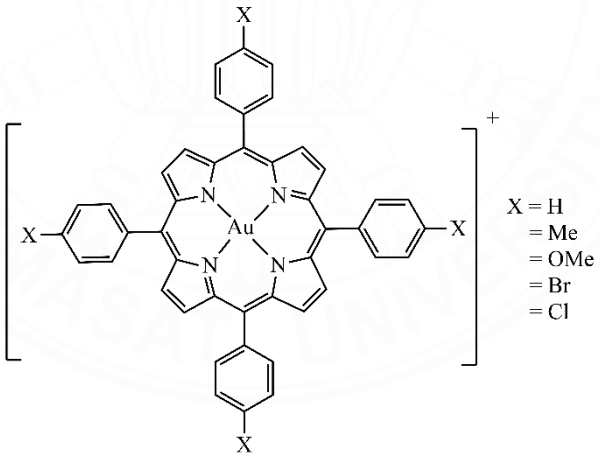

Figure 33 Structure of gold(III) porphyrin complexes

In 2012 Liang S. et al. studied the cytotoxicity activity of new water-soluble gold(III) porphyrin complexes on Sarcoma 180 mouse tumor cell line (S180) and human gastric carcinoma cell line (SGC-7901). The water-soluble gold(III) porphyrin complexes have been synthesized with a different *meso*-substituent group (**Figure 34**).

The cytotoxicity of all compound have been investigated by using MTT assay and compared with gold(III) tetraphenylporphyrin ([AuTPP]Cl) and cisplatin. All compounds were dissolved in DMSO first and then serially diluted in a complete culture medium such that the effective DMSO content did not exceed 1%. Complexes B, D, and E show more antitumor activity active than cisplatin and were close to lead compound gold(III) tetraphenylporphyrin [79].

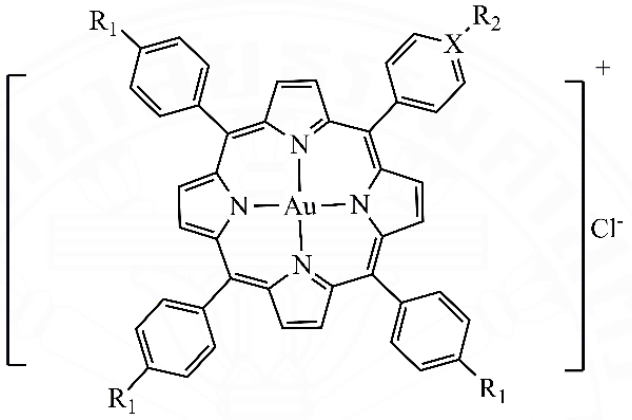

$R_1 = H, \quad R_2 = CH_3, \quad X = N^+I^-$
$R_1 = CO_2^-Na^+, \quad R_2 = CO_2^-Na^+, \quad X = C$
$R_1 = H, \quad R_2 = CO_2^-Na^+, \quad X = C$
$R_1 = SO_3^-Na^-, \quad R_2 = SO_3^-Na^-, \quad X = C$
$R_1 = H, \quad R_2 = NH_3^+Cl^-, \quad X = C$

Figure 34 Structure of water-soluble gold(III) porphyrin complexes

In 2015 Aaron D.L. et al. report the *In vitro* anticancer activity of water-soluble gold(III) porphyrin complexes on the human ovarian cancer cell line(A2780). The octahydroxy gold(III) porphyrin, octamethoxy gold(III) porphyrin, and octahydroxy porphyrin have been synthesized and characterized. The MTT assay has been used to investigate the cytotoxicity of the porphyrin compounds. The octahydroxy gold(III) porphyrin show the highest anticancer activity than other compound with IC_{50} value 9 μM [80].

In 2011 Huasheng C. et al. reported the cytotoxicity of gold(III) porphyrin complexes on mouse tumor cell line (S180). The free-base porphyrin was synthesized by Alder-Longo and Lindsey method. The gold(III) porphyrin complexes (**Figure 35**)

were synthesized by reaction for $KAuCl_4$ with porphyrin ligands in the presence of NaOAc in acetic acid. The cytotoxicity was studied by using MTT assay compared with [AuTPP]Cl and cisplatin. All gold(III) porphyrin complexes exhibited cytotoxicity on S180 cells. This result indicates that the gold atom at center of porphyrin ring has major impact on the effect of the whole compounds. Compound D display more prominent activity than [AuTPP]Cl and cisplatin with IC_{50} value 2.820 μM [81].

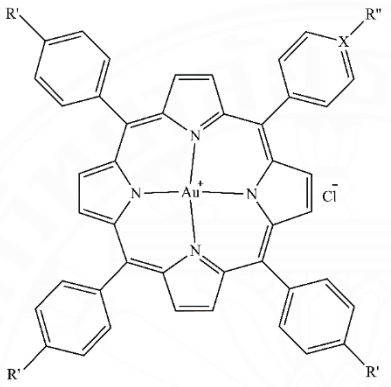

R′	R″
H	H
H	OCH_3
CO_2CH_3	CO_2CH_3
H	CO_2CH_3
H	NO_2
H	-

Figure 35 Structure of gold(III) substituted porphyrin

In 2009 Kim H.C. et al. prepared the novel gold(III) porphyrin complexes (5-hydroxyphenyl-10,15,20-triphenylporphyrinato gold(III) chloride). This compound was synthesized by the standard Schlenk technique and characterized by ^1H NMR, UV-visible spectroscopy, and mass spectrometry. The cytotoxicity of these complexes was studied both *In vitro* and *In vivo*. *In vitro* cytotoxicity was investigated by crystal violet assay with five types of human breast cancer cells including BT474, T47D, MCF7, MDA-MB-231, and SKBR3. These complexes showed higher cytotoxicity than cisplatin with an IC_{50} value in the nanomolar range. *In vivo* studies, the MDA-MB-231 cell was implanted in nude mice and treated with different dosages of gold(III) porphyrin for 4 weeks. The result demonstrated that gold(III) porphyrin complexes exhibited higher antitumor activity than cisplatin due to the tumor volume and tumor weight of mice treated with gold(III) porphyrin were decreased than mice treated with cisplatin group [82].

In 2014 Philipp A. et al. synthesis the novel photoactive porphyrin compounds. The free-base porphyrin and its copper and zinc complexes (**Figure 36**)

have been synthesized and characterized. The singlet oxygen quantum yield of all compound have been investigated upon light irradiation. The free-base porphyrin and zinc(II) complexes exhibited high singlet oxygen quantum yield whereas, the copper(II) complex shows no signal. Moreover, the cytotoxicity of all compounds was investigated by using MTT assay on human mammary carcinoma MCF7 cell and human ovarian cancer A2780 cell in dark and under red light irradiation. The cytotoxicity of all compounds in the dark was rather low. However, when exposed to the light it showed significant cytotoxicity. When compared with free-base porphyrin the metalloporphyrin showed great toxicity than free-base in both conditions. This result shows that the metal in central porphyrin increased the cytotoxicity of porphyrin compounds. Zinc(II) porphyrin and free-base exhibited phototoxicity due to the singlet oxygen evaluation. In the case of copper, complexes were observed the phototoxicity due to the production of hydroxyl radical confirmed by EPS spectroscopy. All compounds exhibited cytotoxicity higher than cisplatin under red light irradiation. Especially, zinc(II) porphyrin complex showed the IC_{50} value down to 0.4 μM [83].

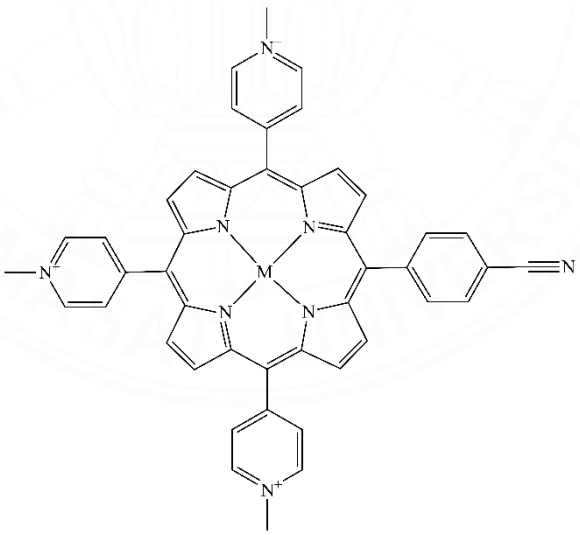

Figure 36 Water-soluble cationic porphyrins

In 2007 Dong H.L. et al. report the synthesis of the porphyrin compounds and their zinc, manganese, and nickel complexes (**Figure 37**). All synthesized compounds were characterized by UV, IR, MS, ^{1}H NMR spectra, and elementary

analysis. The anticancer activity of the metalloporphyrin complexes on liver cancer cells (SMCC-7721) *In vitro* was investigated using an MTT assay compared with ftorafur. The metalloporphyrin complexes exhibited an anticancer activity larger than ftorafur [84].

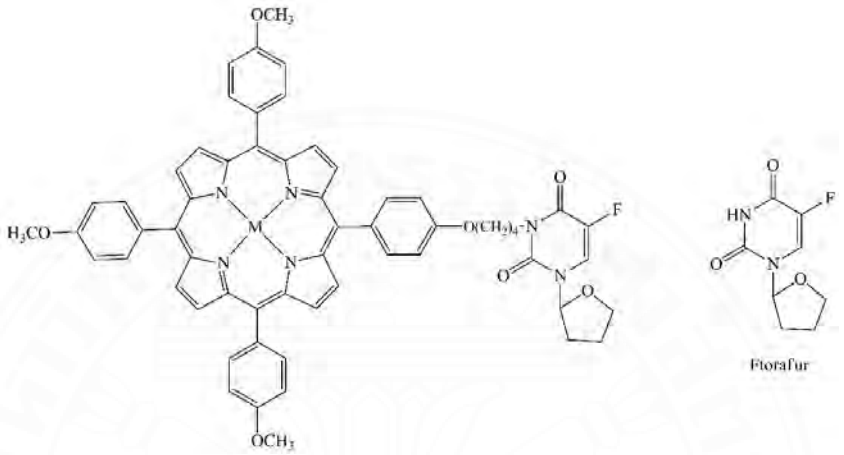

Figure 37 Structure of metalloporphyrin complexes and ftorafur

In 2018 Liu J-C. et al. report the synthesis of the novel heterometallic metal-porphyrinic framework (MPFs). This complex is built from Y and K ions as node and *meso*-tetra(4-carboxyphenyl)porphyrin (TCPP) as a linker. The single-crystal X-ray diffraction studied shown that the complex crystallized in the monoclinic and P2/m space group. *In vitro* cytotoxicity of this complex was evaluated with human breast cancer cells (BT474, SKBr-3, and ZR-75-30) using an MTT assay. These complexes exhibited good anticancer activities with IC_{50} 20 - 30 μM. It was similar to cisplatin and more than TCPP pure ligand. Moreover, the cytotoxicity on normal cell MDCK was investigated. This complex shows no cytotoxicity on MDCK cell with IC_{50} > 100 μM [85].

In 2018, Kaikai D. et al. prepared the nanoparticle of porphyrin and zinc(II) porphyrin complexes of anticancer activity studies. The three porphyrin derivatives, 5,10,15,20-tetrakis(3,4-methoxyphenyl) porphyrin (P1) and it zinc(II) complex (P2) and 5,15-bis(3,4-methoxyphenyl)-10,20-bis(4-methoxyphenylethynyl) zinc porphyrin (ZnP2) have been synthesized and characterized. All compounds were successfully

prepared as nanoparticles through the nanoprecipitation method. The porphyrin nanoparticle shows good water dispensability and passes tumor-targeting properties. The singlet oxygen quantum yield of all compounds was studied, the complex ZnP2 exhibited the highest singlet oxygen quantum yield (79%). The porphyrin nanoparticle demonstrates both photodynamic and photothermal effects. *In vitro* cytotoxicity of porphyrin nanoparticles was investigated using MTT assay on Hela cells. The porphyrin ZnP2 nanoparticles show the best photodynamic therapy efficiency and good biocompatibility in the dark. *In vivo* studies showed that porphyrin ZnP2 nanoparticles present high phototoxicity, low dark toxicity, and good biocompatibility [86].

In 2017 Fatima D. et al. developed the water-soluble gold(III) porphyrin complexes for anticancer application. The gold(III) porphyrin-adamantane chloride and gold(III) porphyrin mono-acetate chloride. The antiproliferative effect of gold(III) porphyrin complexes were studied *In vitro* using MTT assay on human colorectal cell line including HT-29 and HCT-116. All compounds exhibited cytotoxicity on HT-29 and HCT-116 cell lines caused cell cycle arrest in the G_2/M phase. The gold(III) porphyrin mono-acetate chloride exhibited significant antiproliferative effect on HT-29 and HCT-116 with IC_{50} at 24 hours = 3.5 µg/ml, and 3 µg/ml and at 48 = 2 µg/ml, and 1.9 µg/ml, respectively. The gold(III) porphyrin complexes induce apoptosis by intrinsic pathway [87].

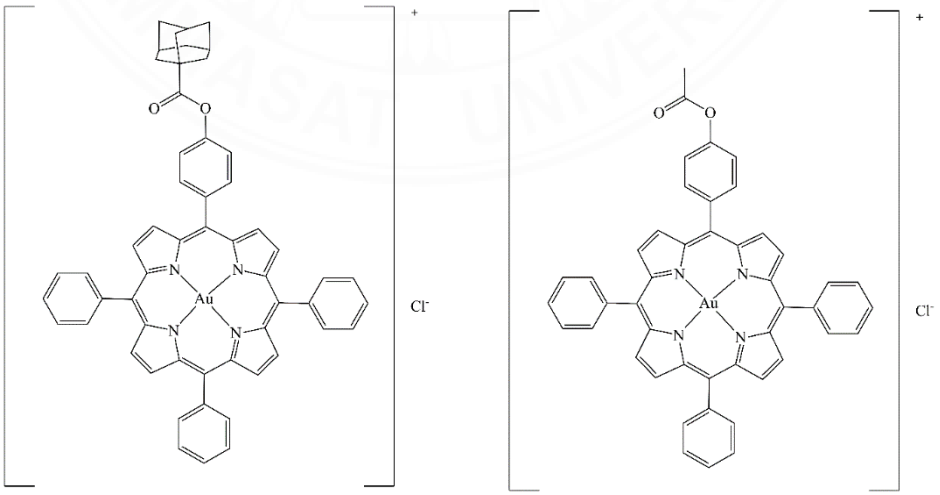

Figure 38 Structure of (a) gold(III) porphyrin-adamantane chloride and (b) gold(III) porphyrin mono-acetate chloride

In 2009 Shuiping T. et al. studied the cytotoxicity of gold(III) tetraphenylporphyrin chloride ([AuTPP]Cl) on colon cancer cells both *In vitro* and *In vivo*. *In vitro* studies, the human colon cancer cell line including SW1116, Colo 205, CRL-238, CCL-2134, and HCT-15 have been used for antiproliferation efficiency studied. The [AuTPP]Cl exhibited significant cytotoxicity on colon cancer cells with IC_{50} values in the range from 0.20 to 3.4 μM. It shows higher anticancer activity than cisplatin. This gold(III) porphyrin induces apoptosis in the colon cancer cell and causes cell cycle arrest in G_0/G_1 phase. *In vivo* studies, the mice bearing tumor cells (colo 205) have been used to study the antitumor efficiency of [AuTPP]Cl. The [AuTPP]Cl significantly inhibited the growth of tumor cells compared with the control group. The antitumor efficiency of [AuTPP]Cl was similar or better than cisplatin. The [AuTPP]Cl showed damage in major organs of mice. The [AuTPP]Cl exhibited low toxicity *In vivo* at the effective concentration [51].

In 2016 Ya-Hong Y. et al. synthesis three novel free-base porphyrin including two Schiff-base porphyrin, 5,10,15-triphenyl-20-[4-(2-(4-formyl)phenoxy)-ethoxy]phenyl porphyrin (H2Pp(1)), 5,10,15-triphenyl-20-[4-(2-(4-hydroxyimino)-phenoxy)ethoxy]phenyl porphyrin (H2Pp(2)) and 5,10,15-triphenyl-20-[4-(2-(4-m-hydroxyanilinodeneformyl)phenoxy)ethoxy]-phenyl porphyrin (H2Pp(3)). Moreover, the metalloporphyrin complexes of porphyrin H2Pp(1) with copper, zinc, and cobalt were synthesized. All compounds were successfully characterized by ^{1}H NMR, UV-Visible, FT-IR spectroscopy, and mass spectrometry. The human epidermal squamous cell carcinoma cell (A-431) and the normal human horn cell (HaCat) were used for evaluating the cytotoxicity of all synthesized compounds *In vitro* using MTT assay. After incubation for 24 hours, all compounds exhibited cytotoxicity on the A-431 cell line with an IC_{50} value in the range 6.6 – 9.8 μM. The three metalloporphyrin show more cytotoxicity than free-base porphyrin. In free metal porphyrin, the introduction of Schiff-base enhances cytotoxicity activity against A-431 cells. In contrast, no toxicity was observed in HaCaT cells with cell viability of over 80% [88].

In 2008 Xiaolan F. et al. report the anticancer activity of the novel porphyrin-based photosensitizer. The 2- (1-hexyloxyethyl) -6, 7- bis [2- (sodium carbonate) ethyl]-1, 3, 5, 8- tetramethyl - 4-vinylporphyrin (P-1) and it isomer 4-(1-hexyloxyethyl)-6, 7-bis[2- (sodium carbonate) ethyl]- 1, 3, 5,8- tetramethyl-2-

vinylporphyrin (P-2) were synthesized and characterized. The photophysical properties indicated that the porphyrin compounds could be utilized as a potential sensitizer for photodynamic therapy due to the strong absorption band at 630 nm. The generation of singlet oxygen of all synthesized porphyrins was investigated using singlet oxygen sensor green (SOSG). The porphyrin P-2 exhibited higher singlet oxygen generation than porphyrin P-1. *In vitro* studies, the three breast cancer cells including marine breast cancer cell 4T1 and human breast cancer cell MCF7 and MDA-MB-231 were used to investigate the phototoxicity of the porphyrin compounds using MTT assay compared with the hematoporphyrin monomethyl ether (HMME). The result shows that porphyrin P-1 and P-2 exhibited highly phototoxicity than HMME and show low dark toxicity. A similar result was observed in *In vivo* study. The porphyrin P-1 and P-2 were found to localize in multiple subcellular organelles, which could induce multiple stress pathways to post PDT treatment, leading to more effective cell destruction [89].

In 2006, Ching T.L. et al. report the cytotoxicity effect of gold(III) tetraphenylporphyrin chloride ([AuTPP]Cl) on hepatocellular carcinoma *In vitro* and *In vivo*. The rat hepatoma cell McA-RH-7777 cells have been used to investigate the cytotoxicity of [AuTPP]Cl. *In vitro* studies using MTT assay the gold(III) porphyrin exhibited higher cytotoxicity on McA-RH-7777 than cisplatin with IC_{50} value 1.6 ± 0.09 μM. *In vivo* studies, the mice with hepatocellular carcinoma (HCC) were treated with different doses of [AuTPP]Cl. The [AuTPP]Cl shows the prolonged the several of HCC-bearing mice. The [AuTPP]Cl induced necrosis as well as apoptosis in the tumor cell, but show no effect in the normal liver tissues [90].

In 2009 Yuk F.T. et al. report the cytotoxicity of [AuTPP]Cl on nasopharyngeal carcinoma (NPC) *In vitro* and *In vivo* compared with cisplatin standard drug. Gold porphyrin complex was synthesized and characterized by NMR spectroscopy, CHN elemental analysis, mass spectrometry, and UV-visible spectroscopy. They have obtained the gold complexes as 70% yield. The human NPC cell SUNE1, C666-1, and cisplatin resistant-variant CNE2 have been used and studied the cytotoxicity of [AuTPP]Cl and cisplatin by using MTT assay. The result shows that the [Au(TPP)]Cl exhibited 100-fold higher potency than cisplatin in killing nasopharyngel carcinoma (NPC) cell. Moreover, the cytotoxicity effect of [AuTPP]Cl and cisplatin were studied on normal/noncancerous cell CCD19Lu and PBMC cells.

The IC_{50} on a normal cell of [AuTPP]Cl is higher than the IC_{50} value on the cancer cells. The effect of [AuTPP]Cl on tumor growth *In vivo* was studied. The safety concentration of the [Au(TPP)]Cl was demonstrated, 3 mg/kg per week is the safe dose of [Au(TPP)]Cl [48].

In 2009, Raymon W. and Chi-Ming C. reported the anticancer properties of gold complexes with dianionic porphyrin and tetradentate ligand. The structure of all compounds is shown in **Figure 39**. The gold porphyrin complexes were prepared by the treatment of $K[AuCl_4]$ or $nBu_4N[AuCl_4]$ with free-base porphyrin ligand in the presence of NaOAc in acetic acid. While the gold complexes with tetradentate Schiff base ligand including salicylideneimines and dimethylglyoxine were obtained by the reaction of free Schiff base ligand with $K[AuCl_4]$ in a CH_2Cl_2/MeOH mixture. Both kinds of gold complexes were obtained around 60 %yield. All compounds have been characterized by spectroscopy technique and single-crystal X-ray diffraction. Moreover, electrochemistry and solubility were studied. In addition, the *In vitro* and *In vivo* anticancer properties have been studied by using NPC (SUNE1, CNE1, CNE2, and C666-1), HL-60, HepG2, HeLa, KB-3-1, and KB-V1 human cancer cell line. The result shows that all compound has the anticancer properties [50].

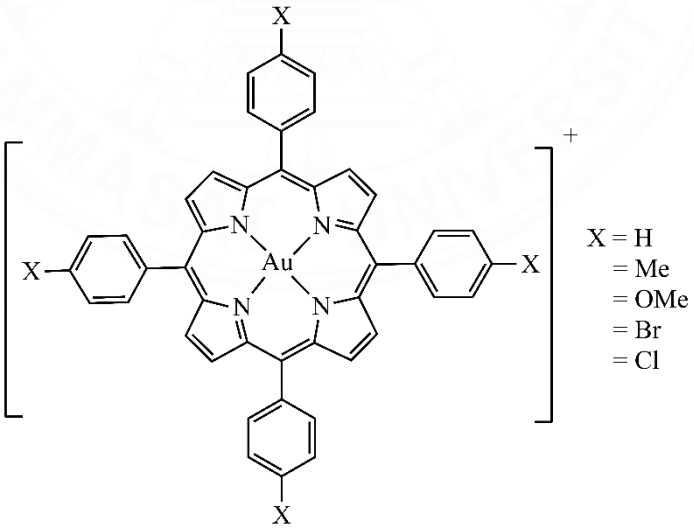

Figure 39 Schematic drawings of gold(III) porphyrin compounds

In 2014, Valentina R. et al. reported the anticancer activity of cationic porphyrins tetra-*meso* (N-methyl-2-pyridyl) porphine (TNPyP2), tetra-*meso* (N-methyl-4-pyridyl) porphine (TMPyP4), and tri-*meso* (N-methyl-4-pyridyl), *meso* (N-tetradecyl-4-pyridyl) porphine (TMPyP4-C14) (**Figure 4**0) *In vivo*. The singlet oxygen generation capacity of all cationic porphyrins was investigated by a 9, 10-dimethyl-lantracene (DMA) photobleaching assay. The PMPyP2 shows the lowest quantum yield singlet oxygen generation due to the steric between 2-methyl-pyridine and 3-pyrrole hydrogen. The cellular uptake and phototoxicity were studied by using melanoma B78-H1 cells. The cellular uptake result indicated that the addition of a lipophilic chain enhances the cellular uptake of the TMPyP4 compound. The photoactivity studied exhibited that without irradiation the porphyrin is not cytotoxic, while under irradiation TMPyP4 and TMPyP4-C14 exhibited more effectiveness than TMPyP2. Moreover, the *In vivo* anticancer activity of all compounds has been observed. The result shows that TMPyP4-C14 is a stronger anticancer drug than the TMPyP4 complex. The cationic porphyrin cause cell death by apoptosis and necrosis [91].

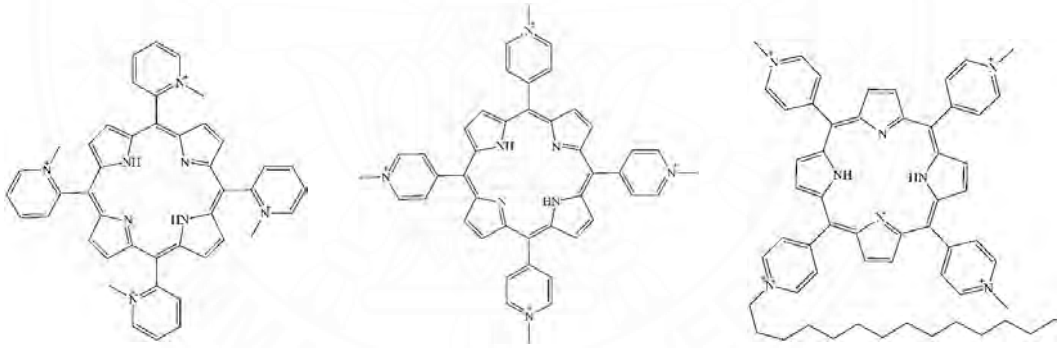

TMPyP2 TMPyP4 TMPyP4-C14

Figure 40 Structure of the cationic porhyrins TMPyP2, TMPyP4, and TMPyP4-C14

In 2013, Zhong O et al. synthesized the gold(III)porphyrin that containing two, three, or four β,β-fused quinolone (**Figure 41**). All synthesized compounds were characterized by CHN elemental analysis, ^{1}H, ^{31}P, and ^{19}F NMR spectroscopy, and mass spectrometry. Moreover, the synthetic complexes were examined for their electrochemical properties in several solvents including THF, pyridine, CH_2Cl_2, and CH_2Cl_2 containing added acid in the form of trifluoroacetic acid. In the absence of added acid, all gold

complexes exhibited reversible one-electron oxidation and several reductions. The first reduction was characterized as an Au^{III}/Au^{II} process [92].

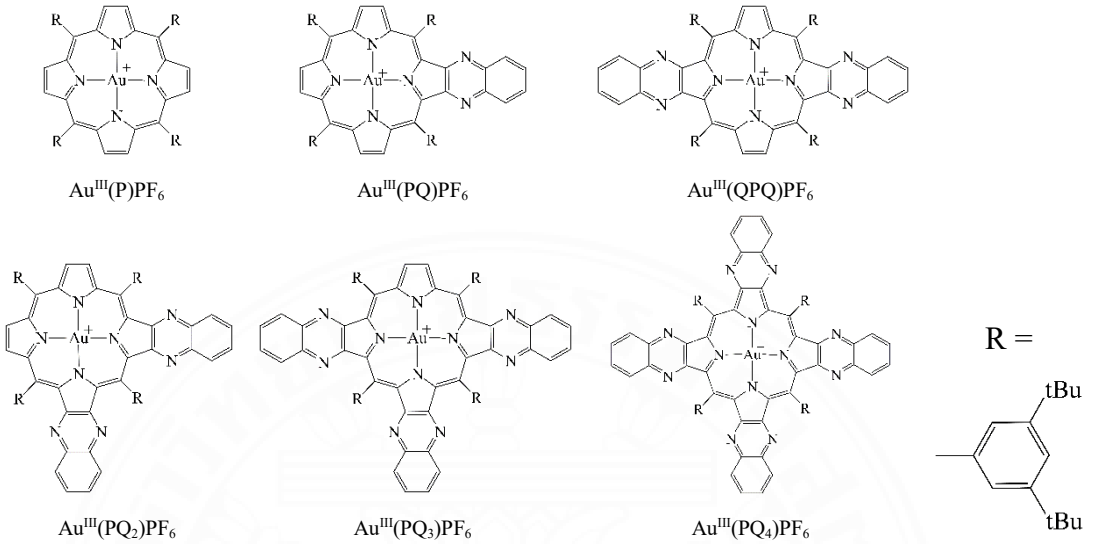

Figure 41 Structures of Gold(III) Quinoxalinoporphyrins

In 2004, Zhoungping O. et al. synthesis the gold(III)porphyrin of the type (P-R)$AuPF_6$ where P = 5,10,15,20-tetrakis(3,5-di-tret-butylphenyl)porphyrin and R is H, NO_2, or NH_2, which is substituted at one of the β-position (**Figure 42**). All compound were characterized by using infrared, UV-visible, ^1H NMR, ^{31}P NMR spectroscopy, mass spectrometry, and CHN elemental analysis. Moreover, electrochemistry has been studied by cyclic voltammetry. In the present study, their reversible reductions are observed under almost all solvent (THF, DMF, CH_2Cl_2, pyridine, PhCN, and toluene) [93].

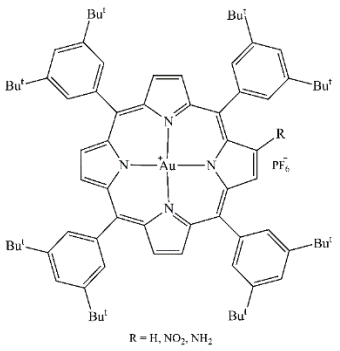

Figure 42 Structure of (P-R)$AuPF_6$ complexes

CHAPTER 3
RESEARCH METHODOLOGY

3.1 Materials

3.1.1 Apparatus

- Nuclear magnetic resonance spectra were recorded at 400 MHz for ^{1}H NMR and at 100 MHz for ^{13}C NMR using a Bruker (FT-NMR advance 400 MHz) spectrometer.
- The FT-IR (4000 - 400 cm^{-1}) spectra were recorded on Perkin Elmer infrared spectrophotometer (spectrum GX). Mass spectra were obtained on Thermo Finnigan mass spectrometer (LCQ Advantage).
- The elemental analysis was carried out on Perkin Elmer (2400) elemental analyzer.
- UV-Vis absorption and fluorescence spectroscopic measurements were carried out on a Shimadzu UV-spectrometer (UV-1700) and a Jasco spectrofluorometer (FP-6200), respectively.
- Thermal gravimetric analysis were recorded on Perkin Elmer (TGA7).
- Electrochemical studies were performed by cyclic voltammeter (Metrohm).
- Electron paramagnetic resonance spectroscopy were recorded on Electron Spin Resonance Spectrometer (JES-X310)
- Cancer cells and normal cells were culture in the CO_2 Incubator (Water Jacket Type CO_2 Incubator APC-50D)

3.1.2 Chemical and Reagents

- *1*-Bromobutane (C_4H_9Br, Assay 99%, Sigma-aldrich, USA)

- *1*-Bromodecane ($C_{10}H_{21}Br$, Assay 98%, Sigma-aldrich, USA)
- *1*-Bromooctane ($C_8H_{17}Br$, Assay 99%, Sigma-aldrich, USA)
- *4*-Hydroxybenzaldehyde ($C_7H_6O_2$, Assay 99%, Sigma-aldrich, USA)
- Acetic acid (CH_3COOH, Assay 100%, AnalaR, USA)
- Acetone (C_3H_6O, Assay 98%, RCI Labscan, Thailand)
- Chloroform ($CHCl_3$, Assay 98%, RCI Labscan, Thailand)
- Chloroform-*d* ($CDCl_3$-*d*, A.R. grade, Cambridge Isotope, USA)
- Copper acetate ($C_4H_6CuO_4$, synthesized by Prohmsatit T.)
- Dichloromethane (CH_2Cl_2, Assay 98%, RCI Labscan, Thailand)
- Dichloromethane (CH_2Cl_2, HPLC grade, Merck, Germany)
- Distilled water (H_2O)
- Dimethyl sufoxide ($(CH_3)_2SO$, Assay 99.9%, RCI Labscan, Thailand)
- Ethanol (C_2H_5OH, Assay 98%, RCI Labscan, Thailand)
- Hexane (C_6H_{14}, Assay 98%, RCI Labscan. Thailand)
- Magnesium sulphate anhydrous ($MgSO_4$, QP Panreac Quimica Sa, Barcelona)
- Methanol (CH_3OH, Assay 98%, RCI Labscan, Thailand)
- Methanol (CH_3OH, HPLC grade, Merck, Germany)
- *N,N*-Dimethylformamide (C_3H_7NO, Analytical grade, MAY&BAKER, England)
- *p*-Anisaldehyde ($C_8H_8O_2$, Assay 99%, Sigma-aldrich, USA)
- Potassium carbonate anhydrous (K_2CO_3, Assay 99%, Unilab, Australia)
- Potassium tetrachloroaurate ($K[AuCl_4]$, Assay 99%, Sigma-aldrich, USA)
- Propionic acid ($C_3H_6O_2$, Assay 95%, Poison, Australia)

- Pyrrole (C_4H_5N, A.R. grade , Aldrich, Steinheim, Germany)
- Silver nitrate ($AgNO_3$, Carlo Erba, Italy)
- Thin layer chromatography (Macherey-nagel, Germany)
- E-MEM(-) medium (Ds Pharma Biomedical Co. Ltd., Japan)
- Fetal bovine serum (use the stocked tube, Gibco, Japan)
- MEM-Non essential amino acids (use the stocked tube, Gibco, Japan)
- L-Glutamine (200mM, use the stocked tube, Gibco, Japan)
- Penicillin and streptomycin solution (use the stocked tube, Gibco, Japan)
- Fungizone (use the stocked tube, Gibco, Japan)
- Phosphate-Buffered Saline (Gibco, Japan)
- Ethylenediaminetetraacetic acid disodium salt dihydrate, ($C_{10}H_{14}N_2Na_2O_8 \cdot 2H_2O$, Nakalai tesque, Japan)
- Tripsin solution (use the stocked tube, Gibco, Japan)
- Thiazolyl Blue Tetrazolium Bromide (Sigma-Aldrich, USA)
- Diff-Quik stain solution I (Gibco, Japan)
- Diff-Quik stain solution II (Gibco, Japan)
- Diff-Quik Fixative solution (Gibco, Japan)

3.2 Method

3.2.1 Sample preparation for characterization

3.2.1.1 Nuclear Magnetic Resonance Spectroscopy (NMR)

For ^1H NMR and ^{13}C NMR, 2 mg of free-base porphyrins were dissolved in chloroform-*d*. The amount of solvent was 1 ml whereas the sample depth was at least 4 cm in the NMR tube.

3.2.1.2 Fourier transform Infrared Spectroscopy (FT-IR)

FT-IR spectra of free-base porphyrins, and metalloporphyrins were recorded in KBr in the 4000-400 cm^{-1} region.

3.2.1.3 Mass spectrometry

The solution of free-base porphyrins, and metalloporphyrins were prepared by dissolved 10 mg of them in dichloromethane (HPLC grade), and made up to 5 ml.

3.2.1.4 The elemental analysis

The sample under test is weighed in using a tin capsule. The required amount is 5 - 10 mg of free-base porphyrins, and metalloporphyrins. After folding the capsule (looking rather like wrapped tin foil) the sample is placed in the autosampler.

3.2.1.5 UV-visible and fluorescence spectroscopy

The free-base porphyrin, and metalloporphyrin were dissolved in dichloromethane at concentration 0.1 mM. Properties of free-base porphyrins and metalloporphyrin with their derivatives characterized by UV-Vis spectroscopy in the wavelength range of 200 - 800 nm and fluorescence spectroscopy in the wavelength range of 530 - 700 nm.

3.2.1.6 Thermal gravimetric analysis (TGA)

The thermal behaviors including the possible phase transition of free-base porphyrins, and metalloporphyrins were studied during the heating process at temperature of 25°C to 900°C. The 10 mg of porphyrins compounds were used and heating under nitrogen flow with scan rate 10°C per minute.

3.2.1.7 Cyclic voltammetry

The free-base porphyrin, and metalloporphyrin were dissolved in dichloromethane at concentration 0.1 mM containing 0.1 M $TBAPF_6$ as electrolyte. Their compounds were tested with a three-electrode system under deaevated conditions. Grassy carbon electrode and platinum electrode were used as working electrode and counter electrode respectively. All potentials were recorded against an Ag/AgCl reference electrode.

3.2.1.8 Electron spin resonance spectroscopy (EPR)

The free-base porphyrin, and metalloporphyrin were dissolved in dichloromethane at concentration 0.1 M**.** The EPR spectra were recorded under magnetic field 3200 – 3800 G.

3.2.2 Synthesis

3.2.2.1 Synthesis of alkyloxybenzaldehydes

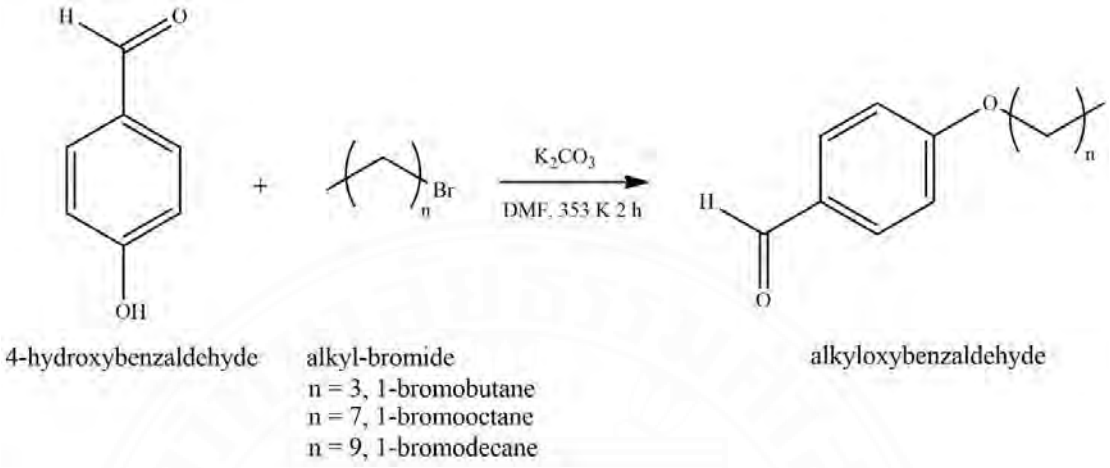

Scheme 1 Synthesis of alkyloxybenzaldehyde

1-Bromoalkane 0.05 mole (*1*-bromobutane 6.8510 g, *1*-bromooctane 8.6368 g, and *1*-bromodecane 11.0590 g) were added into the mixture of *4*-hydroxybenzaldehyde 0.05 mole (6.1060 g) and K_2CO_3 0.05 mole (6.9601 g) in DMF. The resulting reaction mixture was refluxed at 353 K for 2 hours. After refluxing, the reaction mixture was cooled down to room temperature, and then the salt were filtrated and dried to remove solvent. The reaction products was purified by using CH_2Cl_2, and distilled water. Magnesium sulfate anhydrous was used for drying agent. The yellow oil product was afforded [57]. The reaction product was further used without any purification. Butyloxybenzaldehyde **1** was obtained in 60% yield (5.35g). ^{1}H NMR (400 MHz, $CDCl_3$): δ 9.9 (1H, C***H***O), 7.8 (2H, Phenyl, *o*-H), 6.9 (2H, Phenyl, *m*-H), 4.0 (2H, OC***H***$_2$), 1.7 (2H, -OCH$_2$C***H***$_2$), 1.4 (2H, -C***H***$_2$CH$_3$), 0.9 (3H, -C***H***$_3$). ^{13}C NMR (100 MHz, $CDCl_3$): δ 191, 164, 133, 115, 68, 32, 20, 14 ppm. FTIR (NaCl, nujol, cm^{-1}): 3072, 2960, 2873, 2737, 1690, 1603, 1509, 1466, 1389, 1161, 1023, 834. Mass m/z (ESI) calcd for $C_{11}H_{14}O_2$: 178.23. Found 178.8 $[M]^+$. The similarly method was used to prepare both of Octyloxybenzaldehyde **2** and Dectyloxybenzaldehyde **3** with 71% yield (8.41g) and 72% yield (9.57g), respectively.

Octyloxybenzaldehyde **2** was obtained as yellow oil. ^{1}H NMR

(400 MHz, $CDCl_3$): δ 9.9 (1H, C***H***O), 7.8 (2H, Phenyl, *o*-H), 6.9 (2H, Phenyl, *m*-H), 4.0 (2H, OC***H***$_2$), 1.8 (2H, -OCH$_2$C***H***$_2$), 1.4 (2H, -C***H***$_2$CH$_3$), 1.2 (8H, -CH$_2$C***H***$_2$CH$_2$), 0.8 (3H, -C***H***$_3$). ^{13}C NMR (100 MHz, $CDCl_3$): δ 190, 164, 133, 114, 68, 32, 29, 23, 14 ppm. FTIR (NaCl, nujol, cm^{-1}): 3073, 2927, 2856, 2732, 1691, 1602, 1509, 1467, 1395, 1160, 1020, 833. Mass m/z (ESI) calcd for $C_{15}H_{22}O_2$: 234.33. Found 235.3 $[M]^{+\cdot}$

Dectyloxybenzaldehyde **3** was also obtained as yellow oil. ^{1}H NMR (400 MHz, $CDCl_3$): δ 9.8 (1H, C***H***O), 7.7 (2H, Phenyl, *o*-H), 6.9 (2H, Phenyl, *m*-H), 3.9 (2H, OC***H***$_2$), 1.8 (2H, -OCH$_2$C***H***$_2$), 1.4 (2H, -C***H***$_2$CH$_3$), 1.2 (12H, -CH$_2$C***H***$_2$CH$_2$), 0.9 (3H, -C***H***$_3$). ^{13}C NMR (100 MHz, $CDCl_3$): δ 190, 164, 132, 115, 68, 32, 30, 23, 14 ppm. FTIR (NaCl, nujol, cm^{-1}): 3074, 2926, 2855, 2732, 1693, 1602, 1509, 1467, 1393, 1160, 1017, 833. Mass m/z (ESI) calcd for $C_{17}H_{26}O_2$: 262.49. Found 261.2 $[M]^+$.

3.2.2.2 Synthesis of free-base porpohyrins

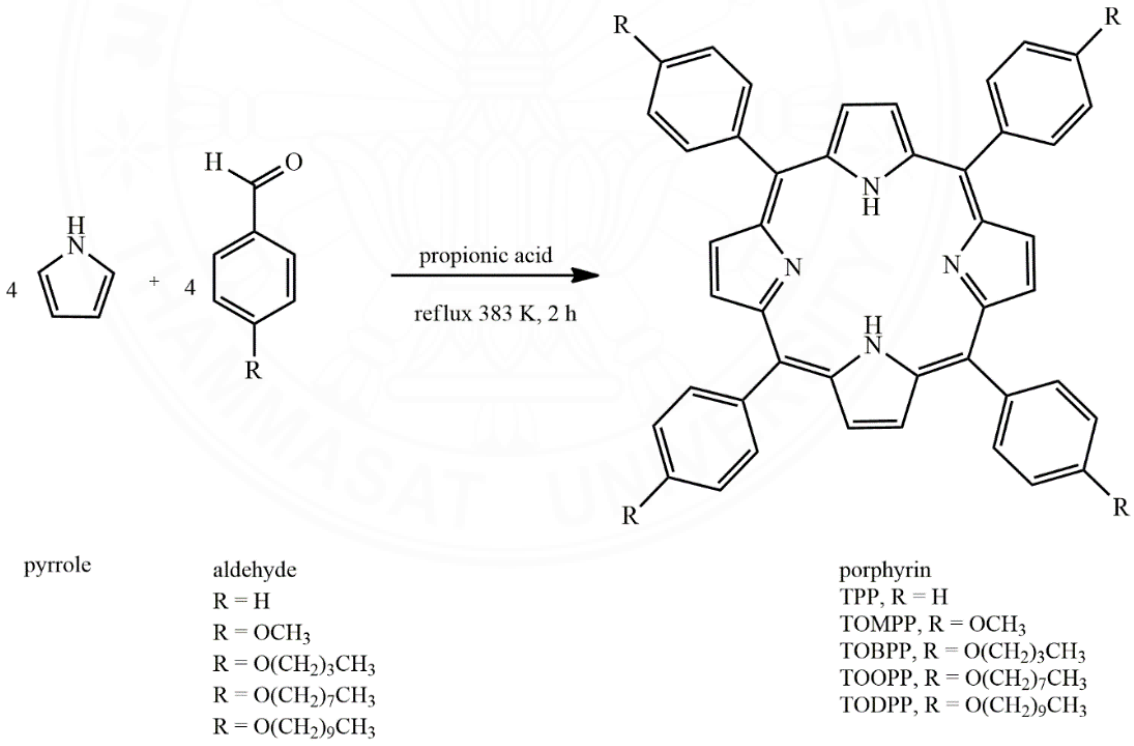

Scheme 2 Synthesis of free-base porphyrins

Free-base porphyrin and its derivatives were synthesized by following a published procedure with slight modification [17]. Pyrrole 0.028 mole (2 mL) and benzaldehyde 0.03 mole (3.18 g) were taken in a 100 mL round bottom flask containing 40 mL of propionic acid. The reaction mixture was stirred and refluxed at 383 K for 2 hours. After refluxing, the reaction mixture was cooled to room temperature, and added 40 mL of ethanol. Then cool down to 4°C overnight. The purple crystals were filtered, washed, and dried by vacuum. The filtration with cold ethanol to removed traces of propionic acid was applied. The crude products were purified by silica gel column chromatography and eluted with the increasing polarity by the mixture of dichloromethane and hexane to afford TPP **4** as a purple crystal in 22% yield (0.4834 g). ^{1}H NMR (400 MHz, $CDCl_3$): δ 8.8 (8H, Pyrrole, *β*-H), 8.2 (8H, Phenyl, *o*-H), 7.7 (8H, Phenyl, *m*-H) ^{13}C NMR (100 MHz, $CDCl_3$): 127.70, 134.56, 131.12, 142.22, 120.15, 126.67 ppm. FTIR (KBr, cm^{-1}): 3310, 3053, 3024, 1597, 1469, 1212, 1177, 966, 794. Elemental analysis; calcd (%) for $C_{44}H_{30}N_4$: C 86.0, H 4.9, N 9.1; found: C 85.9, H 4.9, N 9.1. Mass m/z (ESI) calcd for $C_{44}H_{30}N_4$: 614.7 Found 615.0 $[M+H]^+$. UV-vis (CH_2Cl_2): (λ_{abs}(nm), ε ($10^3M^{-1}cm^{-1}$)): S-band; (417, 327.5), Q-band; (514, 14.1), (548, 6.1), (590, 4.6), (649, 3.9). The TOMPP **5**, TOBPP **6**, TOOPP **7**, and TODPP **8** were prepared similarly to TPP **4**, with changed benzaldehyde to *ρ*-anisaldehyde, butyloxybenzaldehyde, octyloxybenzaldehyde, dectyloxybenzaldehyde, respectively.

The tetrakis(4-methoxyphenyl)porphyrin (TOMPP **5**) was obtained in 26% yield (0.5988 g) as purple crystal. ^{1}H NMR (400 MHz, $CDCl_3$): δ 8.8 (8H, Pyrrole, *β*-H), 8.1 (8H, Phenyl, *o*-H), 7.2 (8H, Phenyl, *m*-H), 4.1 (12H, $-OCH_3$). ^{13}C NMR (100 MHz, $CDCl_3$): 158.75, 134.68, 133.99, 129.97, 127.89, 118.83, 111.44, 54.65 ppm. FTIR (KBr, cm^{-1}): 3316, 2931, 2834, 1607, 1509, 1248, 1174, 966, 804. Elemental analysis; calcd (%) for $C_{48}H_{38}N_4O_4$: C 78.45, H 5.21, N 7.62; found: C 76.42, H 5.75, N 7.42. Mass m/z (ESI) calcd for $C_{48}H_{38}N_4O_4$: 734.84 Found 735.4 $[M+H]^+$. UV-vis (CH_2Cl_2): (λ_{abs}(nm), ε ($10^3M^{-1}cm^{-1}$)): S-band; (421, 296.9), Q-band; (518, 11.9), (555, 8.2), (595, 3.9), (650, 5.2).

The tetrakis(4-butyloxyphenyl)porphyrin (TOBPP **6**) was obtained as purple crystal in 9% yield. ^{1}H NMR (400 MHz, $CDCl_3$): δ 8.9 (8H, Pyrrole, *β*-H), 8.1 (8H, Phenyl, *o*-H), 7.4 (8H, Phenyl, *m*-H), 4.2 ($-OCH_2$), 1.9 ($-OCH_2CH_2$), 1.3

(-CH_2CH_3), 0.9 (-CH_3). ^{13}C NMR (100 MHz, $CDCl_3$): 159.09, 135.32, 134.74, 130.70, 128.76, 119.7, 112.84, 68.14, 31.49, 23.98, 13.84 ppm. FTIR (KBr, cm^{-1}): 3320, 2931, 2868, 1607, 1509, 1245, 1174, 966, 802. Elemental analysis; calcd (%) for $C_{60}H_{62}N_4O_4$: C 79.79, H 6.92, N 6.20; found: C 79.44, H 6.55, N 5.83. Mass m/z (ESI) calcd for $C_{60}H_{62}N_4O_4$: 903.16. Found 903.6 $[M+H]^+$. UV-vis (CH_2Cl_2): (λ_{abs}(nm), ε ($10^3M^{-1}cm^{-1}$)): S-band; (422, 530.6), Q-band; (519, 22.9), (556, 17.3), (595, 8.6), (651, 11.6).

The tetrakis(4-octyloxyphenyl)porphyrin (TOOPP **7**) was obtained in 12% yield as purple crystal. ^{1}H NMR (400 MHz, $CDCl_3$): δ 8.8 (8H, Pyrrole, β-H), 8.2 (16H, Phenyl, *o*-H and *m*-H), 4.2 (-OCH_2), 1.9 (-OCH_2CH_2), 1.3 (-CH_2CH_3), 1.2 (-$CH_2CH_2CH_2$), 0.9 (-CH_3). ^{13}C NMR (100 MHz, $CDCl_3$): 159.07, 135.54, 134.57, 131.78, 128.74, 119.79, 112.82, 68.45, 31.84, 29.64, 29.53, 29.45, 26.22, 22.64, 14.00 ppm. FTIR (KBr, cm^{-1}): 3318, 2927, 2852, 1607, 1509, 1243, 1174, 965, 804. Elemental analysis; calcd (%) for $C_{76}H_{94}N_4O_4$: C 80.95, H 8.40, N 4.97; found: C 81.10, H 8.25, N 4.93. Mass m/z (ESI) calcd for $C_{76}H_{94}N_4O_4$: 1125.57. Found 1127.9 $[M+H]^+$. UV-vis (CH_2Cl_2): (λ_{abs}(nm), ε ($10^3M^{-1}cm^{-1}$)): S-band; (422, 611.7), Q-band; (519, 30.9), (556, 24.7), (595, 15.7), (651, 17.4).

The tetrakis(4-decyloxyphenyl)porphyrin (TODPP **8**) was obtained as purple crystal in 9% yield. ^{1}H NMR (400 MHz, $CDCl_3$): δ 8.8 (8H, Pyrrole, β-H), 8.0 (16H, Phenyl, *o*-H and *m*-H), 4.2 (-OCH_2), 1.9 (-OCH_2CH_2), 1.3 (-CH_2CH_3), 1.2 (-CH_2CH_2), 0.8 (-CH_3). ^{13}C NMR (100 MHz, $CDCl_3$): 159.10, 135.51, 134.51, 130.68, 128.76, 119.77, 112.86, 68.48, 31.88, 29.60, 29.55, 29.53, 29.46, 29.28, 26.20, 22.60, 13.93 ppm. FTIR (KBr, cm^{-1}): 3317, 2924, 2852, 1607, 1509, 1244, 1174, 967, 803. Elemental analysis; calcd (%) for $C_{84}H_{110}N_4O_4$: C 81.37, H 8.94, N 4.52; found: C 81.24, H 8.99, N 4.58. Mass m/z (ESI) calcd for $C_{84}H_{110}N_4O_4$: 1237.17. Found 1239.0 $[M+H]^+$. UV-vis (CH_2Cl_2): (λ_{abs}(nm), ε ($10^3M^{-1}cm^{-1}$)): S-band; (422, 440.5), Q-band; (519, 20.8), (556, 15.7), (595, 8.4), (652, 10.6).

3.2.2.3 Synthesis of copper(II) and silver(II) porphyrin complexes

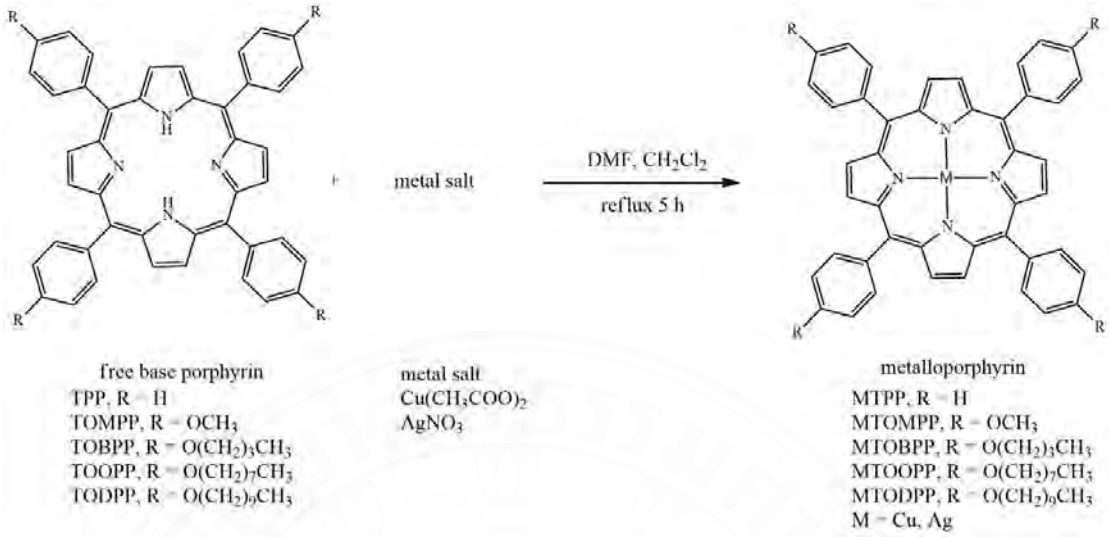

Scheme 3 Synthesis of copper(II) and Silver(II) porphyrin complexes

The copper(II) ion was inserted into the center of each free-base porphyrin by following the modification of published procedure [94]. The copper (II) ion derivative of tetraphenylporphyrin (CuTPP **9**) was obtained in 93%yield (0.4672 g) by refluxing tetraphenylporphyrin (TPP **4**) (0.3 mole, 0.1842 g) with an excess copper acetate [$Cu(OAc)_2 \cdot 3H_2O$] in mixed solvent between DMF (15 mL) and dichloromethane (15 mL) for 5 hours. After refluxing, the reaction mixture was cooled to room temperature. The mixture was kept in 4°C overnight after adding distilled water. Finally, the purple fine crystals were filtrate, washed cold methanol, and dried by vacuum. The reaction products were purified by silica gel column chromatography and eluted with the increasing polarity by the mixture of dichloromethane and hexane to afford pure CuTPP **9** as a purple crystal. FTIR (KBr, cm^{-1}): 3052, 3023, 1600, 1441, 1345, 1165, 793. Elemental analysis; calcd (%) for $CuC_{44}H_{28}N_4$: C 78.15, H 4.17, N 8.28; found: C 76.90, H 3.94, N 8.18. Mass m/z (ESI) calcd for $CuC_{44}H_{28}N_4$: 676.27. Found 677 $[M+H]^+$. UV-vis (CH_2Cl_2): (λ_{abs}(nm), ε ($10^3 M^{-1}cm^{-1}$)): S-band; (415, 415.9), Q-band; (540, 13.8). Other copper porphyrin have been synthesized by using similarly method with CuTPP.

The copper(II) tetrakis(4-methoxyphenyl)porphyrin (CuTOMPP **10**) was synthesized by reacting TOMPP **5** with copper acetate. The product was obtained as purple crystal in 92% yield. FTIR (KBr, cm^{-1}): 2929, 2835,

1607, 1499, 1248, 1173, 804. Elemental analysis; calcd (%) for $CuC_{48}H_{36}N_4O_4$: C 72.42, H 4.52, N 7.03; found: C 60.42, H 4.17, N 6.22. Mass m/z (ESI) calcd for $CuC_{48}H_{36}N_4O_4$: 796.38. Found 797.4 $[M+H]^+$. UV-vis (CH_2Cl_2): (λ_{abs}(nm), ε (10^3 $M^{-1}cm^{-1}$)): S-band; (419, 402.5), Q-band; (541, 18.9).

The copper(II) tetrakis(4-butyloxyphenyl)porphyrin (CuTOBPP **11**) was synthesized by reaction between TOBPP **6** and copper acetate. The product was obtained as purple crystal in 71% yield. FTIR (KBr, cm^{-1}): 2930, 2869, 1607, 1502, 1246, 1174, 799. Elemental analysis; calcd (%) for $CuC_{60}H_{60}N_4O_4$: C 74.77, H 6.23, N 5.82; found: C 74.51, H 6.25, N 5.76. Mass m/z (ESI) calcd for $CuC_{60}H_{60}N_4O_4$: 964.70. Found 965.6 $[M+H]^+$. UV-vis (CH_2Cl_2): (λ_{abs}(nm), ε (10^3 $M^{-1}cm^{-1}$)): S-band; (419, 415.4), Q-band; (541, 24.5).

The copper(II) tetrakis(4-octyloxyphenyl)porphyrin (CuTOOPP **12**) was synthesized by reaction between TOOPP **7** and copper acetate. The product was obtained as purple crystal in 96% yield. FTIR (KBr, cm^{-1}): 2926, 2852, 1607, 1506, 1244, 1174, 804. Elemental analysis; calcd (%) for $CuC_{76}H_{92}N_4O_4$: C 76.83, H 7.75, N 4.73; found: C 68.65, H 6.95, N 4.40. Mass m/z (ESI) calcd for $CuC_{76}H_{92}N_4O_4$: 1187.11. Found 1187.0 $[M+H]^+$. UV-vis (CH_2Cl_2): (λ_{abs}(nm), ε (10^3 $M^{-1}cm^{-1}$)): S-band; (419, 380.4), Q-band; (541, 29.0).

The copper(II) tetrakis(4-dectyloxyphenyl)porphyrin (CuTODPP **13**) was synthesized by reaction between TODPP **8** and copper acetate. The product was obtained as purple crystal in 63% yield. FTIR (KBr, cm^{-1}): 2923, 2852, 1607, 1504, 1246, 1174, 800. Elemental analysis; calcd (%) for $CuC_{84}H_{108}N_4O_4$: C 77.60, H 8.31, N 4.31; found: C 66.91, H 7.30, N 3.80. Mass m/z (ESI) calcd for $CuC_{84}H_{108}N_4O_4$: 1299.32. Found 1303.7 $[M+H]^+$. UV-vis (CH_2Cl_2): (λ_{abs}(nm), ε (10^3 $M^{-1}cm^{-1}$)): S-band; (419, 311.1), Q-band; (541, 14.2).

The synthesis of silver(II) porphyrins were followed the published procedure [60]. The silver(II) tetraphenylporphyrin (AgTPP **14**) was obtained 74.94 % yield (0.2704 g) by refluxing TPP **4** (0.5 mole, 0.3074 g) with an excess silver nitrate ($AgNO_3$) in DMF (15 mL) and dichloromethane (15 mL) for 5 hours. After that reaction was completed, the reaction mixture was cooled to room temperature and kept in 4°C overnight after adding distilled water. The obtained purple crystal was vacuum-filtrated and washed with cold water. Further purification of the

reaction product was carried out over a silica gel column with the mixture of dichloromethane and hexane as eluent to afford AgTPP **14**. FTIR (KBr, cm^{-1}): 1598, 1442, 1243, 794. Elemental analysis; calcd (%) for $AgC_{44}H_{28}N_4$ (720.59): C 73.34, H 3.92, N 7.77; found C 72.98, H 4.11, N 7.56. Mass *m/z* (ESI): found 721.3 $[M+H]^+$. UV-Vis (CH_2Cl_2): (λ_{abs}(nm), Ɛ ($10^3M^{-1}cm^{-1}$)): S-band; (425, 542.7), Q-band; (542, 25.7). Other silver porphyrin have been synthesized by using similarly method with AgTPP

The silver(II) tetrakis(4-methoxyphenyl)porphyrin (AgTOMPP **15**) was obtained as purple crystal in 57.14 % yield. FTIR (KBr, cm^{-1}): 2934, 2833, 1606, 1548, 1250, 1175, 809. Elemental analysis; calcd (%) for $AgC_{48}H_{36}N_4O_4$ (840.69): C 62.47, H 4.53, N 6.13; found C 62.63, H 4.10, N 5.92. Mass *m/z* (ESI): found 841.6 $[M+H]^+$. UV-Vis (CH_2Cl_2): (λ_{abs}(nm), Ɛ ($10^3M^{-1}cm^{-1}$)): S-band; (427, 442.2), Q-band; (542, 22.9).

The silver(II) tetrakis(4-butyloxyphenyl)porphyrin (AgTOBPP **16**) was obtained as purple crystal in 18 % yield. FTIR (KBr, cm^{-1}): 2932, 2834, 1609, 1506, 1248, 1176, 805. Elemental analysis; calcd (%) for $AgC_{60}H_{60}N_4O_4$ (1009.01): C 71.42, H 5.99, N 5.55; found C 74.51, H 6.25, N 5.76. Mass *m/z* (ESI): found 1010.1 $[M+H]^+$. UV-Vis (CH_2Cl_2): (λ_{abs}(nm), Ɛ ($10^3M^{-1}cm^{-1}$)): S-band; (427, 356.5), Q-band; (543, 25.0).

The silver(II) tetrakis(4-octyloxyphenyl)porphyrin (AgTOOPP **17**) was obtained as purple crystal in 63.33 % yield. FTIR (KBr, cm^{-1}): 2934, 2843, 1609, 1506, 1247, 1177, 805. Elemental analysis; calcd (%) for $AgC_{76}H_{92}N_4O_4$ (1233.44): C 73.42, H 7.47, N 4.50; found C 73.19, H 7.71, N 4.21. Mass *m/z* (ESI): found 1233.9 $[M+H]^+$. UV-Vis (CH_2Cl_2): (λ_{abs}(nm), Ɛ ($10^3M^{-1}cm^{-1}$)): S-band; (430, 444.9), Q-band; (544, 22.9).

The silver(II) tetrakis(4-dectyloxyphenyl)porphyrin (AgTODPP **18**) was obtained as purple crystal in 52.24 % yield). FTIR (KBr, cm^{-1}): 2928, 2845, 1609, 1507, 1249, 1177, 805. Elemental analysis; calcd (%) for $AgC_{84}H_{108}N_4O_4$ (1345.65): C 69.71, H 7.59, N 3.80; found C 69.66, H 7.70, N 3.88. Mass *m/z* (ESI): found 1346.0 $[M+H]^+$. UV-Vis (CH_2Cl_2): (λ_{abs}(nm), Ɛ ($10^3M^{-1}cm^{-1}$)): S-band; (430, 590.2), Q-band; (544, 25.9).

3.2.2.4 Synthesis of gold(III) porphyrin complexes

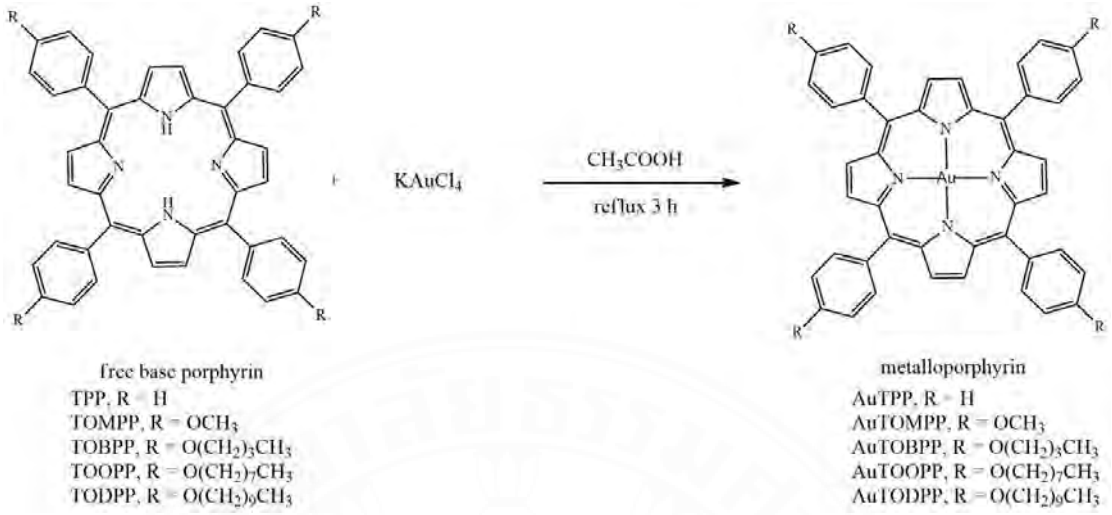

Scheme 4 Synthesis of Gold(III) porphyrin complexes

The gold(III) porphyrin complexes were synthesized with the corresponding free-base by following the published procedure [76]. The gold(III) tetraphenylporphyrin (AuTPP **19**) complex was prepared by refluxing tetraphenylporphyrin (TPP) in glacial acetic acid with sodium acetate and excess $KAuCl_4$ for 3 h. After completion the reaction was checked by TLC. The acetic acid in cured product were removed then washed with CH_2Cl_2 and water for several time until become neutral. The product was future purified by silica gel column chromatography (CH_2Cl_2/MeOH 5/1 v/v) to afford AuTPP as a purple crystalline solid in 16% yield. FTIR (KBr, cm^{-1}): 3123, 3050, 1620, 1488, 1358, 807. Mass m/z (ESI) calcd for $AuC_{44}H_{28}N_4$: 809.6. Found 808.9 Elemental analysis; calcd (%) for $AuC_{44}H_{28}N_4Cl{\cdot}2CH_2Cl_2$: C 54.43, H 3.18, N 5.52; found C 53.13, H 3.22, N 5.50. $[M+H]^+$. UV-Vis (CH_2Cl_2): (λ_{abs}(nm), Ɛ ($10^3M^{-1}cm^{-1}$)): S-band; (406, 87.30), Q-band; (519, 4.5). Other gold(III) porphyrin complexes were synthesis similarly with AuTPP.

The gold(III) tetrakis(4-methoxyphenyl)porphyrin (AuTOMPP **20**) was obtained as purple crystals in 10% yield. . FTIR (KBr, cm^{-1}): 2927, 2837, 1600, 1508, 1290, 1174, 801. Mass m/z (ESI) calcd for $AuC_{48}H_{36}N_4O_4$: 929.8. Found 929.4 $[M+H]^+$. Elemental analysis; calcd (%) for $AuC_{48}H_{36}N_4O_4$ Cl $\cdot 2CH_3OH$:

C 58.34, H 4.31, N 5.44; found C 62.62, H 4.37, N 5.34. λ_{abs}(nm), Ɛ ($10^3M^{-1}cm^{-1}$)): S-band; (418, 77.3), Q-band; (521, 9.9).

The gold(III) tetrakis(4-butyloxyphenyl)porphyrin (AuTOBPP **21**) was obtained as purple crystals in 21% yield. FTIR (KBr, cm^{-1}): 2955, 2831, 1603, 1503, 1278, 1175, 801. Mass m/z (ESI) calcd for $AuC_{60}H_{60}N_4O_4Cl$: 1098.1. Found 1097.4 $[M+H]^+$. Elemental analysis; calcd (%) for $AuC_{60}H_{60}N_4O_4 \cdot CH_2Cl_2$: C 60.13, H 5.13, N 4.60; found C 60.76, H 5.10, N 4.89. λ_{abs}(nm), Ɛ ($10^3M^{-1}cm^{-1}$)): S-band; (419, 77.4), Q-band; (525, 71).

The gold(III) tetrakis(4-octyloxyphenyl)porphyrin (AuTOOPP **22**) was obtained as purple crystal in 18% yield. FTIR (KBr, cm^{-1}): 2924, 2853, 1604, 1503, 1287, 1176, 801. Mass m/z (ESI) calcd for $AuC_{76}H_{92}N_4O_4$: 1322.5. Found 1322.2 $[M+H]^+$. Elemental analysis; calcd (%) for $AuC_{76}H_{92}N_4O_4Cl \cdot CH_2Cl_2$: C 64.09, H 6.57, N 3.88; found C 65.08, H 6.37, N 4.10. λ_{abs}(nm), Ɛ ($10^3M^{-1}cm^{-1}$)): S-band; (419, 73.8), Q-band; (526, 6.2).

The gold(III) tetrakis(4-dectyloxyphenyl)porphyrin (AuTODPP **23**) was obtained as purple crystal in 22% yield. FTIR (KBr, cm^{-1}): 2916, 2856, 1604, 1505, 1287, 1178, 801. Mass m/z (ESI) calcd for $AuC_{84}H_{108}N_4O_4$: 1434.7. Found 1434.9 $[M+H]^+$. Elemental analysis; calcd (%) for $AuC_{84}H_{108}N_4O_4Cl$: C 68.62, H 7.40, N 3.81; found C 67.62, H 7.18, N 3.92. λ_{abs}(nm), Ɛ ($10^3M^{-1}cm^{-1}$)): S-band; (419, 59.9), Q-band; (526, 5.3).

3.2.3 Antibacterial activity

The media was prepared by using nutrient broth 4.00 g and agar 7.50 g in water. The disc of Whatmann No.1 filter paper having a diameter of 5 mm, autoclave priors used. The compound solution (50 µL, 10 mg/L) is applied to the disc then placed over the media. The methanol was served as the control solvent, while penicillin (10 mg/L) was selected for the standard drug. The samples were incubated for 24 hours at 37 ± 2 °C. The inhibition zone was carefully measured in mm. Furthermore, the minimum inhibitory concentration (MIC) and the minimum bactericidal concentration (MBC) have been determined. The minimum inhibitory concentration (MIC) was observed by the micro broth dilution method [95]. Stock solution (1,280 ppm) of all synthesized porphyrins were prepared in DMSO. The test solution was dilute with a nutrient broth medium to reduce the haft of concentration in

a 96-well microplate. Then 50 μL of the bacterial cell was added to each well. The final volume is 100 μL. The microplate was incubated for 18 hours at 37 ± 2 °C. After that 10 μL of 0.18%, resazurin was added to all wells and incubated for 2 hours at 37 ± 2 °C. The MIC value is the lowest concentration of a chemical that prevents the visible growth of a bacteria, which can be observed by the color in the last well change to purple. After that, the minimum bactericidal concentration (MBC) values were investigated by streak result solution from MIC tested that didn't found the bacterial growth (purple solution) on nutrient broth medium, incubated for 18 hours at 37 ± 2 °C. The minimum bactericidal concentration (MBC) is the concentration that results in microbial death.

3.2.4 Anticancer activity

3.2.4.1 Cell lines and cell culture

The human breast cancer cell line MCF7 was maintained in E-MEM(+) medium. The E-MEM(+) medium was supplemented with 10% Fetal bovine serum, 1% MEM-Non essential amino acid, 1% of 200 mM L-Glutamine, 1% of PEST, and 1% Fungizone. The MCF7 cell lines were maintained at 37°C in a humidified incubator with an atmosphere of 5% carbon dioxide. The Rhesus Monkey Kidney Epithelial Cells (LLC-MK2) were supported from department of biology, Silpakorn University.

3.2.4.2 Sample preparation

The Au(III) porphyrin solutions were prepared by dissolving each Au(III) porphyrin complex in dimethylsulphoxide (DMSO) at 15, 10, 5, and 2.5 mM, respectively. The stock solutions were then diluted with E-MEM(+) medium to obtain working concentrations of DMSO at 1% (v/v) and working concentrations of each compound of 150, 100, 50, and 25 μM respectively. In case of AuTPP, this sample have been prepared at lower concentration by dilute with E-MEM(+) medium at final concentration 10, 5, 1, and 0.5 μM respectively.

3.2.4.3 *In vitro* 3-(4,5-dimethylthiazol-2-yl)-2,5-diphenyltetrazolium bromide assay

MCF7 cells were seeded in 96-well plates with a seeding density of 1.0×10^4 cells/well for 24 hours (100 μL). Then, culture medium was changed to control and tested culture media. A control sample was 1% (v/v) DMSO in

E-MEM(+) medium. After that, MTT assay was performed at 24 hours incubation in control and tested culture media. In brief, MTT assay was performed as followed. Experiments were initiated by replacing the culture medium in each well with 100 µL of sample solutions and incubated at 37 ˚C in the 5% CO_2 incubator. After 24 hours of incubation, the tested cultured media were replaced by culture medium with 10% MTT reagent, 10 µl of MTT reagent in 100 µl culture medium. After that, the plates were incubated at 37 ˚C in the 5% CO_2 incubator for 4 h. At the end of the incubation period, the medium was removed and the intracellular formazan was solubilized with 100 µL DMSO and quantified by reading the absorbance at 560 nm on a microplate reader with UV scan instrument. Percentage of cell viability was calculated based on the absorbance measured relative to the absorbance of cells exposed to the negative control. The percentage of cell viability was calculated as follow:

$$\%\ cell\ viability = \frac{OD\ of\ treated\ cells}{OD\ of\ untreated\ cells} \times 100$$

The similarly method were used to studied the cytotoxicity of porphyrin complexes on LLC-MK2 cell lines.

3.2.4.4 Diff-Quik staining

The solution have been removed from 96-well plates, then the Diff-Quik Fixative solution (30 µL) were added in each well. After 10 minute removed the solution and add the Diff-Quik solution I (30 µL) in each well then removed the solution immediately. Repeat this step with Diff-Quik solution II. Finally, washed with distilled water 2 – 3 time and air dried.

CHAPTER 4
RESULTS AND DISCUSSION

4.1 Aldehyde synthesis and characterization

4.1.1 Aldehyde synthesis

The aldehyde with long-chain alkane, including butyloxybenzaldehyde **1**, octyloxybenzaldehyde **2** and decyloxybenzaldehyde **3** (**Figure 44**) were synthesized by following previous method [57]. The 4-hydroxybenzaldehyde, and K_2CO_3 were refluxed with differences type of alkylbromide (1-bromobutane, 1-bromooctane, and 1-bromodecane) in DMF for 2 hours. The representative example scheme of synthesized alkyloxybenzaldehyde is show in **Figure 43**. The butyloxybenzaldehyde **1** was obtained around 60% while, both of octyloxybenzaldehyde **2**, and decyloxybenzaldehyde **3** were obtained over 70%. The characteristic data of all aldehydes were summarized in **Table 2**

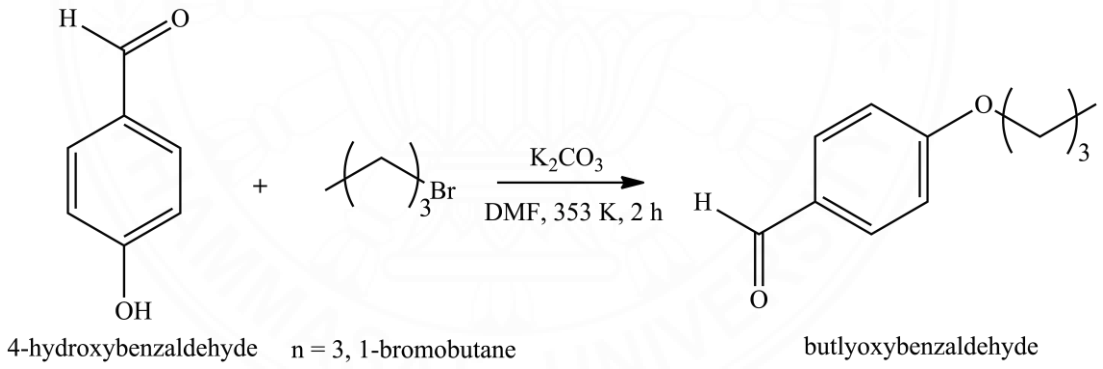

Figure 43 Synthesis of buthyloxybenzaldehyde **1**

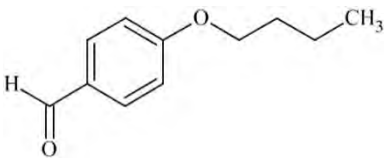

Formula $C_{11}H_{14}O_2$
Butyloxybenzaldehyde **1**

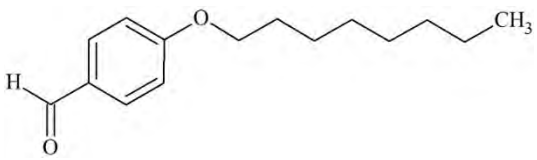

Formula $C_{15}H_{22}O_2$
Octyloxybenzaldehyde **2**

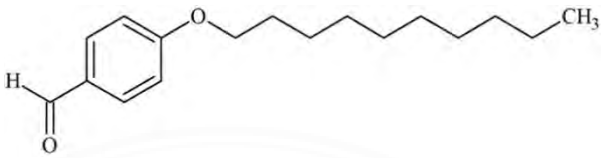

Formula $C_{17}H_{26}O_2$
Decyloxybenzaldehyde **3**

Figure 44 Structure of alkyloxybenzaldehyde

Table 2
Characteristic data of aldehydes **1-3**

Aldehydes	Empirical formula	Yield (%)	Formula weight	MS (m/z) $[M+H]^+$
Butyloxybenzaldehyde **1**	$C_{11}H_{14}O_2$	60	178.2	178.8
Octyloxybenzaldehyde **2**	$C_{15}H_{22}O_2$	71	234.3	235.3
Decyloxybenzaldehyde **3**	$C_{17}H_{26}O_2$	72	262.3	261.2

4.1.2 Aldehyde characterization

The structure of synthesized alkyloxybenzaldehyde has been confirmed by mass spectrometry, ^1H, and ^{13}C NMR spectroscopy, and IR spectroscopy. The result of mass spectrometry founded that the molecular ion peak of alkyloxybenzaldehyde 1, 2, and 3 at m/z = 178.8, 235.3, and 261.2, respectively. For the ^1H NMR spectroscopy, the important characteristic chemical shift of proton at carboxaldehyde (-CHO) was founded at 9.9 ppm, the proton in the phenyl ring was founded range 6.9 - 7.7 ppm. The signal of proton in alkyl long-chain were founded range 0.8 - 4.0 ppm. In addition, the carbon in carboxaldehyde (-CHO) was exhibited the signal peak in ^{13}C NMR spectrum at 190 ppm, and carbon in the phenyl ring in the range 115 -164 ppm, while the carbon in alkyl long-chain in the range 14 - 68 ppm, respectively. Finally, the importance IR signal peak of carboxaldehyde, and alcoxy functional group was founded at 1690 cm^{-1}, and 1161 with 1020 cm^{-1}, respectively

4.1.2.1 Mass spectrometry (MS)

The mass spectrometry have been used to confirm the structure of the alkyloxybenzaldehyde derivative. **Figure 45** shows mass spectrum of butyloxybenzaldehyde **1** (without purification) with shows the strong molecular ion peak $[M+H]^+$ at m/z = 178.8. Furthermore, the fragmentation peaks were founded at m/z = 122.9, that represent the mass of their parent compound (*4*-hydroxybenzaldehyde). In previous report by *M. Rosario M.D.*, they founded the fragmentation reaction of butyloxybenzaldehyde **1** is due to the loss of an alkyl long-chain group at m/z = 162, 148, 134, and 122, respectively [96]. In addition the octyloxybenzaldehyde **2** and, dectyloxybenzaldehyde **3** founded the molecular ion peak $[M+H]^+$ at m/z = 235.3 and 261.2 respectively. The result were confirmed the structure of all alkyloxybenzaldehyde are in agree with the expected structure (**Figure 44**). The mass spectrometry data of all aldehyde were show in **Table 2**

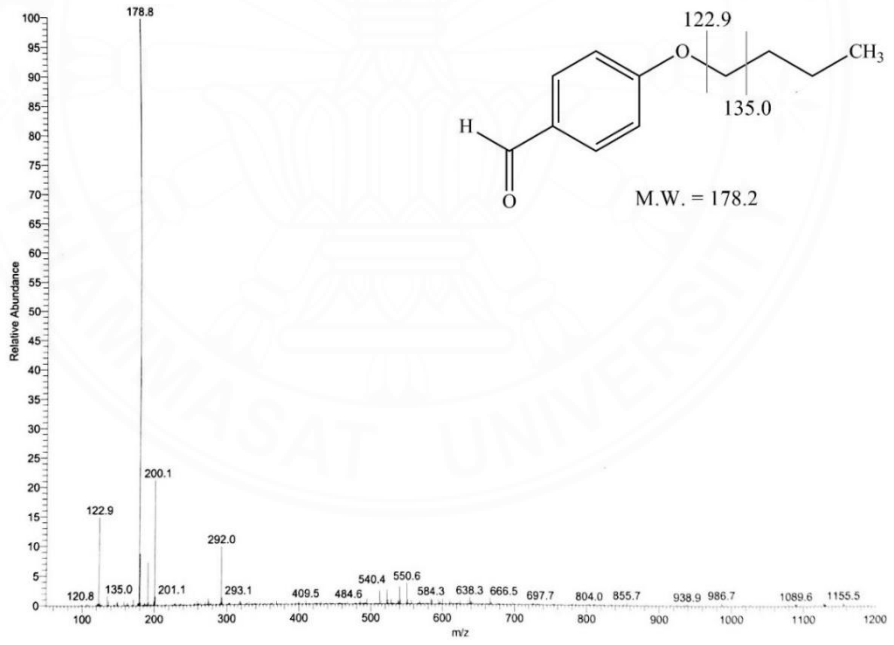

Figure 45 Mass spectrum of butyloxybenzaldehyde **1**

4.1.2.2 Nuclear Magnetic Resonance spectroscopy (NMR)

Nuclear magnetic resonance spectroscopy is used to local the magnetic fields around atomic nuclei and have been used to determining the structure

of organic compounds. So, the structure of the alkyloxybenzaldehyde were confirmed by using ^{1}H NMR and ^{13}C NMR spectroscopy. The representative ^{1}H NMR spectrum of butyloxybenzaldehyde **1** shows in **Figurer 46**. The ^{1}H NMR of butyloxybenzaldehyde **1** exhibits characteristic chemical shift arising from proton at carbonyl group of aldehyde (C***H***O) at 9.9 ppm, due to the magnetic anisotropy the carbonyl group. The *ortho*- and *meta*- proton of phenyl ring were showed two doublets peaks at 7.8 and 6.9 ppm, respectively. Moreover, the signal of proton from alkyl long-chain were observed at 4.0, 1.7, 1.5, and 0.9 ppm, respectively. The triplet peaks at 4.0 ppm was assigned to proton near the alcoxy group of alkyl long-chain (-OC***H***$_2$). The quintet and sextet signal peak at 1.7 and 1.5 ppm were corresponded to methylene proton of alkyl long-chain (-OCH$_2$C***H***$_2$C***H***$_2$-). The methyl (-C***H***$_3$) at the end of alkyl long-chain show the triplet peak at 0.9 ppm. Other benzaldehyde derivatively (octyloxybenzaldehyde **2** and, dectyloxybenzaldehyde **3**) showed similar proton signal as butyloxybenzaldehyde **1**. However, the signal of methylene proton of octyloxybenzaldehyde **2** and, dectyloxybenzaldehyde **3** that were observed the multiplet peak around 1.3 – 1.1 ppm.

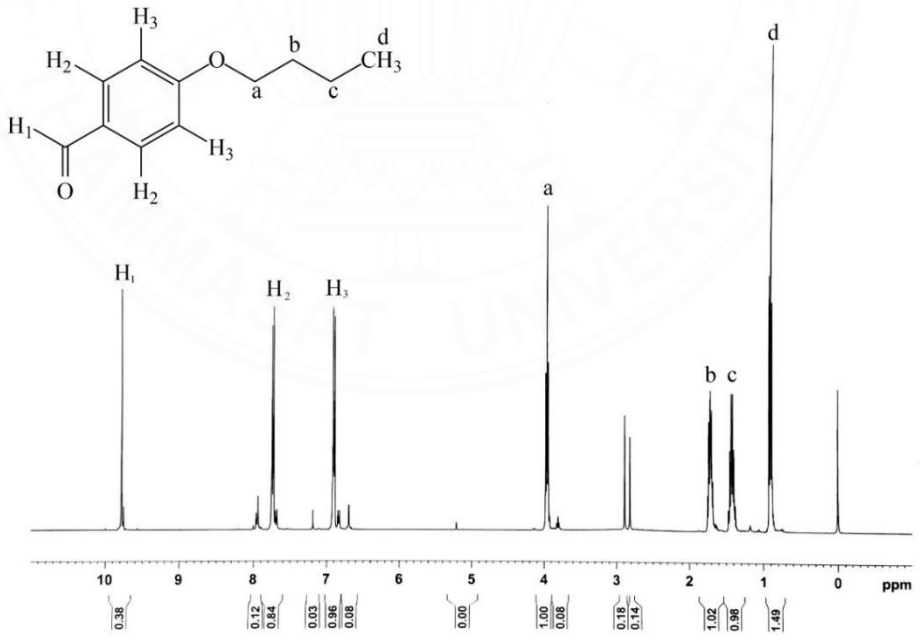

Figure 46 ^{1}H NMR spectrum of butyloxybenzaldehyde **1**

The representative ^{13}C NMR spectrum of butyloxybenzaldehyde **1** was shown in **Figurer 47**. The signal peak at 190.76 ppm was assigned to carbonyl carbon (***C***HO) at C_1 position. The carbon of phenyl ring showed four peaks at the chemical shift between 144.46 – 169.62 ppm. Next, the signal peak of methylene carbon that near the oxygen atom (C_2) was shown at 68.14 ppm, due to the deshielded effect of alcoxy group increased the chemical shift of this carbon atom (C_2) the similar result was reported by *Iannis D.K.* [57]. While, the methylene carbon at C_3 and C_4 position were found the signal at 31.25 and 19.20 ppm, respectively. Finally, the methyl carbon at the end of alkyl long-chain (C_5 position) was shown signal at 13.66 ppm. The similar results were observed in octyloxybenzaldehyde **2** and, dectyloxybenzaldehyde **3**, and the data were summarized in **Table 3**. The NMR result are in agreement with the previous reported by *Debora S.S.C.* [97]. Both ^{1}H and ^{13}C NMR were successfully to confirm the corresponding structure of all alkyloxybenzaldehyde derivative.

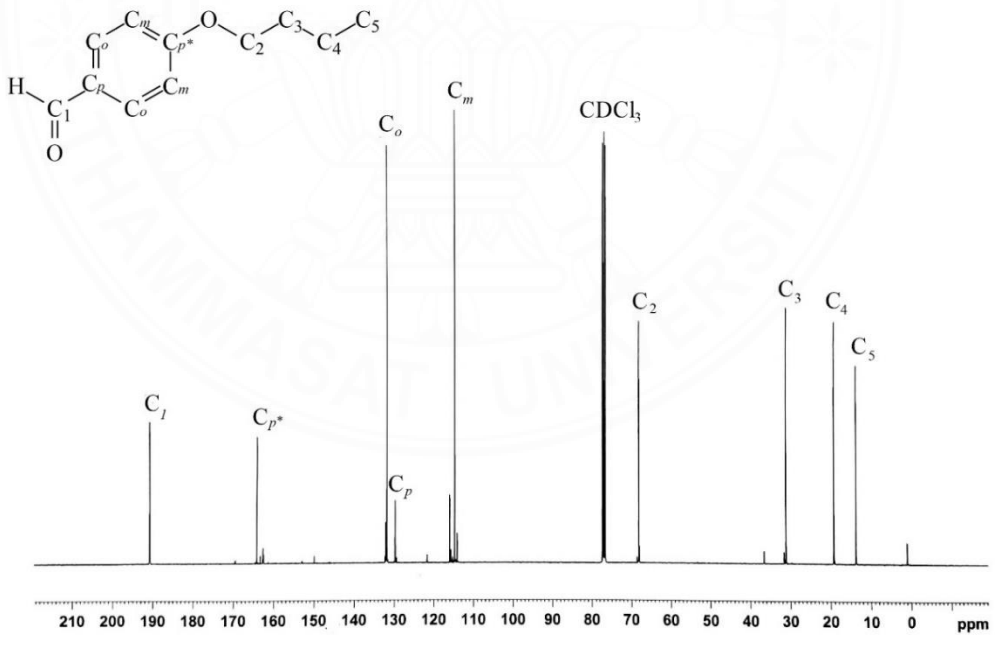

Figure 47 ^{13}C NMR spectrum of butyloxybenzaldehyde **1**

Table 3

^{1}H and ^{13}C NMR spectroscopic data for alkyloxybenzaldehydes **1-3**

Aldehydes	^{1}H NMR (ppm), proton							
	C***H***O	Phenyl, *o*-***H***	Phenyl, *m*-***H***	O***CH***$_2$	OCH$_2$***CH***$_2$	***CH***$_2$CH$_3$	CH$_2$***CH***$_2$CH$_2$	***CH***$_3$
Butyloxybenzaldehyde **1**	9.9 (1H)	7.8 (2H)	6.9 (2H)	4.0 (2H)	1.7 (2H)	1.5 (2H)	-	0.9 (3H)
Octyloxybenzaldehyde **2**	9.9 (1H)	7.8 (2H)	6.9 (2H)	4.0 (2H)	1.8 (2H)	1.4 (2H)	1.2 (8H)	0.8 (3H)
Decyloxybenzaldehyde **3**	9.8 (1H)	7.7 (2H)	6.9 (2H)	3.9 (2H)	1.8 (2H)	1.4 (2H)	1.2 (12H)	0.9 (3H)

Aldehydes	^{13}C NMR (ppm), carbon								
	C*H*O	Phenyl, *p*-***C***	Phenyl, *o*-***C***	Phenyl, *m*-***C***	O***C***H$_2$	OCH$_2$***C***H$_2$	CH$_2$***C***H$_2$CH$_2$	***C***H$_2$CH$_3$	***C***H$_3$
Butyloxybenzaldehyde **1**	190 (1C)	164 (1C)	133 (1C)	115 (1C)	68 (1C)	32 (1C)	-	20 (1C)	14 (1C)
Octyloxybenzaldehyde **2**	190 (1C)	164 (1C)	133 (1C)	114 (1C)	68 (1C)	32 (1C)	29 (4C)	23 (1C)	14 (1C)
Decyloxybenzaldehyde **3**	190 (1C)	164 (2C)	132 (1C)	115 (1C)	68 (1C)	32 (1C)	30 (6C)	23 (1C)	14 (1C)

4.1.2.3 Infrared spectroscopy (IR)

The functional group of alkyloxybenzaldehydes were confirmed by IR spectroscopy technique. That was recorded by nujul in NaCl discs. The data were collected in the 4000 – 400 cm^{-1} region and summarized in **Table 4**. All alkyloxybenzaldehyde show the similarly wavenumber with small peak shift, due to the effect of alkyl long-chain group. **Figurer 48** show the representative IR spectrum of butyloxybenzaldehyde **1**. The C=O stretching of carboxaldehyde was found at 1690 cm^{-1}. The characteristic peak of proton next to the carboxaldehyde group (C-H stretching) showed two peak at 2873 and 2757 cm^{-1}. Then, the alcoxy group (C-O-C) in alkyl long-chain exhibited two characteristic peak at 1161 and 1023 cm^{-1}. Other aldehydes show the characteristic peak of carboxaldehyde functional group at the similarly wavenumber, but the signal of proton next to the carboxaldehyde group of octyloxybenzaldehyde **2** and, dectyloxybenzaldehyde **3** were decreased when the number of carbon in alkyl chain were increased due to the electron donating effect of alkyl long-chain groups. The signal at 3072 cm^{-1} was assigned to the C-H sp^2 stretching of phenyl ring and two signals at 1603 and 1509 cm^{-1} represented the C=C stretching in the phenyl ring. Moreover, the IR spectra of butyloxybenzaldehyde **1** show a C-H sp^3 stretching band of alkyl long-chain at 2960 cm^{-1}. The peaks at 1466 and 1389 cm^{-1} were assigned to CH_3 bend in alkyl long-chain group. The position of alkyl long-chain substitution was confirmed by signal at wavenumber 834 cm^{-1}. This signal was in agreement with the out of plane in the *para* disubsititution. However, the decreasing of wavenumber were observed in octyloxybenzaldehyde **2** and, dectyloxybenzaldehyde **3**. The result of this studies are in agreement with the previous reports [23, 98].

Table 4

The IR data of aldehydes **1** - **3**

Aldehydes	C-H sp^2 str. in phenyl	C-H sp^3 str. in long-chain	C-H str. in aldehyde	C=O str. in aldehyde	C=C str. in phenyl	CH_3 bend	C-O-C ether	Oop, para disubt.
Butyloxybenzaldehyde **1**	3072	2960	2873, 2737	1690	1603, 1509	1466, 1389	1161, 1023	834
Octyloxybenzaldehyde **2**	3073	2927	2856, 2732	1691	1602, 1509	1467, 1395	1160, 1020	833
Decyloxybenzaldehyde **3**	3074	2926	2855, 2732	1693	1602, 1509	1467, 1393	1160, 1017	833

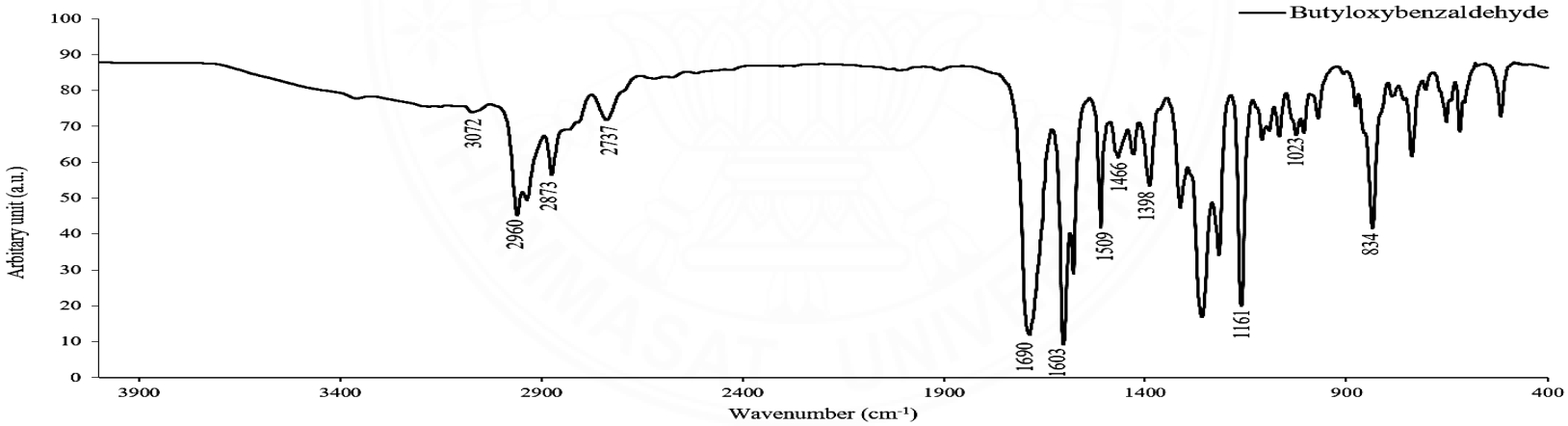

Figure 48 IR spectrum of butyloxybenzaldehyde **1**

4.2 Free-base porphyrin and metalloporphyrin synthesis and characterization

4.2.1 Free-base porphyrin synthesis

The free-base porphyrins, TPP **4** was synthesized by Alder-Longo method [17]. Then other free-base porphyrins including TOMPP **5**, TOBPP **6**, TOOPP **7**, and TODPP **8** (**Figure 50**) were synthesized by a modification of Alder-Longo method [99]. Firstly, heating each aldehyde derivative in propionic acid, followed by adding the same amount of pyrrole. The reaction were magnetically refluxed for 2 hours, then the reaction mixture was cooled to room temperature. The ethanol was added, and cool down to 4°C overnight. The purple crystals were obtained in dark solution. The product dried over vacuum and was further used as starting material for metalloporphyrin synthesis without further purification. The synthesized products were obtained in range 9 to 36% yield, as shown in **Table 5**. The long-chain derivative porphyrins (TOBPP **6**, TOOPP **7**, and TODPP **8**) gave the lower yield than 10%, due to the steric hindrance and the donating group on *para*-position of alkyl long-chain derivative, where will be further studied in chapter 4.6.

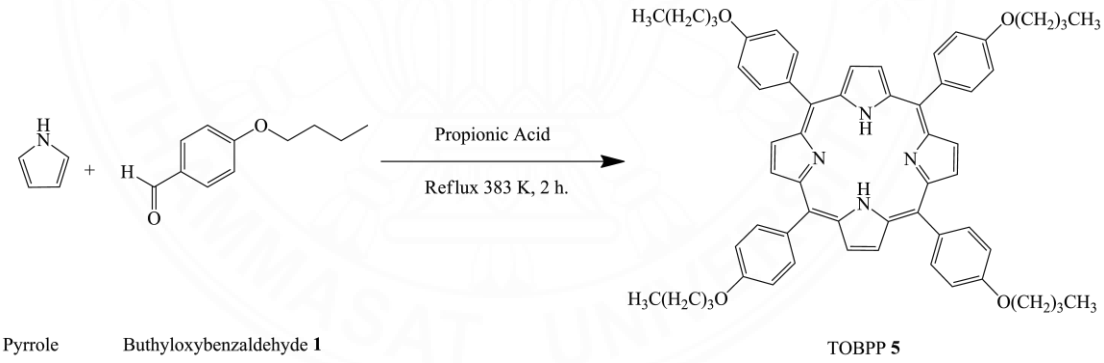

Figure 49 Synthesis of tetrakis(4-butyloxyphenyl)porphyrin (TOBPP **6**)

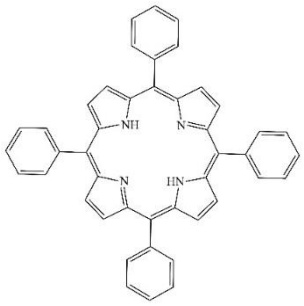

Formula $C_{44}H_{30}N_4$
Tetraphenylporphyrin
TPP **4**

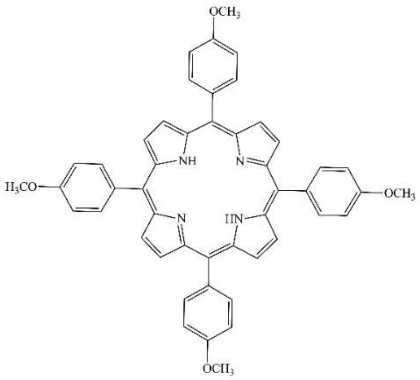

Formula $C_{48}H_{38}N_4O_4$
Tetrakis(4-methoxyphenyl)porphyrin
TOMPP **5**

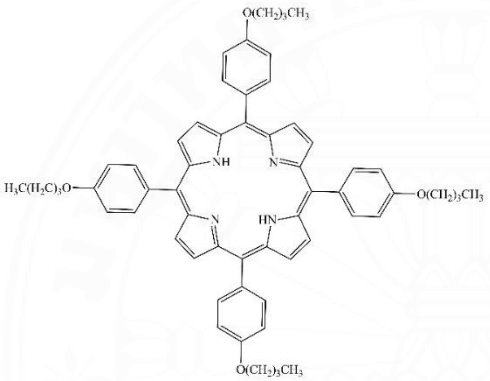

Formula $C_{60}H_{62}N_4O_4$
Tetrakis(4-butyloxyphenyl)porphyrin
TOBPP **6**

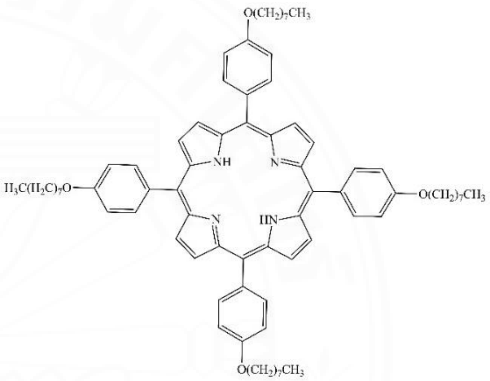

Formula $C_{76}H_{94}N_4O_4$
Tetrakis(4-octyloxyphenyl)porphyrin
TOOPP **7**

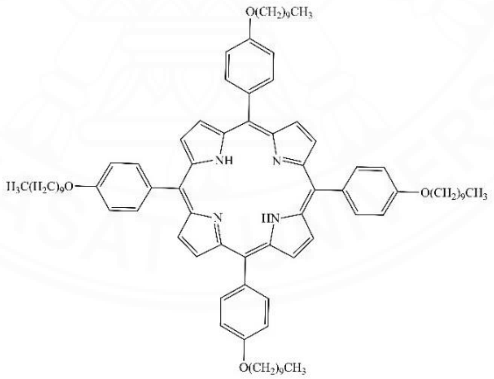

Formula $C_{84}H_{110}N_4O_4$
Tetrakis(4-dectyloxyphenyl)porphyrin
TODPP **8**

Figure 50 structure of free-base porphyrin

Table 5

The characteristic data for free-base porphyrins

Porphyrins	Empirical formula	Yield (%)	Elemental analysis ([a]) %			Formula weight	MS (m/z)
			C	H	N		
TPP **4**	$C_{44}H_{30}N_4$	22	85.9 (86.0)	4.9 (4.9)	9.1 (9.1)	614.7	615.0
TOMPP **5**	$C_{48}H_{38}N_4O_4$	26	76.42 (78.45)	5.75 (5.21)	7.42 (7.62)	734.84	735.4
TOBPP **6**	$C_{60}H_{62}N_4O_4$	9	79.44 (79.79)	6.55 (6.92)	5.83 (6.20)	903.16	903.6
TOOPP **7**	$C_{76}H_{94}N_4O_4$	12	81.10 (80.95)	8.25 (8.40)	4.93 (4.97)	1127.57	1127.9
TODPP **8**	$C_{84}H_{110}N_4O_4$	9	81.24 (81.37)	8.99 (8.94)	4.58 (4.52)	1239.78	1239.0

[a] Theoretical values are given in parentheses

4.2.2 Mtalloporphyrin synthesis

The metalloporphyrin have been interested. The copper(II) porphyrin complexes (CuTPP 9, CuTOMPP 10, CuTOBPP 11, CuTOOPP 12, and CuTODPP 13) and the silver(II) porphyrin complexes (AgTPP 14, AgTOMPP 15, AgTOBPP 16, AgTOOPP 17, and AgTODPP 18) were prepared by a modified procedure from the previous reports [94, 60]. Firstly, each free-base porphyrin have been dissolved in mixed solvent of *N,N*-dimethylformamide and dichloromethane (1:1), then excess copper acetate or silver nitrate were added, and refluxed for 5 hours. After finish the reaction distilled water was added for removing the surplus of metal salt. The purple products were formed after cool to 4°C overnight, and finally purified by silica gel column chromatography (gradient: hexane/dichloromethane; 10 – 50%). The results show that the synthetic products were obtained in a better yield than free-base porphyrin, due to the size of copper(II) ion and silver(II) ion are fitted in to the central hole of porphyrin with a proper oxidation state. The similarly result was reported by *Hongshan H.* for CuTPP [22]. The successful synthesis was obtained due to the long time reaction, more metal salt, and the reaction driving forward. However, some of metalloporphyrin was received in the small yield, suggesting the influence of steric hindrance of *para* substituent. The synthetic route of copper and silver porphyrin complexes are shown in **Figure 51**.

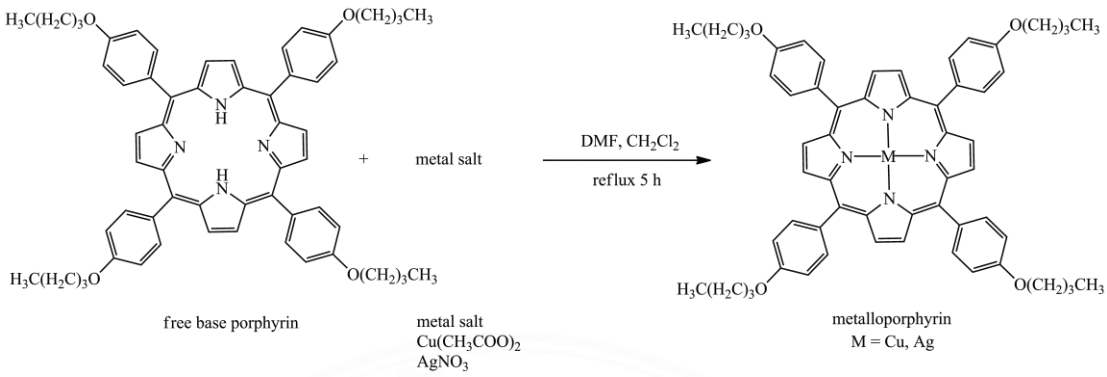

Figure 51 Synthesis of CuTOBPP **11** and AgTOBPP **16**

The gold(III) porphyrin complexes (AuTPP **19**, AuTOMPP **20**, AuTOBPP **21**, AuTOOPP **22**, and AuTODPP **23**) were synthesized by the reaction of $KAuCl_4$ with each free-base porphyrin in the presence of sodium acetate and acetic acid for 3 hours [76]. After remover the excess acetic acid by evaporation the crude product have been dissolved in CH_2Cl_2 and washed with distilled water to remove any unreacted $KAuCl_4$ and sodium acetate. Finally, the products were purified by silica gel column chromatography (dichloromethane/methanol: 5/1 v/v). The gold(III) porphyrin complexes were obtained in yield 10 – 22 %. The structure of metalloporphyrin complexes were illustrated in **Figure 53**. The chloride counter ion is regarded of balance the charge of gold(III) ion.

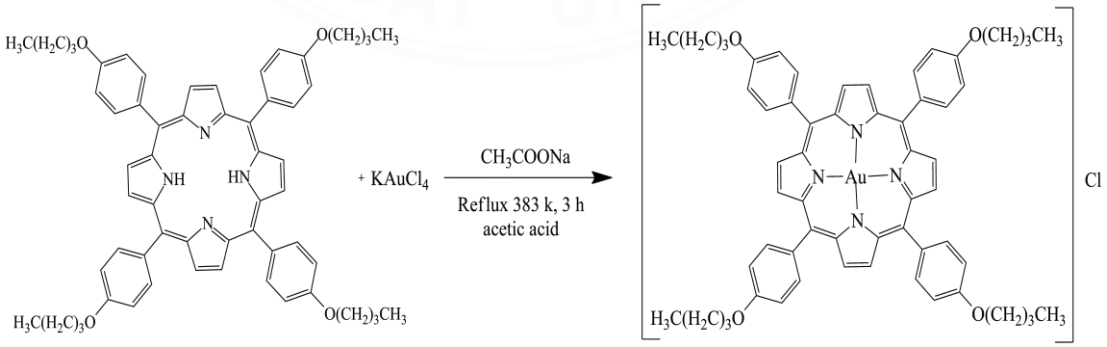

Figure 52 Synthesis of AuTOBPP **21**

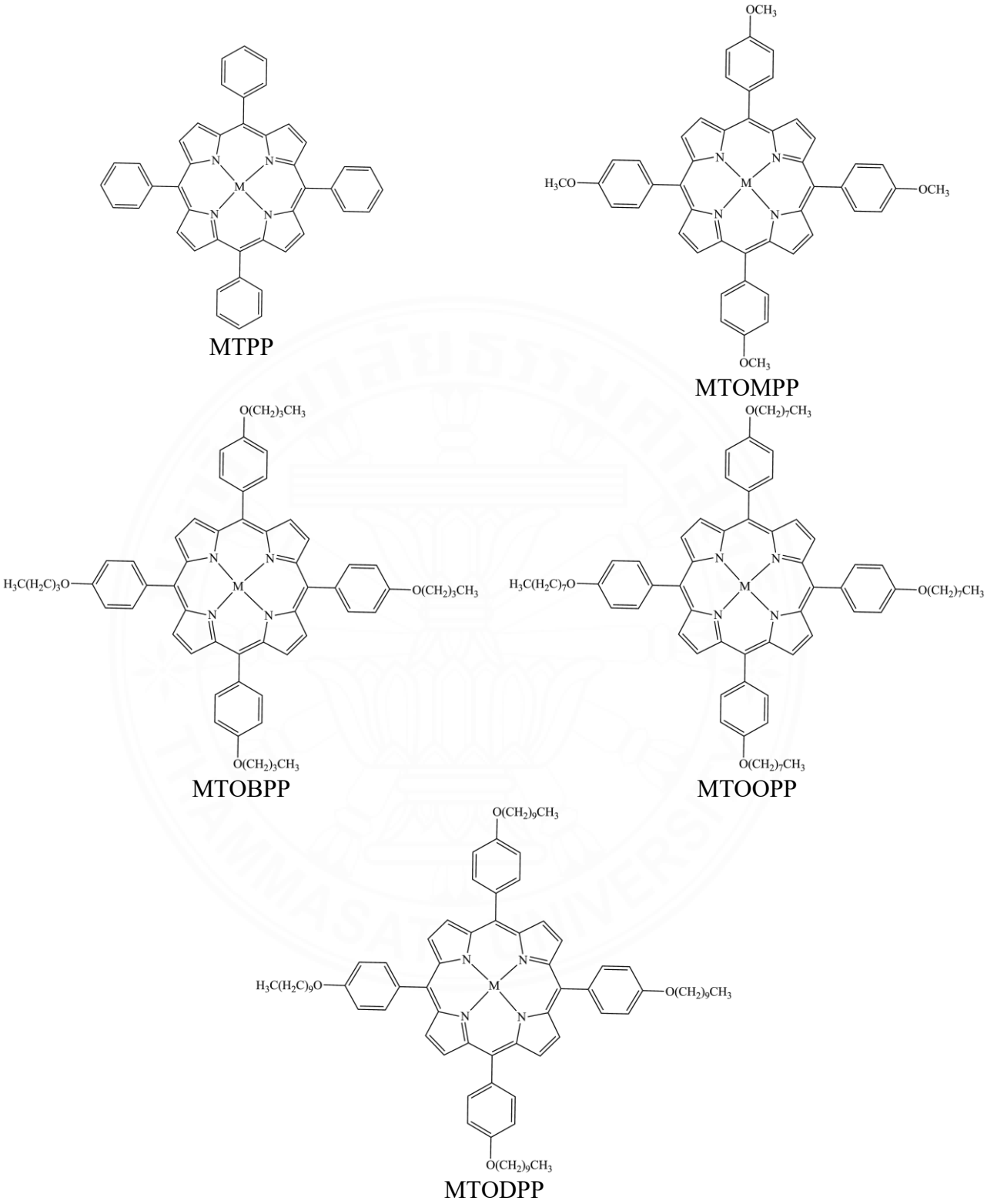

Figure 53 Structure of metalloporphyrin complexes (M = Cu, Ag, and Au)

Table 6

The characteristic data of metalloporphyrin complexes

Porphyrins	Empirical formula	Yield (%)	Elemental analysis ([a]) %		
			C	H	N
CuTPP **9**	$CuC_{44}H_{28}N_4$	93	76.90 (78.15)	3.94 (4.17)	8.18 (8.28)
CuTOMPP **10**	$CuC_{48}H_{36}N_4O_4 \cdot 2.5\ CH_2Cl_2$	92	60.42 (60.14)	4.17 (4.07)	6.22 (5.55)
CuTOBPP **11**	$CuC_{60}H_{60}N_4O_4$	71	74.51 (74.77)	6.25 (6.23)	5.76 (5.82)
CuTOOPP **12**	$CuC_{76}H_{92}N_4O_4 \cdot 2.5\ CH_2Cl_2$	96	68.65 (67.31)	6.95 (6.93)	4.40 (4.00)
CuTODPP **13**	$CuC_{84}H_{108}N_4O_4 \cdot 3\ CH_2Cl_2$	63	66.91 (67.18)	7.30 (7.34)	3.80 (3.60)
AgTPP **14**	$AgC_{44}H_{28}N_4$	74	72.98(73.34)	4.11(3.92)	7.57(7.78)
AgTOMPP **15**	$AgC_{48}H_{36}N_4O_4 \cdot 1.25\ CH_2Cl_2$	57	62.63(62.47)	4.53(4.10)	6.13(5.92)
AgTOBPP **16**	$AgC_{60}H_{60}N_4O_4$	48	74.51(71.42)	6.25(5.99)	5.76(5.55)
AgTOOPP **17**	$AgC_{76}H_{92}N_4O_4 \cdot 0.15\ CH_2Cl_2$	63	73.19(73.39)	7.71(7.47)	4.21(4.50)
AgTODPP **18**	$AgC_{84}H_{108}N_4O_4 \cdot 1.5\ CH_2Cl_2$	52	69.66(69.71)	7.70(7.59)	3.88(3.80)
AuTPP **19**	$[AuC_{44}H_{28}N_4]Cl \cdot 2\ CH_2Cl_2$	16	53.13 (54.43)	3.22 (3.18)	5.50 (5.52)
AuTOMPP **20**	$[AuC_{48}H_{36}N_4O_4]Cl \cdot 2CH_3OH$	10	62.62 (58.34)	4.37 (4.31)	5.34 (5.44)
AuTOBPP **21**	$[AuC_{60}H_{60}N_4O_4]Cl \cdot CH_2Cl_2$	21	60.76 (60.13)	5.10 (5.13)	4.89 (4.60)
AuTOOPP **22**	$[AuC_{76}H_{92}N_4O_4]Cl \cdot CH_2Cl_2$	18	65.08 (64.09)	6.37 (6.57)	4.10 (3.88)
AuTODPP **23**	$[AuC_{84}H_{108}N_4O_4]Cl$	22	67.62 (68.62)	7.18 (7.40)	3.92 (3.81)

[a] Theoretical values are given in parentheses.

Table 7

The mass spectrometric data of metalloporphyrin complexes

Porphyrins	Empirical formula	Formula weight [b]	MS (m/z)
CuTPP **9**	$CuC_{44}H_{28}N_4$	676.27	677.0
CuTOMPP **10**	$CuC_{48}H_{36}N_4O_4$	796.38	797.4
CuTOBPP **11**	$CuC_{60}H_{60}N_4O_4$	964.70	965.6
CuTOOPP **12**	$CuC_{76}H_{92}N_4O_4$	1189.11	1187.0
CuTODPP **13**	$CuC_{84}H_{108}N_4O_4$	1301.32	1303.7
AgTPP **14**	$AgC_{44}H_{28}N_4$	720.6	719.2
AgTOMPP **15**	$AgC_{48}H_{36}N_4O_4$	840.7	841.6
AgTOBPP **16**	$AgC_{60}H_{60}N_4O_4$	1009.0	1010.1
AgTOOPP **17**	$AgC_{76}H_{92}N_4O_4$	1233.4	1233.9
AgTODPP **18**	$AgC_{84}H_{108}N_4O_4$	1345.7	1346.0
AuTPP **19**	$AuC_{44}H_{28}N_4$	809.6	808.9
AuTOMPP **20**	$AuC_{48}H_{36}N_4O_4$	929.8	929.4
AuTOBPP **21**	$AuC_{60}H_{60}N_4O_4$	1098.1	1097.4
AuTOOPP **22**	$AuC_{76}H_{92}N_4O_4$	1322.5	1322.2
AuTODPP **23**	$AuC_{84}H_{108}N_4O_4$	1434.7	1434.9

4.2.3 Free-base porphyrin and metalloporphyrin characterization

The CHN elemental analysis, mass spectrometry, NMR spectroscopy, and IR spectroscopy have been used to confirm the structure of all free-base porphyrins, and metalloporphyrin complexes. The result are summarized in **Table 5 - 7**. The results show that percentage of element, and the molecular ion peak found closely with the theoretical value, which confirmed the structure of all synthesized compounds are the expected structure. Furthermore, the result from IR spectroscopy, free-base porphyrin exhibited the important signal peak of N-H starching and bending vibration in the range from 3,310-3,320 cm^{-1}, and 965-967 cm^{-1}, respectively. Whereas, these two peaks disappeared in the IR spectrum of metalloporphyrin complexes that can be confirmed the metal ion has been coordinated with the porphyrin ligand. In addition, the NMR spectroscopy have been used to confirm the structure of free-base porphyrin. From the ^{13}C NMR spectroscopy, the signal of carbon in porphyrin ring have been found in range 119 -135 ppm, carbon in phenyl ring in range 112 -159 ppm, and carbon in alkyl long-chain in range 13 – 55 ppm. The results of all techniques can confirmed the structure of all free-base porphyrin and metalloporphyrin.

4.2.3.1 CHN elemental analysis

The free-base porphyrin and metalloporphyrin have been characterized by CHN elemental analysis. The data are summarized in **Table 5** and **Table 6**. The elemental analysis data of all synthesized compounds were confirmed the expected structure, and were agreed with theoretical value. However, some synthesized metalloporphyrin complexes have been found synthesis different percentages of carbon, hydrogen, and nitrogen from the theoretical value, due to the trace of solvent in their molecule. The porphyrins have been purified by silica gel column chromatography using hexane, dichloromethane, or methanol as eluent with gradient polarity. After purified the solvent was removed by air-dried. The trapped solvent in the crystal cause a shifted result. Whereas, in case of free-base porphyrin after purification, the solvent has been removed by evaporation so the solvent was completely removed. The results are parallel with theoretical data.

4.2.3.2 Mass spectrometry

Mass spectrometry have been used to confirm the expected structure of free-base porphyrin and metalloporphyrin complexes. The **Figure 54** show

the representative mass spectrum of TOMPP **5**. The mass spectrum displayed the major molecular ion peak $[M+H]^+$ at m/z = 735.4. In addition, other free-base porphyrin exhibited molecular ion peak closely with each the theoretical molecular weight. The fragmentation of free-base porphyrin requires a great deal of energy. Therefore, such fragmentation is not observed to any significant extent. The mass spectrum data of all free-base porphyrins, were displayed in **Table 5**.

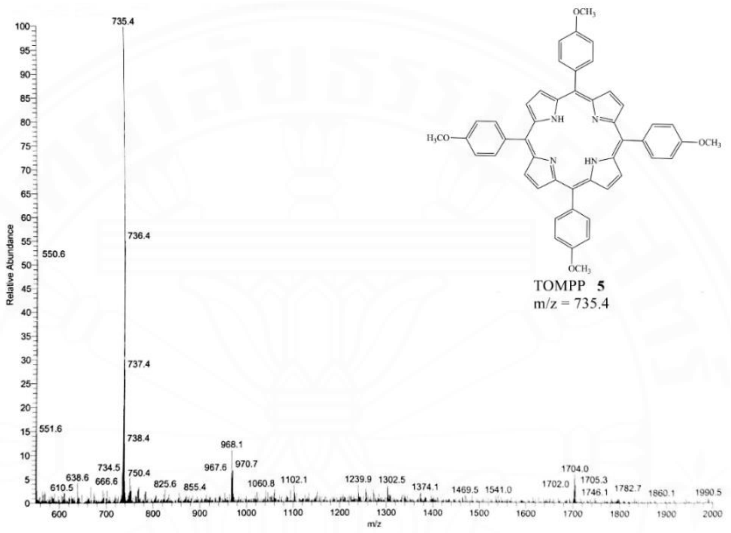

Figure 54 Mass spectrum of TOMPP **5**

Moreover, the mass spectrum data of all metalloporphyrin were displayed in **Table 7**. The CuTOMPP **10**, AgTOMPP **15**, and AuTOMPP **20** were shown as a representative example of mass spectrum of metalloporphyrin complexes (**Figure 55**). This copper(II) porphyrin, silver(II) porphyrin, and gold(III) porphyrin complexes exhibits molecular ion peak $[M+H]^+$ at m/z = 797.4, 841.6, and 929.4, respectively. The mass spectra of CuTOMPP **10** and AgTOMPP **15** have been found the fragmentation peak at m/z = 735.4, represented the losing of copper(II) ion and silver(II) ion. This fragmentation peak can be assigned as TOMPP **5**. The mass spectra of all metalloporphyrin showed very intense molecular ion peaks due to they had high energy from the delocalized electrons in the molecule, which the result similar in free-base porphyrins. The mass spectra have been successfully received to confirm expect corresponding structure of all metalloporphyrin complexes.

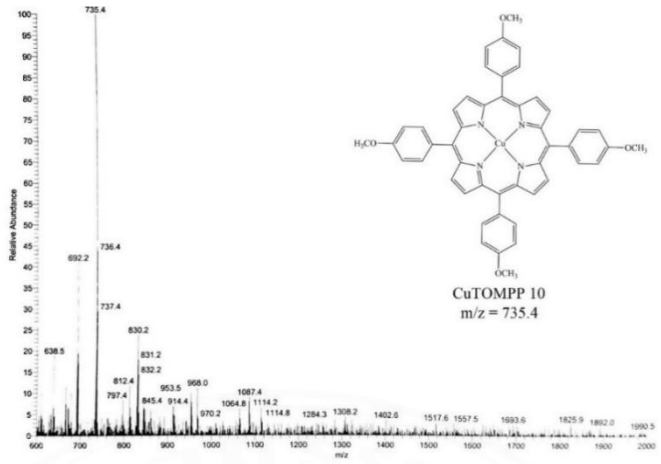

a

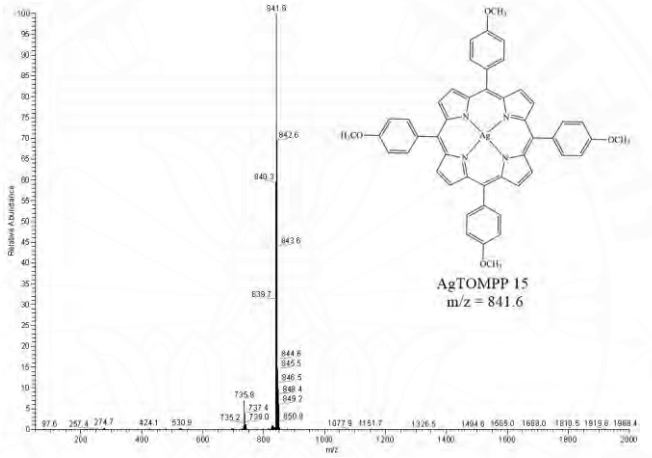

b

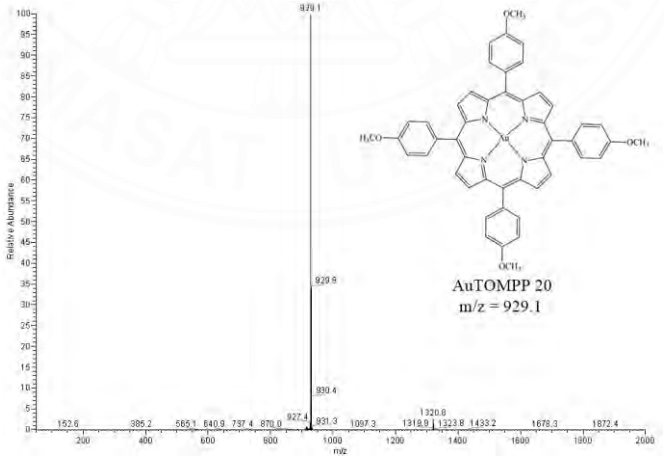

c

Figure 55 Mass spectrum of (a) CuTOMPP **10**, (b) AgTOMPP **15**, and (c) AuTOMPP **20**

4.2.3.3 Nuclear Magnetic Resonance spectroscopy (NMR)

Nuclear magnetic resonance spectroscopy is a spectroscopic technique to observe local magnetic fields around atomic nuclei and have been used to determining the structure of organic compounds. So, the structure of the free-base porphyrin were confirmed by using ^{1}H NMR and ^{13}C NMR spectroscopy. The ^{1}H NMR and ^{13}C NMR spectra of all free-base porphyrins (TPP **4**, TOMPP **5**, TOBPP **6**, TOOPP **7**, and TODPP **8**) have been studied. The spectra of ^{1}H NMR and ^{13}C NMR corresponding to all synthetized free-base porphyrin were obtain in chloroform solvent ($CDCl_3$). The NMR spectral peak have been assigned by comparison with pervious reported [70,73]. The important chemical shift data was concluded in **Table 8**.

The important signal of β-pyrrole protons have found at 8.86 ppm, the phenyl protons in range 8.20 to 8.08 ppm, and 7.77 to 7.21 ppm and the protons in alkyl long-chain in range 0.87 – 4.24 ppm. From the ^{1}H NMR spectrum, the signal of β-pyrrole protons were founded the chemical shift at 8.8 ppm, this result was observed in all free-base porphyrin ^{1}H NMR spectra. The slightly downfield shift from TPP, cause by the deshielding effect. The difference deshielding effect of porphyrins derivative involves with the difference substituent group on phenyl ring. The phenyl protons, at *otho*- and *meta*- position, exhibited signal peak in range from 8.20 to 8.08 and 7.77 to 7.21 ppm, respectively. This similarly results were found in previously reported [32]. The substituted porphyrin derivative show the up field shift of chemical shift value, as a result of *para*-substituent group on the phenyl ring. The substituent groups including –OCH_3, -$O(CH_2)_3CH_3$, -$O(CH_2)_7CH_3$ and –$O(CH_2)_9CH_3$ are electron donating groups, cause the phenyl proton displayed up field chemical shift, due to the shielding effect. From **Table 6** the shielding effect of methoxy group are the lowest, when compared with other long-chain alkyloxy group. The increasing number of carbon in alkyl chain, the shielding effect was increased. The effect of electron donating groups were reported by *Hossein D. et al*. [100]. In addition, the *para*- proton of phenyl ring in TPP had a chemical shift at 7.52 ppm. The proton of *para*-substituent group in TOMPP (-OCH_3) was assigned at 4.10 ppm. The alkyl proton in long-chain (TOOPP and TODPP) were found to be shielded than TOBPP, due to the inductive effect and electron donating of ether group is side chain. The result found in alkyloxybenzaldehyde. The signal of N-H proton were observed in very high field (-2.90 ppm), due to the more shielding effect

of porphyrin ring. The ^{1}H NM spectrum of TOBPP **6** showed in **Figure 56** as a representative example.

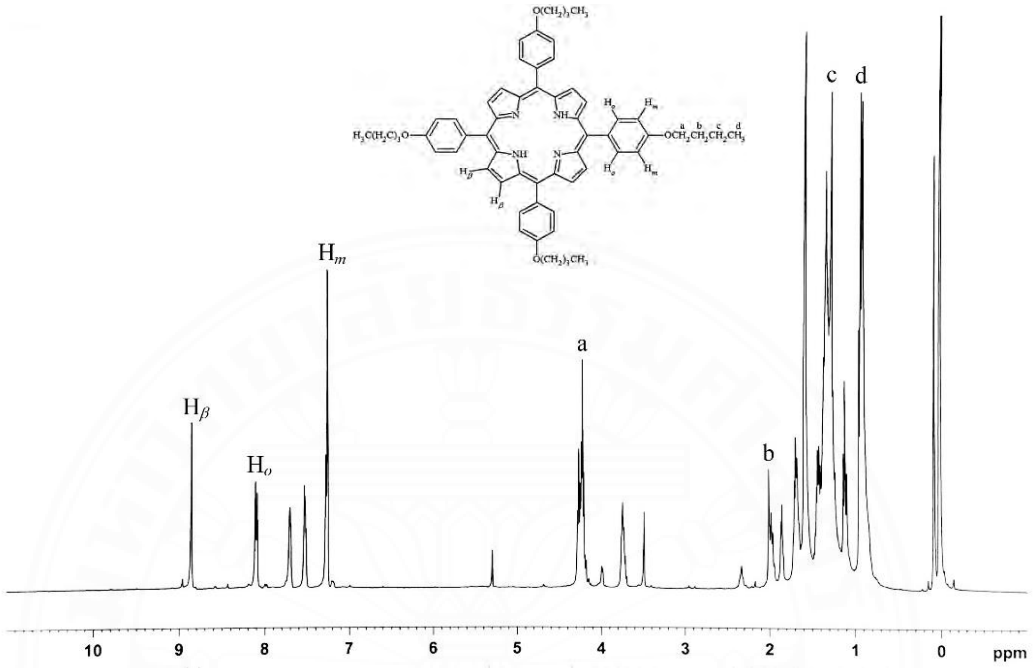

Figure 56 ^{1}H NMR spectrum of TOBPP **6**

The ^{13}C NMR spectrum of TOBPP was shown in **Figure 57** as a representative example, analyzed by using chloroform as solvent. The ^{13}C NMR spectrum of TOBPP was assigned the signal of α-***C***, pyrrole at 135.32 ppm, *β*-***C***, pyrrole at 130.70 ppm and *meso*-***C***, Methane Bridge at 119.70 ppm. The carbons of phenyl ring were obtained the signal at 159.09 (*p**-***C***), 134.74 (*o*-***C***), 128.76 (*p*-***C***) and 112.84 (*m*-***C***) ppm. In addition, the signal of carbon in alkyl long-chain group was displayed in the same range of aldehyde. The similarly result was observed in other free-base porphyrin. The data of ^{13}C NMR of all synthesized porphyrins were concluded in **Table 6**. In metalloporphyrin complexes, the chemical shifts was observed as broad peaks related to ligands information only. The metalloporphyrins were unsuccessful identified due to the paramagnetic properties. Further analysis, including ESR spectroscopy, may be required for studying the information inside into the complexes.

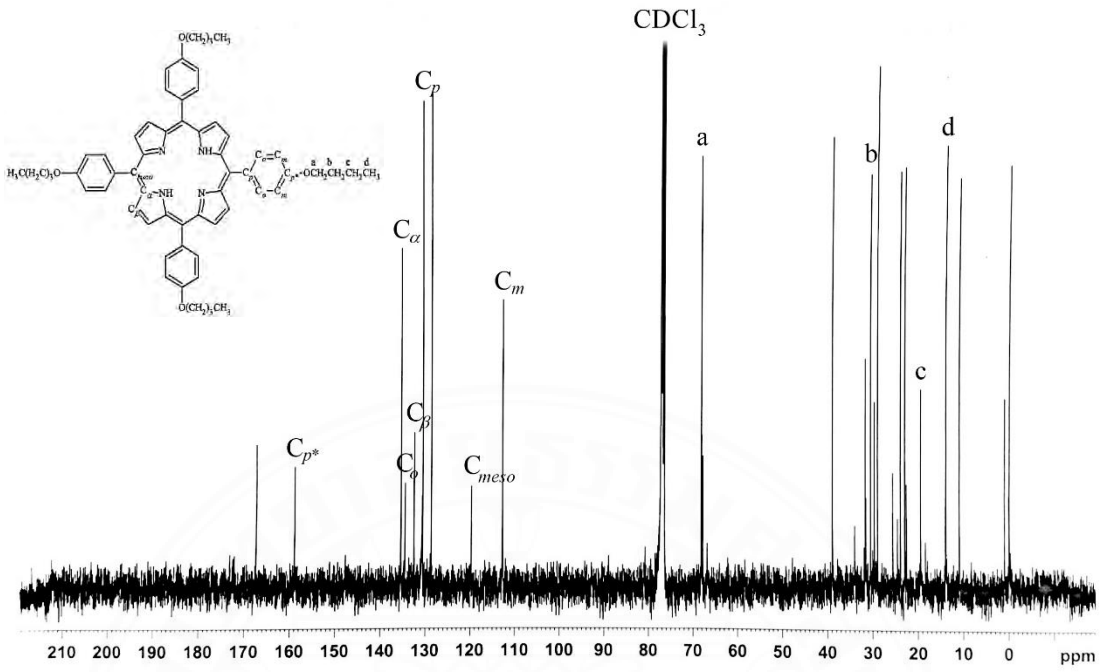

Figure 57 ^{13}C NMR spectrum of TOBPP **6**

Table 8

^{1}H and ^{13}C NMR spectroscopic data for free-base porphyrins

Porphyrins	^{1}H NMR (ppm), proton									
	Pyrrole, *β*-**H**	Phenyl, *o*-***H***	Phenyl, *m*-***H***	Phenyl, *p*-H	OCH_3	OCH_2	OCH_2CH_2	CH_2CH_3	$CH_2CH_2CH_2$	CH_3
TPP **4**	8.85	8.20	7.77	7.52	-	-	-	-	-	-
TOMPP **5**	8.86	8.12	7.29	-	4.10	-	-	-	-	-
TOBPP **6**	8.86	8.11	7.28	-	-	4.24	1.98	1.30	-	0.90
TOOPP **7**	8.86	8.08	7.21	-	-	4.22	1.98	1.30	1.26	0.88
TODPP **8**	8.86	8.08	7.22	-	-	4.22	1.98	1.30	1.26	0.87

Porphyrins	^{13}C NMR (ppm), carbon												
	Phenyl, *p**-***C***	α-***C***	Phenyl, *o*-***C***	*β*-**C**	Phenyl, *p*-***C***	*Meso*-***C***	Phenyl, *m*-***C***	OCH_3	OCH_2	OCH_2CH_2	$CH_2CH_2CH_2$	CH_2CH_3	CH_3
TPP **4**	127.70	-	134.56	131.12	142.22	120.15	126.67	-	-	-	-	-	-
TOMPP **5**	158.75	134.68	133.99	129.97	127.89	118.83	111.44	54.65	-	-	-	-	-
TOBPP **6**	159.09	135.32	134.74	130.70	128.76	119.7	112.84	-	68.14	31.49	-	23.98	13.84
TOOPP **7**	159.07	135.54	134.57	131.78	128.74	119.79	112.82	-	68.45	31.84	29.64, 29.53, 29.45, 26.22, 22.64		14.00
TODPP **8**	159.10	135.51	134.51	130.68	128.76	119.77	112.86	-	68.48	31.88	29.60, 29.55, 29.53, 29.46, 29.28, 26.20, 22.60		13.93

4.2.3.4 Infrared spectroscopy (IR)

IR spectroscopy has been used to characterize all synthesized porphyrin compounds. The IR spectrum were record in KBr disc, and the data were collected in the 4000 - 400 cm^{-1} region. The result were concluded in **Table 9** and **Table 10**. All free-base porphyrin exhibited the important signal peak of N-H starching, and N-H bending vibration in range from 3310-3320 cm^{-1}, and 965-967 cm^{-1}, respectively. However, after coordinated with metal ion. The peak of N-H starching, and N-H bending were disappeared for all metalloporphyrin (**Figure 58**), suggesting the coordinated with metal ions. The similar results were reported by *Zhijie X. et al.* [23] *and Sandeep M. et al*. [101]. That can confirmed, the metal ion (Cu^{2+}, Ag^{2+}, and Au^{3+}) were inserted into the porphyrin ring and replace of hydrogen in pyrrole ring. Furthermore, the signal peak of C-H stretching (long-chain) and C-N stretching in porphyrin ring were showed. The similarly character was found in all porphyrin compounds. When the number of carbon atom in long-chain were increased, the frequency of both signals found to be slightly decreased due to the electronic effect of long-chain substituent. The substituent saturated alkyl chain group exhibited electron delocalize from the para position of the phenyl ring to the electronegativity of the porphyrin. The frequencies were observed downshifts of carbon in alkyl chain substituted group, which related to the interactions intrinsically decrease the bond strength of the molecule [102, 103, 104]. However the signal peak including C=C stretching in phenyl, C-O stretching in alkyl chain and C-H bending in porphyrin of all synthesized porphyrin complexes displayed a small peak shift in IR spectra.

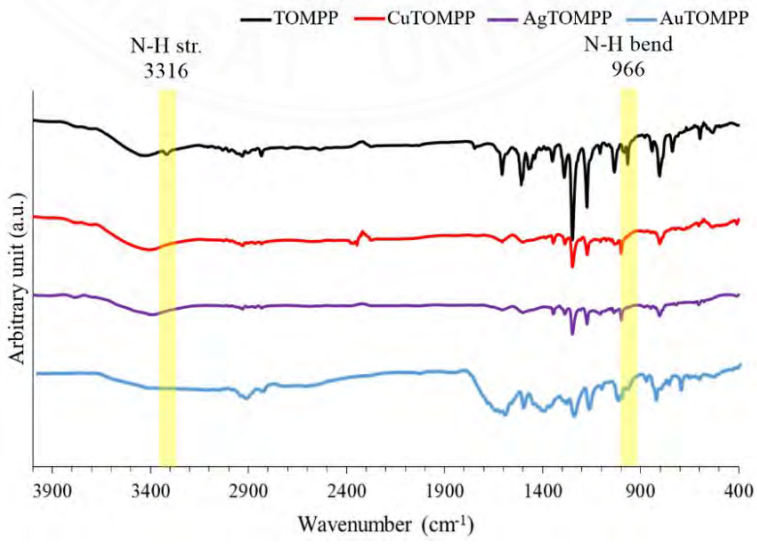

Figure 58 IR spectrum of TOMPP **5**, CuTOMPP **10**, AgTOMPP **15**, and AuTOMPP **20**

Table 9

The IR data of free-base porphyrins

Porphyrins	N-H str. in porphyrin	C-H str. in phenyl and long-chain	C=C str. in phenyl	C-N str. in porphyrin	C-O str. in long-chain	N-H bend in porphyrin	C-H bend in porphyrin
TPP **4**	3310	-	1597, 1469	1212	-	966	794
TOMPP **5**	3316	2931, 2834	1607, 1509	1248	1174	966	804
TOBPP **6**	3320	2931, 2868	1607, 1509	1245	1174	966	802
TOOPP **7**	3318	2927, 2852	1607, 1509	1243	1174	965	804
TODPP **8**	3317	2924, 2852	1607, 1509	1244	1174	967	803

Table 10

The IR data of metalloporphyrin complexes

Porphyrins	C-H str. in phenyl and long-chain	C=C str. in phenyl	C-N str. in porphyrin	C-O str. in long-chain	C-H bend in porphyrin
CuTPP **9**	-	1600, 1441	1345	-	793
CuTOMPP **10**	2929, 2835	1607, 1499	1248	1173	804
CuTOBPP **11**	2930, 2869	1607, 1502	1246	1174	799
CuTOOPP **12**	2926, 2852	1607, 1506	1244	1174	804
CuTODPP **13**	2923, 2852	1607, 1504	1246	1174	800
AgTPP **14**	-	1598, 1442	1243	-	794
AgTOMPP **15**	2934, 2833	1606, 1522	1250	1176	807
AgTOBPP **16**	2932, 2834	1609, 1516	1248	1176	805
AgTOOPP **17**	2931, 2943	1609, 1516	1247	1177	805
AgTODPP **18**	2928, 2845	1609, 1517	1249	1175	805
AuTPP **19**	-	1620, 1488	1358	-	807
AuTOMPP **20**	2927, 2837	1600, 1508	1290	1174	831
AuTOBPP **21**	2955, 2931	1603, 1503	1278	1175	801
AuTOOPP **22**	2924, 2853	1604, 1503	1287	1176	801
AuTODPP **23**	2916, 2856	1604, 1505	1287	1178	801

4.3 UV-visible spectroscopy

The electronic properties of free-base porphyrins and metalloporphyrin complexes have been studied by using UV-visible spectroscopy. The absorption spectra of all compounds were recorded in dichloromethane at concentration 1×10^{-4} mol/dm^3 at room temperature. The absorption data and molar extinction coefficient (ε) of all synthesized porphyrins are summarized in **Table 11**. The absorption spectrum of free-base porphyrin compounds are shown in **Figure 59**.

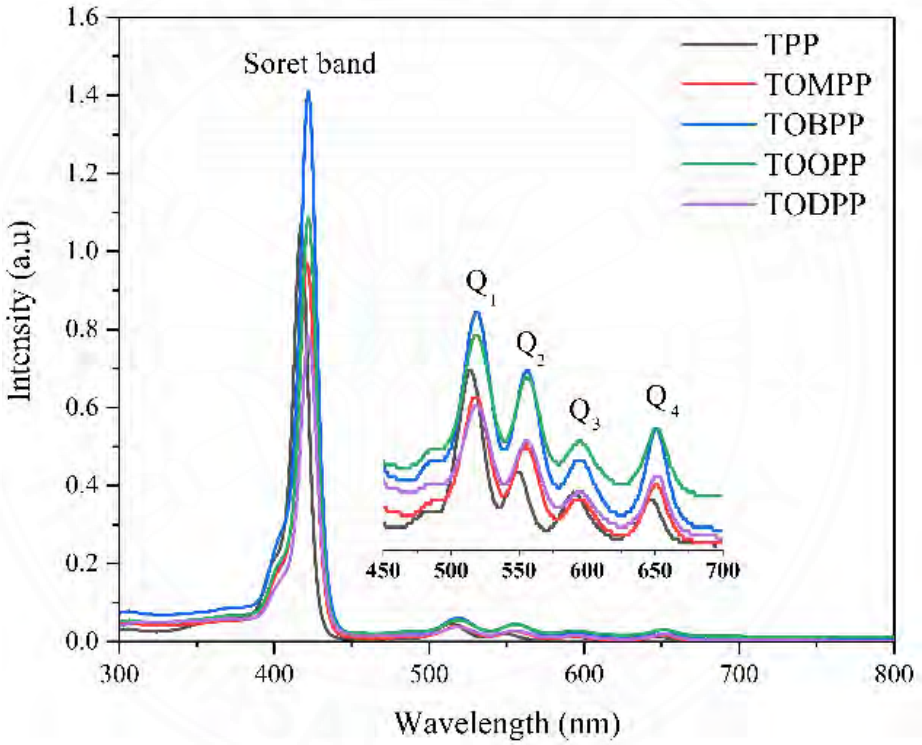

Figure 59 UV-Vis absorption spectra of free-base porphyrin in CH_2Cl_2

The absorption spectra of all free-base porphyrins exhibited a strong absorption (Soret band) at 417-422 nm and four weak absorptions (Q band) in the range 500-700 nm, which can be assigned to π⟶π* electronic transitions. The very intense Soret band assigned to the S0⟶S2 transition, which can be found in a shorter wavelength. On the other hand, the Q bands assigned to the S0⟶S1 transitions, appear in longer-wavelength [105]. According to UV-Vis spectroscopy data, the S band and Q

band of the para-substituted porphyrin move to a small redshift about 4 – 10 nm when compared with TPP due to the steric hindrance and electron effect [106]. According to the experimental results, the Soret band of para-substituent porphyrin was found as a weak absorption peak, resulted from the substituted phenyl and the porphyrin rings were not in the same plane, then the conjugated effect between the phenyl substitutes and porphyrin ring was relatively weak.

All metalloporphyrin exhibited the characteristic absorption spectrum as Soret band with one Q band. The Soret band and Q-band are in range 400 – 430 nm, and 510 – 550 nm, respectively, which can be assigned to $\pi \longrightarrow \pi^*$ electronic transitions. The very intense Soret band assigned to the S0⟶S2 transition is found at shorter wavelengths. In contrast, the Q bands assigned to the S0⟶S1 transitions appear at longer wavelengths [107]. When compared with the corresponding free-base porphyrin λ_{max} of the gold(III) porphyrin complexes are lower than other metalloporphyrin complexes. The shift to the lower λ_{max} of the gold(III) porphyrin complexes is a result of both the trivalent ion of gold and also a result of the greater stability of the gold(III) porphyrin. This results are related to the reported by *Thomas et. al.* [109]. Both of Soret band Q band of metalloporphyrin complexes containing the alkyl long chain moved to a small red-shift compared with MTPP (M = Cu, Ag, and Au). The red shifting of the absorption band is usually an indicator of mixing with the intramolecular charge-transfer character in $\pi \longrightarrow \pi^*$ electronic transitions [108]. Similar results were found in free-base porphyrin. As the experimental results, the functional groups have no effect on the changes in the UV-Vis absorption of complexes due to the para-substituted of porphyrin as the similar electronegativity (electron-donating) moved slightly toward a short wavelength. The absorption spectrum of TOMPP **5**, CuTOMPP **10**, AgTOMPP **15** and AuTOMPP **20** are shown in **Figure 60** for a comparison.

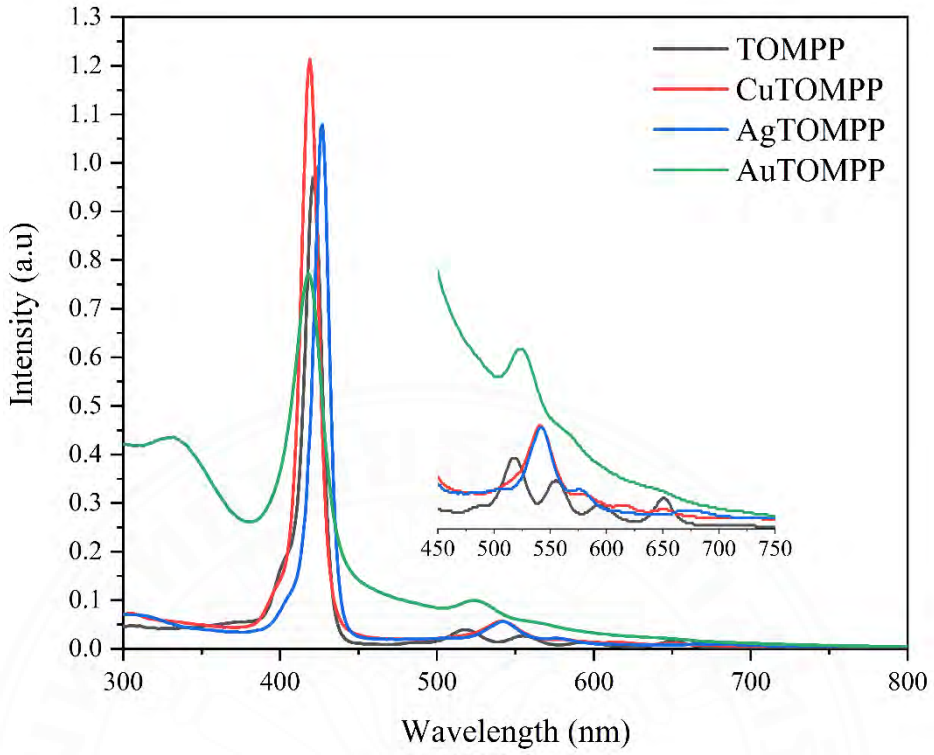

Figure 60 The UV-Vis absorption spectra of TOMPP **5**, CuTOMPP **10**, AgTOMPP **15**, and AuTOMPP **20** in CH_2Cl_2

Comparing each free-base porphyrin with their metalloporphyrin the UV-visible absorption spectra changed significantly. After coordinated with metal ion (Cu^{2+}, Ag^{2+}, and Au^{3+}) some Q bands were absent due to the increasing of $\pi \longrightarrow \pi^*$ electronic transitions energy resulting from interaction from d-orbital electron of metal ion and macrocycle π-band system of porphyrin ring. Furthermore, the symmetry of porphyrin ring was change after H-atom in central hole were substituted by metal ion, therefore their absorption spectra were changed to different extent. In addition, the Soret band of metalloporphyrin compared with the corresponding free-base porphyrin show blue shift (except silver(II) porphyrin complexes exhibited red shift). The generally of the in-plane metalloporphyrin due to the atomic orbital of their metal center in-plane can be overlap more strongly with HOMO energy level of ligand but the LUMO energy level didn't change. So the energy gaps between the excited and ground states increase the result were future discus in chapter 4.8 [110].

Table 11

The absorption data of free-base porphyrin and metalloporphyrin

Porphyrins	Dichloromethane[a]				
	S band (nm)	Q band (nm), $\varepsilon(M^{-1}cm^{-1})$			
		Q_1	Q_2	Q_3	Q_4
TPP **4**	417	514, 14122	548, 6140	590, 4605	649, 3991
TOMPP **5**	421	518, 11941	555, 8266	595, 3980	650, 5205
TOBPP **6**	422	519, 22955	556, 17310	595, 8655	651, 11665
TOOPP **7**	422	519, 30953	556, 24762	595, 15757	651, 17446
TODPP **8**	422	519, 20817	556, 15758	595, 8439	652, 10689
CuTPP **9**	415	-	540, 13863	-	-
CuTOMPP **10**	419	-	541, 18914	-	-
CuTOBPP **11**	419	-	541, 24599	-	-
CuTOOPP **12**	419	-	541, 29084	-	-
CuTODPP **13**	419	-	541, 14292	-	-
AgTPP **14**	425	-	542, 257779	-	-
AgTOMPP **15**	427	-	542, 229512	-	-
AgTOBPP **16**	427	-	543, 250043	-	-
AgTOOPP **17**	430	-	544, 229723	-	-
AgTODPP **18**	430	-	544,259617	-	-
AuTPP **19**	406	519, 1800	-	-	-
AuTOMPP **20**	418	521, 3960	-	-	-
AuTOBPP **21**	419	525, 2840	-	-	-
AuTOOPP **22**	419	526, 2480	-	-	-
AuTODPP **23**	419	526, 2120	-	-	-

[a] All solution were prepared in the concentration of 1×10^{-4} mol/L, in CH_2Cl_2 (n =3, %RSD ≤ 1.6) and measured in the wavelength range of 200-800 nm.

4.4 Fluorescence spectroscopy

The electronic properties of all porphyrin compounds have been investigated by using fluorescence spectroscopy. The emission spectrum of porphyrin compounds was recorded in dichloromethane at concentration 1×10^{-4} mol/dm^3 at room temperature. The excitation and emission wavelength are summarized in **Table 12**. The emission spectra of free-base ligands in CH_2Cl_2 was shown in **Figure 61**.

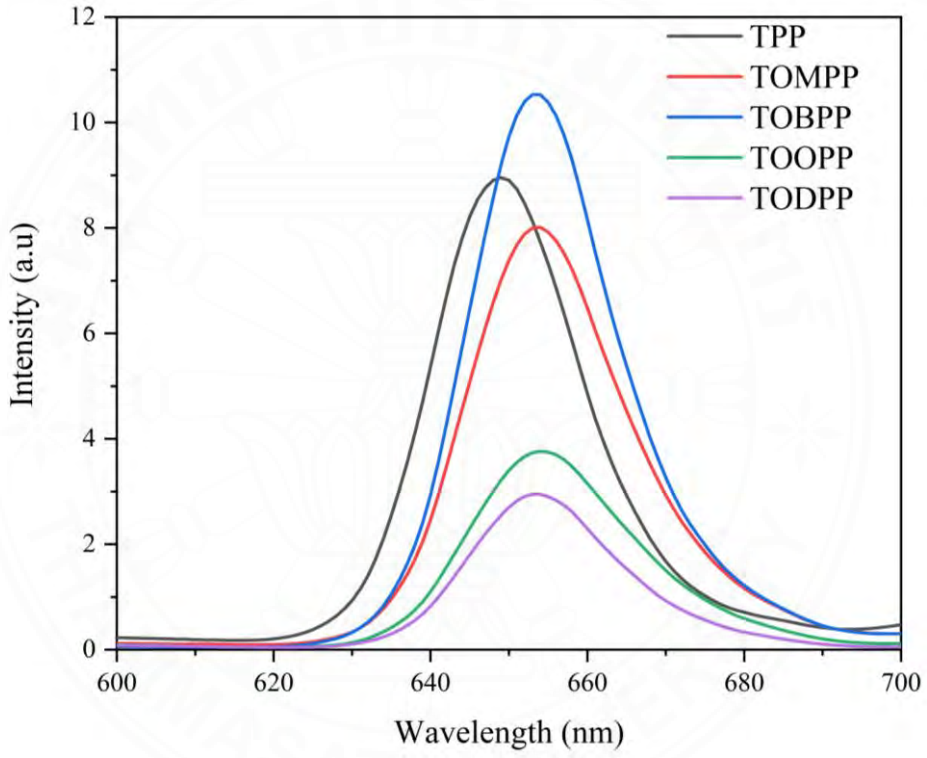

Figure 61 Emission spectra of free-base porphyrin in CH_2Cl_2

When excited free-base porphyrin TOMPP at 534 nm it referred to the Q1 band of absorption spectra. The electron has been excited from the ground state to the excited state from S0 to S1 transition. After vibrational relaxation, the electron released the energy as fluorescence and back to the ground state. The different of emission wavelength and absorption wavelength can be referred to the relative energy gap of the porphyrin compound, the ground state S0 referred to HOMO energy level and the excited state S1 referred to LUMO level. Furthermore, the emission spectra of

metalloporphyrin complexes have been observed. The fluorescence of all copper(II) and silver(II) porphyrins observed around 604 - 609 nm, when excited at 556 nm, except the CuTOMPP 10 (exhibit fluorescence spectra at 654 nm). That can be observed in the emission spectra similarly with the free-base porphyrin TOMPP 5, suggested the loosing of Cu^{2+}. However, the emission spectra show a slight difference, due to the electron-donating ability of alkoxy in the chain [25]. The copper(II) and silver(II) porphyrins exhibited the blue shift when compared with free-base porphyrin caused by the interaction between the metal ion in the porphyrinic substituents and the solvent molecules [111]. The gold(III) porphyrin complexes were excited at each λ_{max}, and exhibited two or three emission peaks appeared in the range 500 – 900 nm. The results revealed that the energy gap of metalloporphyrin was higher than the corresponding free-base porphyrin. The emission data of all compounds were summarized in **Table 12**.

The energy difference between HOMO and LUMO was calculated in terms of the relative energy gap (E_{gap}). In previous report, Jayant Dharma suggest the equation for calculate the energy gab from intersection of UV-vis absorption (Q band) referred to the energy for exciting electrons from ground state to excited state and fluorescence emission referred to energy that electron release from excited state back to ground state following this equation [141].

$$E_{gap} = hc/\lambda$$

When h = Planks constant (6.626 x 10-34 J.s)

c = speed of light (3.0 x 108 ms^{-1})

1 eV = 1.602 x 10^{-19} J

The energy gap of free-base porphyrin has been calculated. The estimated energy gaps of free-base porphyrin were obtained at 1.90 eV this result is in agreement with the previous work by *Ventura B. et. al*. They reported the energy gab of TPP at 1.92 eV [113]. Moreover, the energy gap of metalloporphyrin has been tried to calculate. The copper porphyrin is around 2.16 – 2.17 eV, silver porphyrin is around 2.13 – 2.14 eV, and gold porphyrin is around 2.00 - 2.20 eV, respectively.

Table 12

Emission spectra data of free-base porphyrin and metalloporphyrin

Porphyrins	Dichloromethane	
	Absorption wavelength (nm)	Emission wavelength (nm)
TPP **4**	529	649
TOMPP **5**	534	654
TOBPP **6**	534	654
TOOPP **7**	534	654
TODPP **8**	534	654
CuTPP **9**	556	605
CuTOMPP **10**	556	654
CuTOBPP **11**	556	604
CuTOOPP **12**	556	605
CuTODPP **13**	556	605
AgTPP **14**	557	605
AgTOMPP **15**	557	607
AgTOBPP **16**	557	604
AgTOOPP **17**	557	605
AgTODPP **18**	557	609
AuTPP **19**	406	611, 650, 824
AuTOMPP **20**	418	503, 718, 848
AuTOBPP **21**	419	658, 858
AuTOOPP **22**	419	659, 854
AuTODPP **23**	419	657, 854

4.5 Electron paramagnetic resonance spectroscopy (EPR)

The magnetic properties and oxidation state of metal ion in metalloporphyrin complexes have been studied by using Electron Paramagnetic Resonance (EPR) spectroscopy. The electron paramagnetic resonance of all synthesized porphyrins have been investigated by diluting each porphyrin in dichloromethane at concentration 0.01 M. The EPR signal of porphyrin compounds are generated by interaction of the delocalized π electrons of the porphyrin ring or the unpaired electron of the metal ion with the magnetic field. In previous report *Minbo L. et al.* reported the EPR signal of TPP by measured in solid sample [106]. This EPR spectrum exhibited nine distinct lines due to the coupling between the porphyrin's nitrogen atoms. However, in this studied all free-base porphyrin didn't found the EPR signal

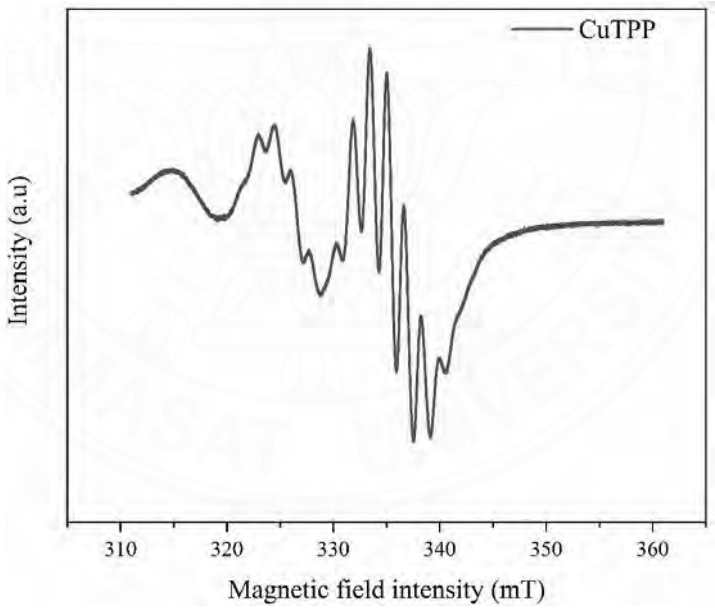

Figure 62 The EPR spectrum of CuTPP **9**

However, The EPR spectra of the copper(II) porphyrin exhibited strong metal properties. There was a significant characteristic about the EPR signals generated by Cu^{2+}. The EPR signal of copper(II) porphyrin complexes are in agree with previous reported [114]. The Cu exhibit a strong paramagnetic property because its d electron

orbit is unpaired. The intensity of the EPR signals generated by Cu^{2+} was enough to cover up the free radicals' signals. Therefore, only the EPR signals of the metal ion could be measured in the EPR spectrum of CuTPP [115]. Other copper(II) porphyrin complexes show similarly result with CuTPP. In the specific case of the CuTPP derivatives are a consequence of the paramagnetic condition of the molecule due to the odd electron in the Cu(II) ion. It is well known that in the case of paramagnetic complexes the interactions of the generated magnetic field and the odd electron are considerably large and lead to chemical displacements much bigger that those associated to the ring current of the aromatic macrocycle. EPR spectra were measured by means of solution of copper(II) porphyrin complexes in dichloromethane at 300 K in anisotropic state (shown in **Figure 62**). A rich super hyperfine structure in the ESR spectra, especially for CuTOBPP **10** is due to the copper(II) coordination with nitrogen ligand atoms in the square planar geometry. A very poor base line in the spectrum of CuTPP 9 inhibits correct determination of g⊥. The g// and g⊥are ranged from 2.0799 to 2.0898 and 2.0034 to 2.0086, respectively.

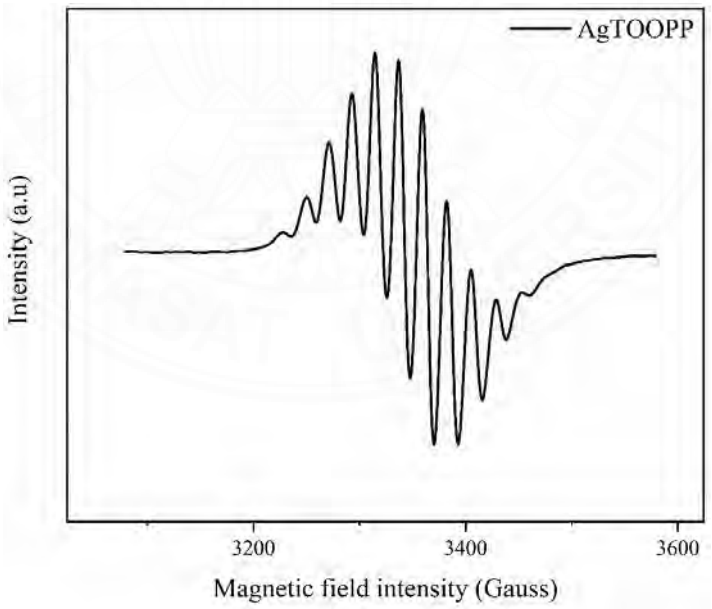

Figure 63 The EPR spectrum of AgTOOPP **17**

The electron spin resonance spectroscopy (ESR) is a good tool to investigate silver porphyrin complexes, providing valuable information about oxidation state, ligand type, and symmetry. **Figure 63** show the representative EPR spectrum of silver(II) porphyrin complexes. The pattern is symmetric one consisting of eleven line with an equal separation around 24 Gauss. Because of the overlapping of the two set of nine nitrogen hyperfine lines, where each set corresponds to hyperfine interactions between the unpaired electron and four equivalent nitrogen atoms with a nuclear spin. The splitting into two sets is due to the hyperfine interaction with the spin of one-half of the silver nucleus. The g values are calculated at 2.0357 – 2.0573. These values are in agreement with reported by *Fritz K. et al.* [116]. The appearance of the ESR signal from silver porphyrin complexes show that they have an unpaired electron with high density on Ag. This result confirmed that all of the silver(II) porphyrin must contained silver(II) ion in the structure [117].

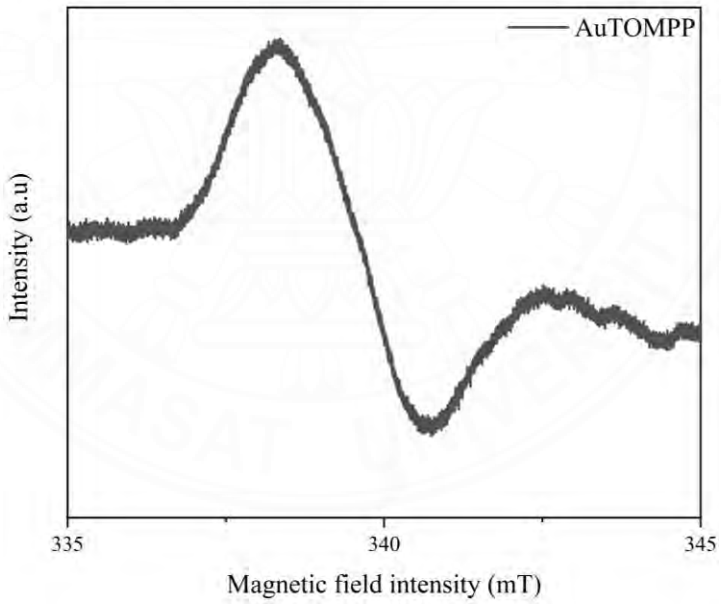

Figure 64 The EPR spectrum of AuTOMPP **20**

All gold(III) porphyrin complexes were observed the sharp signal peak centered around 337 mT. The g value are calculated at 2.0015 which is assigned to the gold(III) porphyrin π-anion radical. This g value are in agreement with previous report for gold(III) tetraarylporphyrin derivatives [118]. In previous work by Adolfo M. et al

reported the broad signal at g = 2.065. The large g value (2.065) is the characteristic of the metal-centered radical of Au(II) phthalocyanine [119]. The broad signal of AuTOMPP **20** was shown as the representative example for all Au(III) porphyrins. The absence of the broad peak due to the Au(II) species clearly indicates that the site of electron transfer changes from the metal to the porphyrin ligand confirmed by the DFT calculation. The result shows that at the ground state the electron was delocalized in *para*-substituent group (**Figure 73**).

Table 13

g value of metalloporphyrin complexes

Porphyrins	g value	
	$g_{\parallel}$	$g_{\perp}$
CuTPP **9**	2.0802	2.0086
CuTOMPP **10**	2.0799	2.0082
CuTOBPP **11**	2.0849	2.0061
CuTOOPP **12**	2.0851	2.0060
CuTODPP **13**	2.0898	2.0034
AgTPP **14**	2.05622	
AgTOMPP **15**	2.03583	
AgTOBPP **16**	2.03715	
AgTOOPP **17**	2.05716	
AgTODPP **18**	2.05739	
AuTPP **19**	2.000204	
AuTOMPP **20**	2.001453	
AuTOBPP **21**	2.001981	
AuTOOPP **22**	2.002187	
AuTODPP **23**	2.002360	

4.6 Electrochemical properties

The electrochemical properties of free-base porphyrin and the metalloporphyrin complexes were investigated by cyclic voltammetry. The glassy carbon was used as working electrode, platinum rod was used as counter electrode, while Ag/AgCl electrode was used as reference electrode. The cyclic voltammetry data were obtained at scan rate 100 mV/s. All porphyrin solution were of 1 x 10^{-4} M concentrations containing 1.0 M $TBAPF_6$ in dichloromethane. The total volume of samples solution was 25 cm^3. The peak of ferrocene has been found at 0.47 V. The electrochemical data are conclude in **Table 14**. The **Figure 65** shown the cyclic voltammogram of TPP **4** as representative.

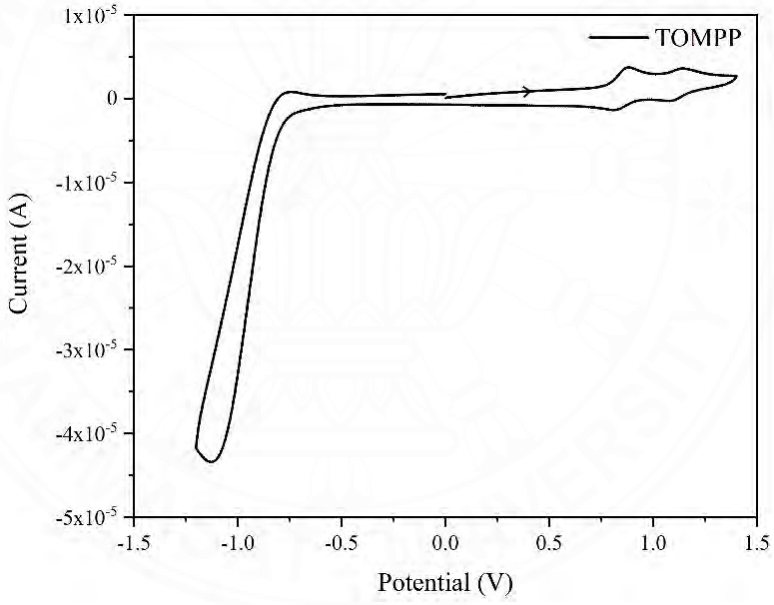

Figure 65 Cyclic voltammograms of TOMPP **5**

The tetraphenylporphyrin (TPP **4**) showed two reversible on electron oxidation of the porphyrin ring at $E_{1/2}$ = 0.97 V and $E_{1/2}$ = 1.30 V and one electron quasi-reversible reduction at $E_{1/2}$ = -0.94 V. There oxidation potential were in agreement with previous report by *Rainer et al.* [120]. Other free-base porphyrin exhibited the redox behavior similar the TPP **4** with oxidation potential at $E_{1/2}$ = 0.85 V and $E_{1/2}$ = 1.10 V and reduction potential at $E_{1/2}$ = -0.94 V.

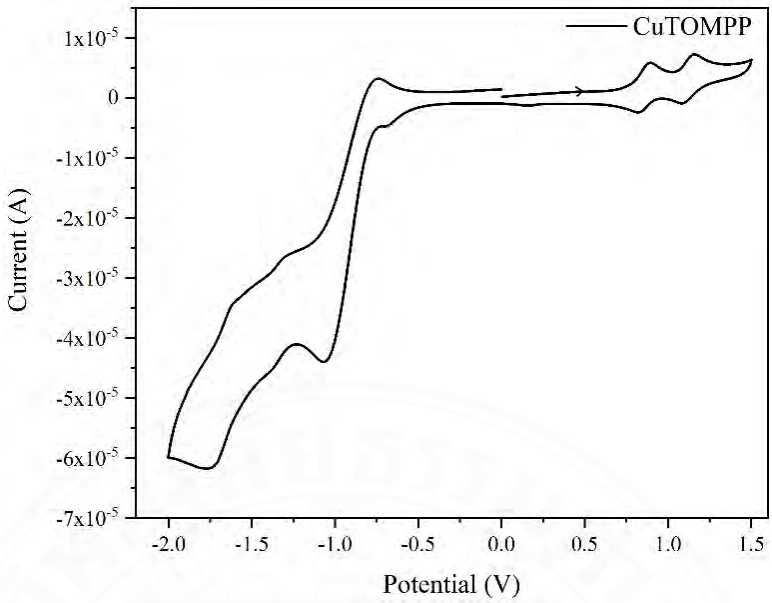

Figure 66 Cyclic voltammograms of CuTOMPP **10**

All copper(II) porphyrin complexes show two reversible one-electron oxidation and a quasi-reversible reduction. The measured half-wave potentials for one- and two-electron oxidations agree well with literature values [121, 122] and they can be assigned to the oxidation potential of CuTPP [123] as; [CuTPP] →$[CuTPP]^{+}$ →$[CuTPP]^{2+}$. The copper(II) tetraphenylporphyrin complex (CuTPP **9**) shows two reversible one-electron oxidation occurring at +0.97 V and +1.35 V and exhibited a quasi-reversible reduction at -0.88 V. Other copper(II) porphyrin exhibited the redox behavior similar the CuTPP **9** with oxidation potential at $E_{1/2}$ = 0.82 – 0.86 V and $E_{1/2}$ = 1.12 – 1.27 V and reduction potential at $E_{1/2}$ = -0.89 – -0.94 V.

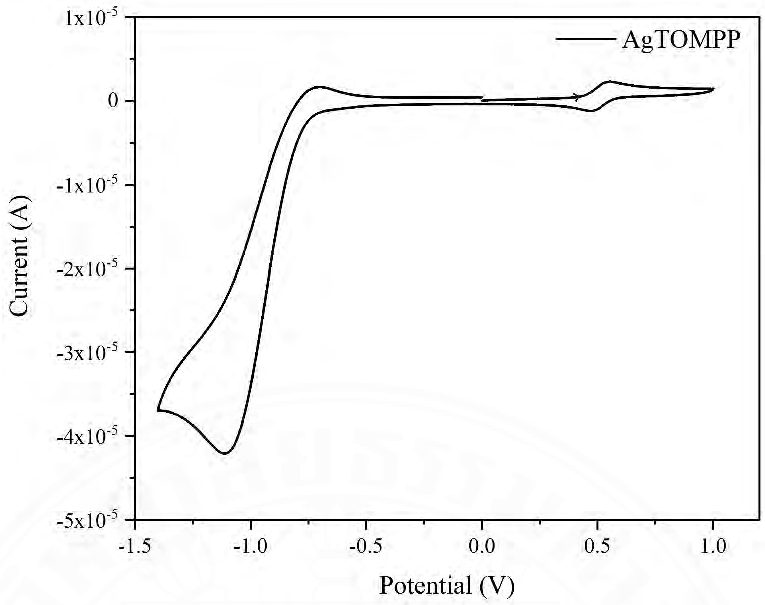

Figure 67 Cyclic voltammograms of AgTOMPP **15**

The redox behavior of silver(II) porphyrin complexes have been studied. All silver(II) porphyrin complexes show one reversible one-electron oxidation and a quasi-reversible reduction. The oxidation of the silver(II) porphyrin complexes is accomplished at lower potential $E_{1/2}$ = 0.46 - 0.57 V [124], and the reduction were founded at -0.90 to -0.94 V. The oxidation and reduction potential of silver(II) porphyrin involves the Ag(II)/Ag(III) transition and reversible Ag(II)/Ag(I) process [125, 126].

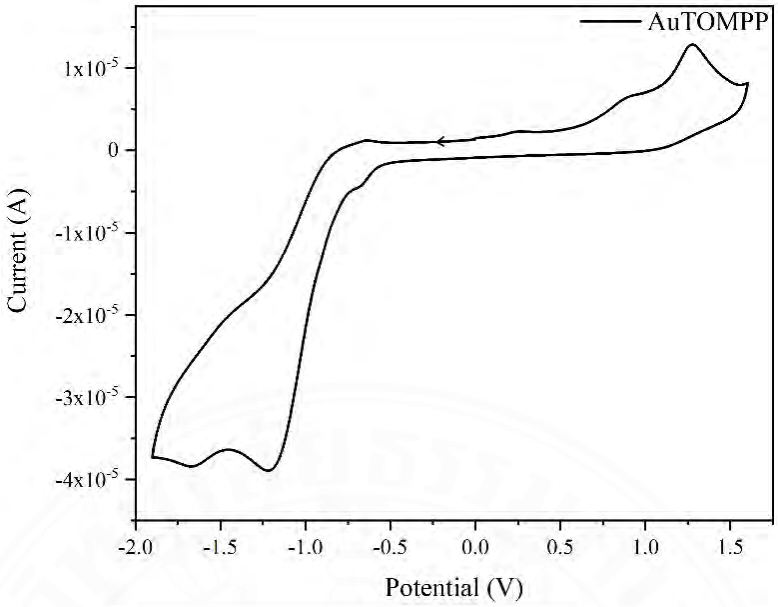

Figure 68 Cyclic voltammogram of AuTOMPP **20**

The first and second reduction peak of gold(III) porphyrin complexes have been reported [118, 128, 129]. The cyclic voltammogram of AuTPP is characterized by the reduction peak at -0.66, -1.20 and -1.60 V [131]. The electron donating group shift the reduction potential negatively. Other gold(III) porphyrin complexes exhibited two irreversible reduction peak (-0.6 and -1.2V). Whereas, AuTOMPP show three reduction peak at -0.66, -1.20 and -1.63V. The reduction potential are assigned as coming from a stepwise reduction of the porphyrin ring leading to π-anion radical. In general, the oxidation potential of gold(III) porphyrin were not observed when scan from oxidation to reduction potential, however the oxidation peak have been observed when scan start at reduction to oxidation potential. All gold(III) porphyrin complexes exhibited the two irreversible oxidation peak at 0.7 and 1.2V, respectively (AuTPP **19** show oxidation potential at 0.35 and 1.17V).

After coordination with metal ion the oxidation of silver(II) porphyrin exhibited at lower potential than the oxidation of corresponding copper(II) and gold(III) porphyrin complexes. Because the oxidation product of the copper(II) porphyrin is copper(II) complexes with oxidized porphyrin ligand ($[Cu(II)L]^+$) whereas, oxidation product of silver(II) porphyrin is $[Ag(III)L]^+$. This result are the general trend observed within Periodic Table. An electron is more readily removed from a larger ion of

identical change and valence electron configuration. In case of the porphyrin ligand presenting the donor atoms in a rigidly fixed arrangement, the larger Ag(III) ion presumably also fits better than the very small Cu(III) ion. The oxidation to the +3 ion generates a small ion and, in the square-planar coordination environment of the porphyrin, very stable d^8 ion that is isoelectronic to the equally stable platinum(II) porphyrin complex.

When compared in each group of synthesized porphyrin. The first oxidation potential (formation of the radical cation) is decreasing linearly with respect to the increasing of long-chain alkoxyl substituent on *para*-substitution (**Table 13**). The substituent is an electrons donating group, thus leading to an increase electrons density in the complexes, therefore to a decreasing oxidation potential. Most of complexes show a second oxidation wave (formation of the di-cation) at more positive than the first one by ca. 0.38 to 0.41 V, in agreement with the previous reports [132]. Interestingly, the reversibility of the reduction potential of all complexes were enhanced by adding electrons to the electrochemical cell as an internal standard of potential, reduction potential -0.86 to -0.93 V, suggesting some mediation of heterogeneous electrons transfer to the platinum electrode. This reduction would correspond to the formation of the porphyrin compounds.

Potential difference between the first ring oxidation and first ring reduction of synthesized porphyrin compounds can related to the energy gap HOMO and LUMO of the porphyrin π-ring system. The result are show in **Table 14.** After coordinated the energy gap of the corresponding porphyrin are decrease follow CuL > AgL > AuL (L = TPP, TOMPP, TOBPP, TOOPP, and TODPP) due to the electron density of metal ion. The result was confirmed by DFT calculation (chapter 4.8).

Table 14

The electrochemical data of free-base porphyrins and metalloporphyrin complexes

Porphyrins	Oxidation Potential (V)		ΔOx	Reduction Potential (V)			$\Delta E_{1/2}$ (V)
	I	II		I	II	III	
TPP **4**	0.97	1.32	0.35	-0.94	-	-	1.90
TOMPP **5**	0.85	1.13	0.28	-0.95	-	-	1.80
TOBPP **6**	0.85	1.11	0.26	-0.95	-	-	1.79
TOOPP **7**	0.84	1.11	0.27	-0.95	-	-	1.79
TODPP **8**	0.84	1.12	0.28	-0.94	-	-	1.77
CuTPP **9**	0.97	1.34	0.37	-0.87	-	-	1.84
CuTOMPP **10**	0.88	1.12	0.24	-0.90	-	-	1.78
CuTOBPP **11**	0.84	1.28	0.44	-0.91	-	-	1.75
CuTOOPP **12**	0.84	1.29	0.45	-0.93	-	-	1.77
CuTODPP **13**	0.85	1.27	0.42	-0.91	-	-	1.76
AgTPP **14**	0.57	-	-	-0.90	-	-	1.46
AgTOMPP **15**	0.51	-	-	-0.92	-	-	1.43
AgTOBPP **16**	0.47	-	-	-0.94	-	-	1.40
AgTOOPP **17**	0.47	-	-	-0.91	-	-	1.37
AgTODPP **18**	0.46	-	-	-0.91	-	-	1.37
AuTPP **19**	0.36	1.17	0.81	-0.66	-1.20	-1.60	1.02
AuTOMPP **20**	0.75	1.25	0.50	-0.66	-1.20	-1.63	1.37
AuTOBPP **21**	0.71	1.25	0.54	-0.66	-1.20	-	1.35
AuTOOPP **22**	0.74	1.27	0.53	-0.66	-1.21	-	1.40
AuTODPP **23**	0.75	1.26	0.51	-0.66	-1.22	-	1.41

4.7 Thermal gravimetric analysis (TGA)

The thermal behavior of free-base porphyrin and metalloporphyrin complexes has been investigated by using Thermal gravimetric analysis (TGA). The free-base porphyrins and metalloporphyrin complexes were determined the decomposition temperature by using the thermal gravimetric analysis (TGA) under nitrogen atmosphere with a heating rate of 10°C/min, from 10 – 900°C. **Figure 69** show the representative TGA curve of TOBPP **6**.

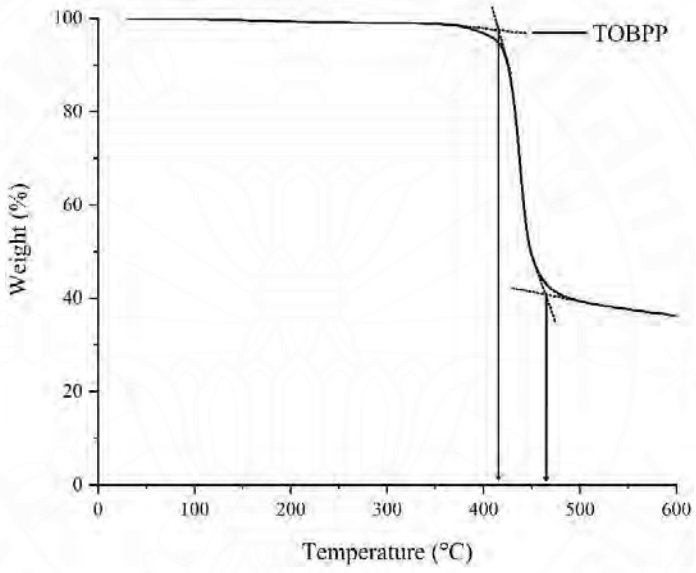

Figure 69 Thermal gravimetric analysis (TGA) curves of TOBPP **6**

The TOBPP **6** exhibited one step decomposition at 415°C referred to the porphyrin ring decomposition with weight loss more than 60%. Other free-base porphyrin showed the porphyrin ring decomposition between 398 – 426°C. While, the TOMPP **5** exhibited two step weight loss at 407°C and 465°C, respectively. The decomposition step at 407°C is attributed to remove the methoxy group in the structure, while at 465°C is porphyrin ring decomposition. This result have been reported by *Xiuhua W. et al.* [133]. The observation decomposition temperature of the free-base porphyrin showed higher thermal stability in rang for 398 – 426°C due to the condensation of pyrrole with alkyl chain aldehyde will afford the remarkable stability

to porphyrin. The trend of decomposition temperature of free-base porphyrin found in the range of TODPP > TOOPP > TOBPP > TPP, related with the increasing number of carbon in alkyl long chain on the para- position of the phenyl ring. However, the metalloporphyrin didn't follow this trend.

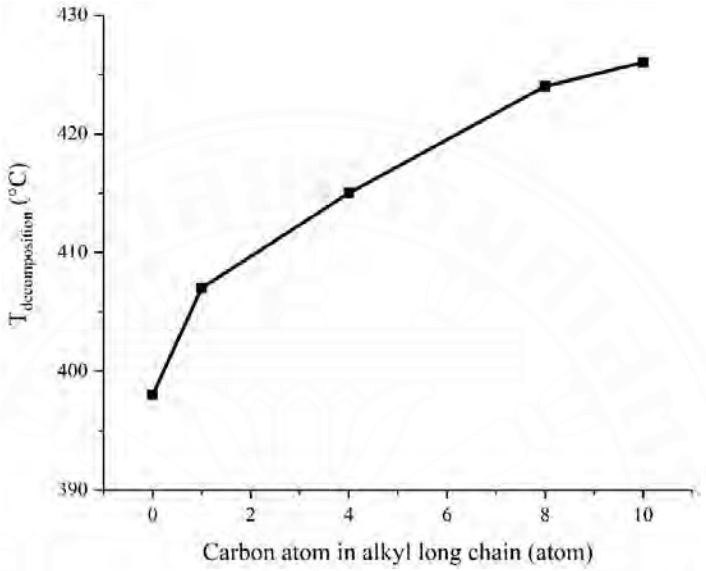

Figure 70 Correlation between decomposition temperatures with number of carbon in alkyl chain porphyrins

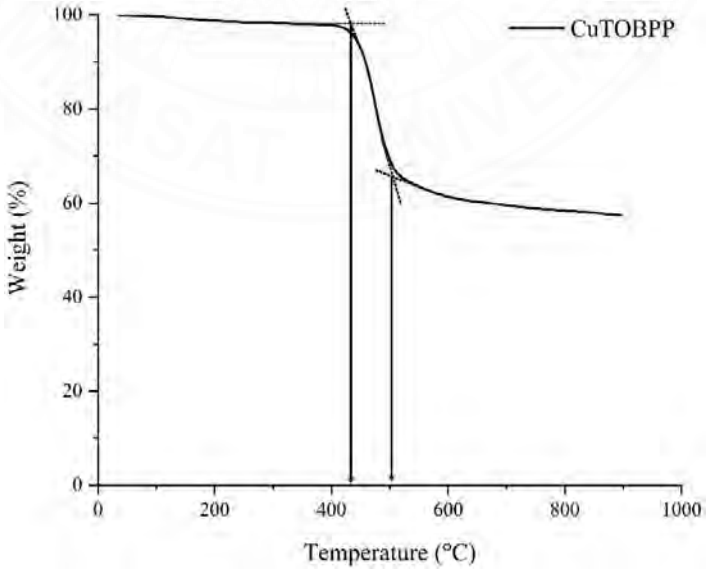

Figure 71 Thermal gravimetric analysis (TGA) curves of CuTOBPP **11**

The copper(II) porphyrin complexes exhibited one step decomposition. The decomposition process in range 459 – 535°C, which corresponding weight loss of 40 – 80% is consistent with the porphyrin ring decomposition. Some of copper(II) porphrin complexes found small weight loss of 3 – 6% at 100 – 200°C which is referred to the elimination of small molecule impurity. The representative TGA curve of CuTOBPP **11** was shown in **Figure 7**1.

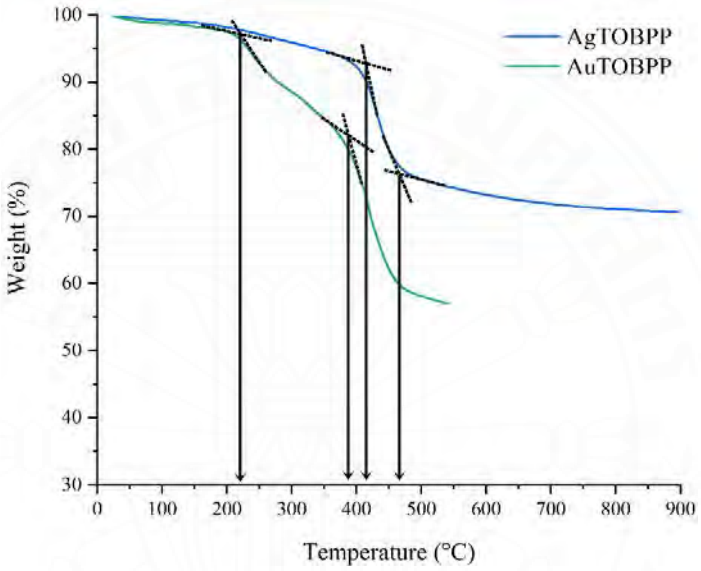

Figure 72 Thermal gravimetric analysis (TGA) curves of AgTOBPP **16** and AuTOBPP **21**

The **Figure 72** shows the representative TGA curve of silver(II) and gold(III) porphyrin complexes. The AgTOBPP exhibited quasi two-step decomposition and AuTOBPP exhibited two-step decomposition due to the final product of silver and gold porphyrin complexes are silver(I) oxide and gold(I) oxide. When increasing the temperature to around 250°C the gold and silver porphyrin pull the electron from the *meso*-substituent group resulted in a weak bond between the *meso*-substituent group and the porphyrin ring when the temperature increase around 250°C the bond between the *meso*-substituent group and porphyrin core was broken. After that temperature increase to 400°C the porphyrin ring has been broken. It is referred to porphyrin decomposition process. A similar result was found in another metalloporphyrin. The

decomposition temperature and weight loss with the corresponding temperature are summarized in **Table 15**.

The metalloporphyrin complexes (copper and silver) exhibited the greatest thermal stability than the corresponding free-base porphyrin due to the copper(II) and silver(II) ion in porphyrin ligand were obtained that a shorter bond distance between the diametrically opposed carbon atom in *meso*-position than pure ligand included the bond distance between metal ion and nitrogen in complexes structure and the copper(II) ion and silver(II) ion fitted in the porphyrin ligand center hole. This result reveals that coordination with metal ions has been improved thermal stability in metalloporphyrin complexes. However, the gold(III) porphyrin complexes exhibited lower thermal stability than the corresponding metalloporphyrin complexes and free-base porphyrin ligand due to the dealkylation process in range 270 - 350°C. In addition, the decomposition temperature of metalloporphyrin shown that the MTPP (M = Cu, Ag, and Au) exhibited the higher thermal stability than other corresponding metalloporphyrin derivatives due to the electron delocalized in porphyrin ring increases the stability of MTPP complexes. Whereas, the electrons of other porphyrin ligands were delocalized in the alkyl group resulted in decreasing the stability of the porphyrin ring. So the decomposition temperature of other porphyrin ligand is lower than TPP. This result will be confirmed by DFT calculation. Furthermore, it could be explained by structure packing. A previous report by *Hunter C.A. et al.* explained the crystalline structure and corresponding stability of metalloporphyrin has appeared from the electrostatic and weak interaction [142]. For all compounds, an evident feature in the crystalline phase is their successive layer arrangements. The crystal structure of porphyrin is from the interaction of proton from phenyl ring group of one molecule with the π system of other. For example, in the case of TPP, the interaction between TPP molecules is from two acidic nitrogen atoms of basic character, and the other is the conjugation system of π electron. This π system interacts with C–H bonds of the phenyl groups of the nearest porphyrin molecule. However, the metalloporphyrin acidic nitrogen atoms are not present due to four nitrogen atoms in the porphyrin ring have been coordinated with the metal ions. Whereas, the π system remains to interact with C-H bonds of the phenyl group of the nearest molecule. These interactions are electrostatic, according to the short distance ($d_{N–H}$) between the nitrogen atoms of one molecule and the protons of the phenyl group of another molecule. A previous work by *Minerva G. et al.* reported

the correlation of temperature of melting with the crystallographic distances. When N–H and interplanar distances are closer, it needs more energy to break the lattice until the melting process occurs. However, in the case of metalloporphyrin, the decomposition temperature is inverse with the $d_{N\text{-}H}$. If $d_{N\text{-}H}$ is short the decomposition temperature is high [112]. The current study, the decomposition temperature of MTPP is higher than other corresponding metalloporphyrins, due to the chain substituents. It can be hindered the packing of porphyrin, and make the distance ($d_{N–H}$) between the porphyrin ring longer than MTPP. As a result of the decomposition temperature of the other metalloporphyrins are lower than MTPP.

Table 15

Decomposition temperatures of free-base porphyrins, and metalloporphyrin complexes

Porphyrins	Stage I		Stage II	
	T_{decomp}/°C	Weight loss/%	T_{decomp}/°C	Weight loss/%
TPP **4** [112]	-	-	398	74.4
TOMPP **5** [133]	407	18.7	465	81.6
TOBPP **6**	-	-	415	60.1
TOOPP **7**	-	-	424	71.5
TODPP **8**	-	-	426	72.1
CuTPP **9**	-	-	535	88.2
CuTOMPP **10**	-	-	459	49.2
CuTOBPP **11**	-	-	475	42.7
CuTOOPP **12**	-	-	469	54.6
CuTODPP **13**	-	-	467	49.3
AgTPP **14**	-	-	540	37.6
AgTOMPP **15**	-	-	546	39.5
AgTOBPP **16**	-	-	432	29.2
AgTOOPP **17**	-	-	434	64.0
AgTODPP **18**	-	-	432	60.3
AuTPP **19**	350	5.0	475	20.0
AuTOMPP **20**	330	13.0	414	41.0
AuTOBPP **21**	276	18.0	404	58.0
AuTOOPP **22**	270	18.0	412	58.0
AuTODPP **23**	273	18.0	407	57.0

4.8 DFT calculation

To explore the electronic structure of the tetraphenylporphyrin derivatives containing different *meso*-substituent groups (phenyl, methoxyphenyl, butyloxyphenyl, octyloxyphenyl, and dectyloxyphenyl) and metal (copper, silver, and gold) complexes, density functional theory (DFT) calculations were performed at the B3LYP method with 6-31G, and GenECP 6d basic set for C, H, N, and O atoms and LANL2DZ for the Cu, Ag, and Au atoms level in the Gaussian 09 program [134, 135]. The optimization structure of TPP revealed the planar conformation of the porphyrin core. However, the saddled conformation have been found in the other free-base porphyrin derivative. The MTPP (M = Cu, Ag, and Au) also showed a planar structure similar to free ligand. Whereas, the metalloporphyrin derivative exhibited the saddled structure similarly to each free-base porphyrin. The optimization structure of MTOMPP (M = H_2, Cu, Ag, and Au) are shown in **Figure 73** as representative. The *meso*-phenyl groups were shown to be angled with respect to the mean plan in range 60° - 70°.

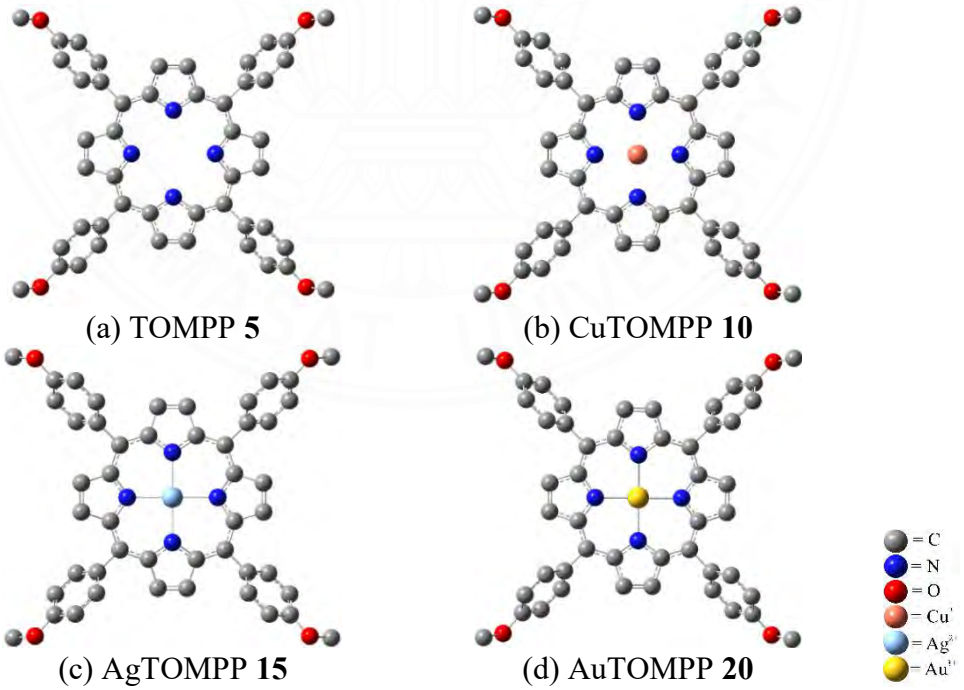

Figure 73 DFT optimization structure of (a) TOMPP **5**, (b) CuTOMPP **10**, (c) AgTOMPP **15**, (d) AuTOMPP **20** analogue calculated using B3LYP/6-31G and LANL2DZ *in vacuo*

The electron density map of free-base porphyrins and metalloporphyrin complexes have been studied. The electron densities of HOMO and HOMO-1 are mainly distributed on the porphyrin ring and could be characterized as porphyrin π-orbitals. The electron contribution from phenyl ring of TPP were not observed in HOMO orbitals (HOMO to HOMO-3). However, the electrons delocalized in p-orbital of free-base porphyrin derivatives (TOMPP, TOBPP, TOOPP, and TODPP) have been discovered in the frontier side HOMO-2 orbital. Whereas, LUMO orbital (LUMO to LUMO+2) exhibited atomic contribution localized over the π*-orbitals of the porphyrin ring. The electron contribution on phenyl substituent group was observed in LUMO+3. The representative frontier molecular orbitals of free-base porphyrin (TOMPP) are shown in **Figure 74**.

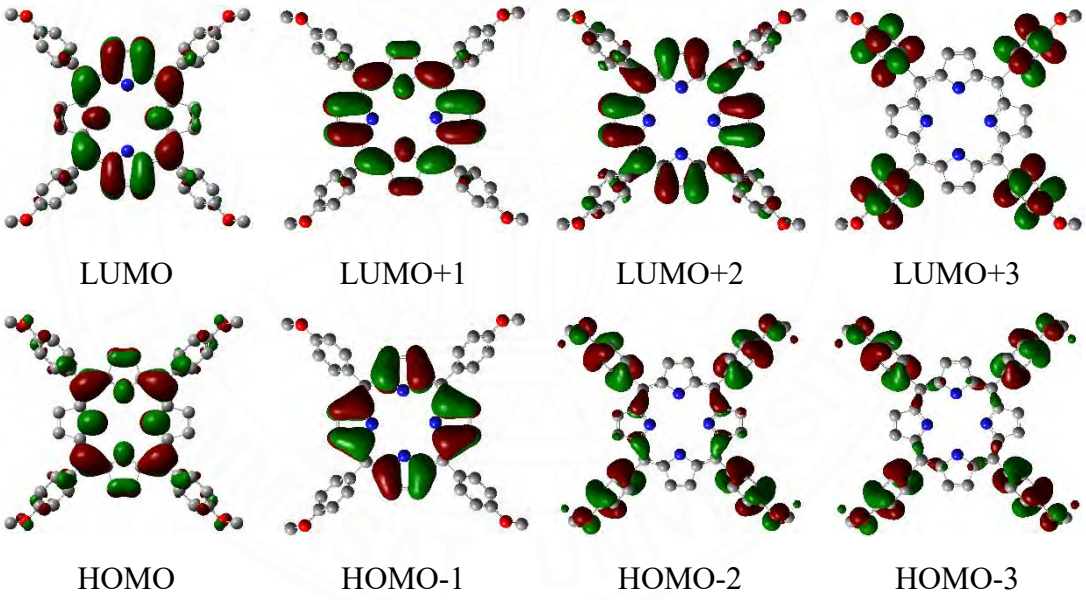

Figure 74 Frontier molecular orbitals of TOMPP **5** calculated using B3LYP/6-31G *in vacuo*

In case of metalloporphyrin complexes, the MTPP (M = Cu, Ag, and Au) have been found electron densities of HOMO (HOMO to HOMO-3) distribution on porphyrin ring and characterized as porphyrin π-orbitals similarly in free-base TPP. Moreover, the electron contribution from d-orbital of metal ion was observed in HOMO orbital (CuTPP observed in HOMO-2 orbital). While the electron densities of LUMO

(LUMO to LUMO+2) are mainly distributed on porphyrin ring and can be assigned as porphyrin π*-orbitals. Other metalloporphyrin derivatives show the electron distribution on para-substituent group in HOMO orbitals (HOMO to HOMO-2). On the other hand, LUMO and LUMO+1 exhibited atomic contributions localized over π*-orbitals of the porphyrin ring.

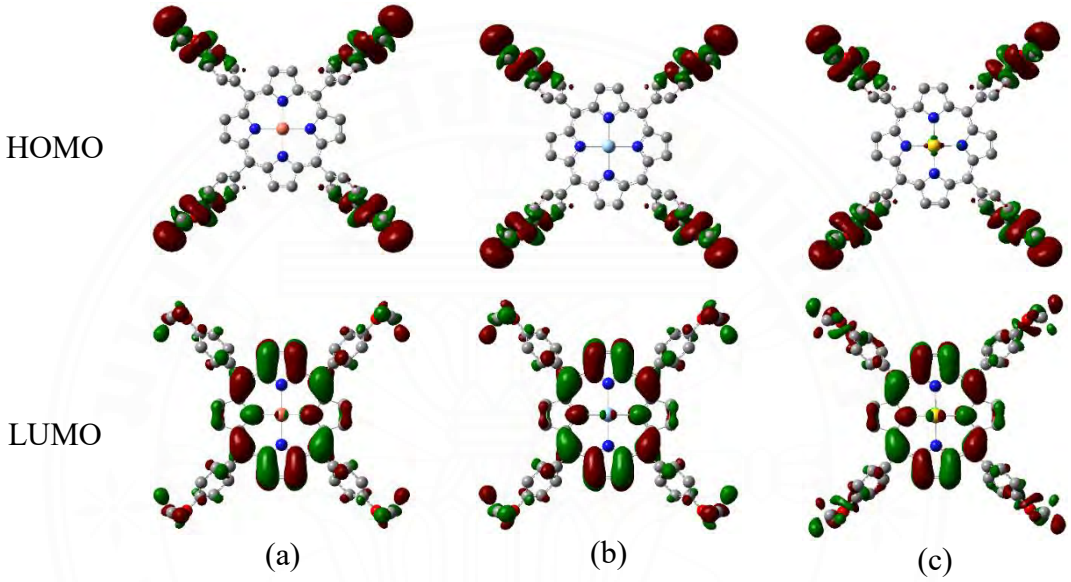

Figure 75 Frontier molecular orbitals of (a) CuTOMPP **10**, (b) AgTOMPP **15**, and (c) AuTOMPP **20** calculated using B3LYP/6-31G and LANL2DZ *in vacuo*

The HOMO and LUMO energy level of free-base porphyrins and metalloporphyrin complexes have been calculated and summarized in **Table 16**. **Figure 76**(a) show the HOMO and LUMO energy level of free-base porphyrins. The TPP has been found HOMO energy level at -4.91 eV, and LUMO at -2.20 eV. While the HOMO and LUMO energy level of other porphyrin derivative are range -4.60 eV and -2.00 eV, respectively. The result revealed that the TPP exhibited higher energy band gap than other free-base porphyin. This result explanted that the porphyrin derivative (TOMPP, TOBPP, TOOPP, and TODPP) exhibited the red shift in absorption spectra due to the smaller band gap than TPP. Similar results were also found in metalloporphyrin complexes. The MTPP exhibited the lowest HOMO and LUMO energy level than other corresponding

metalloporphyrin similar with free-base porphyrin. However, the trend of HOMO and LUMO energy level are follow: MTPP < MTOMPP < MTOBPP < MTOOPP < MTODPP (M = H_2, Cu, Ag, and Au). This trend are explain the first ring redox potential (**Table 14**). Furthermore, after coordinated with metal ion the energy band gap of porphyrin compounds have been decrease compared with the corresponding free-base porphyrin follow by CuL > AgL > AuL (L = TPP, TOMPP, TOBPP, TOOPP, and TODPP). This trend were explained in electrochemical studied of metalloporphyrin (**Table 14**). The energy level diagram of MTOMPP (M = H_2, Cu, Ag, and Au) is show in **Figure 76**(b) for the representative energy level diagram.

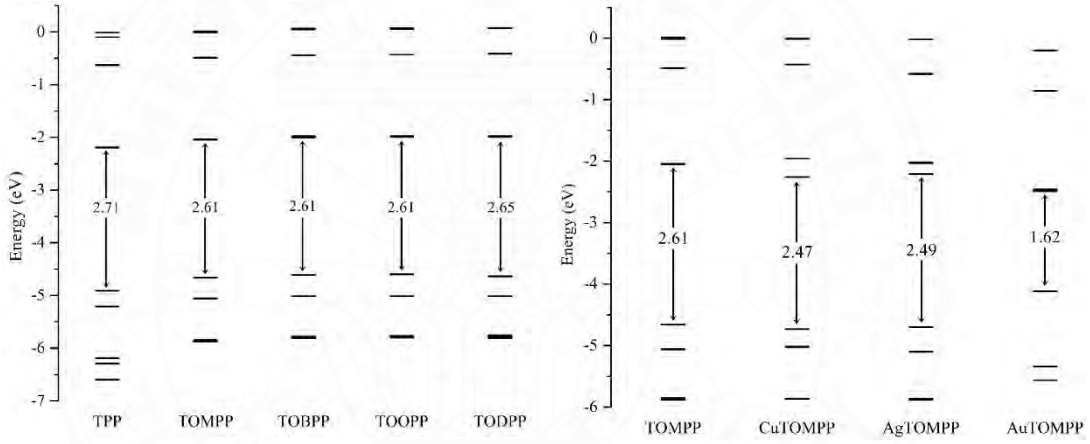

Figure 76 Calculated HOMO and LUMO energy level of (a) free-base porphyrin and (b) MTOMPP (M = H_2, Cu, Ag, and Au) *in vacuo* from DFT calculations at the B3LYP/6-31G, and GenECP 6d and LANL2DZ level of theory

Table 16

Calculated HOMO and LUMO energy level of free-base porphyrin and metalloporphyrin *in vacuo* from DFT calculations at the B3LYP/6-31G, GenECP 6d and LANL2DZ level of theory

Porphyrins	Molecular orbital (#)	Energy (eV)	Band gap energy (eV)
TPP **4**	LUMO (162)	-2.20	2.71
	HOMO (161)	-4.91	
TOMPP **5**	LUMO (194)	-2.05	2.61
	HOMO (193)	-4.66	
TOBPP **6**	LUMO (242)	-2.00	2.61
	HOMO (241)	-4.61	
TOOPP **7**	LUMO (306)	-1.99	2.61
	HOMO (305)	-4.60	
TODPP **8**	LUMO (338)	-1.99	2.65
	HOMO (337)	-4.64	
CuTPP **9**	LUMO (171)	-2.41	2.57
	HOMO (170)	-4.98	
CuTOMPP **10**	LUMO (203)	-2.26	2.47
	HOMO (202)	-4.73	
CuTOBPP **11**	LUMO (251)	-2.23	2.50
	HOMO (250)	-4.73	
CuTOOPP **12**	LUMO (315)	-2.20	2.47
	HOMO (314)	-4.67	
CuTODPP **13**	LUMO (347)	-2.21	2.50
	HOMO (346)	-4.71	
AgTPP **14**	LUMO (171)	-2.36	2.59
	HOMO (170)	-4.95	
AgTOMPP **15**	LUMO (203)	-2.21	2.49
	HOMO (202)	-4.70	
AgTOBPP **16**	LUMO (251)	-2.19	2.50
	HOMO (250)	-4.69	

Table 16

Calculated HOMO and LUMO energy level of free-base porphyrin and metalloporphyrin *in vacuo* from DFT calculations at the B3LYP/6-31G, GenECP 6d and LANL2DZ level of theory (cont.)

Porphyrins	Molecular orbital (#)	Energy (eV)	Band gap energy (eV)
AgTOOPP **17**	LUMO (315)	-2.15	2.49
	HOMO (314)	-4.64	
AgTODPP **18**	LUMO (347)	-2.16	2.51
	HOMO (346)	-4.67	
AuTPP **19**	LUMO (179)	-2.66	1.61
	HOMO (178)	-4.27	
AuTOMPP **20**	LUMO (211)	-2.49	1.62
	HOMO (210)	-4.11	
AuTOBPP **21**	LUMO (259)	-2.48	1.61
	HOMO (258)	-4.09	
AuTOOPP **22**	LUMO (323)	-2.42	1.65
	HOMO (322)	-4.07	
AuTODP **23**	LUMO (355)	-2.44	1.65
	HOMO (354)	-4.09	

4.9 Biological activity

One of the most interesting applications of porphyrin compounds is biological activity, especially antibacterial and anticancer activity. The antibacterial activity has been studied using the disc diffusion method. The representatives for gram-positive and gram-negative bacteria are *Staphylococcus aureus* and *Escherichia coli*, respectively. The porphyrin solution was dissolved in DMSO to obtain a concentration of 10 mg/L. The antibacterial screening data indicate that both metalloporphyrin complexes (copper and silver) are more potent antibacterial against than free-base porphyrin, compared to the corresponding porphyrin ligands. The CuTOMPP **15** and AgTODPP **19** exhibited more effective antibacterial activity than other complexes. Moreover, the minimum inhibitory concentration (MIC) and the minimum bactericidal concentration (MBC) of metalloporphyrin complexes have been investigated. All copper(II) porphyrin complexes show MIC value of *S. aureus* as 320 ppm, *E. coli* as 160 ppm and MBC value of both bacterial as 640 ppm. In case of silver porphyrin complexes MIC value of *S. aureus* as 320 ppm, *E. coli* as 160 ppm, MBC value of *S. aureus* as 640 ppm, *E. coli* as 160 ppm.

The most interesting application of gold porphyrin complexes is anticancer. Started by Chi-Ming in 2003 try to modified five different types of gold porphyrin complex and gold 1a (AuTPP) and gold 1c (AuTOMPP) are showed the lower IC_{50} value than cisplatin. Currently, the cytotoxicity of porphyrin compounds have been studied by MTT assay using SKBR3 and MCF7 cell line as cancer cell. All sample were dissolved in 1%DMSO at concentration 150, 100, 50, and 25 μM. For the SKBR3, the CuTOBPP show the low IC_{50} at 25.22 μM. In case of Au(III) porphyrin complexes, the cytotoxicity were effected in MCF7 cell lines. At the same concentration, AuTPP and AuTOMPP showed the most prominent anticancer activity with lower cell viability than other compounds with IC_{50} value 4.30 μM and 25.35 μM, respectively. Furthermore, the cytotoxicity on normal cell (LLC-MK2) have been investigated. All metalloporphyrin complexes exhibited non-cytotoxicity in LLC-MK2 cell lines in all studied concentration (25 – 150 μM in 1%DMSO) with cell viability more than 70 %.

4.9.1 Antibacterial activity

The antibacterial activity of free-base porphyrin and metalloporphyrin (copper and silver) complexes has been investigated using disc diffusion method [73]. The *Staphylococcus aureus* (ATCC 25923) and *Escherichia coli* (ATCC 25922) were used as testing bacterial representatives for gram-positive and gram-negative bacteria, respectively. The penicillin was used as positive control and DMSO solvent was used for control experiments, which DMSO had no discernible biological effect. The antibacterial potential of all samples are summarized in **Table 17**, as the diameter of the inhibition zone. The results reveal that all free-base porphyrin, metalloporphyrin (copper and silver) complexes were found to be active against both *Staphylococcus aureus* (ATCC 25923) and *Escherichia coli* (ATCC 25922), also the inhibition zone was greater than the control solvent (DMSO).

Table 17
Antibacterial screening data of free-base porphyrin and metalloporphyrin complexes

Porphyrins	*Staphylococcus aureus*	*Escherichia coli*
	Inhibition zone (mm)	Inhibition zone (mm)
TPP **4**	7.5	6.5
TOMPP **5**	8.0	6.5
TOBPP **6**	6.8	6.5
TOOPP **7**	7.5	6.5
TODPP **8**	7.3	6.5
CuTPP **9**	13.0	6.5
CuTOMPP **10**	14.0	8.0
CuTOBPP **11**	8.0	6.5
CuTOOPP **12**	10.5	7.3
CuTODPP **13**	9.0	8.5
AgTPP **14**	7.5	7.5
AgTOMPP **15**	7.5	7.5
AgTOBPP **16**	11.5	10.0
AgTOOPP **17**	11.5	11.4
AgTODPP **18**	12.5	11.5
DMSO	6.8	6.5
Penicillin	12.5	8.0

In case of free-base porphyrin, the TOMPP 5 shown the greatest zone of inhibition of 8.0 mm against *S. aureus*, while the inhibition zone of *E. coli* was observed at 6.5 mm. Among all of free-base porphyrin, the antibacterial activity of the free-base porphyrin showed the maximum zone of inhibition in the order as follow: TOMPP > TPP ⩾ TOOPP ⩾ TOBPP ⩾ TODPP. The similarly trend were observed in both of against *S. aureus*, and *E. coli*. The antibacterial screening data indicate that both of metalloporphyrin complexes are more potent antibacterial against than free-base porphyrin, compared to the corresponding porphyrin ligands. The copper(II) porphyrin complexes, the CuTOMPP **14** shows the maximum inhibition zone of *S. aureus* at 14.0, and shows 8.0 mm of inhibition zone against *E. coli*. The trend of inhibition zone were founded similarly in free-base porphyrin. For the silver(II) porphyrin complexes, the AgTODPP exhibited more effective antibacterial activity than other silver(II) porphyrin complexes. The more efficiency resulted from the length of alkyl long-chain group in porphyrin structure [136]. The similarly result was reported by Tovmasyan A. *et al*. [137]. The standard drug penicillin showed 23 mm inhibition against *S.aureus*, the *E.coli* is a penicillin resistant.

The minimum inhibitory concentration (MIC) and the minimum bactericidal concentration (MBC) of metalloporphyrin complexes were summarized in **Table 18**. The minimum inhibitory concentration (MIC) of all metalloporphyrin was determined against both of *Staphylococcus aureus* (ATCC 25923) and *Escherichia coli* (ATCC 25922). All copper(II) porphyrin complexes show MIC value at concentration 320 ppm for bacterial strain *S. aureus*, and 160 ppm for bacterial strain *E. coli.* Furthermore, the minimum bactericidal concentration (MBC) value of all copper(II) porphyrin were founded in the same concentration for both of tested bacterial at 640 ppm. Whereas the CuTPP **9** founded MBC value for *E. coli* at 320 ppm. These silver(II) porphyrins displayed activity of MIC value against *S. aureus* and *E. coli* at concentration 320 ppm and 160 ppm respectively, excepting AgTODPP **18** shows MIC value of *E. coli* at concentration 80 ppm. Then, the concentration did not show growth was considered to be the MBC for the test in microbial death. The MBC value of all silver(II) porphyrins were founded in the same concentration at 640 ppm for *S. aureus*, excepting AgTPP **14** and AgTODPP **18** exhibit in concentration at 320 ppm. Whereas, the MBC value for *E. coli* was shown at 160 ppm, except AgTODPP **18** found in

concentration at 80 ppm. The AgTODPP **18** was considerably more achieve (MIC = 320 and MBC 80 ppm) than other porphyrins complexes, suggesting that the alkyl long-chain may easily penetrate lipid barriers of the bacteria cell [138].

Table 18

The MIC and MBC value of metalloporphyrin complexes **9** – **13**

Porphyrins	minimum inhibitory concentration (MIC/ppm)		minimum bactericidal concentration (MBC/ppm)	
	S. aureus	*E. coli*	*S. aureus*	*E. coli*
CuTPP **9**	320	160	640	320
CuTOMPP **10**	320	160	640	640
CuTOBPP **11**	320	160	640	640
CuTOOPP **12**	320	160	640	640
CuTODPP **13**	320	160	640	640
AgTPP **14**	320	160	320	160
AgTOMPP **15**	320	160	640	160
AgTOBPP **16**	320	160	640	160
AgTOOPP **17**	320	160	640	160
AgTODPP **18**	320	80	320	80

4.9.2 Anticancer activity

The anticancer activity of copper(II) porphyrin and gold(III) porphyrin complexes was investigated in human breast cancer cell lines using MTT assay [130, 131]. The inhibitory concentrations were evaluated from the dose dependence of surviving cells 24 hours after exposure to each metalloporphyrin complexes. The inhibitory concentrations required to inhibit cell growth by 50% compared with control (IC_{50} values) were evaluated from the dose dependence of cells 24 hours after exposure compounds. The cast shortly of CuTOOPP **12** and CuTODPP **13** was explained, due to the incomplete soluble in DMSO. The other copper(II) porphyrin complexes have been investigated on SKBR3 and MCF7 cell lines. The results show that all copper(II) porphyrin complexes exhibited cytotoxicity against both

cancer cells. For the SKBR3, the CuTOBPP show the lower IC_{50} at 25.22 μM than other compounds. While all testing complexes exhibited cytotoxicity to MCF7 cell lines with IC_{50} greater than 100 μM. Furthermore, the *In vitro* cytotoxicity of TPP was studied (data not show). Base on MTT assay, TPP present the cytotoxicity on SKBR3 and MCF7 cell line with IC_{50} value 143.29 and 100.33 μM, respectively. The CuTPP is more effective than TPP to treat SKBR3 cancer cell. This result indicates that the presence of copper(II) ion in the center of porphyrin ligand can increase the anticancer activity of porphyrin compounds. The redox-active of copper(II) complexes will stimulate the production of reactive oxygen species that cause DNA damage in cancer cells [139]. **Figure 77** show %viability of SKBR3 and MCF7 cells after treated with copper(II) porphyrin complexes for 24 h.

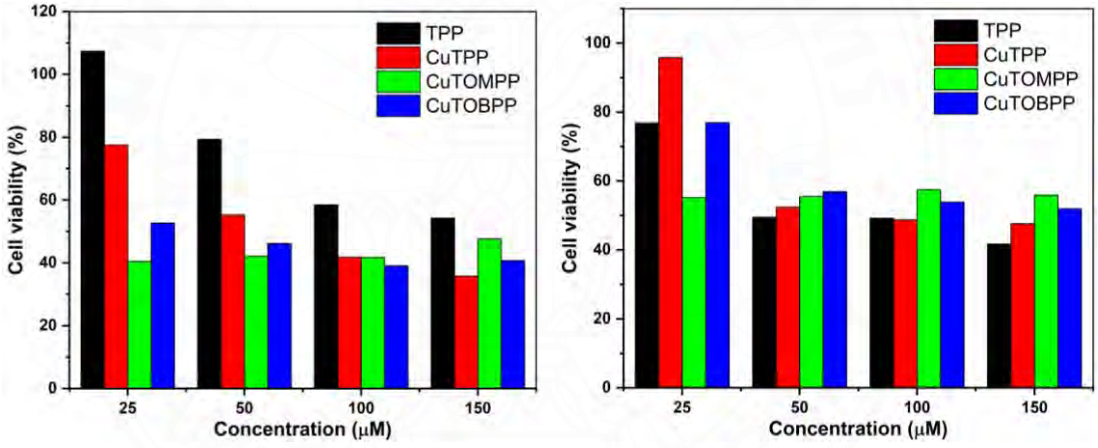

Figure 77 cell viability of (a) SKBR3 and (b) MCF7 cells after treated with copper(II) porphyrin complexes

In case of gold(III) porphyrin complexes, all complexes exhibited the cytotoxicity effect in MCF7 cell lines. At the same concentration, AuTPP **19** and AuTOMPP **20** show the most prominent anticancer activity with lower cell viability than other compounds. The MCF7 cell can survived in 1% DMSO after 24 hours with %cell viability more than 90% and 80%, respectively. It was indicated that the DMSO has no effect on killing MCF7 cell lines. **Figure 78** shows the representative images of Diff-Quik stained MCF7 cell line after treated with 25 μM of gold(III) porphyrin

complexes for 24 hours. The result shows that the cell in 1%DMSO, AuTOBPP **21**, AuTOOPP **22**, and AuTODPP **23** show the morphology of cell similar with the control that means non-cytotoxicity for MCF7 cells line. However, the AuTPP **19** and AuTOMPP **20** reveal the different cell growth from control, suggesting the possibility of cytotoxicity for MCF7 cells line. The staining demonstrated level of cell cytotoxicity of gold(III) porphyrin complexes from the highest to lowest, as followed AuTPP > AuTOMPP ≥ AuTOBPP ≥ AuTOOPP ≥ AuTODPP, respectively

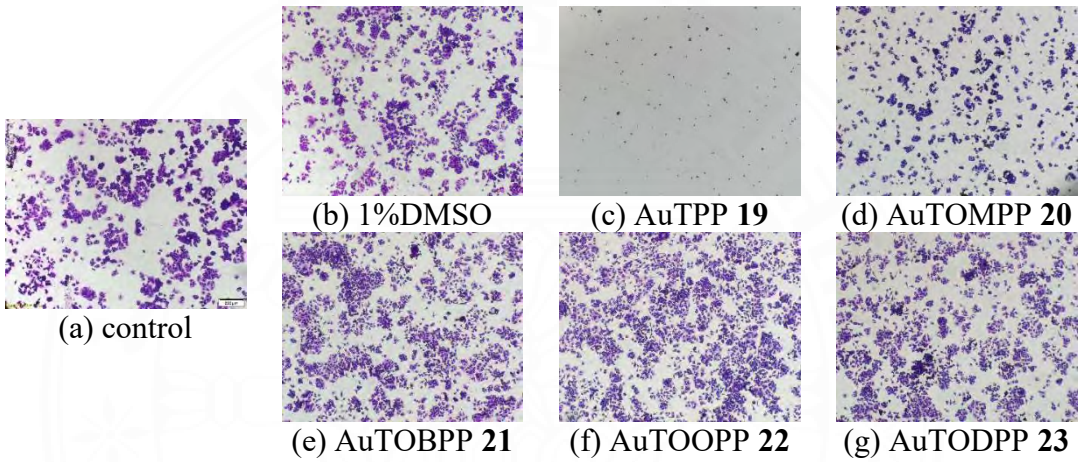

Figure 78 Representative images of Diff-Quik stained MCF7 cell line (a) control, (b) 1%DMSO, and 25 μM of (c) AuTPP, (d) AuTOMPP, (e) AuTOBPP, (f) AuTOOPP, and (g) AuTODPP.

The inhibitory concentrations required to inhibit cell growth by 50% compared with control (IC_{50} values) were evaluated from the dose dependence of cells 24 hours after exposing to the compounds. The AuTOMPP exhibited IC_{50} value as 25.35 ± 7.14 μM. Regarding the AuTPP, this complex exhibited cell viability lower than 2% at all test concentrations. Therefore, working concentrations of AuTPP complex for cytotoxicity test on MCF7 cell lines were lower than concentrations of other compounds (10, 5, 1, and 0.5 μM) and the IC_{50} value at 4.30 μM was calculated. However, IC_{50} of AuTOBPP, AuTOOPP, and AuTODPP cannot be calculated, because the cell viability are higher than 80% at all dose. The gold(III) ion in the gold(III) porphyrin complexes is *iso*-electronic to platinum(II) and it has a similar square-planar structure as in the case of cisplatin. The cytotoxicity studied using MTT assay shown

that all gold(III) porphyrin complexes exhibit the anticancer efficacy in human breast cancer cell (MCF7). Especially, AuTPP and AuTOMPP exhibit significantly reduce the survival of MCF7 cell lines. The *In vitro* cytotoxicity of 5,10,15,20-tetraphenylporphyrin (TPP) was studied. Base on MTT assay, TPP present the cytotoxicity in MCF7 cell line with IC_{50} value 100.33 µM. Comparing the IC_{50} value obtain from TPP, CuTPP, and AuTPP, the AuTPP is more significantly effective than TPP to treat MCF7 cell lines with 23.33 time and 27.31-fold than CuTPP. This result indicates that the presence of gold(III) ion in the center of porphyrin ligand can increase the anticancer activity of porphyrin complexes. Previously, the mechanism of gold(III) porphyrin complexes induce cell death is not completely understood. Initially, the mechanism of gold(III) porphyrin was thought to similarly with cisplatin, that binding of cancer DNA. However, the mechanism of AuTPP induces cell death has been proposed by Chi-ming C. *et al.* they report that the AuTPP induces apoptosis through mitochondrial dysfunction and Bcl-2 protein suppression. In addition, AuTPP can abrogate the cell cycle at G_0-G_1 [140].

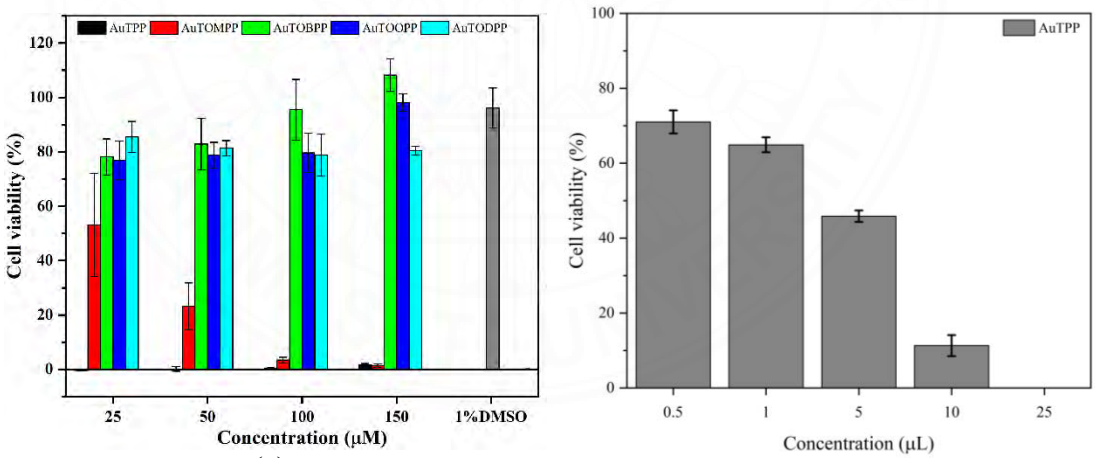

Figure 79 Cell viability of MCF7 cell lines after treat with (a) gold(II) porphyrin complexes at concentration 25 – 150 µM for 24 hour, (b) AuTPP at concentration 0.5 – 25 µM for 24 hour.

The cytotoxicity of copper(II) porphyrin (CuTPP, CuTOMPP, and CuTOBPP), and gold(III) porphyrin complexes (AuTPP, and AuTOMPP) to

normal cells have been investigated by MTT assay using Rhesus Monkey Kidney Epithelial Cells (LLC-MK2). All complexes show non-cytotoxicity on LLC-MK2 cell lines. All metalloporphyrin complexes exhibited non-cytotoxicity in LLC-MK2 cell lines in all concentration with cell viability more than 70 %. While, the AuTPP show non-cytotoxicity at concentration lower than 5 μM. The CuTPP, CuTOMPP, and CuTOBPP exhibited IC_{50} value in LLC-MK2 cell as 145.25, 151.98, and 155.17 μM, respectively. Whereas, the IC_{50} value of AuTPP and AuTOMPP in LLC-MK2 are 27.78 and 178.12 μM, respectively as determined by the MTT assay. Comparing the IC_{50} value obtained from the cancer cell lines (MCF7) with normal cells (LLC-MK2) of AuTPP and AuTOMPP are about 6.4 and 7.0 fold more toxic to cancer cells, respectively (**Table 19**). The results revealed that both copper(II) porphyrin and gold(III) porphyrin exhibited cytotoxicity to the cancer cells (MCF7) and non-toxicity to normal cells (LLC-MK2). When compared with the famous chemotherapy drug cisplatin the CuTOBPP and AuTOMPP exhibited the lower IC_{50} value on SKBR3 and MCF7 cell, both compounds have potential to develop as an anticancer drug in future.

Table 19

IC_{50} value of gold(III) porphyrin complexes in MCF7 and LLC-MK2 cell lines

Porphyrins	IC_{50} (μM)		
	SKBR3	MCF7	LLC-MK2
TPP **4**	143.29	100.33	-
CuTPP **9**	89.62	117.47	145.25
CuTOMPP **10**	N/A	N/A	151.98
CuTOBPP **11**	25.22	141.14	155.17
AuTPP **19**	-	4.30 ± 1.30	27.78
AuTOMPP **20**	-	25.35 ± 7.14	178.12
AuTOBPP **21**	-	N/A	N/A
AuTOOPP **22**	-	N/A	N/A
AuTODPP **23**	-	N/A	N/A
Cisplatin [82]	76.3	20.1	-

- not observed, N/A – can't be calculate

CHAPTER 5
CONCLUSIONS AND RECOMMENDATIONS

The alkyloxybenzaldehyde derivative were successfully synthesized and characterized with high reaction yield more than 60% yield. The *meso*-aryl long-chain porphyrin derivative were prepared by modification of Alder-Longo method. The series of free-base porphyrin contain different *meso*-substituent groups (phenyl, methoxyphenyl, butyloxtphenyl, octyloxyphenyl, and dectyloxyphenyl) were obtained in range 9 – 26% yield. Moreover, the metalloporphyrin complexes (copper, silver, and gold) of each free-base porphyrin were successfully synthesized and characterized.

The UV-visible absorption spectra of free-base porphyrin exhibited a strong absorption (Soret band) with four weak absorption (Q band), while all metalloporphyrin complexes displayed a single Soret band with only one Q band due to the symmetry change of metalloporphyrin complexes. Both of Soret band Q band of metalloporphyrin complexes containing the alkyl long-chain were moved to a small red-shift compared with MTPP (M = Cu, Ag, and Au). When excited the free-base porphyrin at 530 nm, the synthesized porphyrin exhibited fluorescence spectra at 654 nm. The calculated energy gap of all free-base porphyrin were observed at 1.90 eV. For the fluorescence studied of metalloporphyrin complexes (copper and silver) were show the low fluorescence intensity around 605 nm, when excited at the maximum absorption of the Q band, whereas, gold(III) porphyrin complexes shown two high emission intensity peak in range 650 – 850 nm. The metalloporphyrin exhibited strong EPR signal. Especially for Cu(II) porphyrin, due to the unpaired d-electron. The intensity of the EPR signals generated by Cu^{2+} was enough to cover up the free radicals' signals with the g parallel and g perpendicular as 2.08 and 2.00, respectively. The ESR signal of silver porphyrin complexes confirmed that these compounds must contained silver(II) ion in the structure with the g value as 2.05. Similarly the gold(III) porphyrin exhibited g value at 2.01. The electrochemical studied show that free-base porphyrin and their copper(II) and gold(III) porphyrin complexes exhibited two reversible one electron oxidation and one electron quasi-reversible reduction, whereas silver(II) porphyrin complexes exhibiter one reversible oxidation peak. The potential difference between

the first ring oxidation and first ring reduction of all synthesized compounds can related to the energy gap HOMO and LUMO of the porphyrin π-system. After coordinated the energy gap of the corresponding porphyrin are decrease follow CuL > AgL > AuL (L = TPP, TOMPP, TOBPP, TOOPP, and TODPP) due to the electron density of metal ion. The thermal stability of all synthesized compounds were measured by thermal gravimetric analysis (TGA). All of synthesized compounds were found to be highly thermal stability as over 400°C. The trend of thermal stability was follow: TODPP > TOOPP > TOBPP > TOMPP > TPP. The metalloporphyrin complexes were found to be the highly thermal stability than pure ligand. The MTPP (M = Cu(II), Ag(II), Au(III)) exhibited higher thermal stability than other corresponding metalloporphyrin derivatives, due to the electron delocalized in porphyrin ring increases the stability of MTPP complexes.

For the antibacterial activity indicates that the synthesized compounds is found to be sensitive against both of *Staphylococcus aureus* (ATCC 25923) and *Escherichia coli* (ATCC 25922). The TOMPP **5**, CuTOMPP **10**, and AgTODPP **18** show higher zone of inhibition than other compounds in each series. The minimum inhibitory concentration (MIC) and the minimum bactericidal concentration (MBC) of the metalloporphyrin complexes were investigated. All metalloporphyrin found the MIC value of *S. aureus* and *E. coli* at 320 and 160 ppm, respectively excepting AgTODPP **18** displayed MIC value of *E. coli* at 80 ppm. While the MBC value of copper(II) porphyrin complexes were found at 640 ppm for both of bacterial strain. Whereas, silver(II) porphyrin exhibited MBC value for *S. aureus* and *E. coli* at 640 ppm and 160 ppm, respectively. Excepting, AgTPP **14** and AgTODPP **18** show MBC value at 320 ppm for *S. aureus* and at 80 ppm for against *E. coli* of AgTODPP **18**.

The cytotoxicity to MCF7 and SKBR3 cell lines were studied by MTT assay. The copper(II) porphyrin showed cytotoxicity against both cancer cells. For the SKBR3, the CuTOBPP **11** show the lowest IC_{50} at 25.22 μM, while for MCF7 all copper(II) porphyrin exhibited IC_{50} value over than 100 μM. In case of gold(III) porphyrin complexes, the cell cytotoxicity test of MCF7 cell lines demonstrated markedly high cytotoxicity effects of AuTPP **19** and AuTOMPP **20** complexes with IC_{50} value at 4.30 ± 1.30 μM and 25.35 ± 7.14 μM, respectively. Whereas, AuTOBPP **21**, AuTOOPP **22**, and AuTODPP **23** complexes exhibited low cytotoxicity effects or

low anticancer activity on MCF7 cell line with cell viability higher than 80%. The metalloporphyrin complexes exhibited non-cytotoxic on LLC-MK2 cells. Although, the AuTPP **19** show non-cytotoxic at concentration lower than 5 μM. However, of LLC-MK2 for copper(II) porphyrin complexes were founded more than 145 μM. The IC_{50} of AuTPP **19** and AuTOMPP **20** are 27.78 and 178.12 μM, respectively.

REFERENCES

[1] Harrison HR, Hodder OJR, Hodgkin DC. Crystal and molecular structure of 8,12-diethyl-2,3,7,13,17,18-hexamethylcorrole. Journal of the Chemical Society B: Physical Organic. 1971(0):640-5.

[2] Dayan FE, Dayan EA. Porphyrins: one ring in the colors of life: a class of pigment molecules binds King George III, vampires and herbicides. American Scientist. 2011;99(3):236-43.

[3] Moss GP. Nomenclature of tetrapyrroles. European Journal of Biochemistry. 1988;178:277-328

[4] Kumar R, Sankar M. Synthesis, spectral, and electrochemical studies of electronically tunable beta-substituted porphyrins with mixed substituent pattern. Inorganic Chemistry. 2014;53(24):12706-19.

[5] Vicente MG, Smith K. Porphyrins and derivatives synthetic strategies and reactivity profiles. Current Organic Chemistry. 2000;4(2):139-74.

[6] Tatsumi K, Hoffmann R. Metalloporphyrins with unusual geometries. 1. Mono-, di-, triatom-bridged porphyrin dimers. Journal of the American Chemical Society. 1981;103(12):3328-41.

[7] Heme Biology: world scientific; 2011.

[8] Mense SM, Zhang L. Heme: a versatile signaling molecule controlling the activities of diverse regulators ranging from transcription factors to MAP kinases. Cell Research. 2006;16(8):681-92.

[9] Pareek S, Sagar N, Sharma S, Kumar V, Agarwal T, Aguilar G, et al. Chlorophylls: Chemistry and Biological Functions. In: Elhadi MY editor. Fruit and Vegetable Phytochemicals: Chemistry and Human Health, 2nd Edition. 2017. p. 269-84 (15).

[10] Krasnovsky AA, Jr. Chlorophyll isolation, structure and function: major landmarks of the early history of research in the Russian Empire and the Soviet Union. Photosynthesis Research. 2003;76(1-3):389-403.

[11] Rizzo G, Laganà AS. A review of vitamin B12. Molecular Nutrition. 2020. p. 105-29.

[12] Proinsias K, Giedyk M, Gryko D. Vitamin B12: chemical modifications. Chemical Society Reviews. 2013;42(16):6605-19.

[13] Farber G, Keller W, Kratky C. 68. Coenzyme f430 from methanogenic bacteria: complete assignment of configuration based on an X-ray analysis of 12,13-diepi-f430 pentamethyl ester and on NMR spectroscopy. Helvetica Chimica Acta. 1991;74:697 - 716.

[14] McDonnell AM, Dang CH. Basic review of the cytochrome p450 system. Journal of the Advanced Practitioner in Oncology. 2013;4(4):263-8.

[15] Rothemund P. Formation of porphyrins from pyrrole and aldehydes. Journal of the American Chemical Society. 1935;57(10):2010-1.

[16] Rothemund P. A new porphyrin synthesis. The synthesis of porphin[1]. Journal of the American Chemical Society. 1936;58(4):625-7.

[17] Adler AD, Longo FR, Shergalis W. Mechanistic investigations of porphyrin syntheses. I. Preliminary studies on *ms*-tetraphenylporphin. Journal of the American Chemical Society. 1964;86(15):3145-9.

[18] Lindsey JS, Hsu HC, Schreiman IC. Synthesis of tetraphenylporphyrins under very mild conditions. Tetrahedron Letters. 1986;27(41):4969-70.

[19] Arsenault GP, Bullock E, MacDonald SF. Pyrromethanes and porphyrins therefrom[1]. Journal of the American Chemical Society. 1960;82(16):4384-9.

[20] Boudif A, Momenteau M. Synthesis of a porphyrin-2,3-diacrylic acid using a new '3 + 1' type procedure. Journal of the Chemical Society, Chemical Communications. 1994(18):2069-70.

[21] Vicente MD, Smith KM. Syntheses and functionalizations of porphyrin macrocycles. Current Organic Synthesis. 2014;11(1):3-28.

[22] He H, Dubey M, Zhong Y, Shrestha M, Sykes AG. 2-(1-Acetyl-2-oxopropyl)-5,10,15,20-tetraphenylporphyrin and its transition-metal complexes. European Journal of Inorganic Chemistry. 2011: 3731–38.

[23] Xu Z, Mei Q, Hua Q, Tian R, Weng J, Shi Y, et al. Synthesis, characterization, energy transfer and photophysical properties of ethynyl bridge linked porphyrin–naphthalimide pentamer and its metal complexes. Journal of Molecular Structure. 2015;1094:1-8.

[24] Tan Q, Zhang X, Mao L, Xin G, Zhang S. Novel zinc porphyrin sensitizers for dye-sensitized solar cells: Synthesis and spectral, electrochemical, and photovoltaic properties. Journal of Molecular Structure. 2013;1035:400-6.

[25] Lu F, Zhang J, Zhou Y, Zhao Y, Zhang B, Feng Y. Novel D–π–A porphyrin dyes with different alkoxy chains for use in dye-sensitized solar cells. Dyes and Pigments. 2016;125:116-23.

[26] Esteves CHA, Iglesias BA, Li RWC, Ogawa T, Araki K, Gruber J. New composite porphyrin-conductive polymer gas sensors for application in electronic noses. Sensors and Actuators B: Chemical. 2014;193:136-41.

[27] Kladsomboon S, Kerdcharoen T. A method for the detection of alcohol vapours based on optical sensing of magnesium 5,10,15,20-tetraphenyl porphyrin thin film by an optical spectrometer and principal component analysis. Analytica Chimica Acta. 2012;757:75-82.

[28] James D, Scott SM, Ali Z, O'Hare WT. Chemical sensors for electronic nose systems. Microchimica Acta. 2004;149(1-2):1-17.

[29] Suslick K, Rakow N, Kosal M, Chou J-H. The materials chemistry of porphyrins and metalloporphyrins. Journal of Porphyrins and Phthalocyanines. 2000;4:407-13.

[30] Song F, Ma P, Chen C, Jia J, Wang Y, Zhu P. Room temperature NO_2 sensor based on highly ordered porphyrin nanotubes. Journal of Colloid and Interface Science. 2016;474:51-7.

[31] La Penna M, Alvarez MG, Yslas EI, Rivarola V, Durantini EN. Photodynamic activity of 5,10,15,20-tetrakis(4-methoxyphenyl)porphyrin on the Hep-2 human carcinoma cell line: effect of light dose and wavelength range. Bioorganic Chemistry. 2001;29(3):130-9.

[32] Meng S, Xu Z, Hong G, Zhao L, Zhao Z, Guo J, et al. Synthesis, characterization and *In vitro* photodynamic antimicrobial activity of basic amino acid-porphyrin conjugates. European Journal of Medicinal Chemistry. 2015;92:35-48.

[33] Yslas EI, Rivarola V, Durantini EN. Synthesis and photodynamic activity of zinc(II) phthalocyanine derivatives bearing methoxy and trifluoromethylbenzyloxy substituents in homogeneous and biological media. Bioorganic & Medicinal Chemistry. 2005;13(1):39-46.

[34] Philippova TO, Galkin BN, Zinchenko OY, Rusakova MY, Ivanitsa VA, Zhilina ZI, et al. The antimicrobial properties of new synthetic porphyrins. Journal of Porphyrins and Phthalocyanines. 2003;7:755-60.

[35] Mondal D, Bera S. Porphyrins and phthalocyanines: promising molecules for light-triggered antibacterial nanoparticles. Advances in Natural Sciences: Nanoscience and Nanotechnology. 2014;5(3).

[36] Amos-Tautua BM, Songca SP, Oluwafemi OS. Application of Porphyrins in Antibacterial Photodynamic Therapy. Molecules. 2019;24(13).

[37] Sudhakar A. History of cancer, ancient and modern treatment methods. Journal of Cancer Science & Therapy. 2009;1(2):1-4.

[38] World Health Organization. Cancer [Internet]. 2020 [cited 2020 Nov 24]. Available from: https://www.who.int/health-topics/cancer#tab=tab_1.

[39] National Cancer Institute, Department of Medical Services, Ministry of Pubic Health. Hospital-Based Cancer Registry 2019. Bangkok: New Thammada Press; 2020.

[40] American Cancer Society. Global Cancer Facts & Figures 4th Edition. Atlanta: American Cancer Society; 2018.

[41] Janet LS, Irvin SS. Anticancer drug. Encyclopedia Britannica [Internet]. 2018 [cited 2020 Nov 24]. Available from: https://www.britannica.com/science/anticancer-grug.

[42] National Cancer Institute. Type of Cancer Treatment [Internet]. 2020 [cited 2020 Nov 24]. Availble from: https://www.cancer.gov/about-cancer/treatment/types.

[43] Romero-Canelon I, Sadler PJ. Next-generation metal anticancer complexes: multitargeting via redox modulation. Inorganic Chemistry. 2013;52(21):12276-91.

[44] American Cancer Society. Chemotherapy [Internet]. 2020 [cited 2020 Nov 24]. Availbel from: https://www.cancer.org/treatment/treatments-and-side-effects/treatment-types/chemotherapy.html.

[45] Dasari S, Tchounwou PB. Cisplatin in cancer therapy: molecular mechanisms of action. European Journal of Pharmacology. 2014;740:364-78.

[46] Kauffman GB, Pentimalli R, Doldi S, Hall MD. Michele Peyrone (1813-1883), Discoverer of Cisplatin. Platinum Metals Review. 2010;54(4):250-6.

[47] Alderden RA, Hall MD, Hambley TW. The discovery and development of cisplatin. Journal of Chemical Education. 2006;83(5):728.

[48] To YF, Sun RW, Chen Y, Chan VS, Yu WY, Tam PK, et al. Gold(III) porphyrin complex is more potent than cisplatin in inhibiting growth of nasopharyngeal carcinoma *In vitro* and *In vivo*. International Journal of Cancer. 2009;124(8):1971-9.

[49] Milacic V, Dou QP. The tumor proteasome as a novel target for gold(III) complexes: implications for breast cancer therapy. Coordination Chemistry Reviews. 2009;253(11-12):1649-60.

[50] Sun RW-Y, Che C-M. The anti-cancer properties of gold(III) compounds with dianionic porphyrin and tetradentate ligands. Coordination Chemistry Reviews. 2009;253(11-12):1682-91.

[51] Tu S, Wai-Yin Sun R, Lin MC, Tao Cui J, Zou B, Gu Q, et al. Gold (III) porphyrin complexes induce apoptosis and cell cycle arrest and inhibit tumor growth in colon cancer. Cancer. 2009;115(19):4459-69.

[52] Temelli B, Unaleroglu C. Synthesis of *meso*-tetraphenyl porphyrins via condensation of dipyrromethanes with N-tosyl imines. Tetrahedron. 2009;65(10):2043-50.

[53] Wang M-C, Sue L-S, Liau B-C, Ko B-T, Elango S, Chen J-H. Mercury complexes of *meso*-Tetra-(*p*-cyanophenyl)porphyrin and N-methylporphyrin: *meso*- Tetra(*p*-cyanophenyl)porphyrinatomercury(II) and Chloro(*N*-methyl-*meso*- tetraphenylporphyrinato)-mercury(II). Inorganic Chemistry. 2001;40(23):6064-8.

[54] Lee Y-Y, Chen J-H, Hsieh H-Y. Metal complexes of *meso*-tetra-(*p*-chlorophenyl)porphyrin and *meso*-tetra-(*p*-bromophenyl)porphyrin: Tl[(p-Cl)$_4$tpp](OAc) and In[(p-X)$_4$tpp](OAc) [X=Cl, Br, tpp=5,10,15,20-tetraphenylporphyrinate]. Polyhedron. 2003;22(13):1633-9.

[55] Maestrin APJ, Tedesco AC, Neri CR, Gandini MEF, Serra OA, Iamamoto Y. Synthesis, spectroscopy and photosensitizing properties of

hydroxynitrophenylporphyrins. Journal of the Brazilian Chemical Society. 2004;15:708-13.

[56] Ghosh A, Selvamani T, Jose DA, Das A, Mukhopadhyay I. Generation of nanostructures by the aggregation of porphyrin derivatives with long alkane chain in mix-solvent. Journal of Nanomaterials. 2007;2007:1-8.

[57] Kostas ID, Coutsolelos AG, Charalambidis G, Skondra A. The first use of porphyrins as catalysts in cross-coupling reactions: a water-soluble palladium complex with a porphyrin ligand as an efficient catalyst precursor for the Suzuki–Miyaura reaction in aqueous media under aerobic conditions. Tetrahedron Letters. 2007;48(38):6688-91.

[58] Wang C, Yang G, Li J, Mele G, Slota R, Broda M, et al. Novel *meso*-substituted porphyrins: Synthesis, characterization and photocatalytic activity of their TiO_2-based composites. Dyes and Pigments. 2009;80(3):321-8.

[59] Sun E, Sun Z, Yuan M, Wang D, Shi T. The synthesis and properties of *meso*-tetra(4-alkylamidophenyl)porphyrin liquid crystals and their Zn complexes. Dyes and Pigments. 2009;81(2):124-30.

[60] Liao JX, Zhao HB, Yang DL, Chen L, Wang BY. {*meso*-Tetrakis[*p*-(heptyloxy)phenyl]-porphyrinato}silver(II). Acta Crystallographica Section E Structure Reports Online. 2011;67(Pt 9):m1316.

[61] Taesch J, Dang TT, Heitz V. Efficient synthesis and Suzuki cross-coupling reactions of *meso*-tetrakis(2,6-dimethyl-4-triflyloxyphenyl)porphyrin. Tetrahedron Letters. 2012;53(3):333-7.

[62] Zhang YJ, Shi J, Liu W, Yu M. 5, 10, 15, 20-Tetra (N-long-chain-alkyl carbazole) porphyrin and their lanthanide complexes. Synthesis and Reactivity in Inorganic, Metal-Organic, and Nano-Metal Chemistry. 2013;43(5):640-6.

[63] Pinto VH, Carvalhoda-Silva D, Santos JL, Weitner T, Fonseca MG, Yoshida MI, et al. Thermal stability of the prototypical Mn porphyrin-based superoxide dismutase mimic and potent oxidative-stress redox modulator Mn(III) *meso*-tetrakis(*N*-ethylpyridinium-2-yl)porphyrin chloride, MnTE-2-PyP^{5+}. Journal of Pharmaceutical and Biomedical Analysis. 2013;73:29-34.

[64] Nandi G, Sarkar S. High yield synthesis of oxo-tungsten(V) porphyrin: Structural characterization of the hydrolyzed products. Inorganica Chimica Acta. 2014;410:106-10.

[65] Xu Z, Mei Q, Weng J, Huang W. Synthesis, characterization and properties of covalently linked porphyrin–naphthalimide pentamer and its metal complexes. Journal of Molecular Structure. 2014;1074:687-94.

[66] Misra R, Gautam P. *Meso*-tetrakis(ferrocenylethynylphenyl) porphyrins: Synthesis and properties. Journal of Organometallic Chemistry. 2015;776:83-8.

[67] Luguya R, Jaquinod L, Fronczek FR, Vicente MGH, Smith KM. Synthesis and reactions of *meso*-(*p*-nitrophenyl)porphyrins. Tetrahedron. 2004;60(12):2757-63.

[68] Wu Y-h, Chen L, Yu J, Tong S-l, Yan Y. Synthesis and spectroscopic characterization of *meso*-tetra (Schiff-base substituted phenyl) porphyrins and their zinc complexes. Dyes and Pigments. 2013;97(3):423-8.

[69] Fedulova IN, Bragina NA, Novikov NV, Ugol'nikova OA, Mironov A. Synthesis of lipophilic tetraphenylporphyrins to design lipid-porphyrin ensembles. Bioorganicheskaya Khimiya. 2007;33(6):635-9.

[70] Li J, Tang T, Li F, Li M. The synthesis and characterization of novel liquid crystalline, *meso*-tetra[4-(3,4,5-trialkoxybenzoate)phenyl]porphyrins. Dyes and Pigments. 2008;77(2):395-401.

[71] Zhang Z, Duan Y, Zhang L, Yu M, Li J. Synthesis, crystal structure of two new Zn(II), Cu(II) porphyrins and their catalytic activities to ethylbenzene oxidation. Inorganic Chemistry Communications. 2015;58:53-6.

[72] Huang G, Mo L-Q, Cai J-L, Cao X, Peng Y, Guo Y-A, et al. Environmentally friendly and efficient catalysis of cyclohexane oxidation by iron *meso*-tetrakis(pentafluorophenyl)-porphyrin immobilized on zinc oxide. Applied Catalysis B: Environmental. 2015;162:364-71.

[73] Kooriyaden FR, Sujatha S, Arunkumar C. Synthesis, spectral, structural and antimicrobial studies of fluorinated porphyrins. Polyhedron. 2015;97:66-74.

[74] Xu X-J, Xue Z, Qi Z-D, Hou A-X, Li C-H, Liu Y. Antibacterial activities of manganese(II) ebselen–porphyrin conjugate and its free components on

Staphylococcus aureus investigated by microcalorimetry. Thermochimica Acta. 2008;476(1-2):33-8.

[75] Zhao L, Li M, Liu M, Zhang Y, Wu C, Zhang Y. Porphyrin-functionalized porous polysulfone membrane towards an optical sensor membrane for sorption and detection of cadmium(II). Journal of Hazardous Materials. 2016;301:233-41.

[76] Fleischer EB, Laszlo A. Synthesis of a gold porphyrin. Inorganic and Nuclear Chemistry Letters. 1969;5(5):373-6.

[77] Nyarko E, Hara T, Grab DJ, Habib A, Kim Y, Nikolskaia O, et al. *In vitro* toxicity of palladium(II) and gold(III) porphyrins and their aqueous metal ion counterparts on *Trypanosoma brucei brucei* growth. Chemico-Biological Interactions. 2004;148(1-2):19-25.

[78] Che CM, Sun RW, Yu WY, Ko CB, Zhu N, Sun H. Gold(III) porphyrins as a new class of anticancer drugs: cytotoxicity, DNA binding and induction of apoptosis in human cervix epitheloid cancer cells. Chemical communications (Cambridge). 2003(14):1718-9.

[79] Sun L, Chen H, Zhang Z, Yang Q, Tong H, Xu A, et al. Synthesis and cancer cell cytotoxicity of water-soluble gold(III) substituted tetraarylporphyrin. Journal of Inorganic Biochemistry. 2012;108:47-52.

[80] Lammer AD, Cook ME, Sessler JL. Synthesis and anti-cancer activities of a water-soluble gold(III) porphyrin. Journal of Porphyrins and Phthalocyanines. 2015;19(1-03):398-403.

[81] Chen H, Yang Q, Sun L, Zhang Z, Tong H, Xu A, et al. Synthesis and biological evaluation of gold(III) substituted tetraarylporphyrin chlorides as anticancer reagents. Journal of Chemical Research. 2011;35(3):190-4.

[82] Chow KH, Sun RW, Lam JB, Li CK, Xu A, Ma DL, et al. A gold(III) porphyrin complex with antitumor properties targets the Wnt/β-catenin pathway. Cancer Research. 2010;70(1):329-37.

[83] Antoni PM, Naik A, Albert I, Rubbiani R, Gupta S, Ruiz-Sanchez P, et al. (Metallo)porphyrins as potent phototoxic anti-cancer agents after irradiation with red light. Chemistry. 2015;21(3):1179-83.

[84] Li DH, Diao JL, Yu KG, Zhou CH. Synthesis and anticancer activities of porphyrin induced anticancer drugs. Chinese Chemical Letters. 2007;18(11):1331-4.

[85] Liu JC, Gu JJ, Zhang YS. Synthesis, crystal structure, and anti-breast cancer activity of a novel metal-porphyrinic complex [YK(TCPP)$(OH)_2$.$(solvents)_x$]. Brazilian Journal of Medical and Biological Research. 2017;51(1):e6858.

[86] Ding K, Zhang Y, Si W, Zhong X, Cai Y, Zou J, et al. Zinc(II) Metalated porphyrins as photothermogenic photosensitizers for cancer photodynamic/photothermal synergistic therapy. ACS Applied Materials & Interfaces. 2018;10(1):238-47.

[87] Dandash F, Leger DY, Fidanzi-Dugas C, Nasri S, Bregier F, Granet R, et al. *In vitro* anticancer activity of new gold(III) porphyrin complexes in colon cancer cells. Journal of Inorganic Biochemistry. 2017;177:27-38.

[88] Yao Y-H, Luo Y, Li J, Zhang F-X. Synthesis of novel porphyrin derivatives and their cytotoxic activities against a431 cells. Helvetica Chimica Acta. 2016;99(1):24-9.

[89] Feng X, Shi Y, Xie L, Zhang K, Wang X, Liu Q, et al. Synthesis, characterization, and biological evaluation of a porphyrin-based photosensitizer and its isomer for effective photodynamic therapy against breast cancer. Journal of Medicinal Chemistry. 2018;61(16):7189-201.

[90] Lum CT, Yang ZF, Li HY, Wai-Yin Sun R, Fan ST, Poon RT, et al. Gold(III) compound is a novel chemocytotoxic agent for hepatocellular carcinoma. International Journal of Cancer. 2006;118(6):1527-38.

[91] Rapozzi V, Zorzet S, Zacchigna M, Della Pietra E, Cogoi S, Xodo LE. Anticancer activity of cationic porphyrins in melanoma tumour-bearing mice and mechanistic *In vitro* studies. Molecular Cancer. 2014;13(1):75.

[92] Ou Z, Khoury T, Fang Y, Zhu W, Sintic PJ, Crossley MJ, et al. Gold(III) porphyrins containing two, three, or four beta,beta'-fused quinoxalines. Synthesis, electrochemistry, and effect of structure and acidity on electroreduction mechanism. Inorganic Chemistry. 2013;52(5):2474-83.

[93] Ou Z, Kadish KM, E W, Shao J, Sintic PJ, Ohkubo K, et al. Substituent effects on the site of electron transfer during the first reduction for gold(III) porphyrins. Inorganic Chemistry. 2004;43(6):2078-86.

[94] Zyablikova ES, Bragina NA, Mironov AF. Covalent-bound Conjugates of Fullerene C60 and Metal Complexes of Porphyrins with Long-chain Substituents. Mendeleev Communications. 2012;22(5):257-9.

[95] Vollekova A, Kost'alova D, Kettmann V, Toth J. Antifungal activity of *Mahonia aquifolium* extract and its major protoberberine alkaloids. Phytotherapy Research. 2003;17(7):834-7.

[96] Domingues MR, MG SM, Vale CA, Neves MG, Cavaleiro JA, Ferrer-Correia AJ, et al. Do charge-remote fragmentations occur under matrix-assisted laser desorption ionization post-source decompositions and matrix-assisted laser desorption ionization collisionally activated decompositions? Journal of the American Society for Mass Spectrometry. 1999;10(3):217-23.

[97] Costa DS, Martino T, Magalhaes FC, Justo G, Coelho MG, Barcellos JC, et al. Synthesis of *N*-methylarylnitrones derived from alkyloxybenzaldehydes and antineoplastic effect on human cancer cell lines. Bioorganic & Medicinal Chemistry. 2015;23(9):2053-61.

[98] Hu J, Pavel I, Moigno D, Wumaier M, Kiefer W, Chen Z, et al. Fourier-transform Raman and infrared spectroscopic analysis of 2-nitro-tetraphenylporphyrin and metallo-2-nitro-tetraphenylporphyrins. Spectrochimica Acta Part A: Molecular and Biomolecular Spectroscopy. 2003;59(9):1929-35.

[99] Rojkiewicz M, Kuś P, Kozub P, Kempa M. The synthesis of new potential photosensitizers [1]. Part 2. Tetrakis-(hydroxyphenyl)porphyrins with long alkyl chain in the molecule. Dyes and Pigments. 2013;99(3):627-35.

[100] Dehghani H, Shaterian M. New cationic sandwich-type intermediate sitting-atop complexation between *meso*-tetraarylporphyrins and tantalum(V) chloride: synthesis, spectroscopic characterization and photoluminescence study. Bulletin of the Korean Chemical Society. 2009;30(11):2792-4.

[101] Mishra S, Kaur S, Tripathi SK, Mahajan CG, Saini GSS. Fourier-transform infrared spectroscopic studies of dithia tetraphenylporphine. Journal of Chemical Sciences. 2006;118(4):361-9.

[102] Xu K, Rankin JG, Lash TD. Infrared spectroscopy of geoporphyrins: I. Analysis of geochemically significant nickel(II) porphyrins. Vibrational Spectroscopy. 1998;18(2):157-74.

[103] Udal'tsov AV, Bolshakova AV, Vos JG. Highly ordered surface structure of large-scale porphyrin aggregates assembled from protonated TPP and water. Journal of Molecular Structure. 2014;1065-1066:170-8.

[104] Tyulyaeva EY, Lomova TN. Interaction of Silver(II) and gold(III) *meso*-tetraphenylporphine complexes with concentrated sulfuric acid. Russian Journal of Coordination Chemistry. 2001;27(6):433-8.

[105] Zhou Y, Ngo KT, Zhang B, Feng Y, Rochford J. Synthesis, Electronic and photophysical characterization of π-conjugated *meso*-ferrocenyl-porphyrin fluorescent redox switches. Organometallics. 2014;33(24):7078-90.

[106] Lan M, Zhao H, Yuan H, Jiang C, Zuo S, Jiang Y. Absorption and EPR spectra of some porphyrins and metalloporphyrins. Dyes and Pigments. 2007;74(2):357-62.

[107] Fodor MA, Horváth O, Fodor L, Grampp G, Wankmüller A. Photophysical and photocatalytic behavior of cobalt(III) 5,10,15,20-tetrakis(1-methylpyridinium-4-yl)porphyrin. Inorganic Chemistry Communications. 2014;50:110-2.

[108] Chen C-T, Hsieh Sl. Synthesis and characterization of push-pull porphyrins. Journal of the Chinese Chemical Society. 1997;44:23-31.

[109] Thomas DW, Martell AE. Metal chelates of tetraphenylporphine and of some p-substituted derivatives[1,2]. Journal of the American Chemical Society. 1959;81(19):5111-9.

[110] Valicsek Z, Horváth O. Application of the electronic spectra of porphyrins for analytical purposes: The effects of metal ions and structural distortions. Microchemical Journal. 2013;107:47-62.

[111] Boscencu R. Microwave synthesis under solvent-free conditions and spectral studies of some mesoporphyrinic complexes. Molecules. 2012;17(5):5592-603.

[112] Gamboa M, Campos M, Torres LA. Study of the stability of 5,10,15,20-tetraphenylporphine (TPP) and metalloporphyrins NiTPP, CoTPP, CuTPP, and ZnTPP by differential scanning calorimetry and thermogravimetry. The Journal of Chemical Thermodynamics. 2010;42(5):666-74.

[113] Ventura B, Flamigni L, Marconi G, Lodato F, Officer DL. Extending the porphyrin core: synthesis and photophysical characterization of porphyrins with π-conjugated *β*-substituents. New Journal of Chemistry. 2008;32(1):166-78.

[114] Al-Resayes SI, Shakir M, Shahid N, Azam M, Khan AU. Synthesis, spectroscopic characterization and *In vitro* antimicrobial studies of Schiff base ligand, H_2L derived from glyoxalic acid and 1,8-diaminonaphthalene and its Co(II), Ni(II), Cu(II) and Zn(II) complexes. Arabian Journal of Chemistry. 2016;9(3):335-43.

[115] Güner S, Şener MK, Dinçer H, Köseoğlu Y, Kazan S, Koçak MB. EPR studies on Cu^{2+} and Co^{2+} complexes of tetraaza porphyrin derivatives. Journal of Magnetism and Magnetic Materials. 2006;300(1):e530-e3.

[116] Kneubühl FK, Koski WS, Caughey WS. An Electron spin resonance study of silver porphyrin[1]. Journal of the American Chemical Society. 1961;83(7):1607-9.

[117] Ghazzali M, Abu-Youssef MAM, Larsson K, Hansson Ö, Amer A, Tamm T, et al. Synthesis, EPR and DFT calculations of rare Ag(II)porphyrins and the crystal structure of [Zn(II)*tetrakis*(4-bromo-2-thiophene)porphyrin]. Inorganic Chemistry Communications. 2008;11(9):1019-22.

[118] Kadish KM, Wenbo E, Ou Z, Shao J, Sintic PJ, Ohkubo K, et al. Evidence that gold(III) porphyrins are *not* electrochemically inert: facile generation of gold(II) 5,10,15,20-tetrakis(3,5-di-*tert*-butylphenyl)porphyrin. Chemical communications (Cambridge). 2002(4):356-7.

[119] MacCragh A, Koski WS. The Phthalocyanine of Gold[1]. Journal of the American Chemical Society. 1965;87(11):2496-7.

[120] Lippert R, Shubina TE, Vojnovic S, Pavic A, Veselinovic J, Nikodinovic-Runic J, et al. Redox behavior and biological properties of ferrocene bearing porphyrins. Journal of Inorganic Biochemistry. 2017;171:76-89.

[121] Wahab A, Bhattacharya M, Ghosh S, Samuelson AG, Das PK. quadratic nonlinearity of one- and two-electron oxidized metalloporphyrins and their switching in solution. The Journal of Physical Chemistry B. 2008;112(10):2842-7.

[122] Kadish KM, Morrison MM. Substituent effects on the redox reactions of tetraphenylporphyrins. Bioinorganic Chemistry. 1977;7(2):107-15.

[123] Wolberg A, Manassen J. Electrochemical and electron paramagnetic resonance studies of metalloporphyrins and their electrochemical oxidation products. Journal of the American Chemical Society. 1970;92(10):2982-91.

[124] Kadish KM, Lin XQ, Ding JQ, Y. T. Wu, Araullo C. A Reinvestigation of Silver Porphyrin Electrochemistry. Reactions of Ag(III), Ag(II), and Ag(I). Inorganic Chemistry. 1986;25:3236-42.

[125] Antipas A, Dolphin D, Gouterman M, Johnson EC. Porphyrins. 38. Redox potentials, charge transfer transitions, and emission of copper, silver, and gold complexes. Journal of the American Chemical Society. 1978;100(24):7705-9.

[126] Kadish K, Davis DG, Fuhrhop JH. Unusual oxidation states of metalloporphyrins: octaethylporphinatosilver(III) perchlorate. Angewandte Chemie International Edition in English. 1972;11(11):1014-6.

[127] Fukuzumi S, Ohkubo K, Zhu W, Sintic M, Khoury T, Sintic PJ, et al. Androgynous porphyrins. Silver(II) quinoxalinoporphyrins act as both good electron donors and acceptors. Journal of the American Chemical Society. 2008;130(29):9451-8.

[128] Ou Z, Kadish KM, E W, Shao J, Sintic PJ, Ohkubo K, et al. Substituent effects on the site of electron transfer during the first reduction for gold(III) porphyrins. Inorganic Chemistry. 2004;43(6):2078-86.

[129] Preiss S, Melomedov J, Wunsche von Leupoldt A, Heinze K. Gold(III) tetraarylporphyrin amino acid derivatives: ligand or metal centred redox chemistry? Chemical Science. 2016;7(1):596-610.

[130] Konieczna N, Romaniuk-Drapala A, Lisiak N, Toton E, Paszel-Jaworska A, Kaczmarek M, et al. Telomerase inhibitor $TMPyP_4$ alters adhesion and migration of breast-cancer cells MCF7 and MDA-MB-231. International Journal of Molecular Sciences. 2019;20(11).

[131] Pucelik B, Sulek A, Drozd A, Stochel G, Pereira MM, Pinto SMA, et al. Enhanced cellular uptake and photodynamic effect with amphiphilic fluorinated porphyrins: The role of sulfoester groups and the nature of reactive oxygen species. International Journal of Molecular Sciences. 2020;21(8).

[132] Sun E-j, Cheng X-l, Wang D, Tang X-x, Yu S-j, Shi T-s. Synthesis and properties of 5,10,15,20-tetra(4-lauroylimidophenyl)porphyrin and its metal complexes. Solid State Sciences. 2007;9(11):1061-8.

[133] Wei X, Du X, Chen D, Chen Z. Thermal analysis study of 5,10,15,20-tetrakis (methoxyphenyl) porphyrins and their nickel complexes. Thermochimica Acta. 2006;440(2):181-7.

[134] Balanay MP, Kim DH. DFT/TD-DFT molecular design of porphyrin analogues for use in dye-sensitized solar cells. Physical Chemistry Chemical Physics. 2008;10(33):5121-7.

[135] Mangione G, Sambi M, Carlotto S, Vittadini A, Ligorio G, Timpel M, et al. Electronic structure of CuTPP and CuTPP(F) complexes: a combined experimental and theoretical study II. Physical Chemistry Chemical Physics. 2016;18(36):24890-904.

[136] Kumar SV, Scottwell SO, Waugh E, McAdam CJ, Hanton LR, Brooks HJ, et al. Antimicrobial properties of tris(homoleptic) ruthenium(II) 2-pyridyl-1,2,3-triazole "Click" complexes against pathogenic bacteria, including methicillin-resistant *Staphylococcus aureus* (MRSA). Inorganic Chemistry. 2016;55(19):9767-77.

[137] Tovmasyan A, Babayan N, Poghosyan D, Margaryan K, Harutyunyan B, Grigoryan R, et al. Novel amphiphilic cationic porphyrin and its Ag(II) complex as potential anticancer agents. Journal of Inorganic Biochemistry. 2014;140:94-103.

[138] Burda WN, Fields KB, Gill JB, Burt R, Shepherd M, Zhang XP, et al. Neutral metallated and *meso*-substituted porphyrins as antimicrobial agents against gram-positive pathogens. European Journal of Clinical Microbiology & Infectious Diseases. 2012;31(3):327-35.

[139] Tan SJ, Yan YK, Lee PP, Lim KH. Copper, gold and silver compounds as potential new anti-tumor metallodrugs. Future Medicinal Chemistry. 2010;2(10):1591-608.

[140] Sun RW, Li CK, Ma DL, Yan JJ, Lok CN, Leung CH, et al. Stable anticancer gold(III)-porphyrin complexes: effects of porphyrin structure. Chemistry. 2010;16(10):3097-113.

[141] Jaynt D. Simple Method of Measuring the Band Gap Energy Value of TiO_2 in the Powder Form using a UV/Vis/NIR Spectrometer. Application note. PerkinElmer, Inc. 1 – 3.

[142] Christopher AH, Jeremy KMS. The Nature of π- π Interactions. Journal of the American Chemical Society. 1990;112:5525-34.

APPENDICES

APPENDIX A

MASS SPECTROMETRY

Mass spectrum of alkyloxtbenzaldehyde

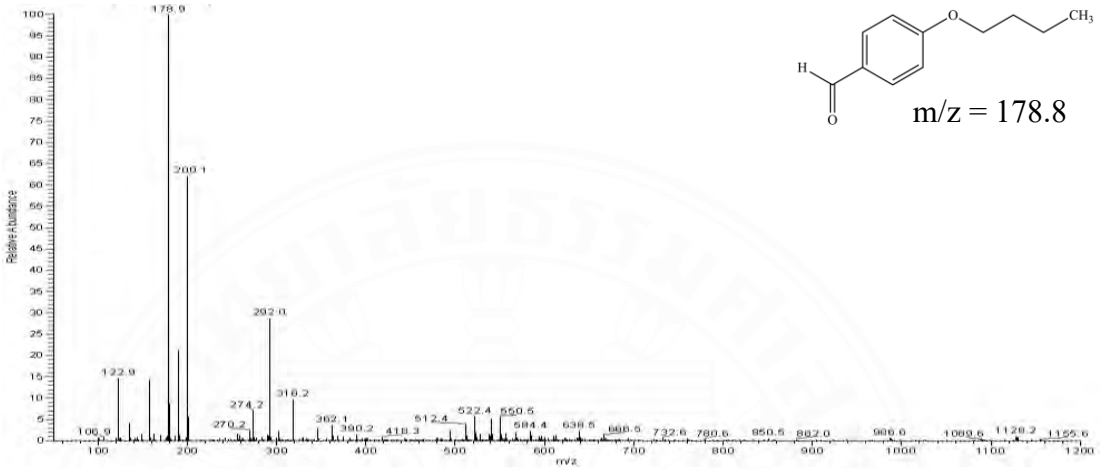

Figure A1 mass spectrum of butyloxybenzaldehyde 1

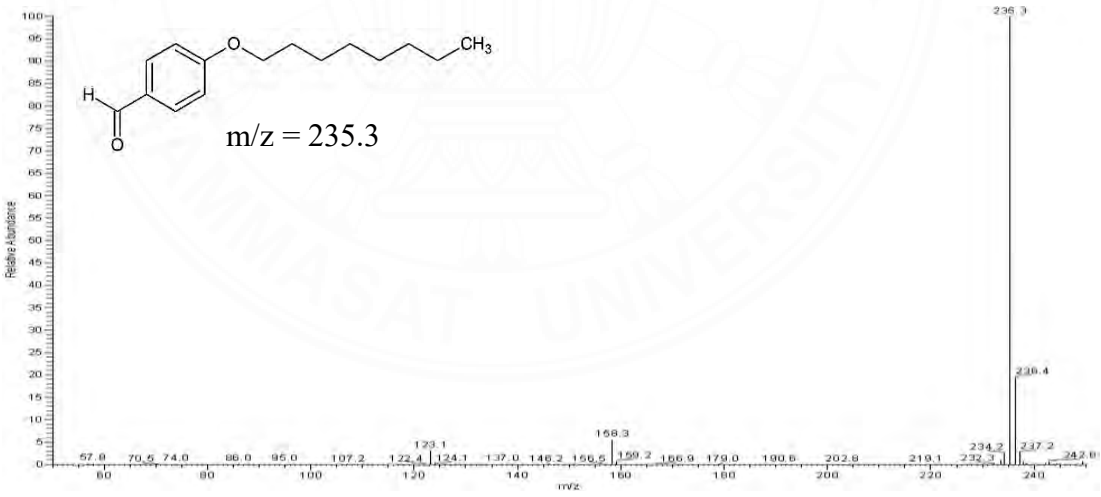

Figure A2 mass spectrum of octyloxybenzaldehyde 2

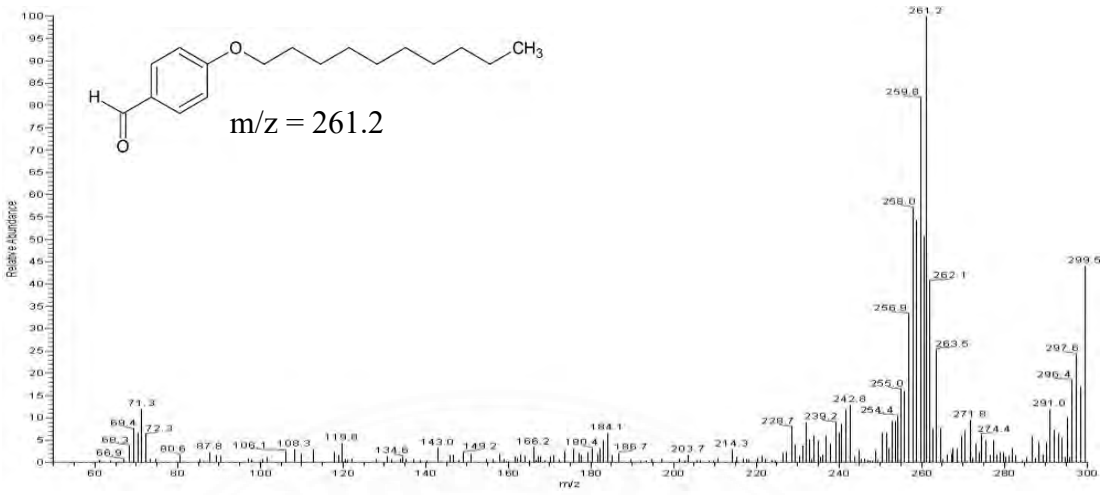

Figure A3 mass spectrum of decyloxybenzaldehyde 3

Mass spectrum of free-base porphyrin

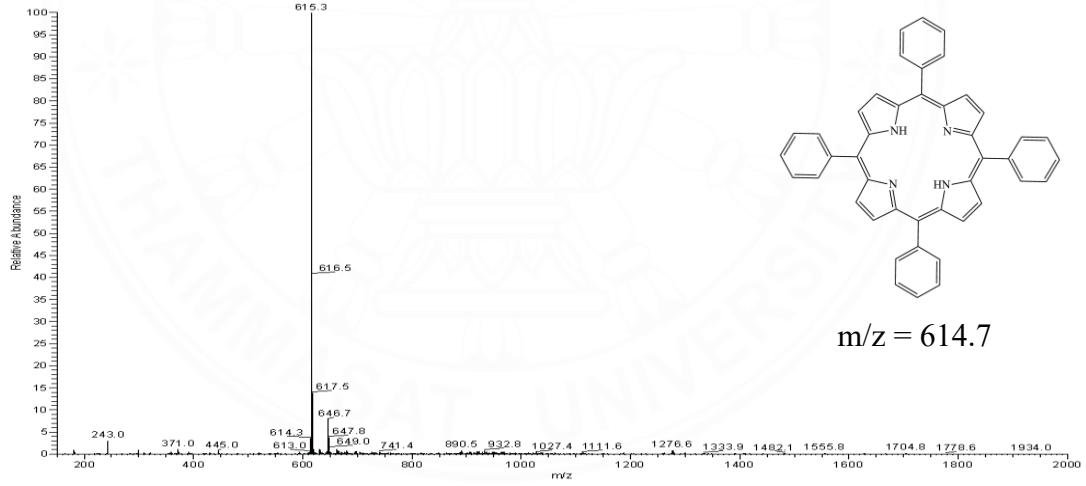

Figure A4 mass spectrum of TPP 4

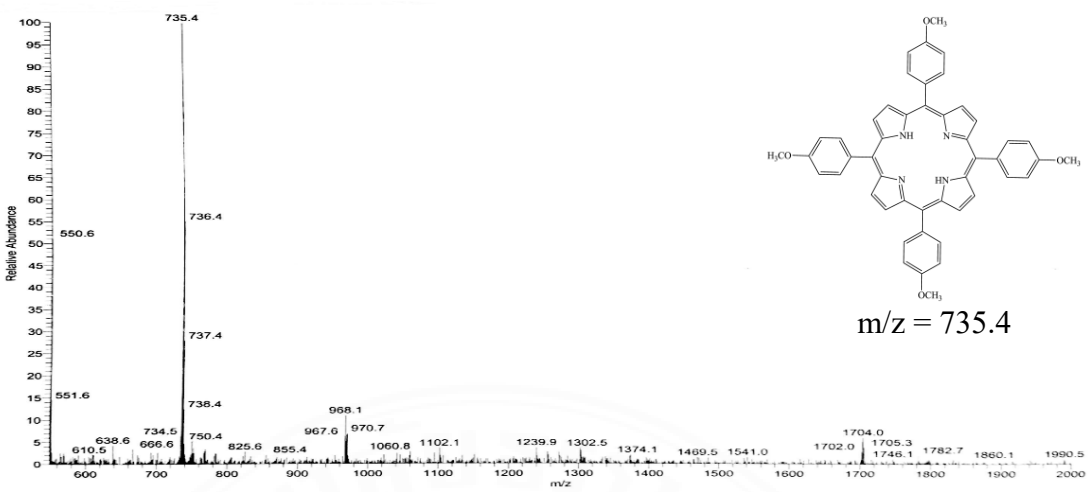

Figure A5 mass spectrum of TOMPP 5

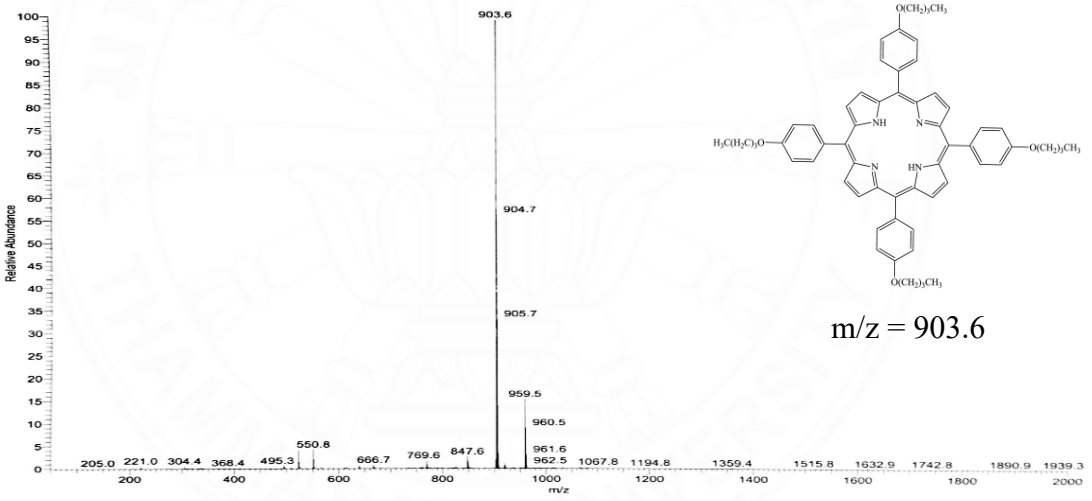

Figure A6 mass spectrum of TOBPP 6

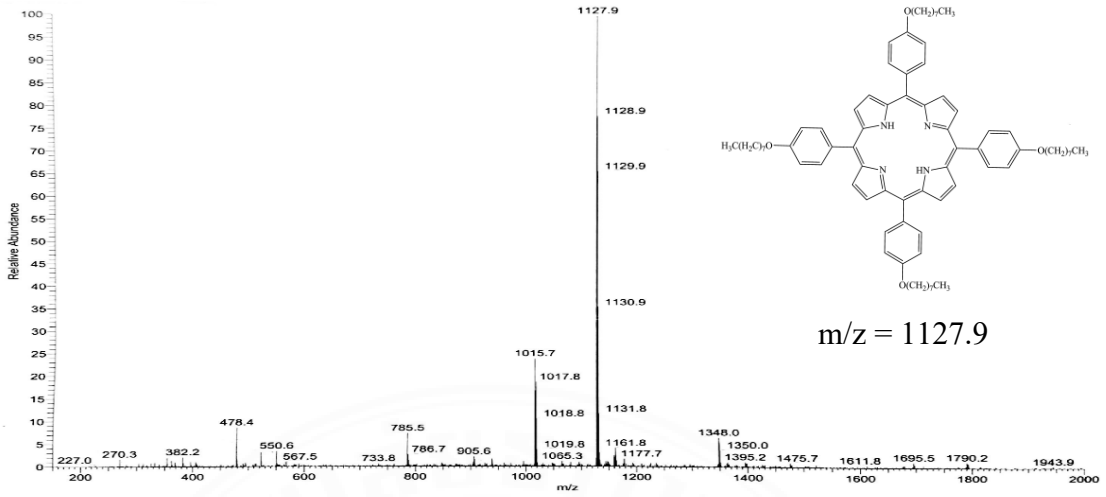

Figure A7 mass spectrum of TOOPP 7

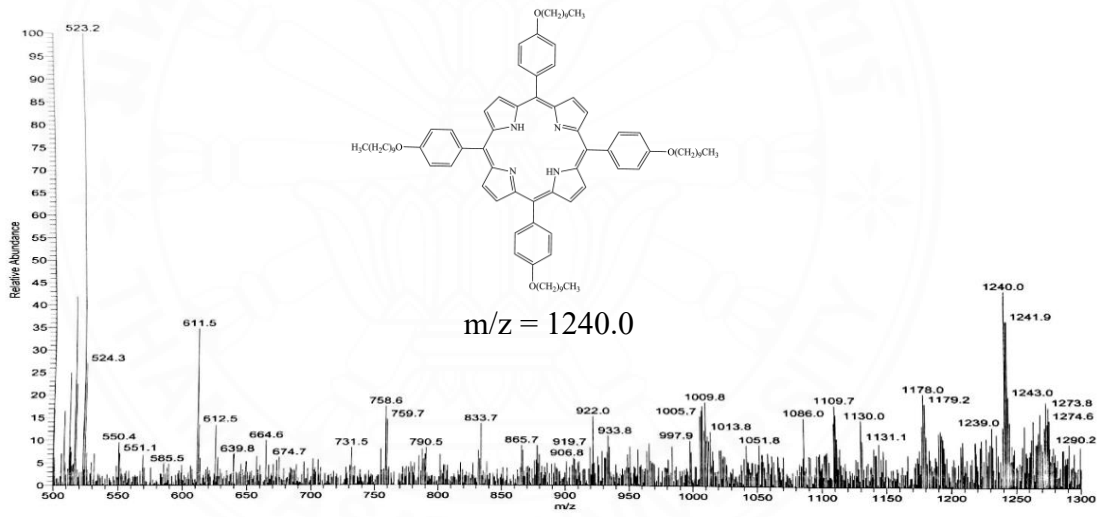

Figure A8 mass spectrum of TODPP 8

Mass spectrum of copper(II) porphyrin complexes

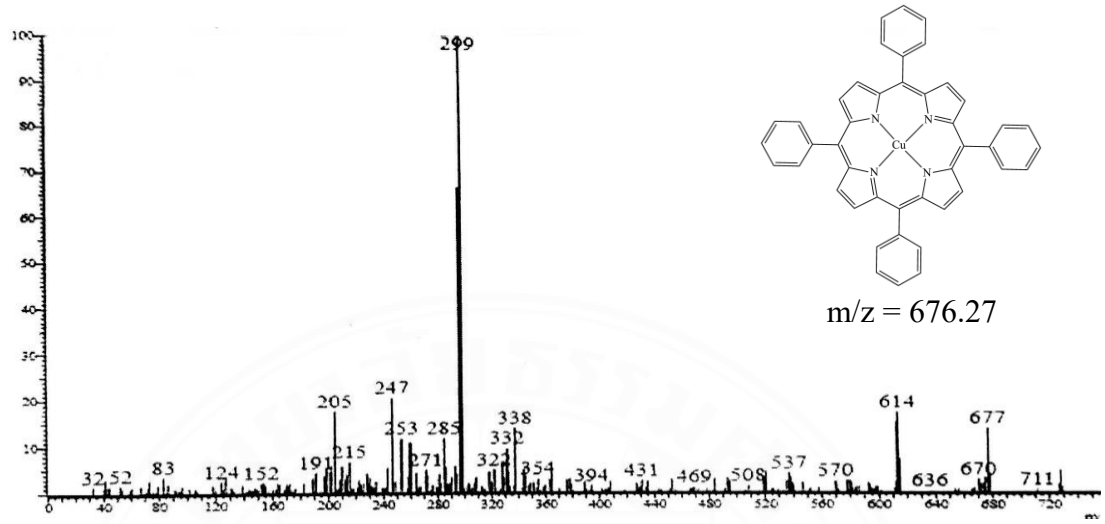

Figure A9 mass spectrum of CuTPP 9

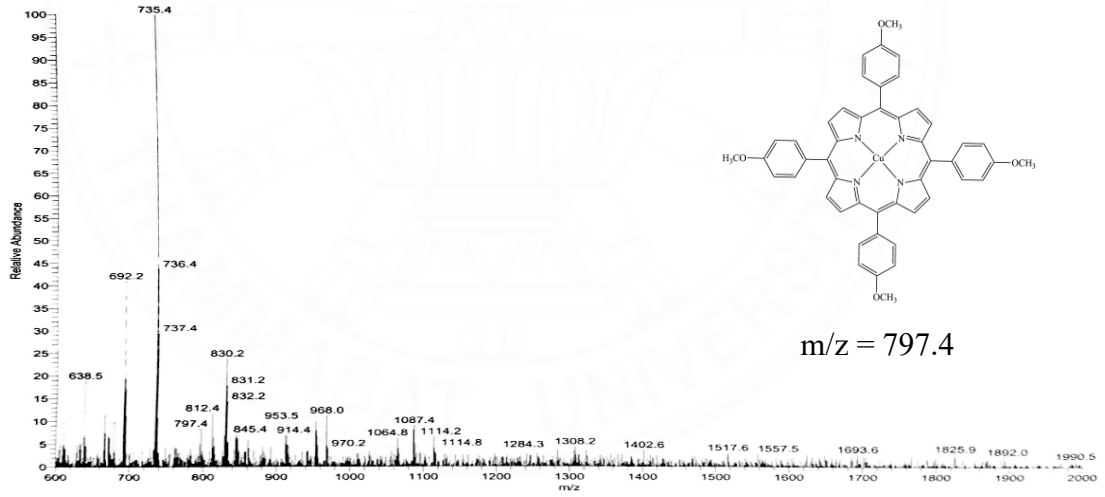

Figure A10 mass spectrum of CuTOMPP 10

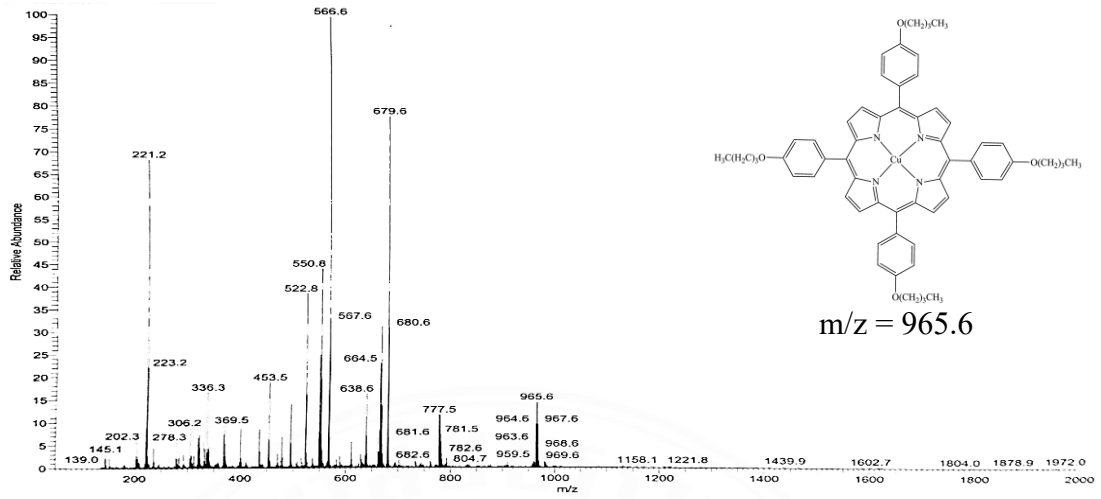

Figure A11 mass spectrum of CuTOBPP 11

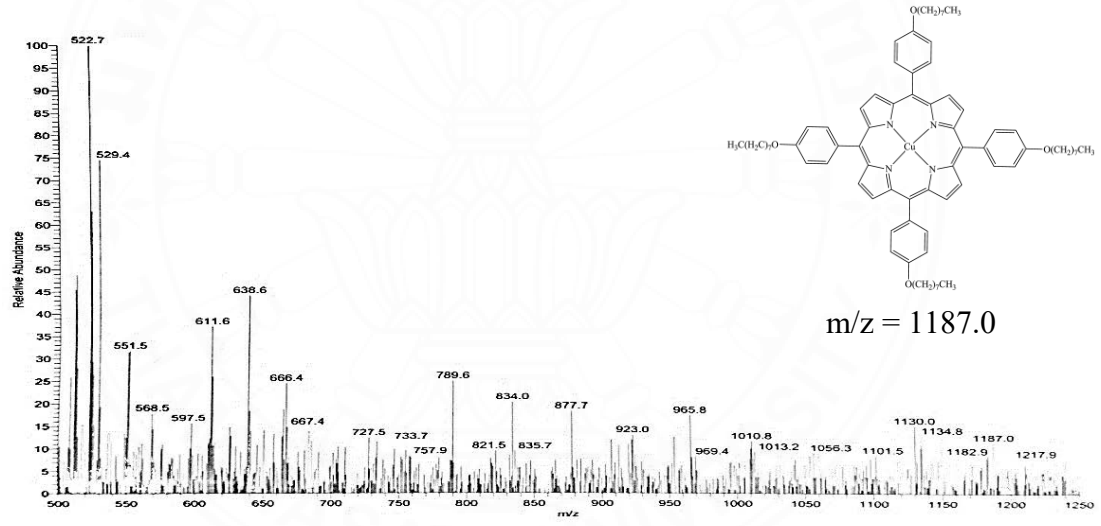

Figure A12 mass spectrum of CuTOOPP 12

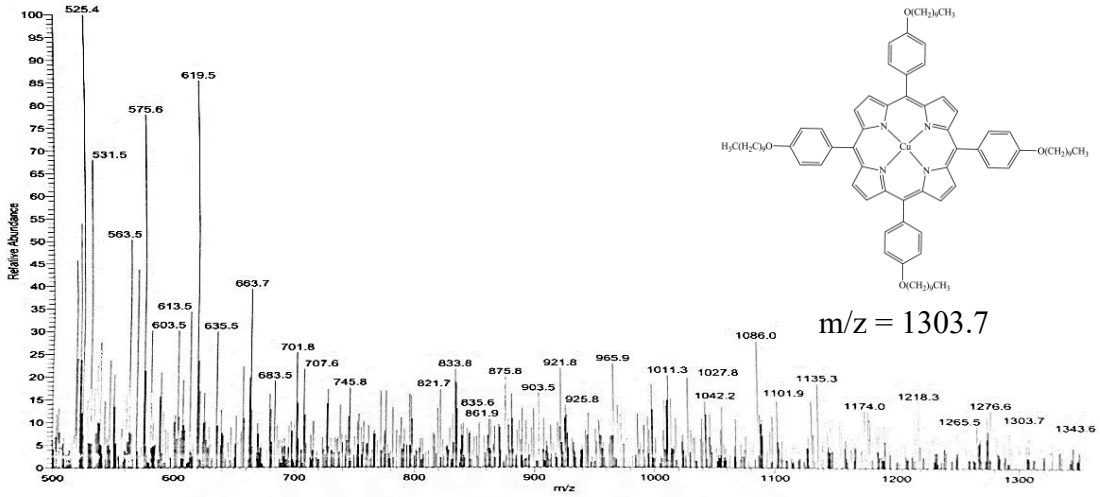

Figure A13 mass spectrum of CuTODPP 13

Mass spectrum of silver(II) porphyrin complexes

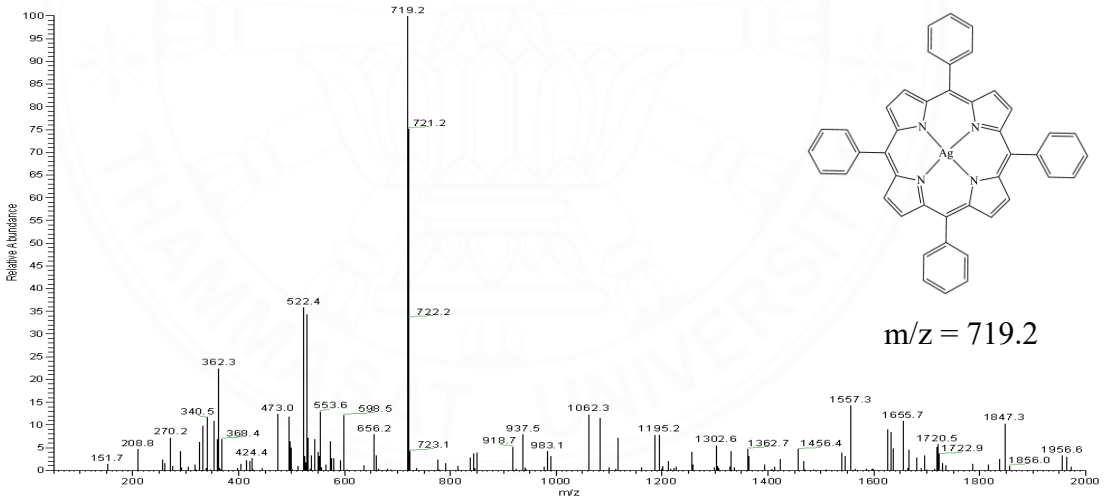

Figure A14 mass spectrum of AgTPP 14

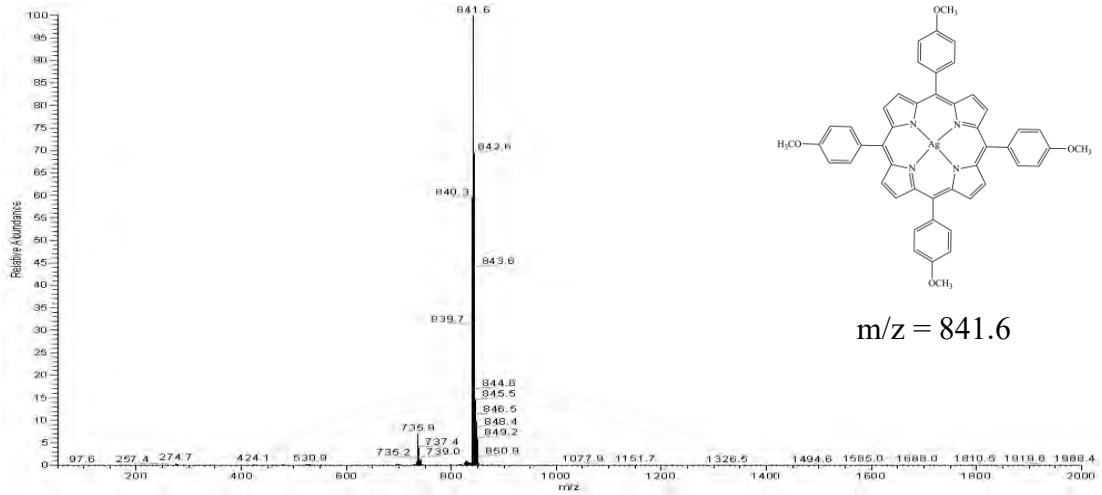

Figure A15 mass spectrum of AgTOMPP 15

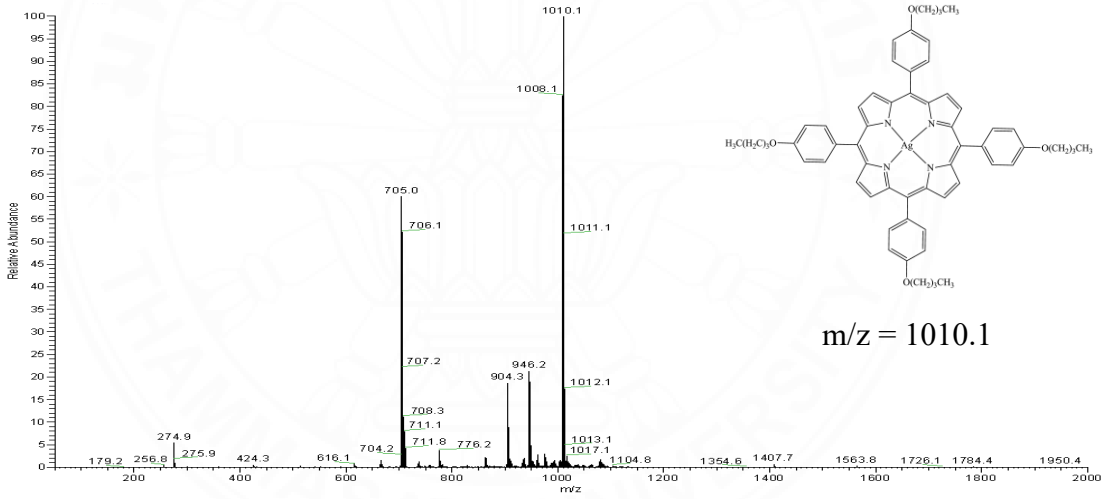

Figure A16 mass spectrum of AgTOBPP 16

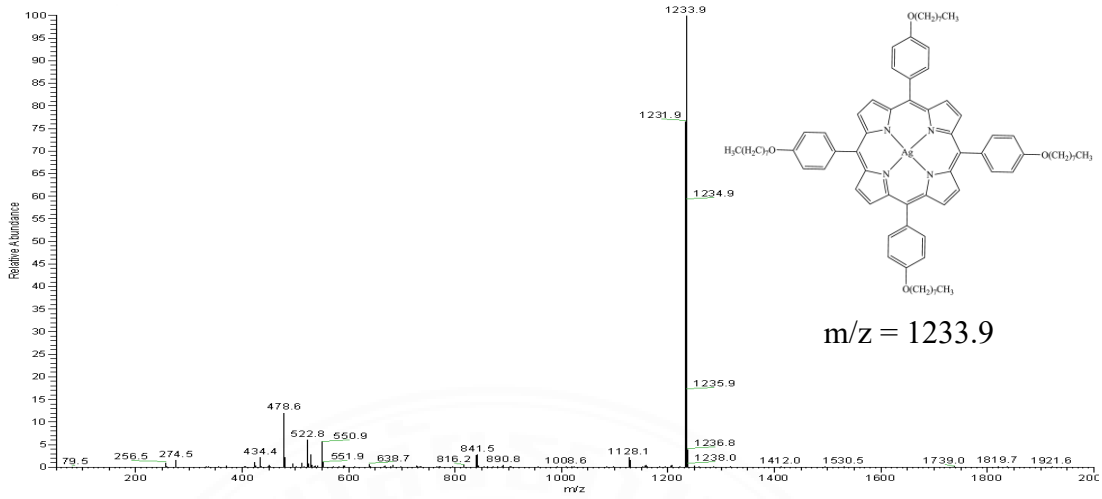

Figure A17 mass spectrum of AgTOOPP 17

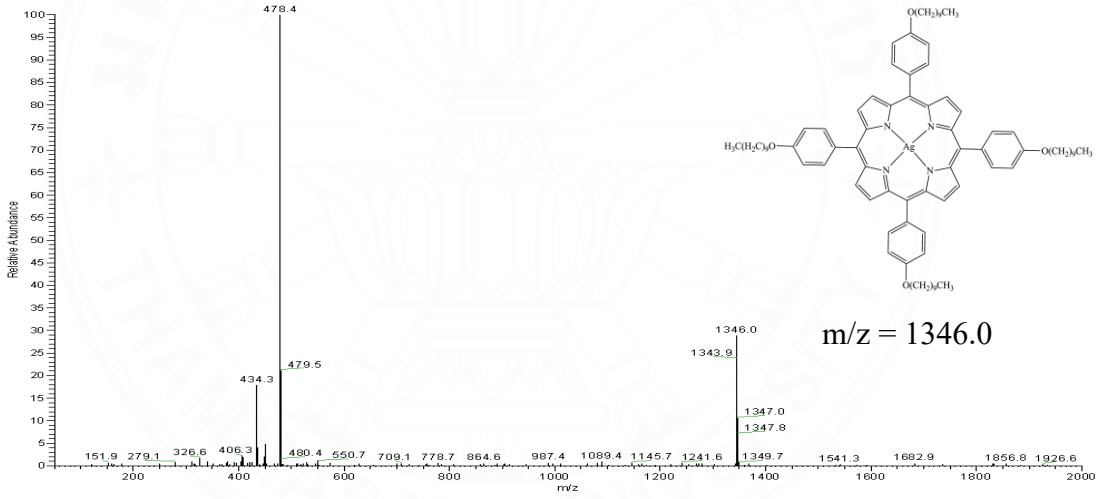

Figure A18 mass spectrum of AgTODPP 18

Mass spectrum of gold(III) porphyrin

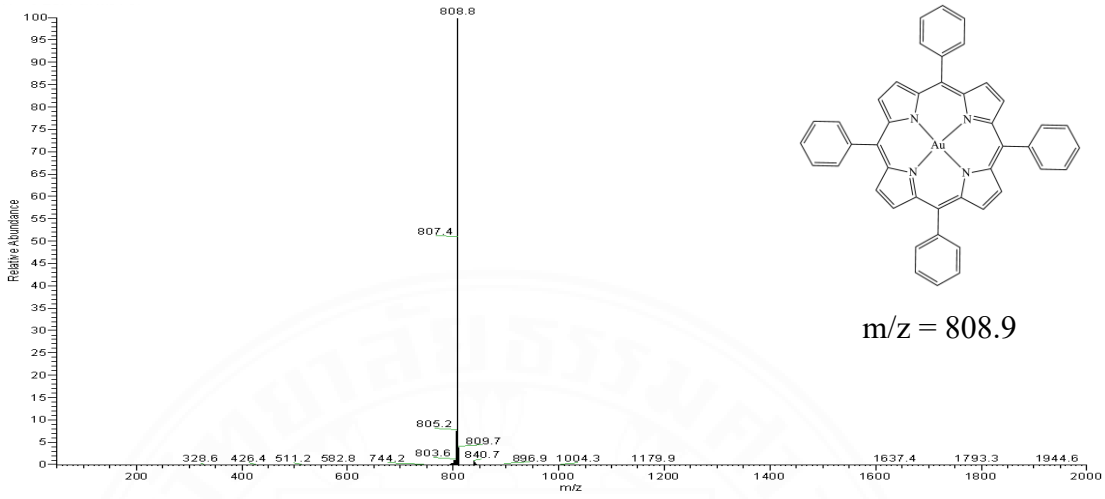

Figure A19 mass spectrum of AuTPP 19

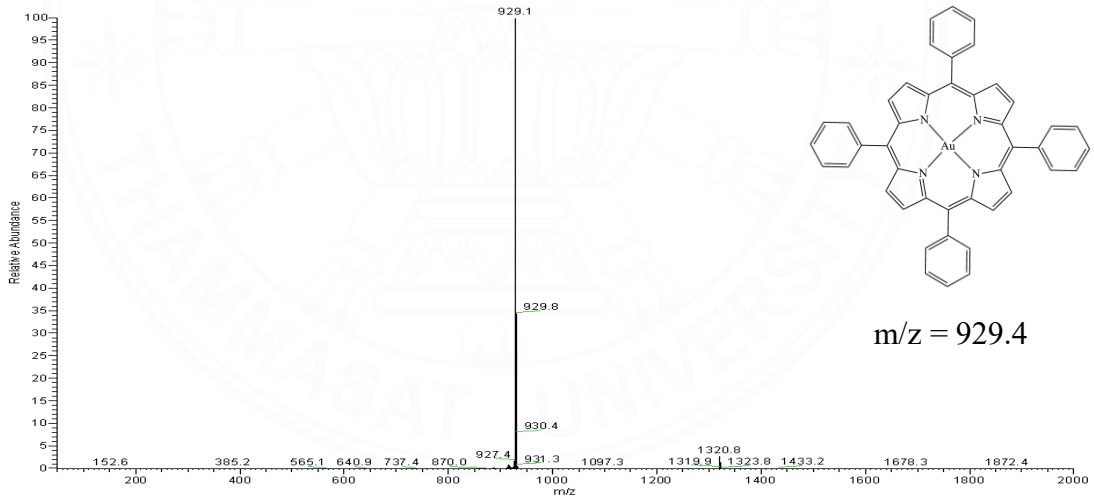

Figure A20 mass spectrum of AuTOMPP 20

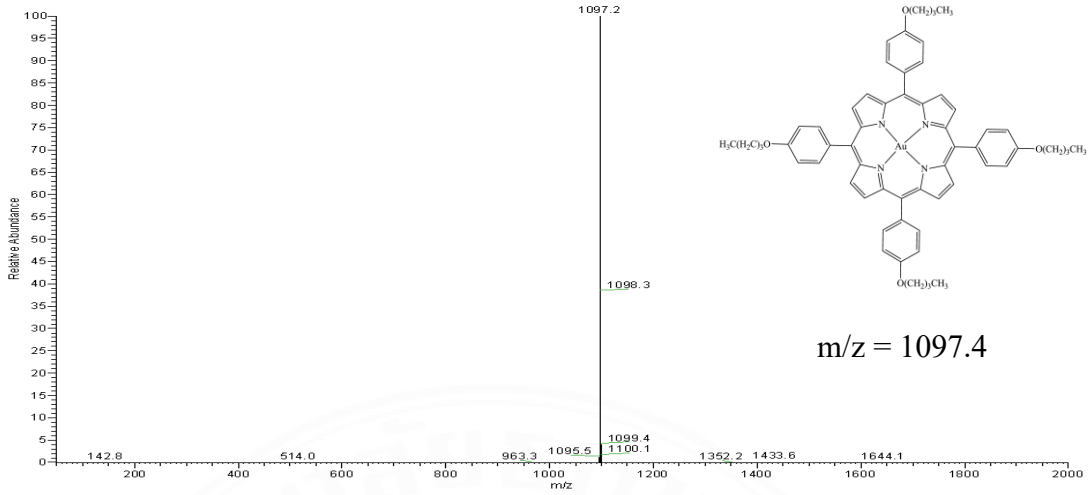

Figure A21 mass spectrum of AuTOBPP 21

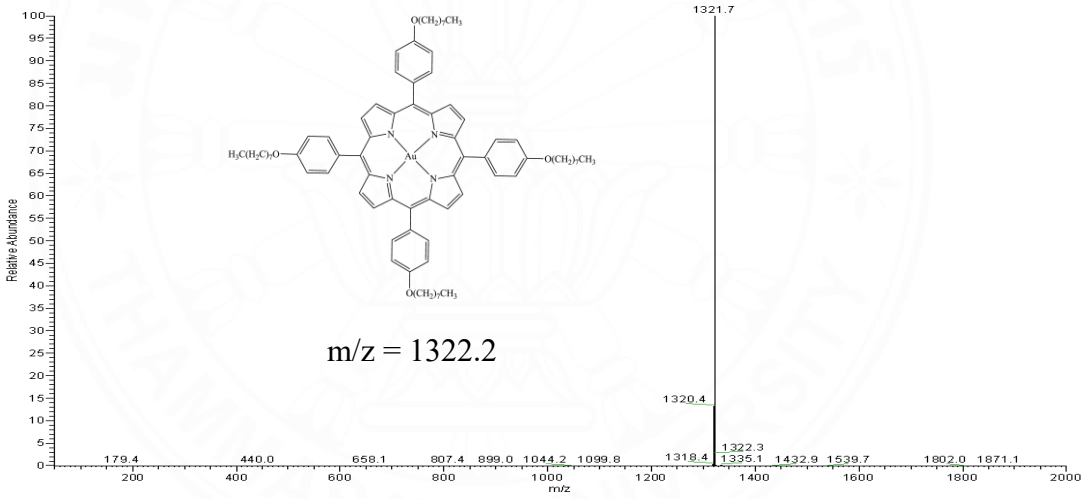

Figure A22 mass spectrum of AuTOOPP 22

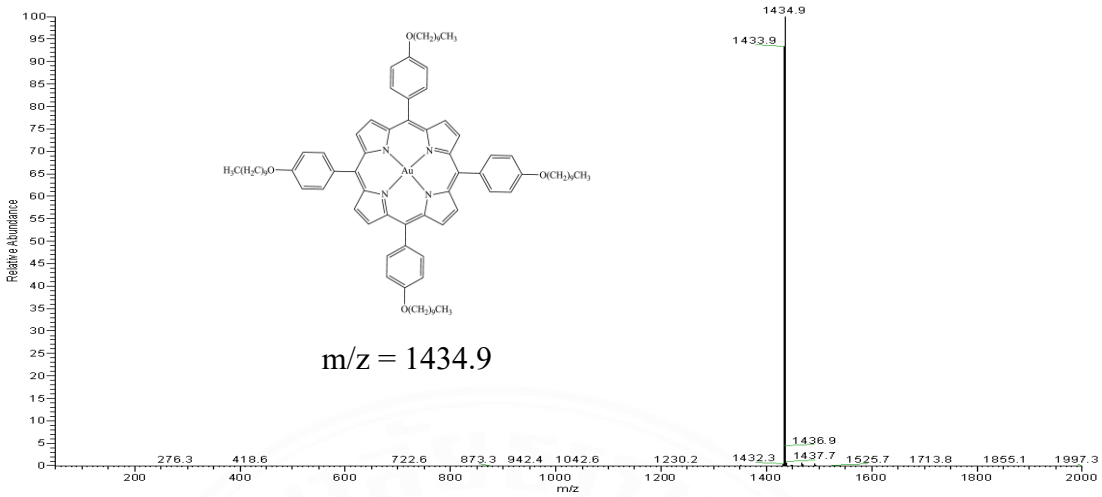

Figure A23 mass spectrum of AuTODPP 23

APPENDIX B

NEUCLEAR MAGNETIC RESONANCE SPCETROSCOPY

^{1}H NMR spectrum of alkyloxybenzaldehyde

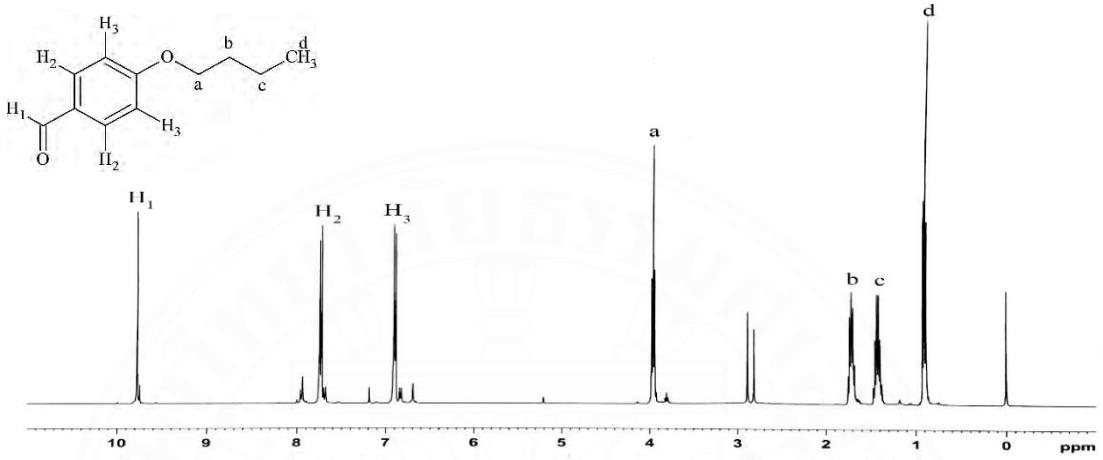

Figure B1 The ^{1}H NMR spectrum of butyloxybenzaldehyde 1 in chloroform-d

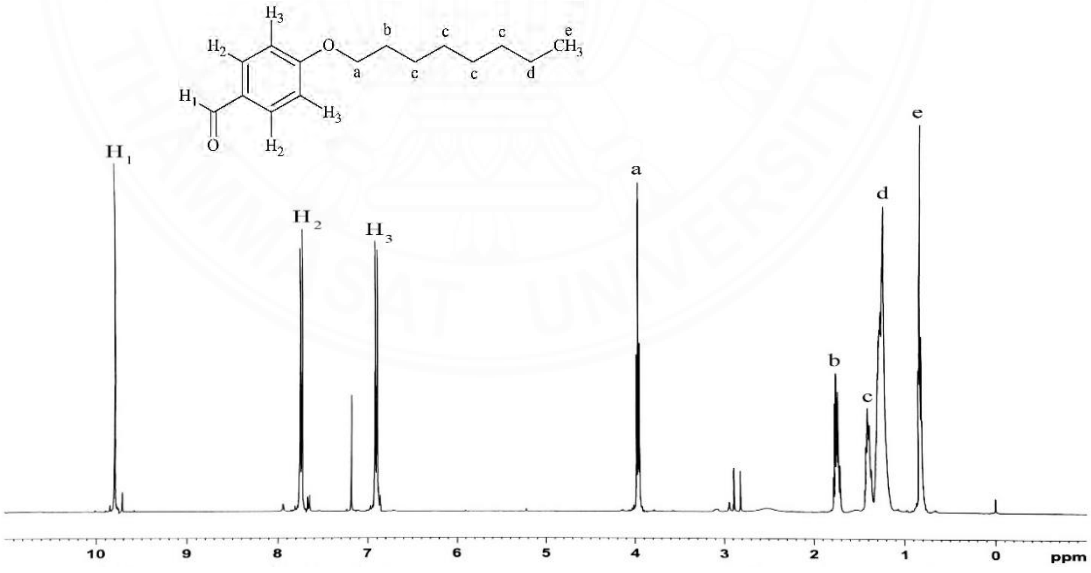

Figure B2 The ^{1}H NMR spectrum of octyloxybenzaldehyde 2 in chloroform-d

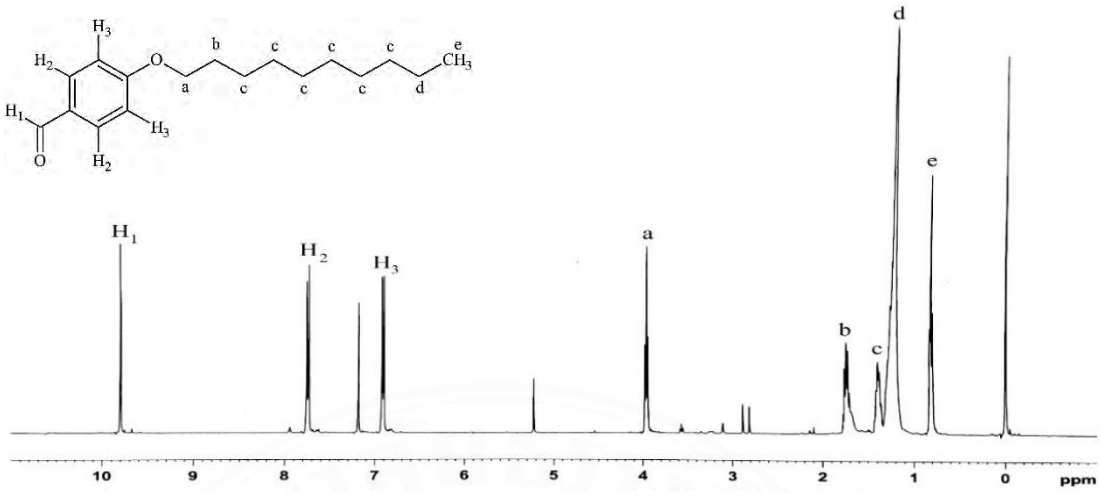

Figure B3 The ^{1}H NMR spectrum of dectyloxybenzaldehyde 3 in chloroform-d

^{13}C NMR spectrum of alkyloxybenzaldehyde

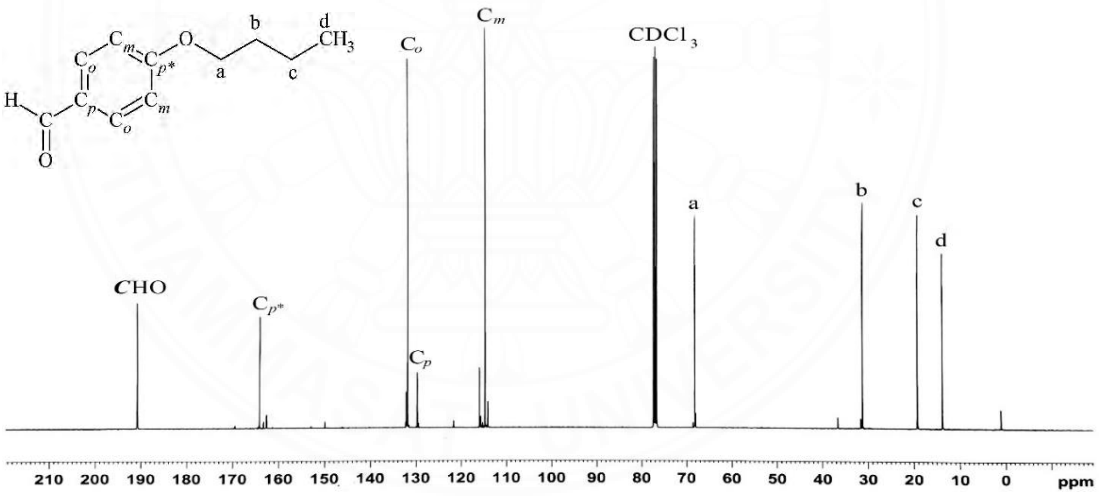

Figure B4 The ^{13}C NMR spectrum of butyloxybenzaldehyde 1 in chloroform-d

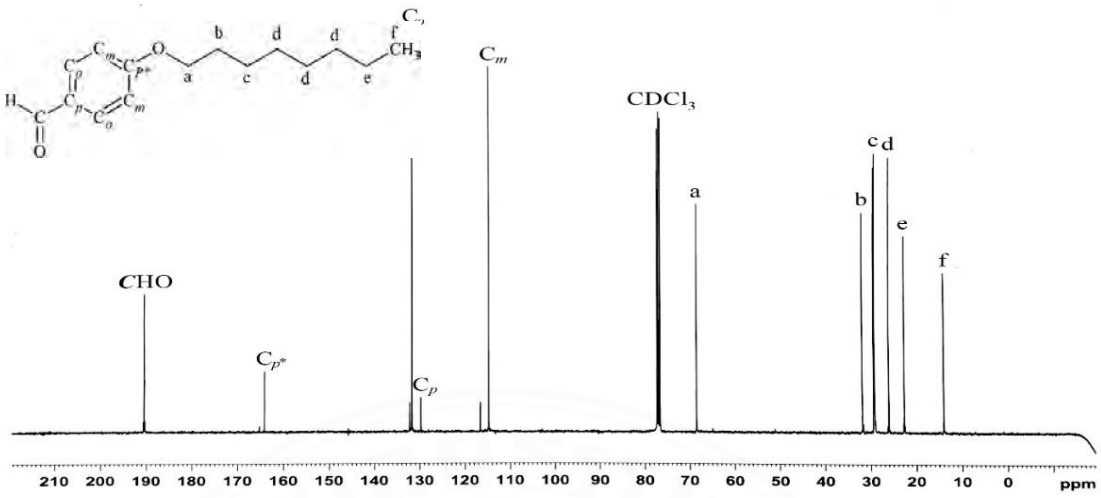

Figure B5 ^{13}C NMR spectrum of octyloxybenzaldehyde 2 in chloroform-d

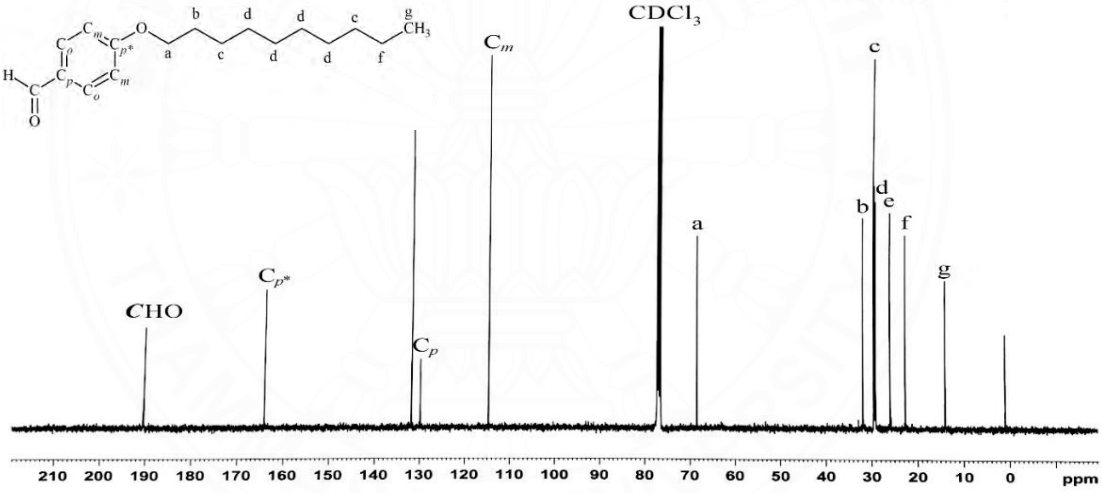

Figure B6 The ^{13}C NMR spectrum of dectyloxybenzaldehyde 3 in chloroform-d

^{1}H NMR spectrum of free-base porphyrin compounds

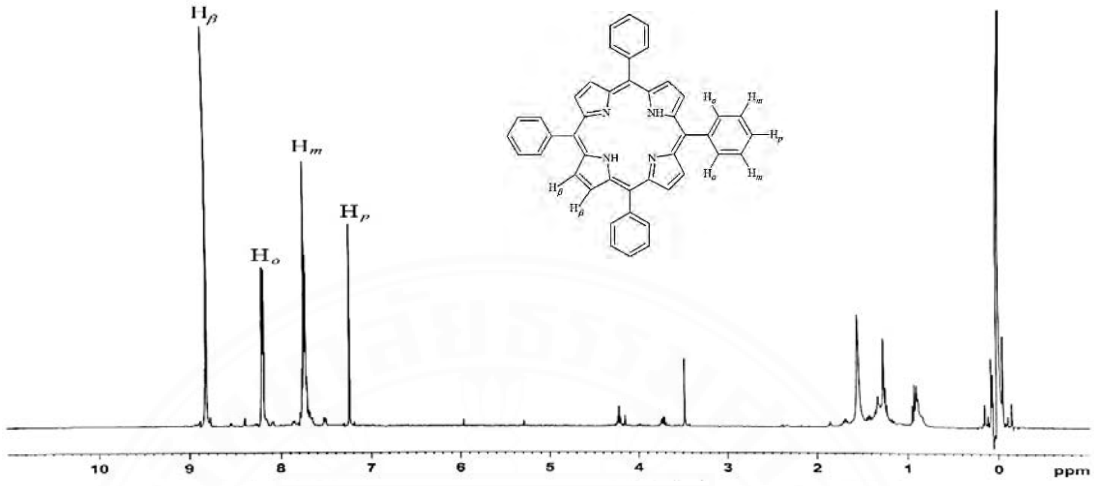

Figure B7 The ^{1}H NMR spectrum of TPP 4 in chloroform-d ($CDCl_3$)

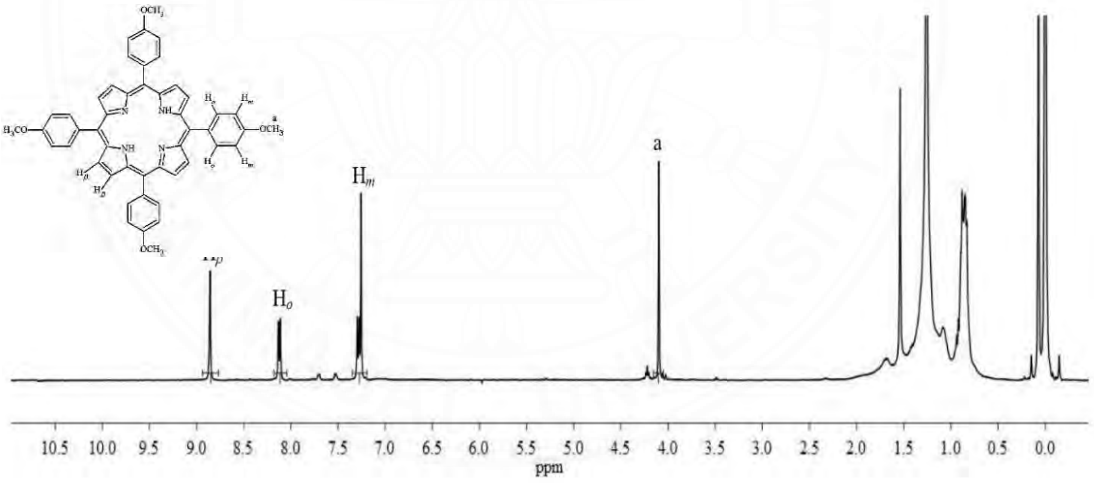

Figure B8 The ^{1}H NMR spectrum of TOMPP 5 in chloroform-d ($CDCl_3$)

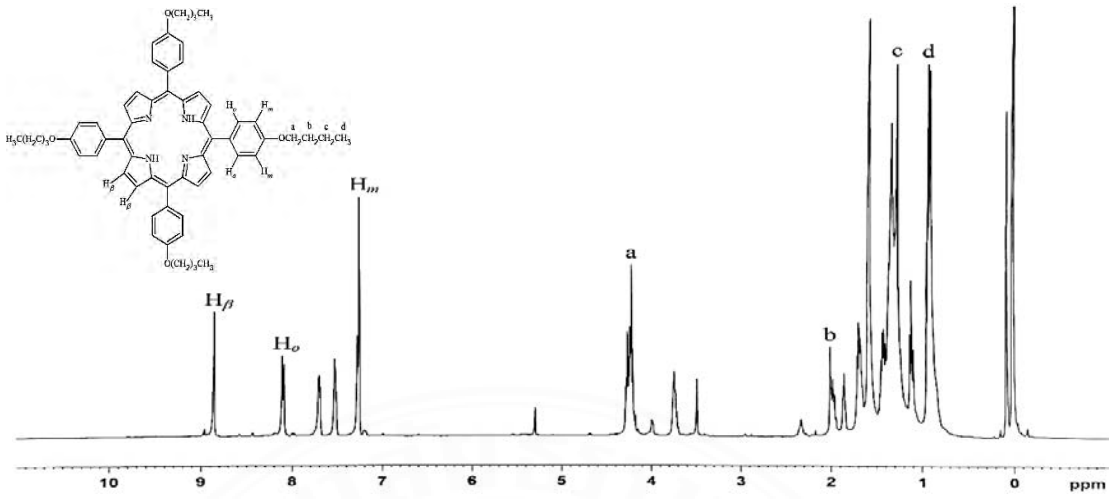

Figure B9 The ^{1}H NMR spectrum of TOBPP 6 in chloroform-d ($CDCl_3$)

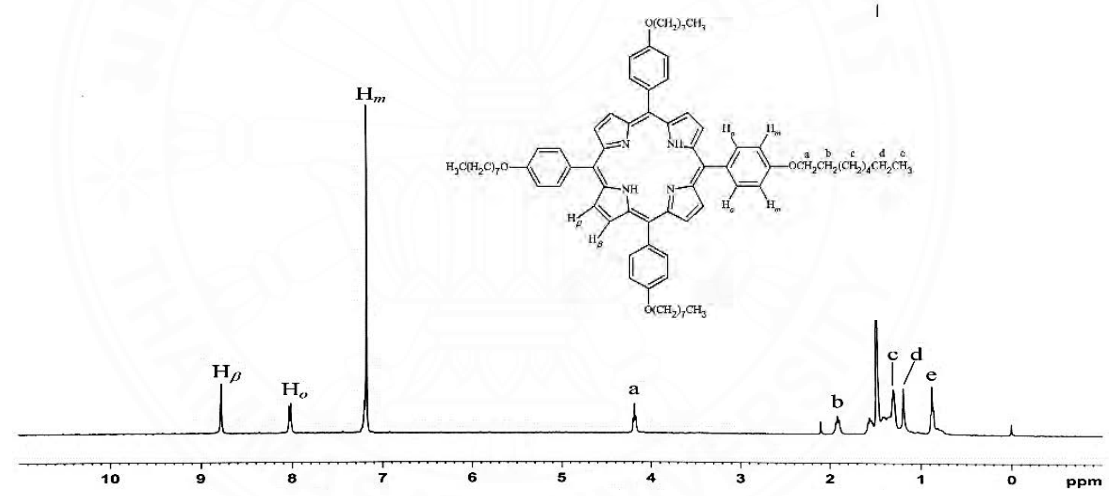

Figure B10 The ^{1}H NMR spectrum of TOOPP 7 in chloroform-d ($CDCl_3$)

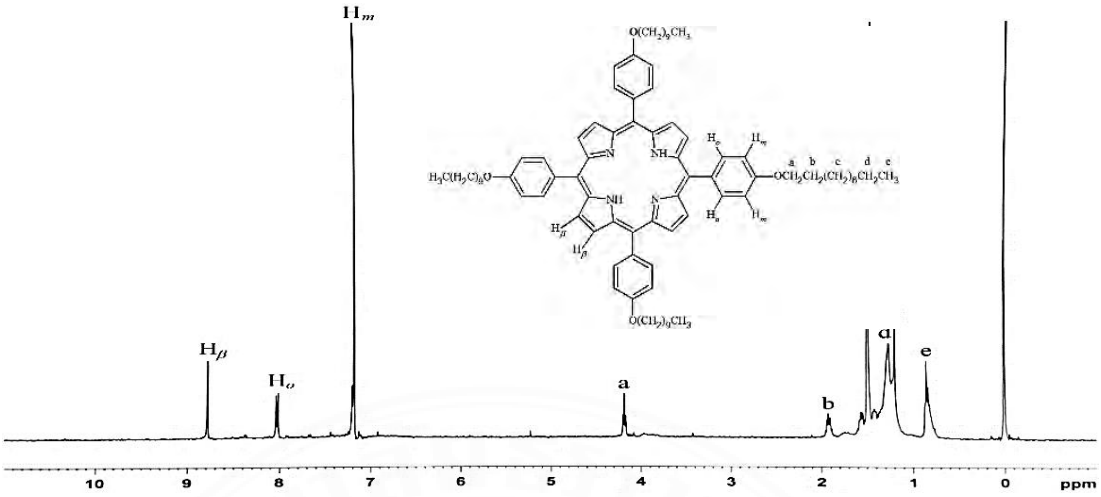

Figure B11 The ^{1}H NMR spectrum of TODPP 8 in chloroform-d ($CDCl_3$)

^{13}C NMR spectrum of free-base porphyrin compopunds

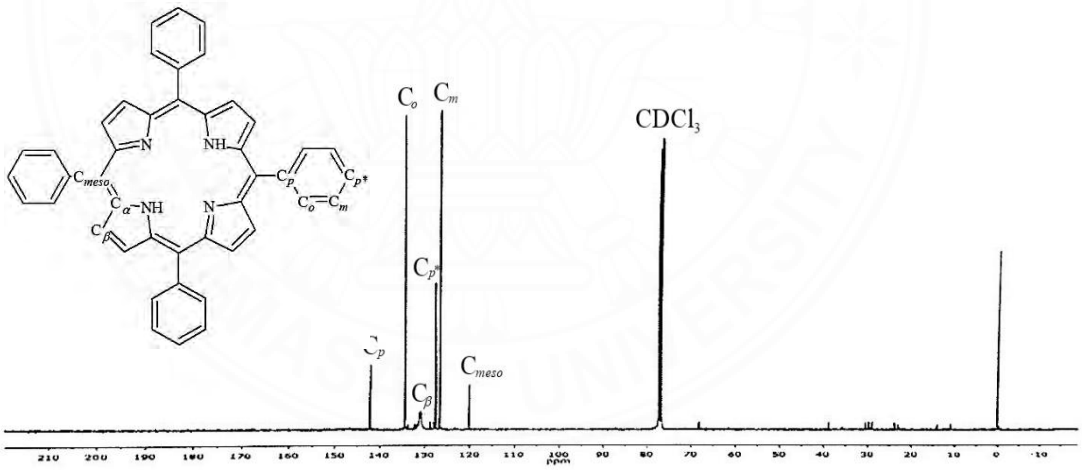

Figure B12 The ^{13}C NMR spectrum of TPP 4 in chloroform-d ($CDCl_3$)

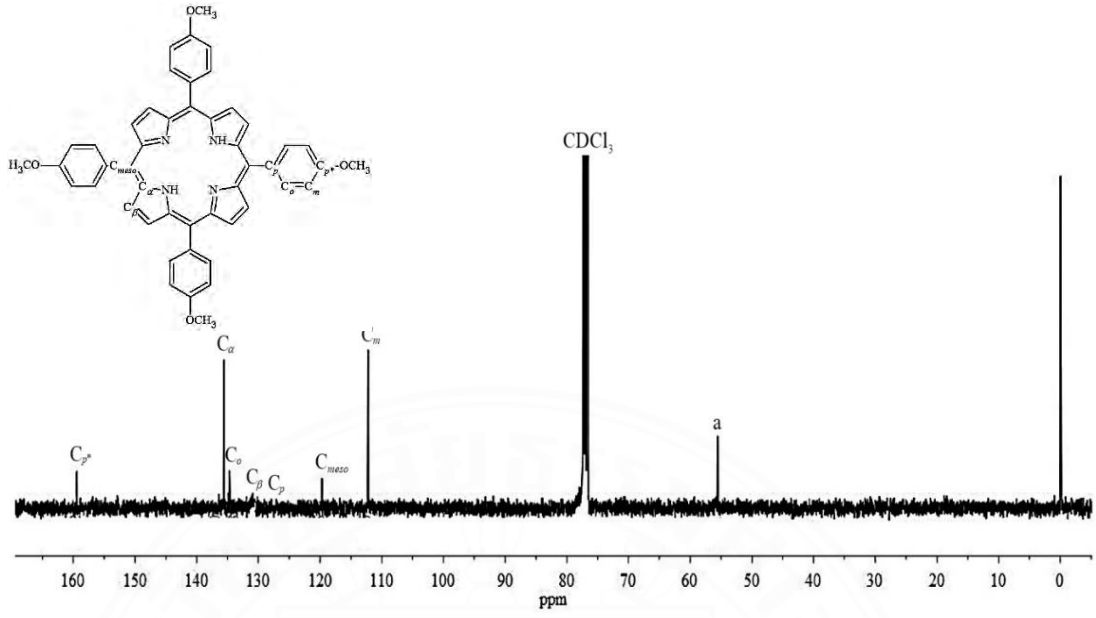

Figure B13 The ^{13}C NMR spectrum of TOMPP 5 in chloroform-d ($CDCl_3$)

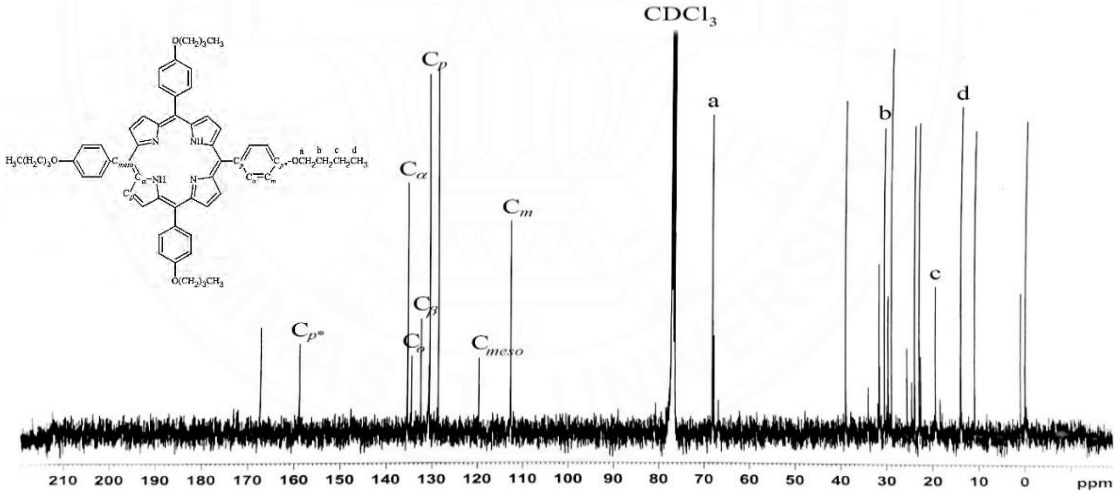

Figure B14 The ^{13}C NMR spectrum of TOBPP 6 in chloroform-d ($CDCl_3$)

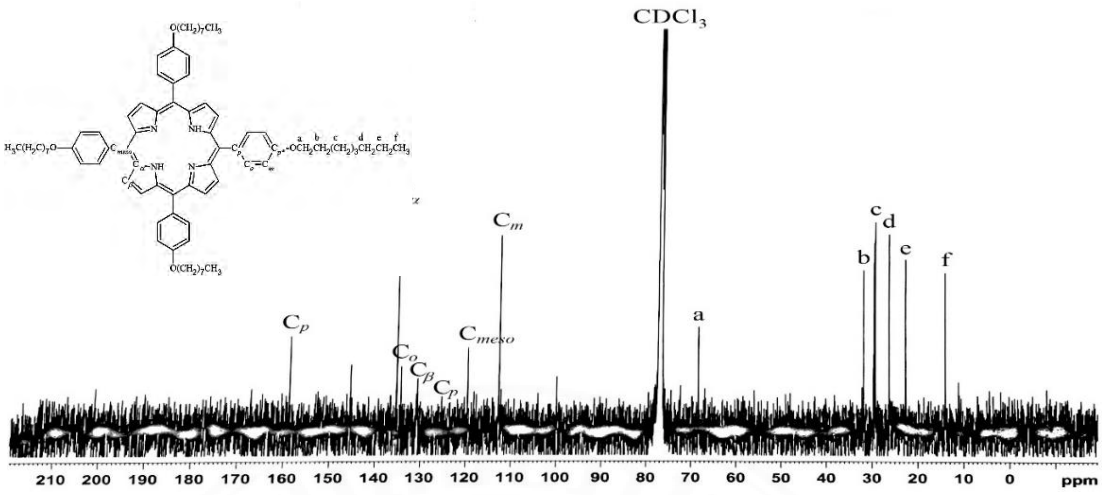

Figure B15 The ^{13}C NMR spectrum of TOOPP 7 in chloroform-d ($CDCl_3$)

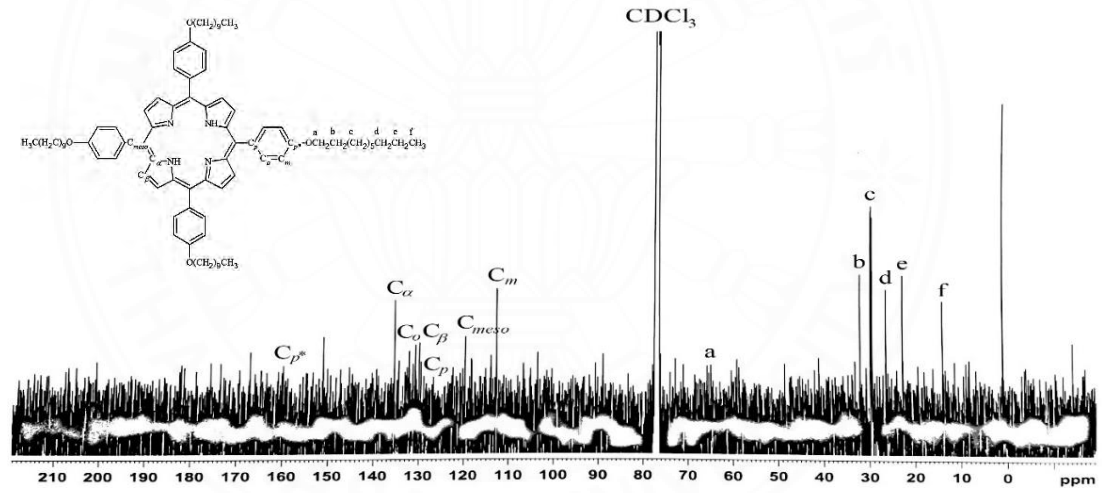

Figure B16 The ^{13}C NMR spectrum of TODPP 8 in chloroform-d ($CDCl_3$)

APPENDIX C
INFRARED SPECTROSCOPY

IR spectra of alkyloxybenzaldehyde

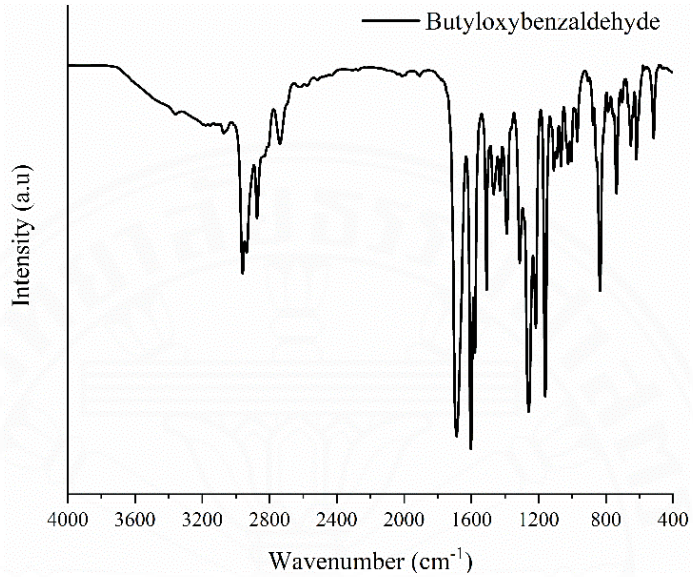

Figure C1 The IR spectrum of butyloxybenzaldehyde 1

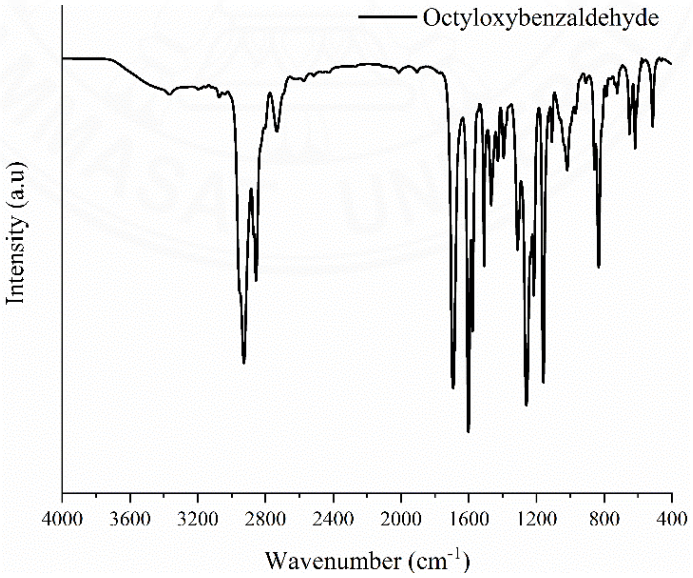

Figure C2 The IR spectrum of octyloxybenzaldehyde 2

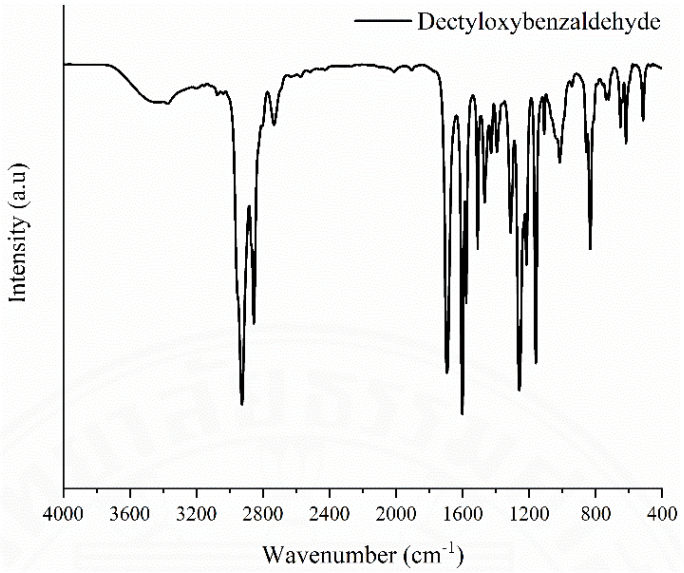

Figure C3 The IR spectrum of dectyloxybenzaldehyde 3

IR spectra of free-base porphyrin

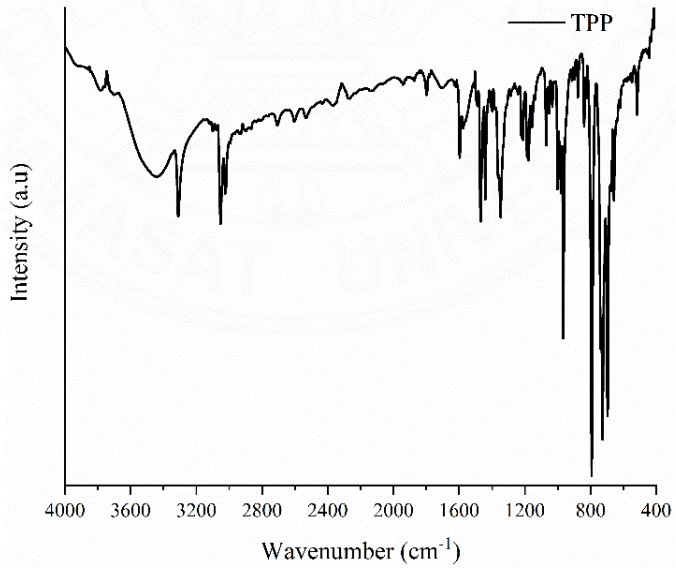

Figure C4 The IR spectrum of TPP 4

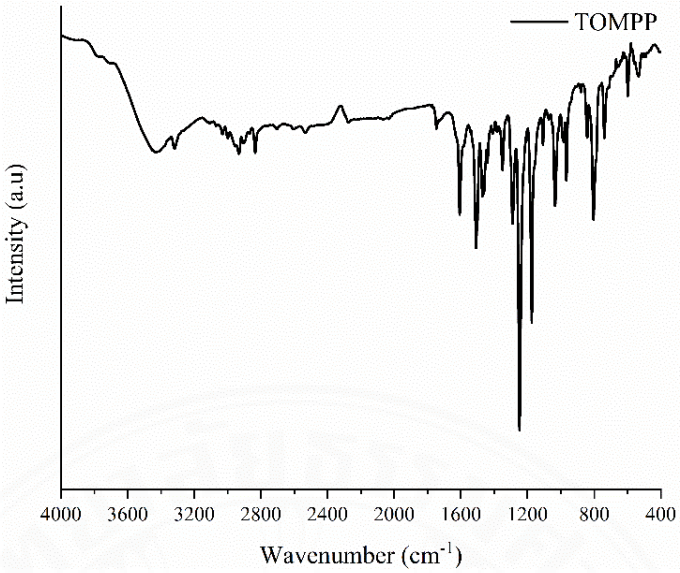

Figure C5 The IR spectrum of TOMPP 5

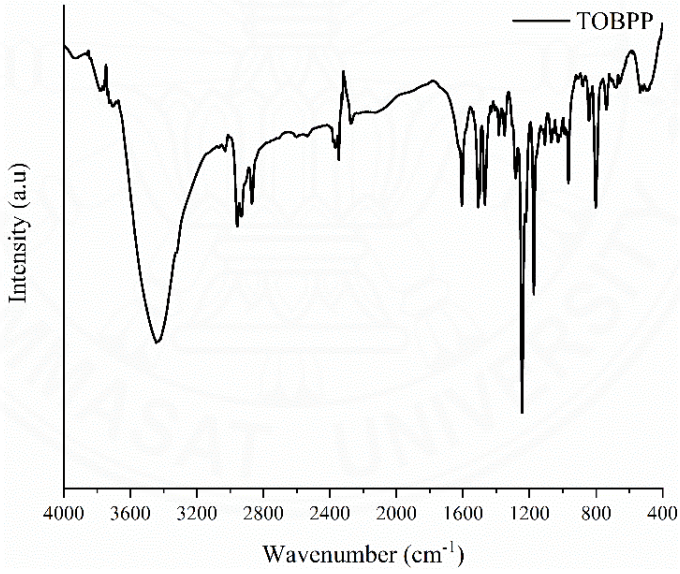

Figure C6 The IR spectrum of TOBPP 6

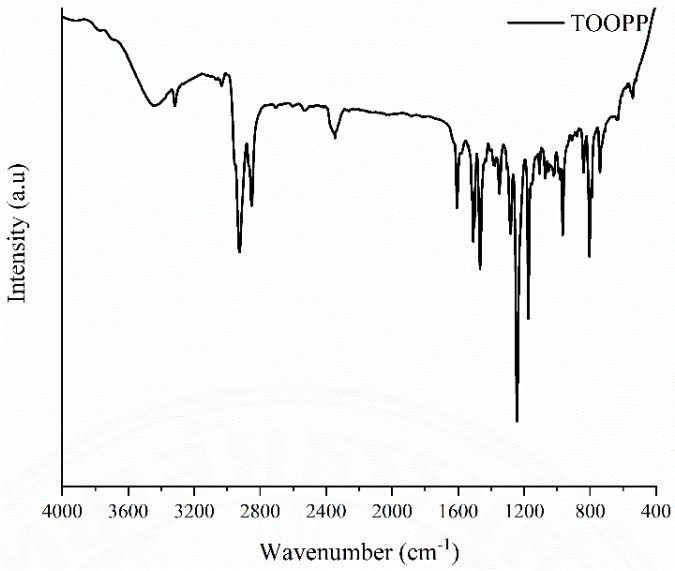

Figure C7 The IR spectrum of TOOPP 7

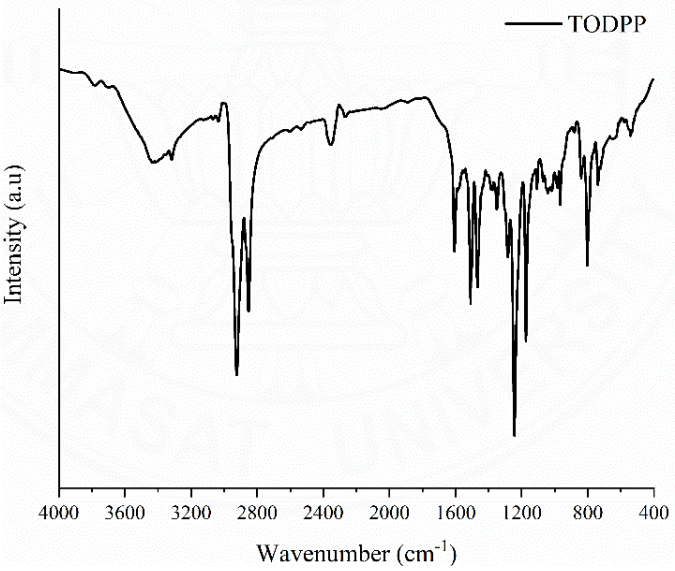

Figure C8 The IR spectrum of TODPP 8

IR spectra of copper(II) porphyrin complexes

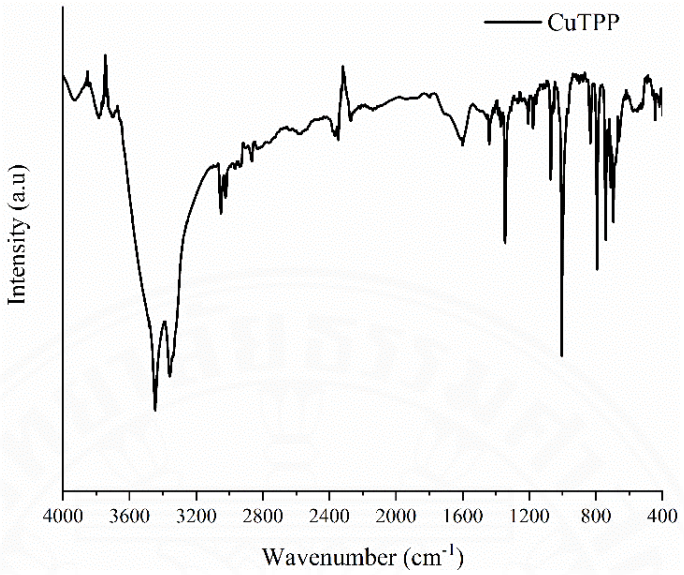

Figure C9 The IR spectrum of CuTPP 9

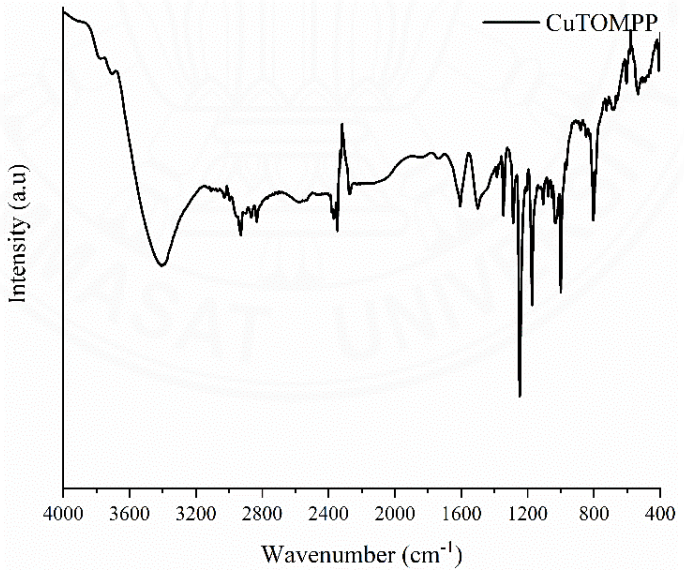

Figure C10 The IR spectrum of CuTOMPP 10

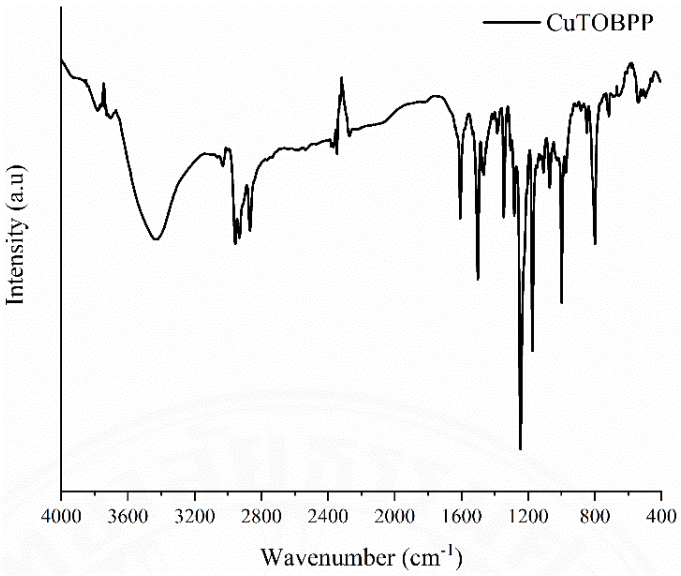

Figure C11 The IR spectrum of CuTOBPP 11

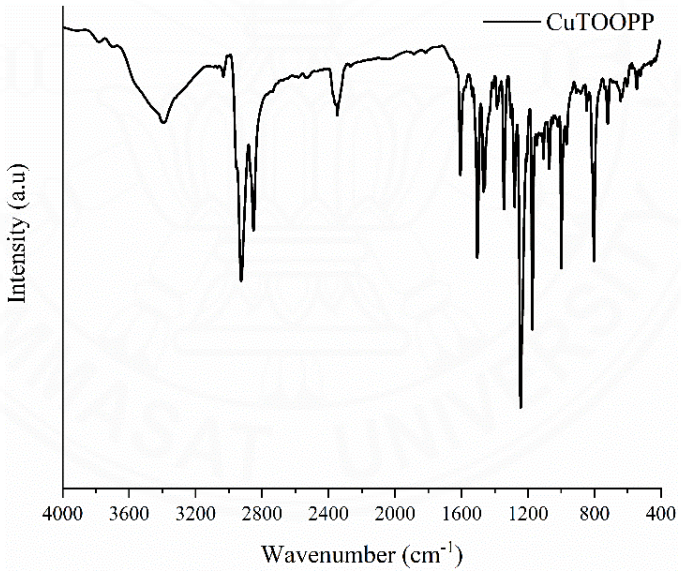

Figure C12 The IR spectrum of CuTOOPP 12

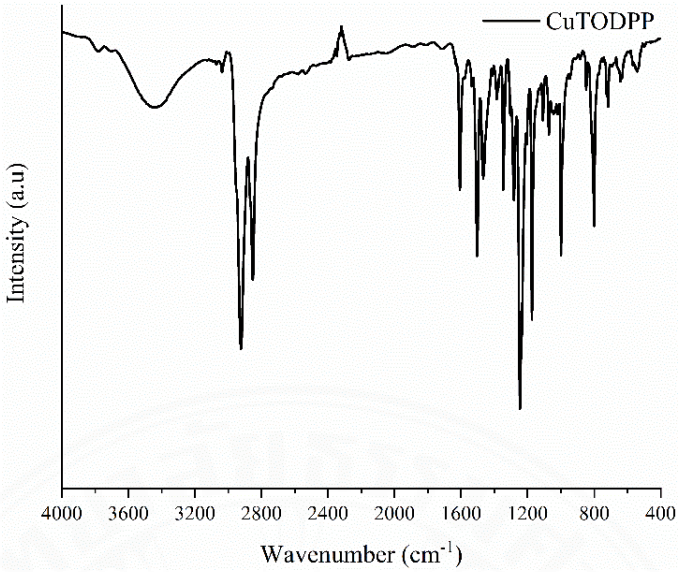

Figure C13 The IR spectrum of CuTODPP 13

IR spectra of silver(II) porphyrin complexes

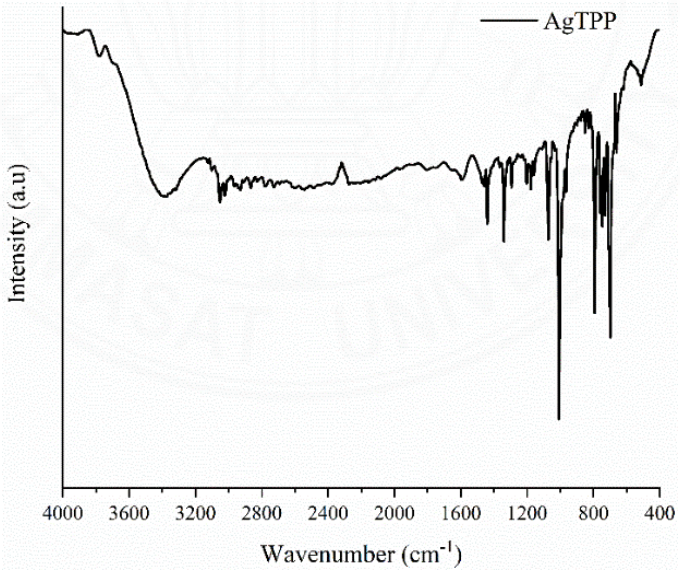

Figure C14 The IR spectrum of AgTPP 14

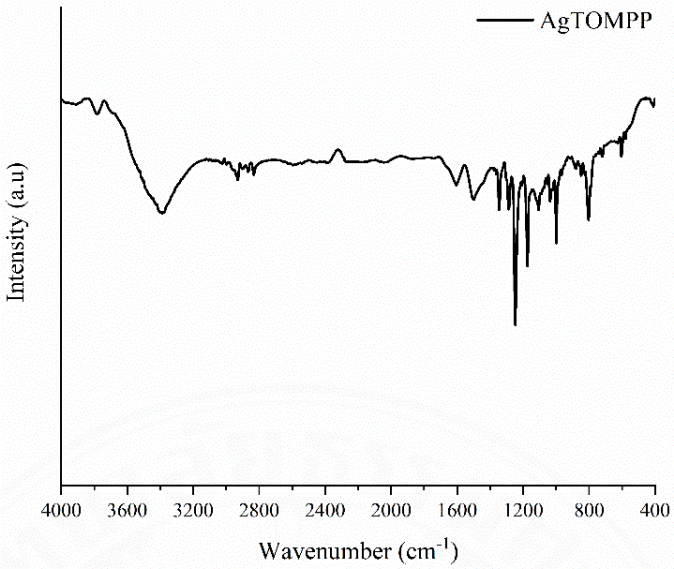

Figure C15 The IR spectrum of AgTOMPP 15

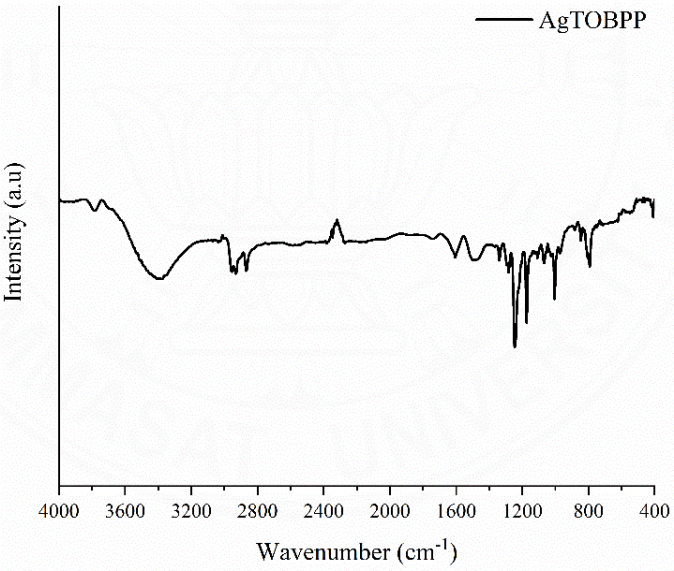

Figure C16 The IR spectrum of AgTOBPP 16

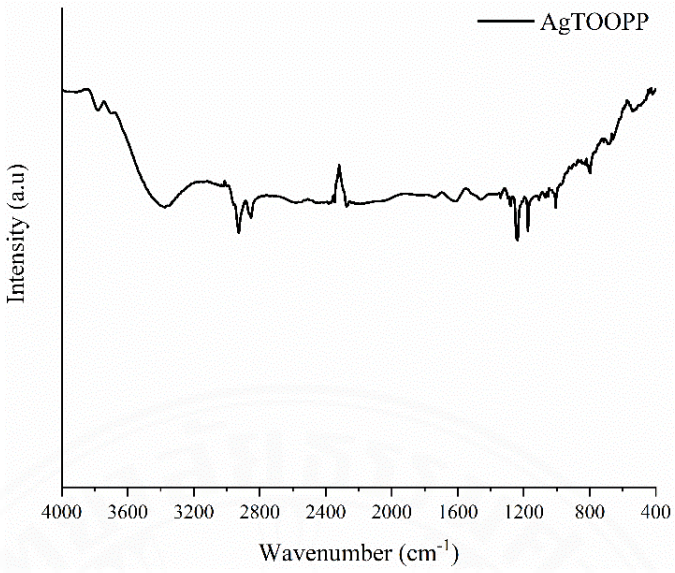

Figure C17 The IR spectrum of AgTOOPP 17

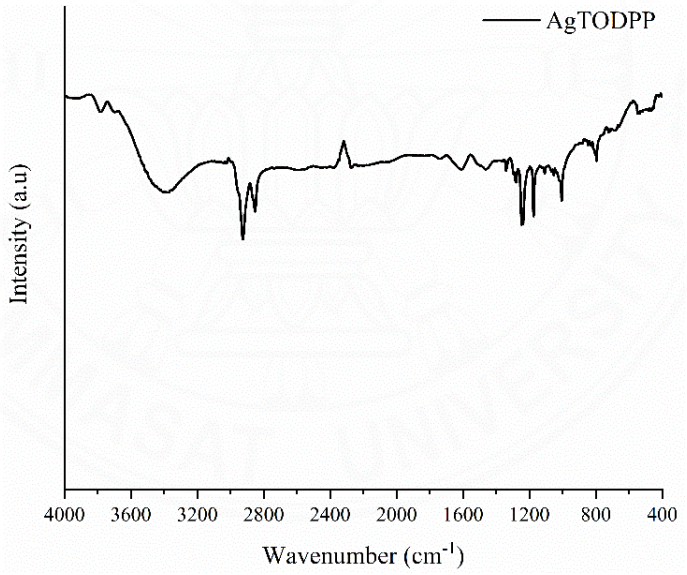

Figure C18 The IR spectrum of AgTODPP 18

IR spectra of gold(III) porphyrin complexes

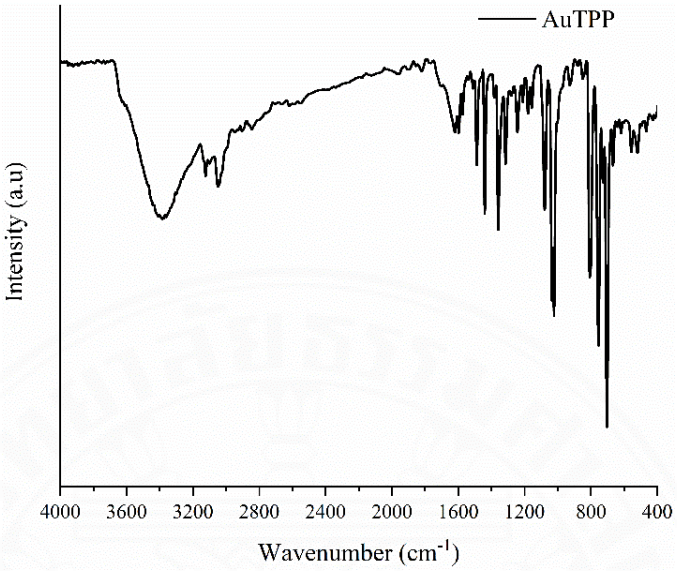

Figure C19 The IR spectrum of AuTPP 19

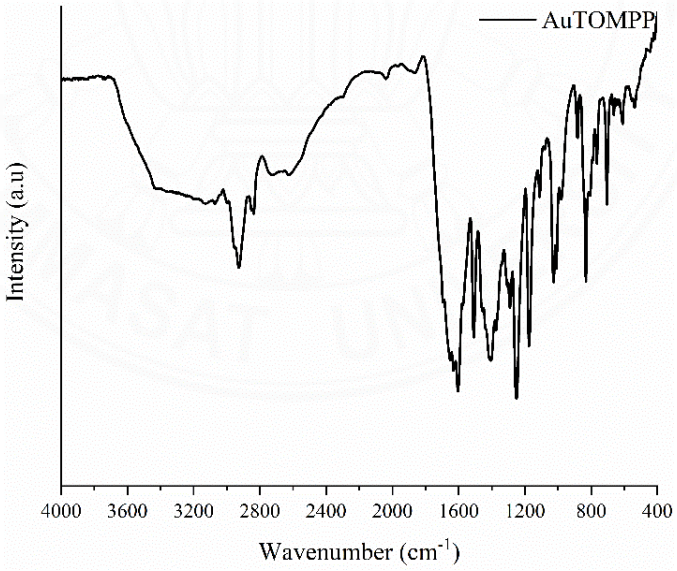

Figure C20 The IR spectrum of AuTOMPP 20

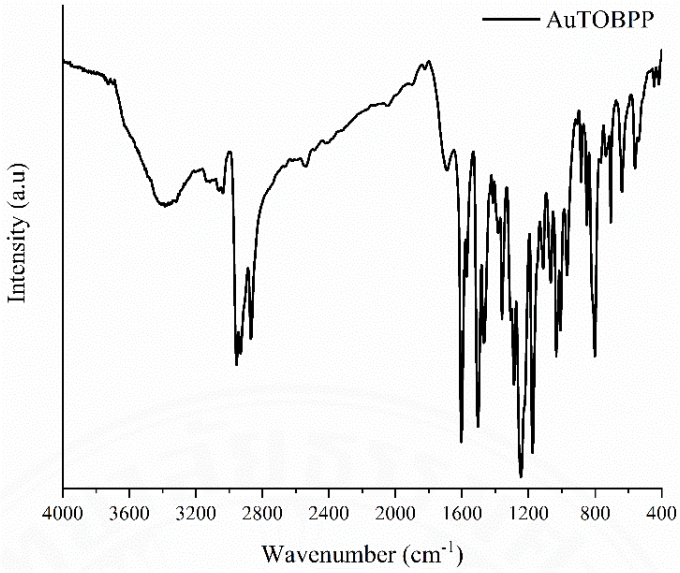

Figure C21 The IR spectrum of AuTOBPP 21

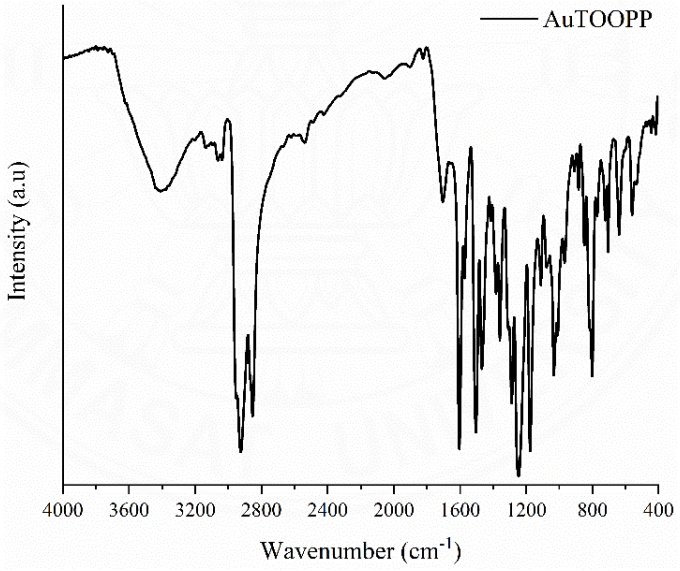

Figure C22 The IR spectrum of AuTOOPP 22

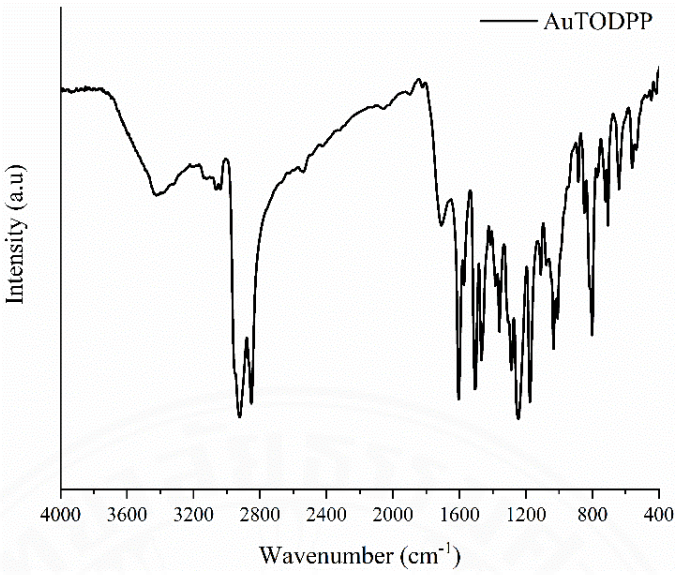

Figure C23 The IR spectrum of AuTODPP 23

APPENDIX D

UV-VISIBLE ABSORPTION SPCETROSCOPY

UV-Visible absorption spectra of free-base porphyrins in dichloromethane

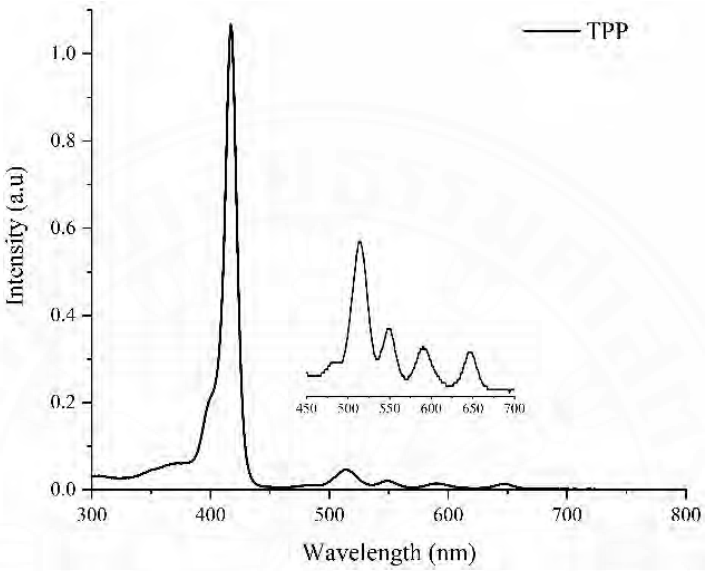

Figure D1 UV-Vis absorption spectra of TPP 4

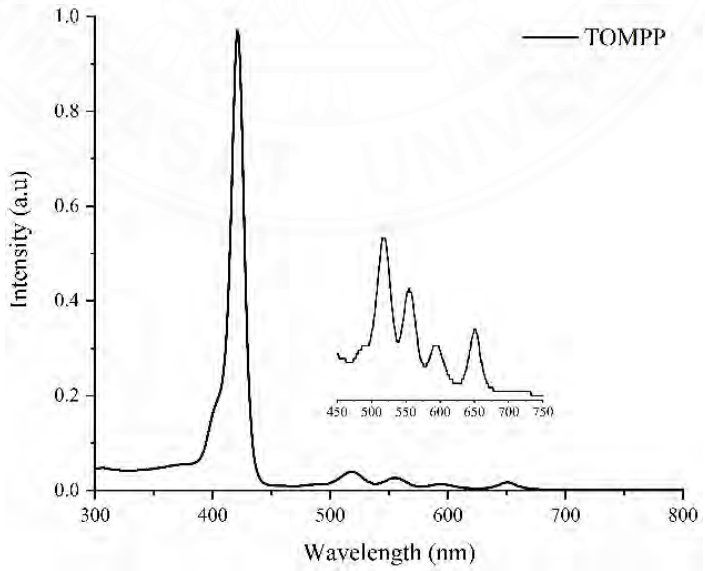

Figure D2 UV-Vis absorption spectra of TOMPP 5

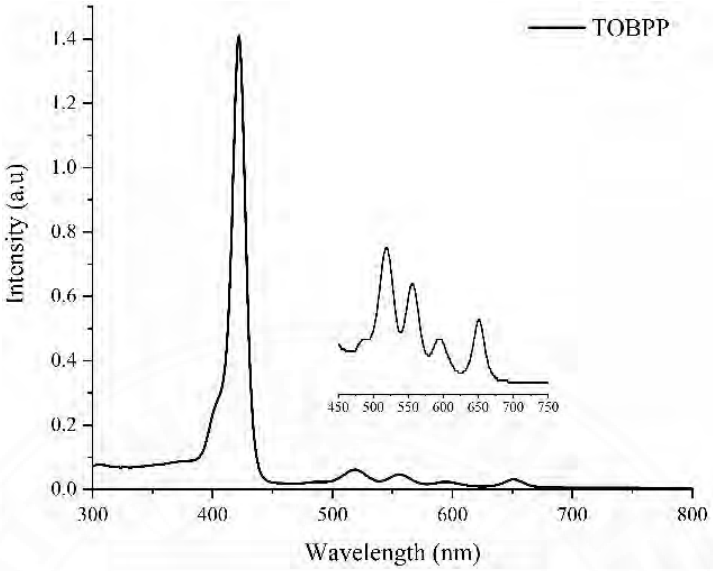

Figure D3 UV-Vis absorption spectra of TOBPP 6

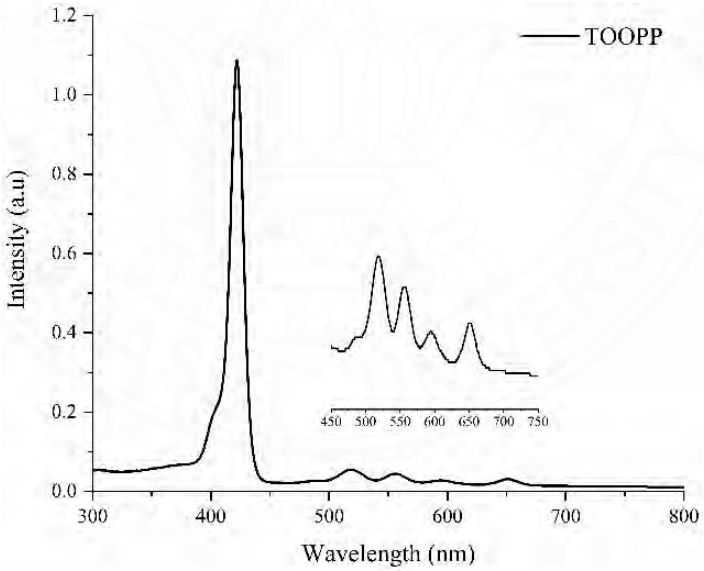

Figure D4 UV-Vis absorption spectra of TOOPP 7

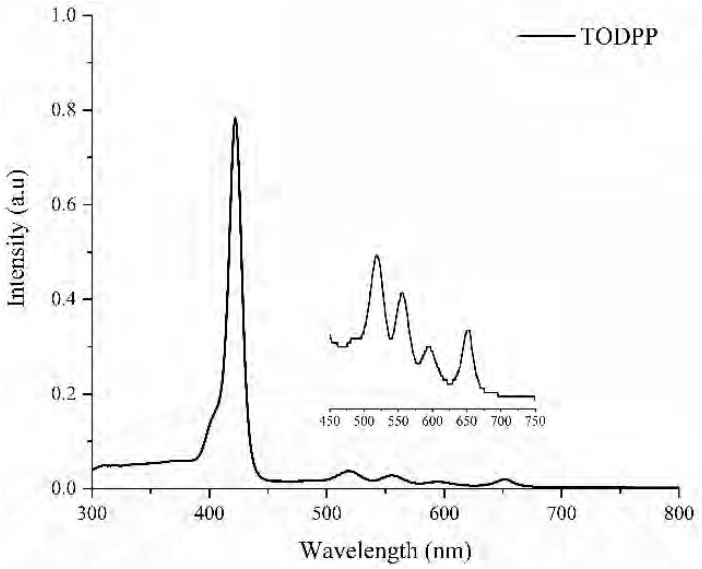

Figure D5 UV-Vis absorption spectra of TODPP 8

UV-Visible absorption spectra of copper(II) porphyrin complexes in dichloromethane

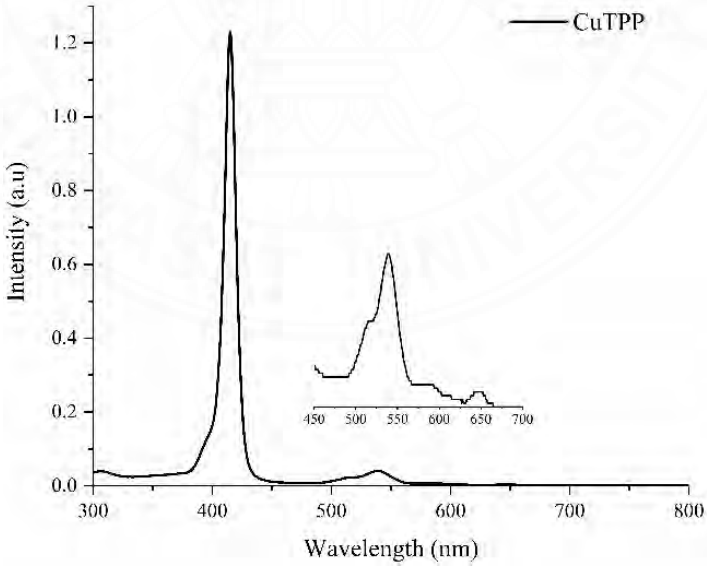

Figure D6 UV-Vis absorption spectra of CuTPP 9

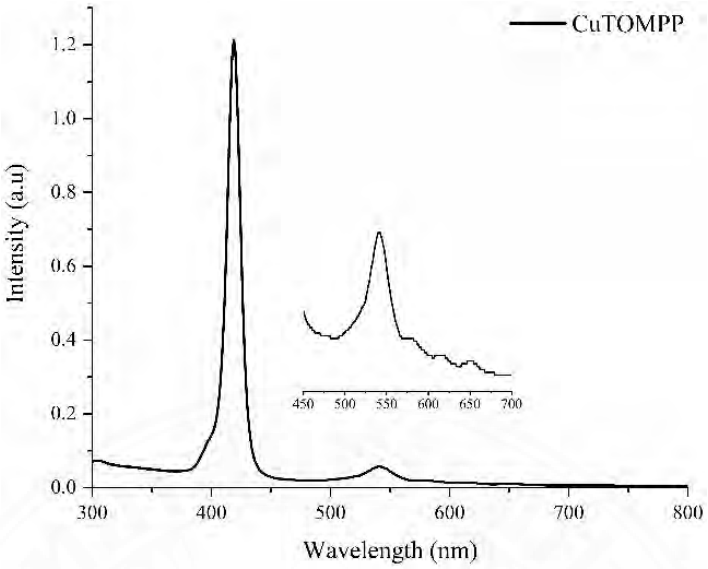

Figure D7 UV-Vis absorption spectra of CuTOMPP 10

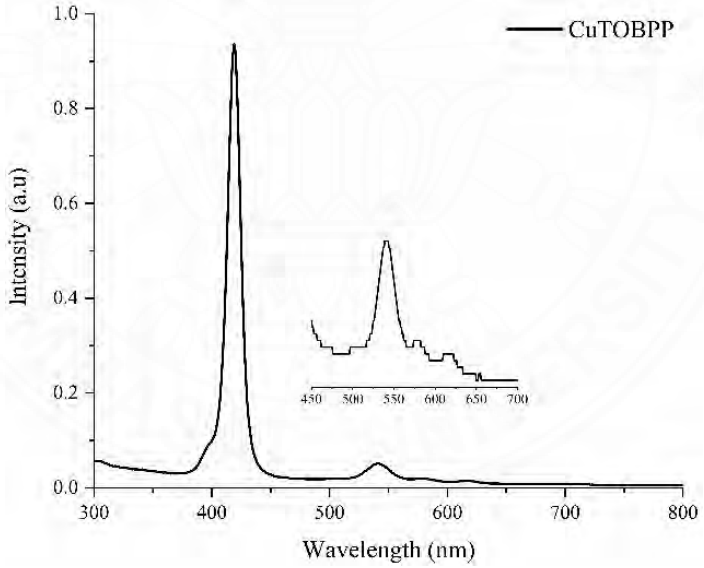

Figure D8 UV-Vis absorption spectra of CuTOBPP 11

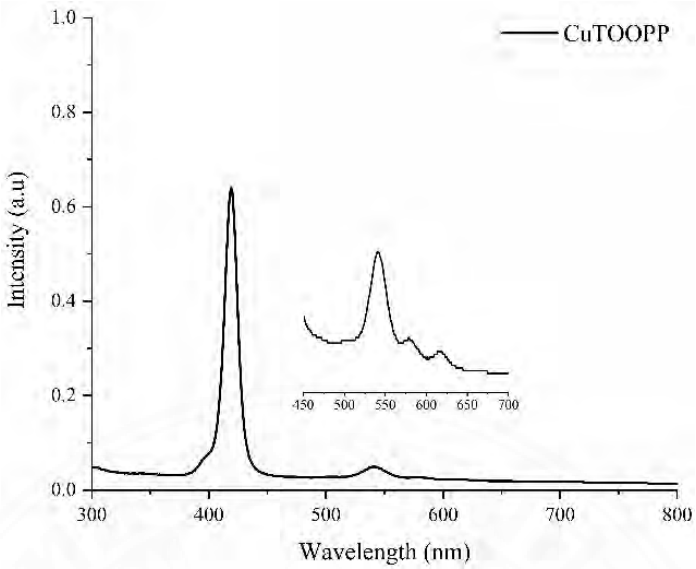

Figure D9 UV-Vis absorption spectra of CuTOOPP 12

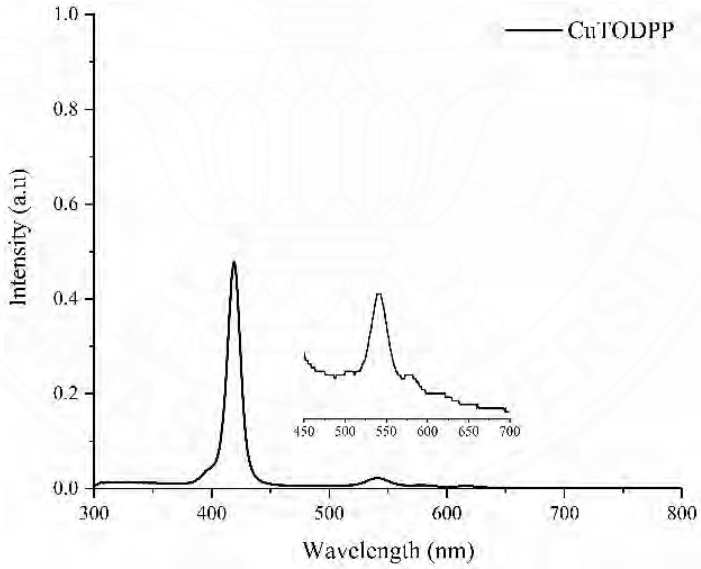

Figure D10 UV-Vis absorption spectra of CuTODPP 13

UV-Visible absorption spectra of silver(II) porphyrin complexes in dichloromethane

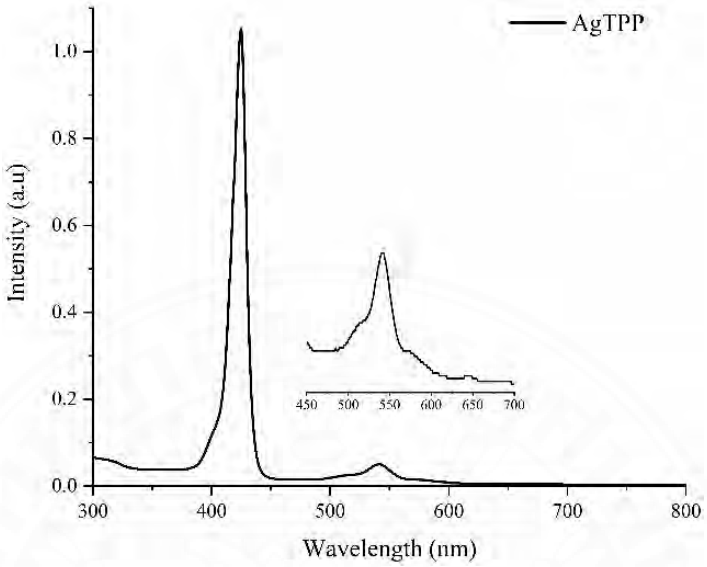

Figure D11 UV-Vis absorption spectra of AgTPP 14

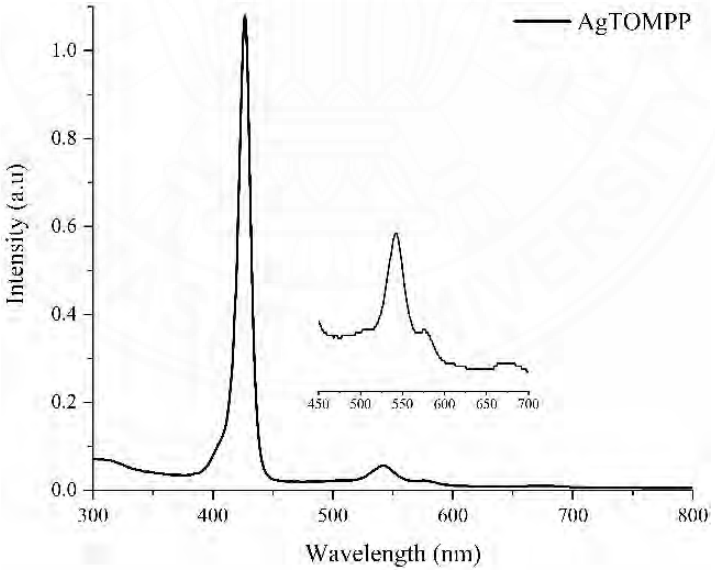

Figure D12 UV-Vis absorption spectra of AgTOMPP 15

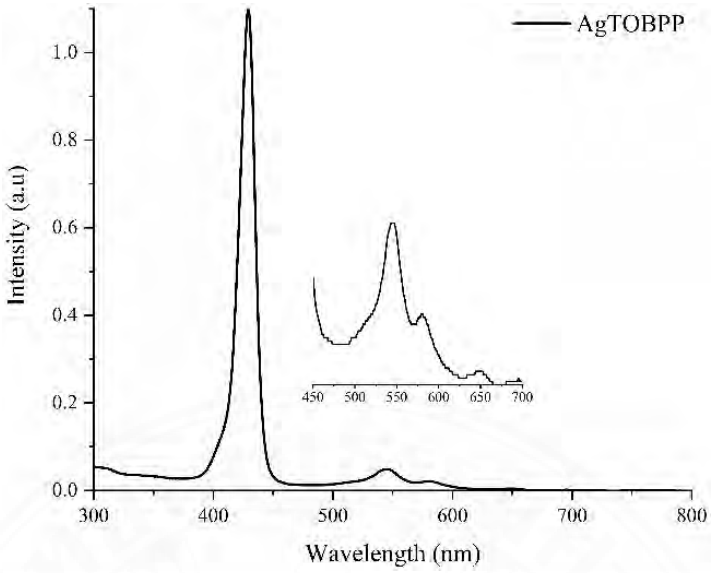

Figure D13 UV-Vis absorption spectra of AgTOBPP 16

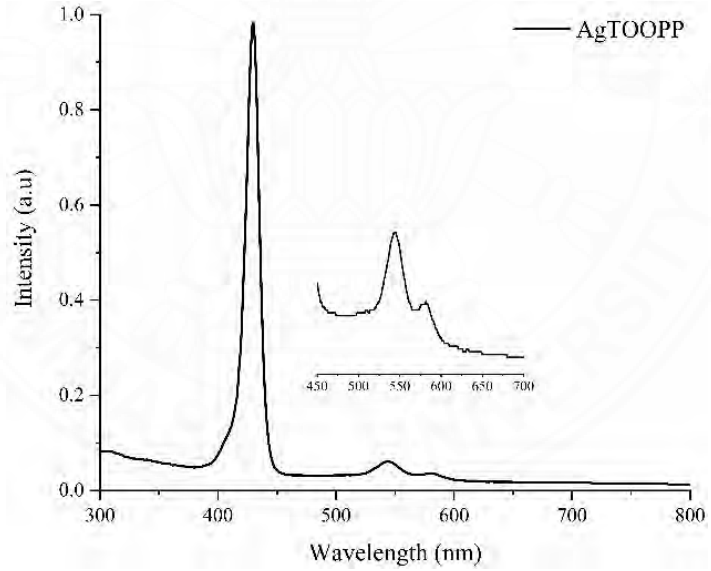

Figure D14 UV-Vis absorption spectra of AgTOOPP 17

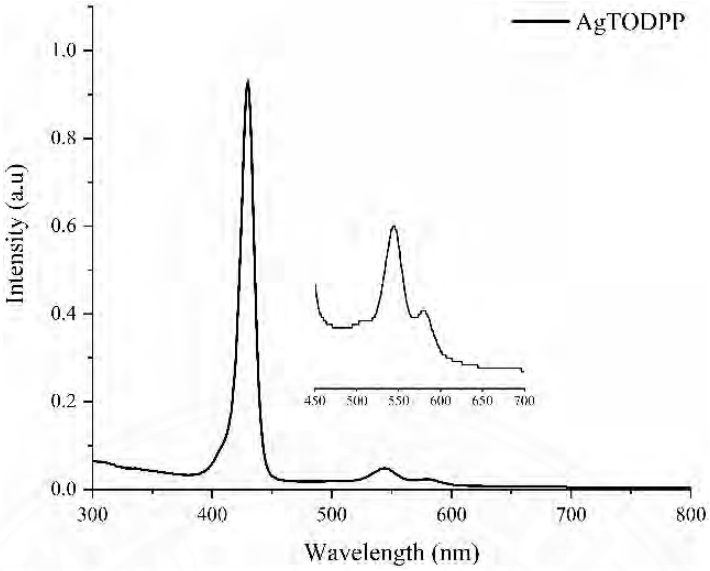

Figure D15 UV-Vis absorption spectra of AgTODPP 18

UV-Visible absorption spectra of gold(III) porphyrin complexes in dichloromethane

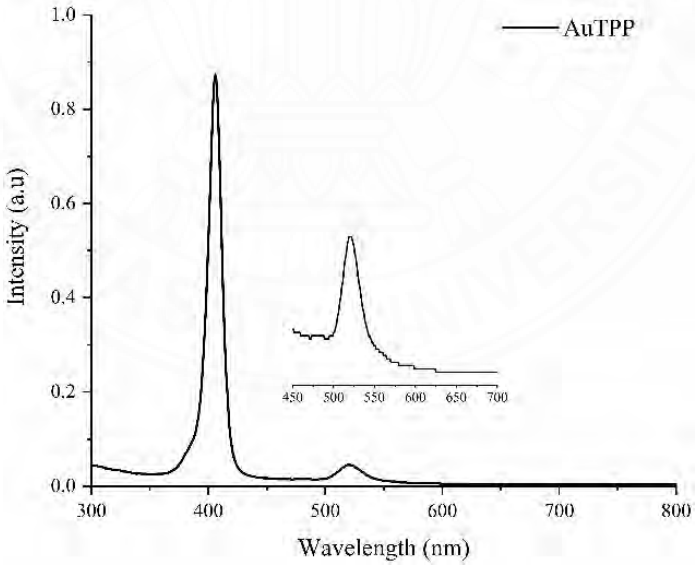

Figure D16 UV-Vis absorption spectra of AuTPP 19

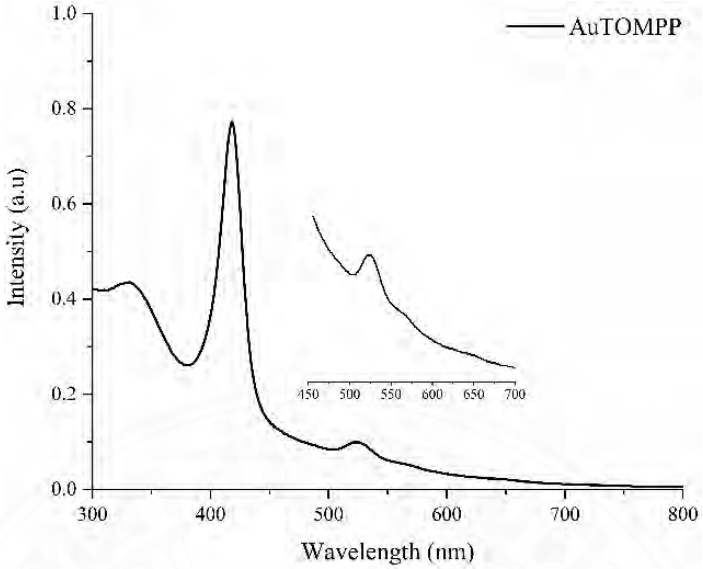

Figure D17 UV-Vis absorption spectra of AuTOMPP 20

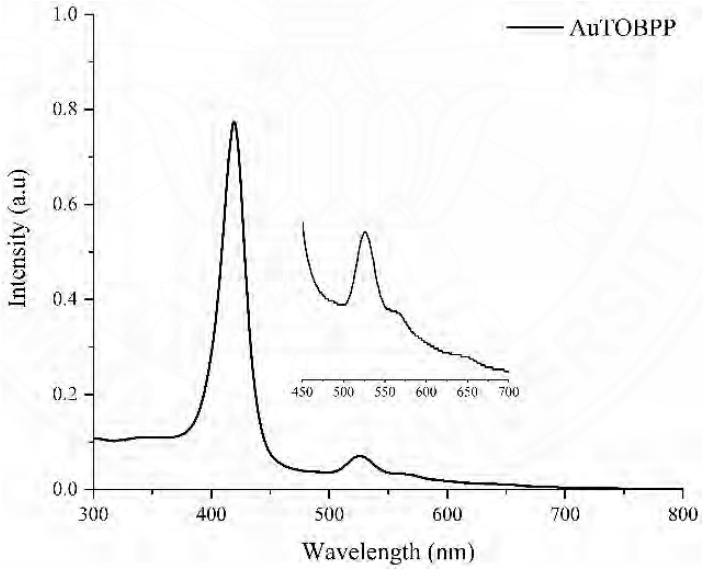

Figure D18 UV-Vis absorption spectra of AuTOBPP 21

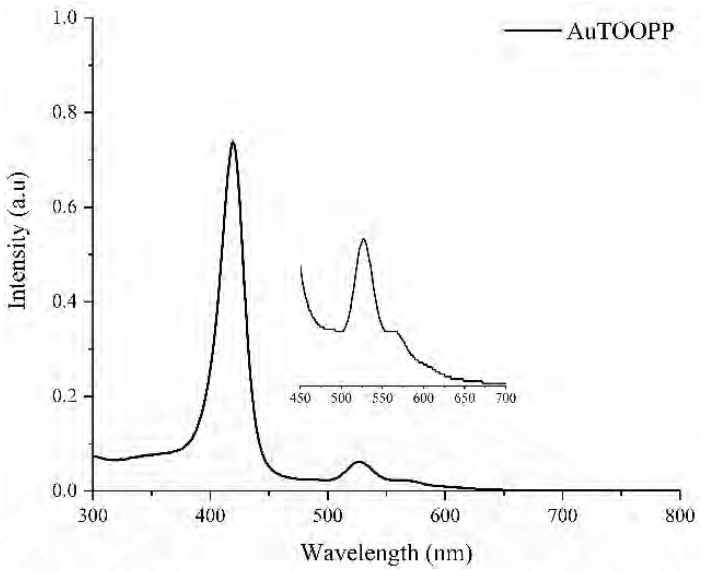

Figure D19 UV-Vis absorption spectra of AuTOOPP 22

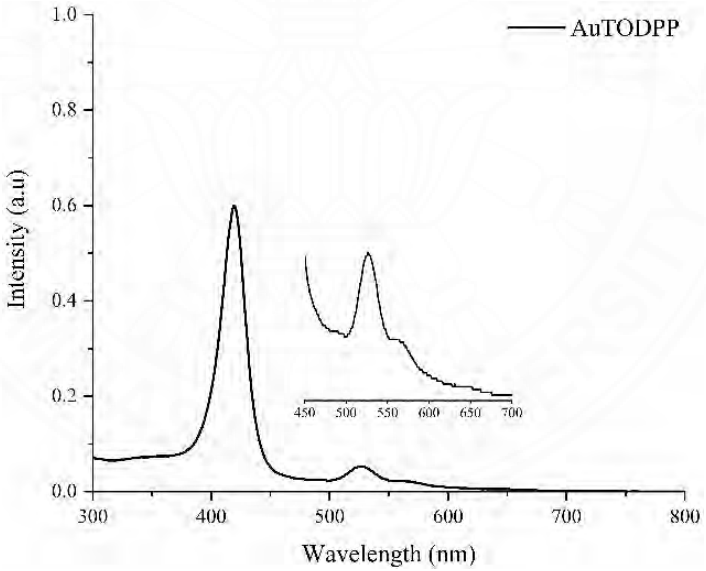

Figure D20 UV-Vis absorption spectra of AuTODPP 23

APPENDIX E
FLUORESCENCE SPECTROSCOPY

Fluorescence spectra of free-base porphyrins

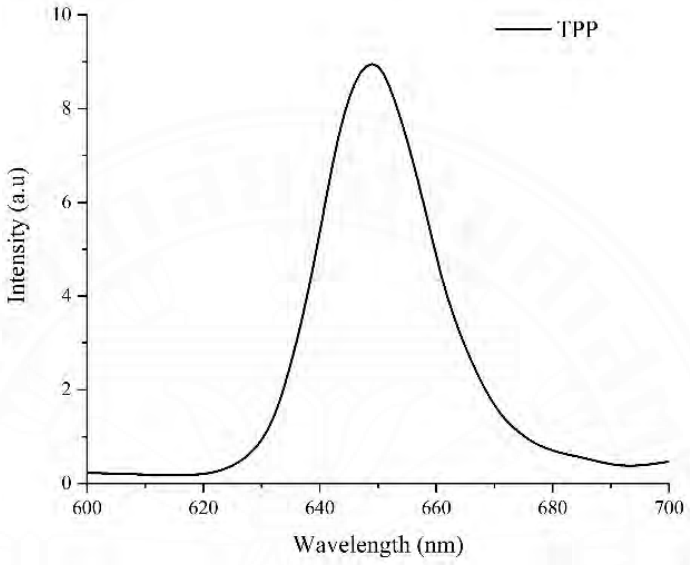

Figure E1 Fluorescence spectra of TPP 4

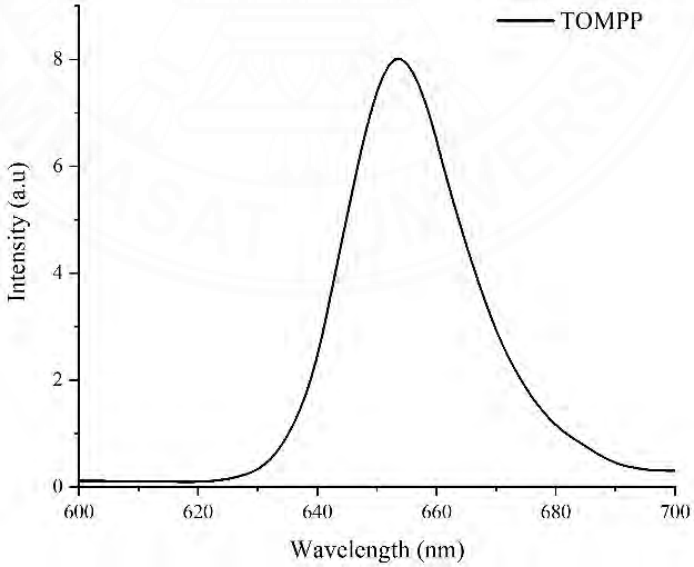

Figure E2 Fluorescence spectra of TOMPP 5

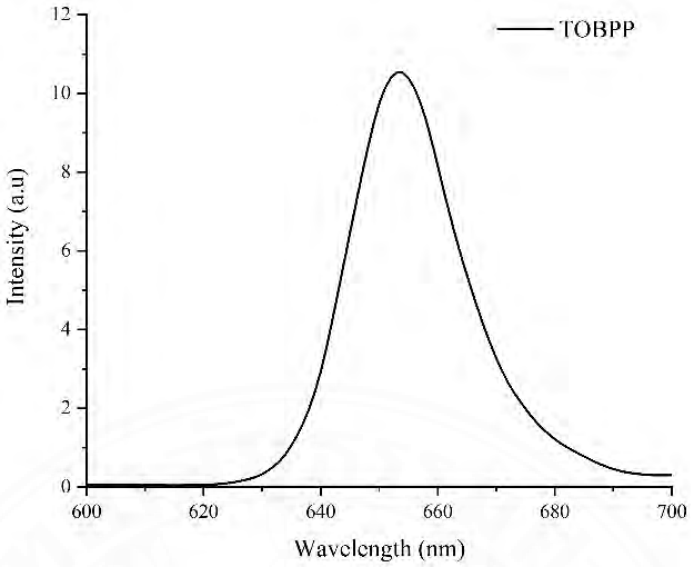

Figure E3 Fluorescence spectra of TOBPP 6

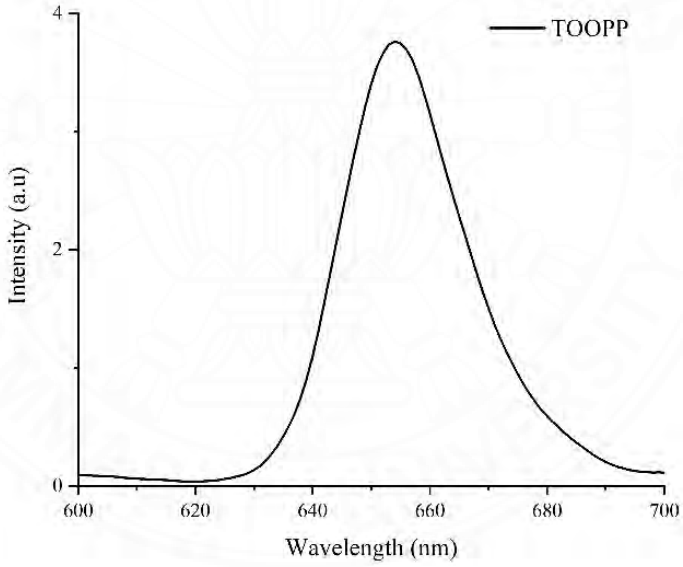

Figure E4 Fluorescence spectra of TOOPP 7

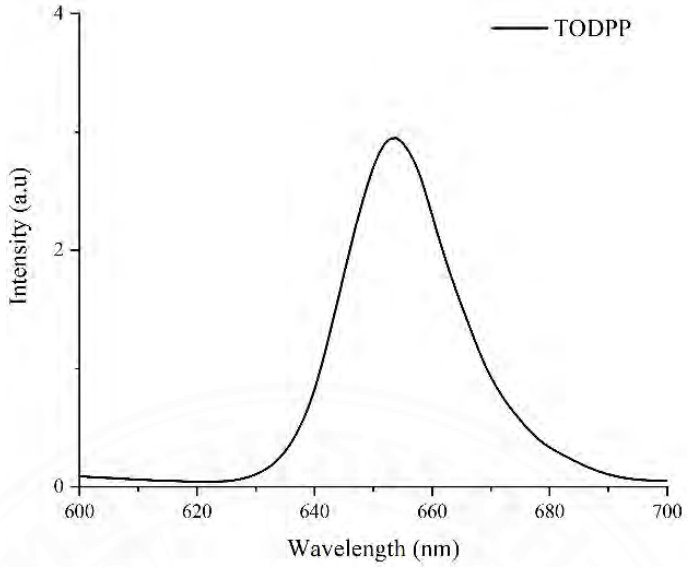

Figure E5 Fluorescence spectra of TODPP 8

Fluorescence spectra of copper(II) porphyrin complexes

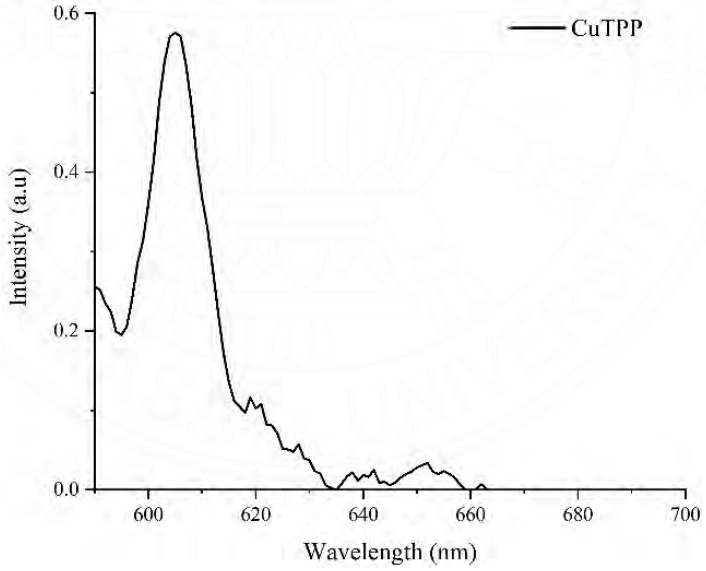

Figure E6 Fluorescence spectra of CuTPP 9

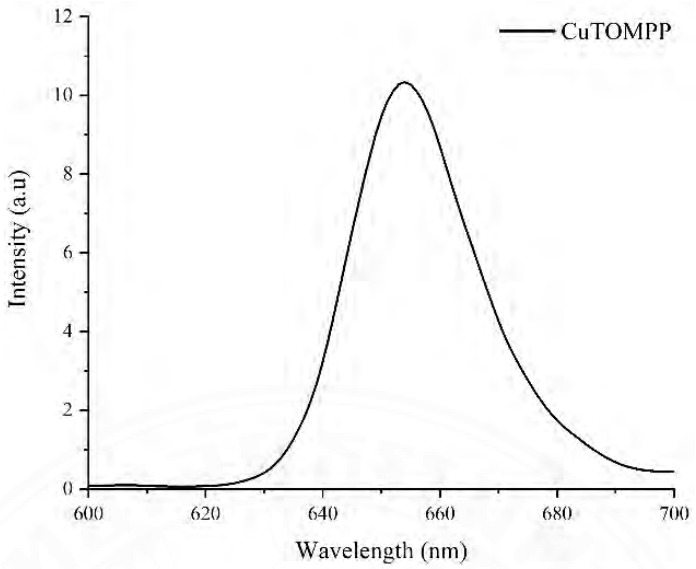

Figure E7 Fluorescence spectra of CuTOMPP 10

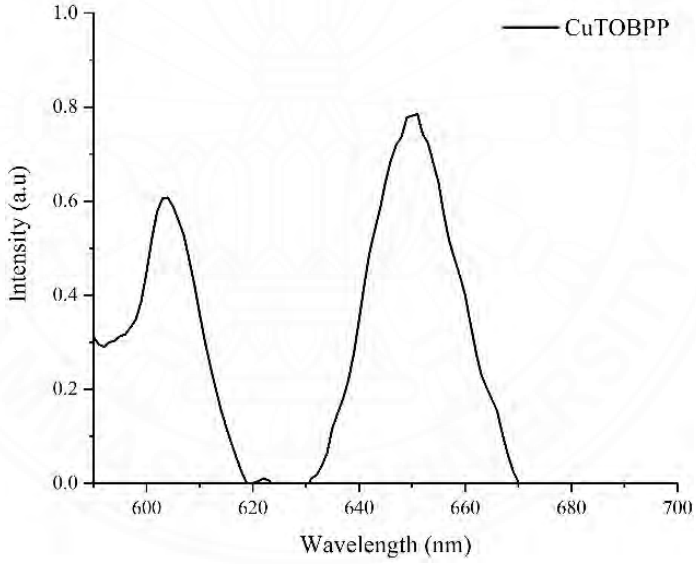

Figure E8 Fluorescence spectra of CuTOBPP 11

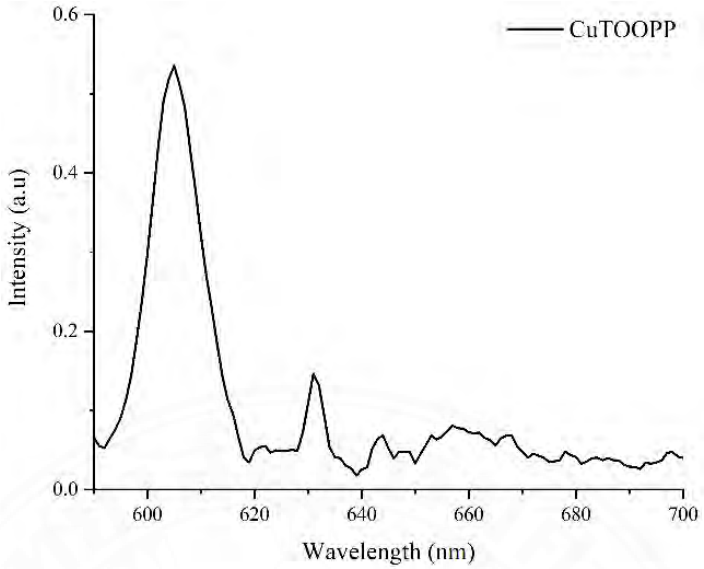

Figure E9 Fluorescence spectra of CuTOOPP 12

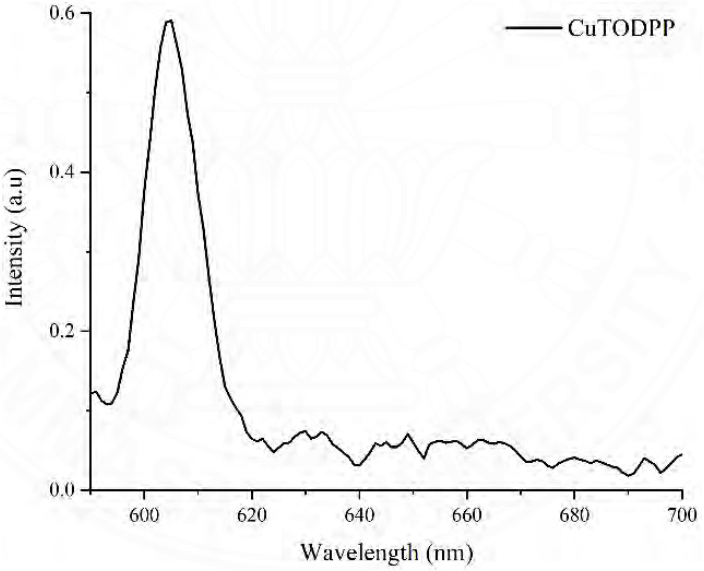

Figure E10 Fluorescence spectra of CuTODPP 13

Fluorescence spectra of silver(II) porphyrin complexes

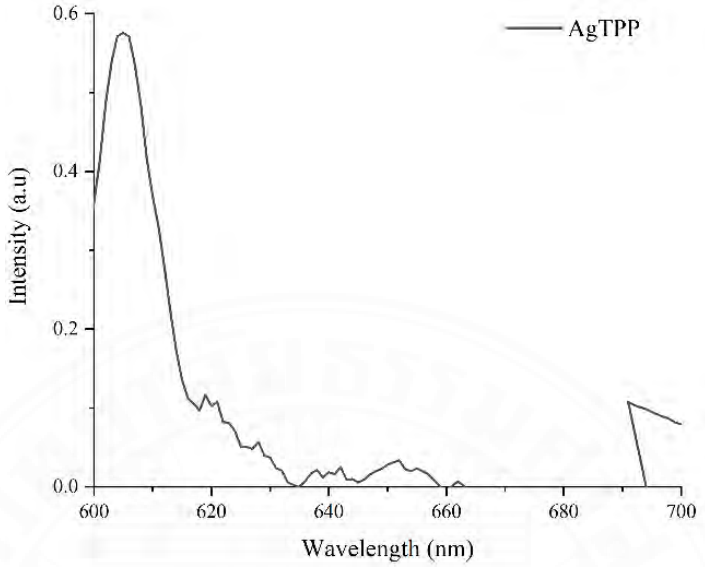

Figure E11 Fluorescence spectra of AgTPP 14

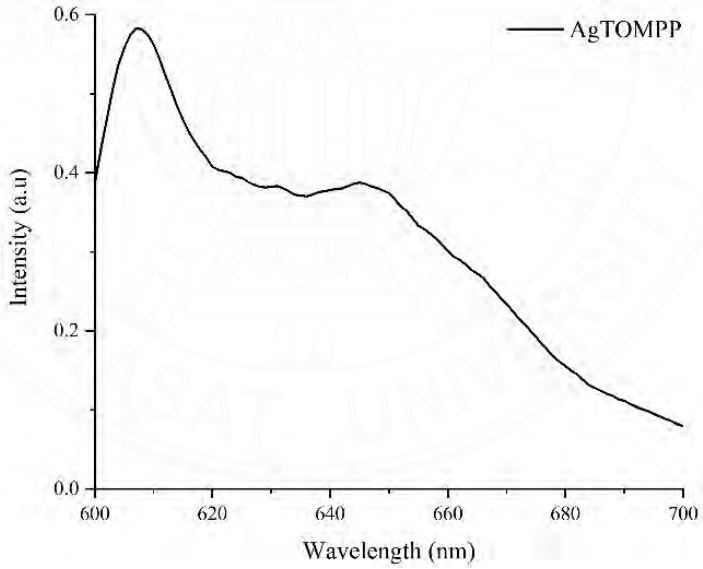

Figure E12 Fluorescence spectra of AgTOMPP 15

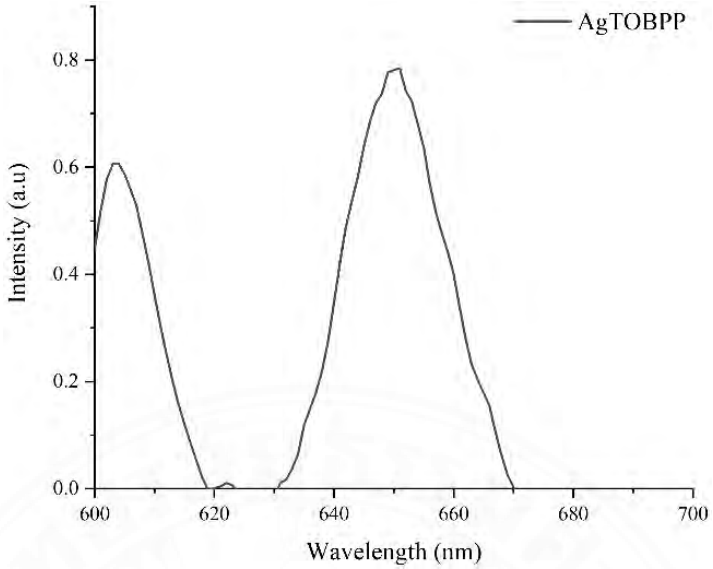

Figure E13 Fluorescence spectra of AgTOBPP 16

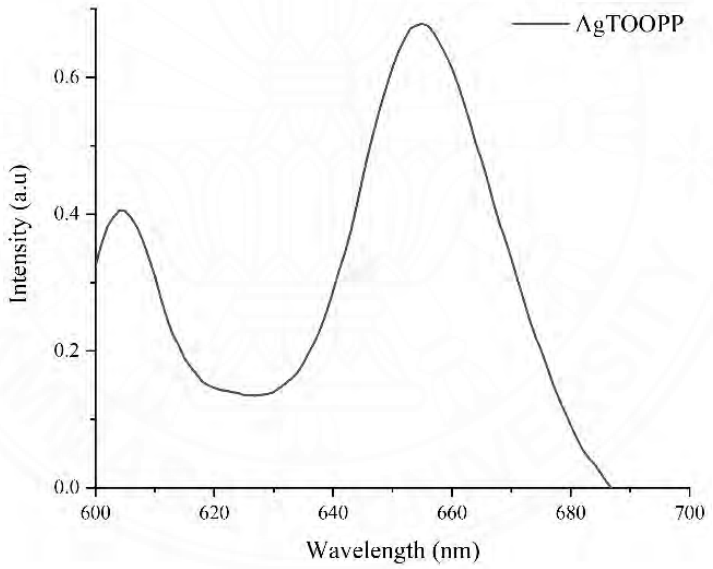

Figure E14 Fluorescence spectra of AgTOOPP 17

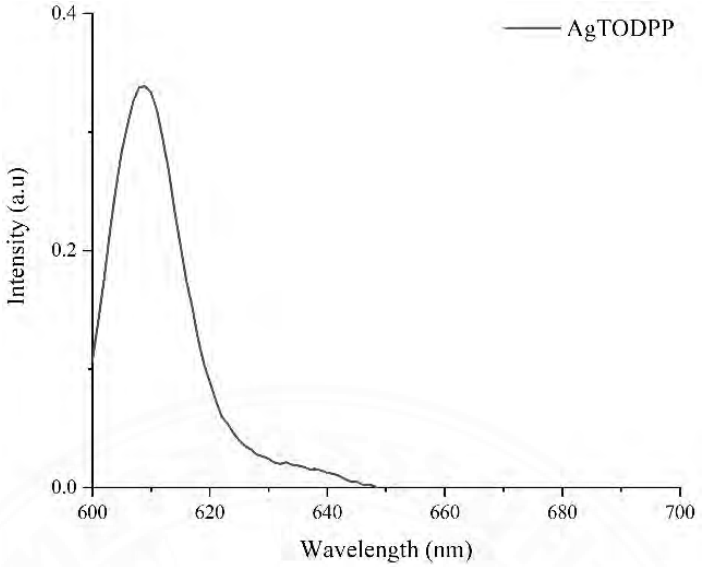

Figure E15 Fluorescence spectra of AgTODPP 18

Fluorescence spectra of gold(III) porphyrin complexes

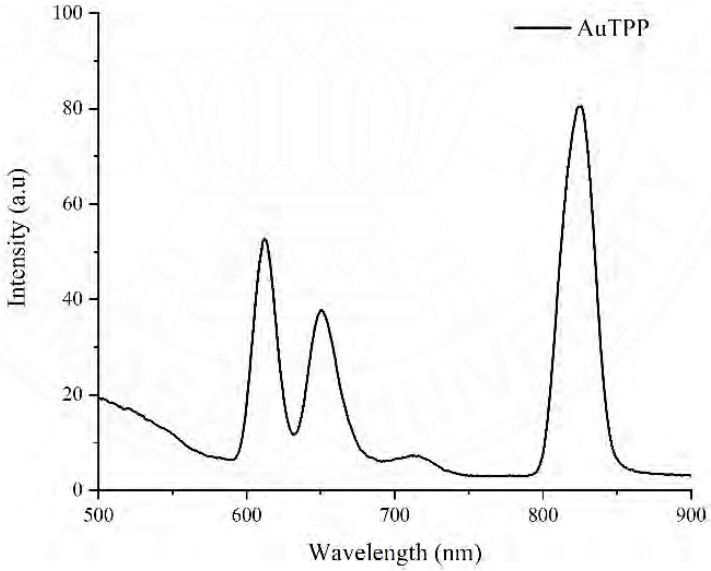

Figure E16 Fluorescence spectra of AuTPP 19

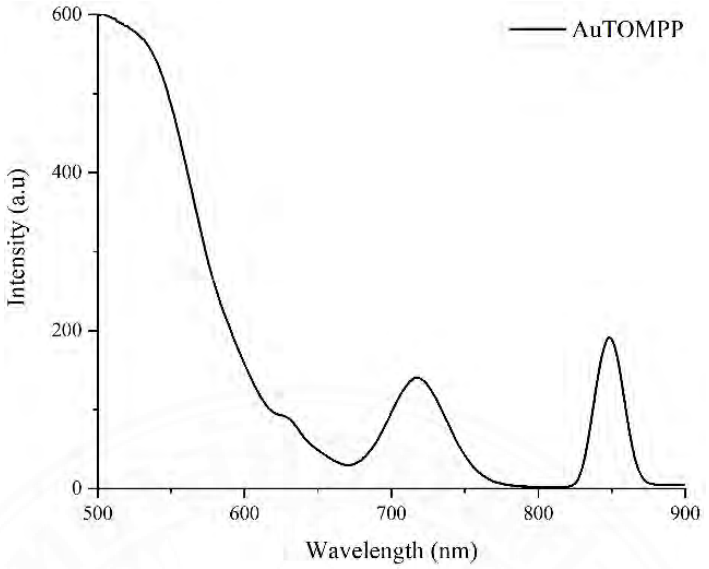

Figure E17 Fluorescence spectra of AuTOMPP 20

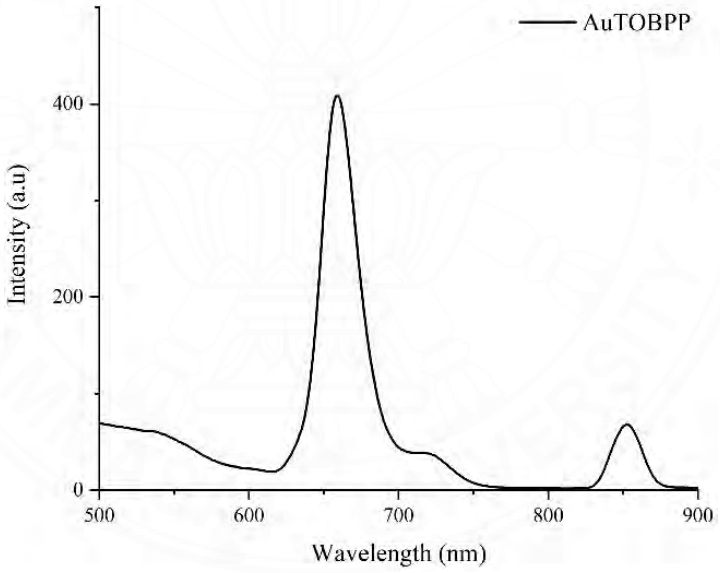

Figure E18 Fluorescence spectra of AuTOBPP 21

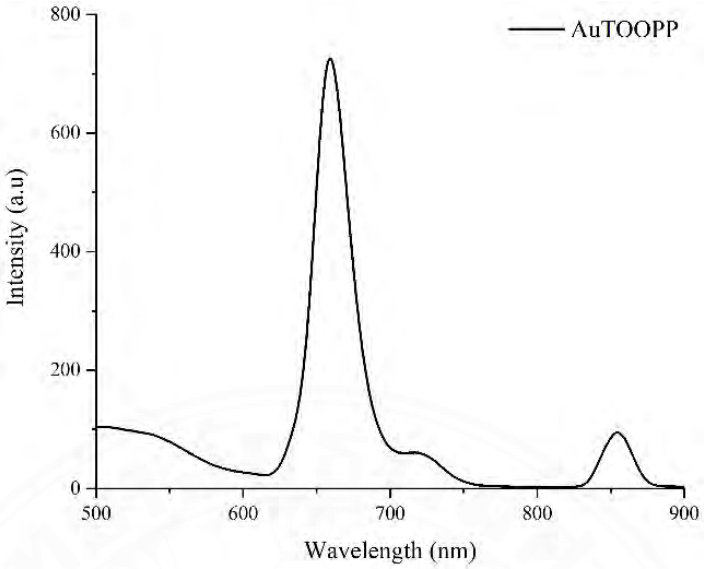

Figure E19 Fluorescence spectra of AuTOOPP 22

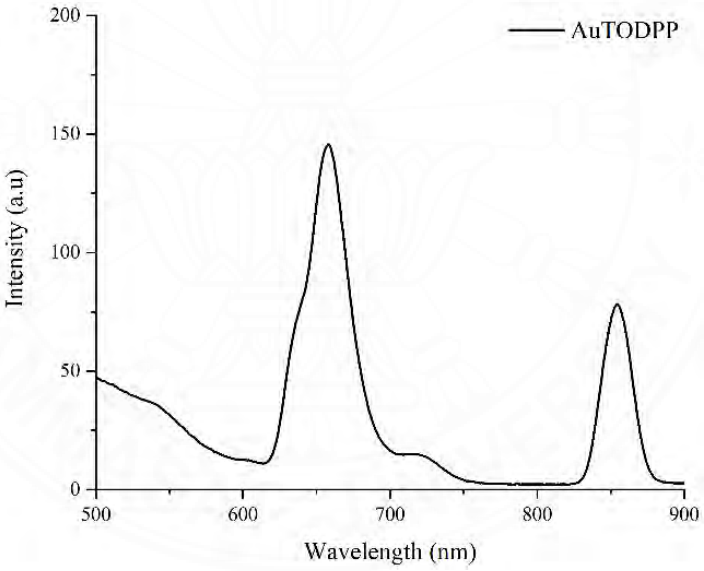

Figure E20 Fluorescence spectra of AuTODPP 23

APPENDIX F

ELECTRON PARAMAGNETIC RESONANCE SPECTROSCOPY

EPR spectrum of copper(II) porphyrin complexes

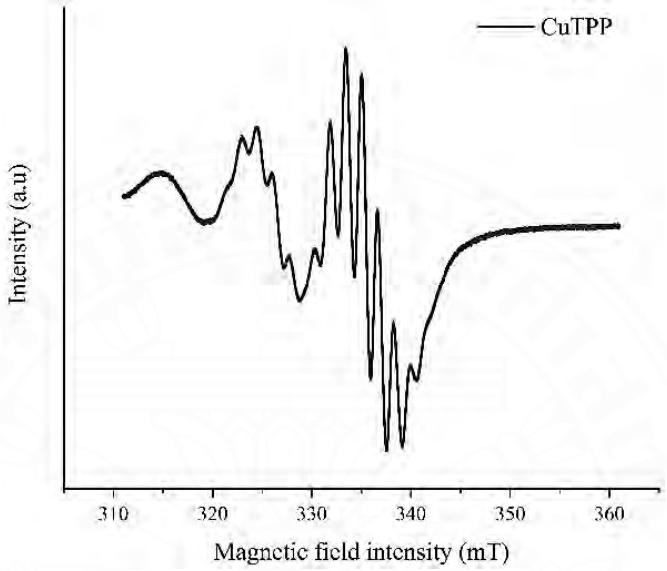

Figure F1 EPR spectrum of CuTPP 9

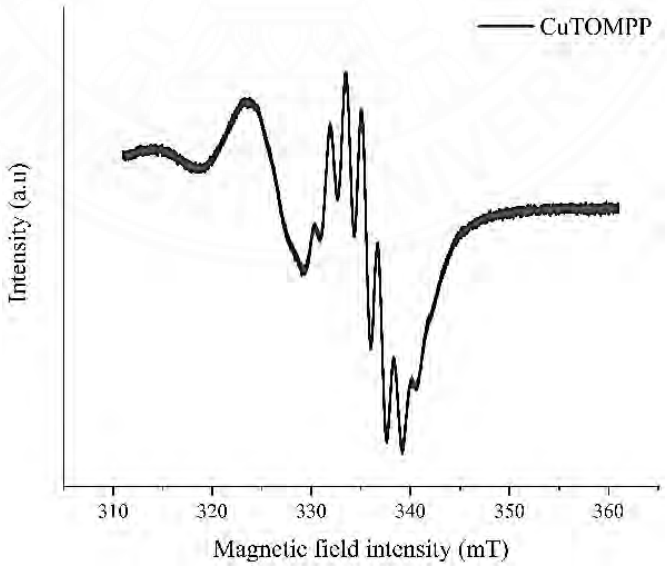

Figure F2 EPR spectrum of CuTOMPP 10

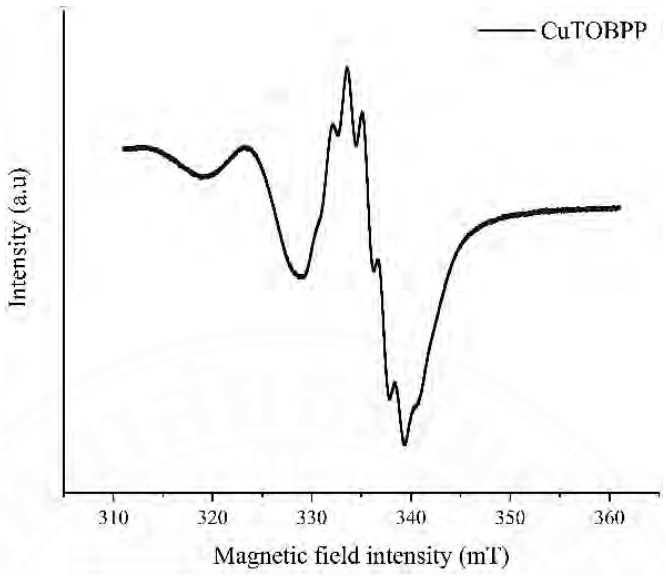

Figure F3 EPR spectrum of CuTOBPP 11

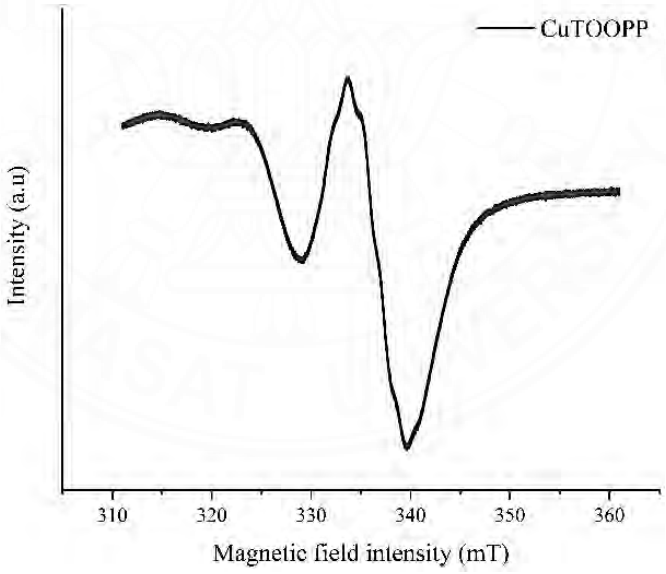

Figure F4 EPR spectrum of CuTOOPP 12

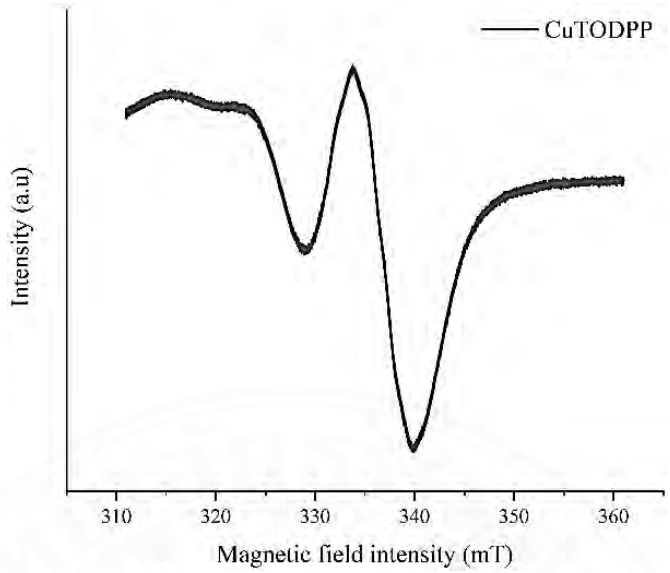

Figure F5 EPR spectrum of CuTODPP 13

EPR spectrum of silver(II) porphyrin complexes

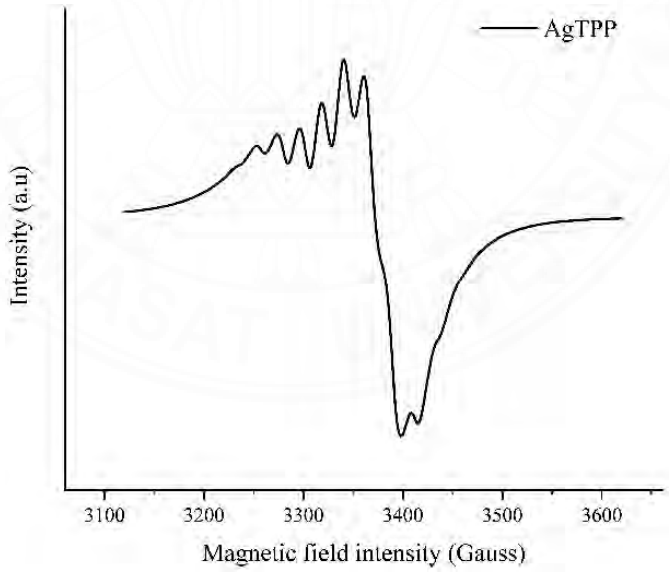

Figure F6 EPR spectrum of AgTPP 14

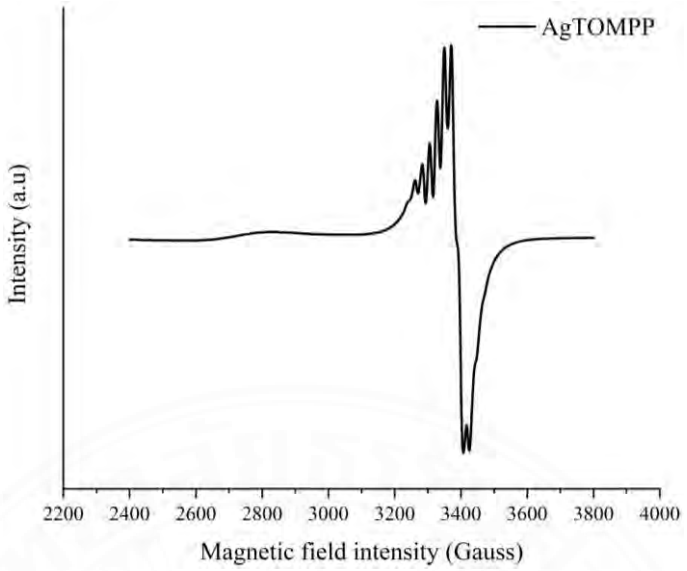

Figure F7 EPR spectrum of AgTOMPP 15

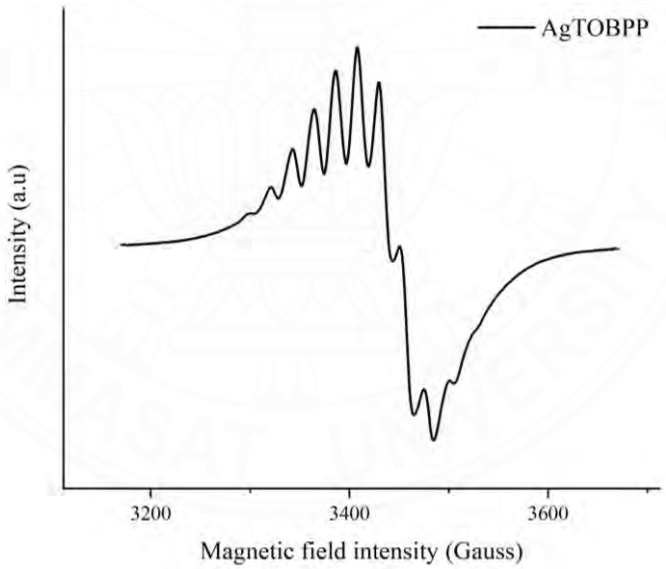

Figure F8 EPR spectrum of AgTOBPP 16

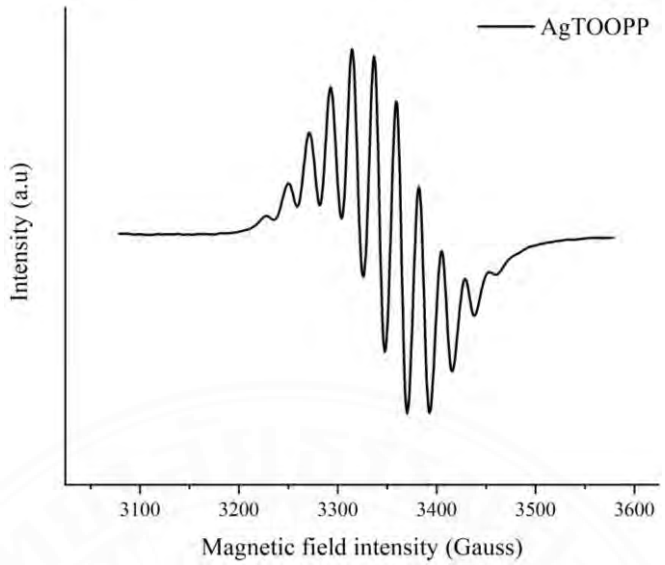

Figure F9 EPR spectrum of AgTOOPP 17

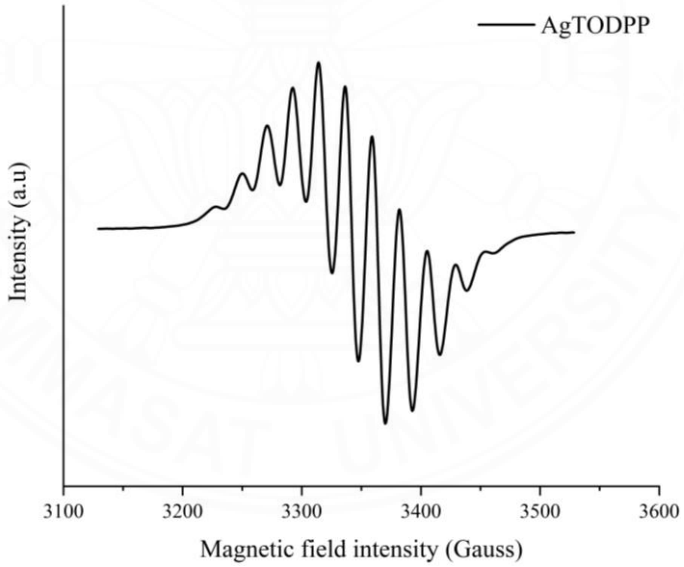

Figure F10 EPR spectrum of AgTOMPP 18

EPR spectrum of gold(III) porphyrin complexes

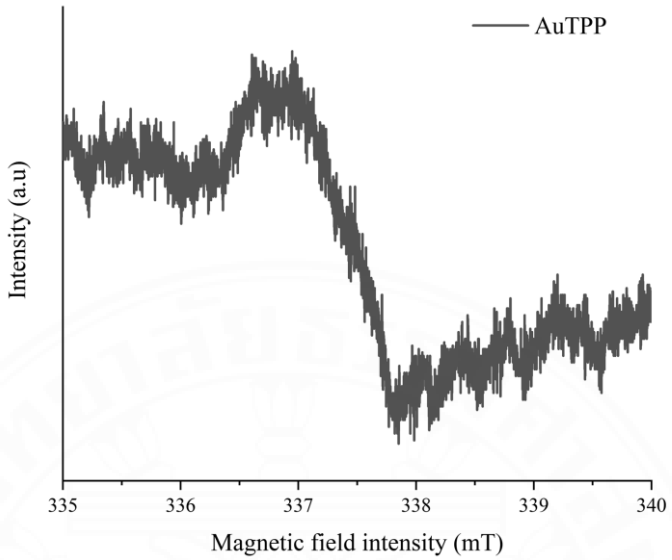

Figure F11 EPR spectrum of AuTPP 19

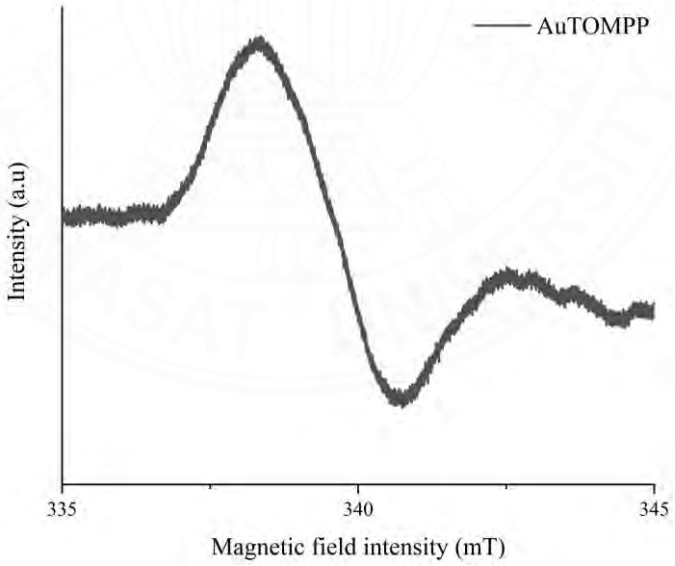

Figure F12 EPR spectrum of AuTOMPP 20

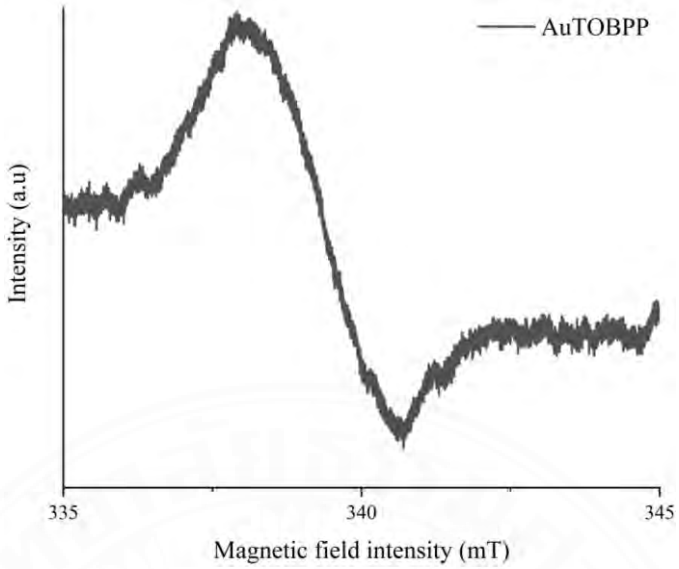

Figure F13 EPR spectrum of AuTOBPP 21

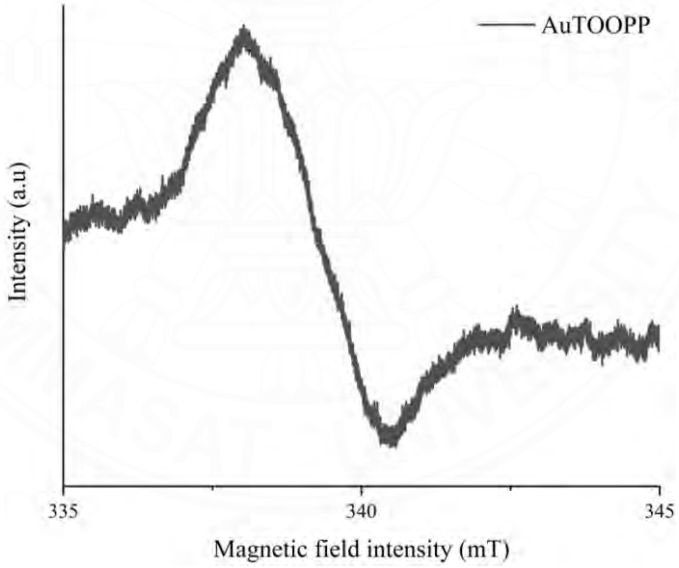

Figure F14 EPR spectrum of AuTOOPP 22

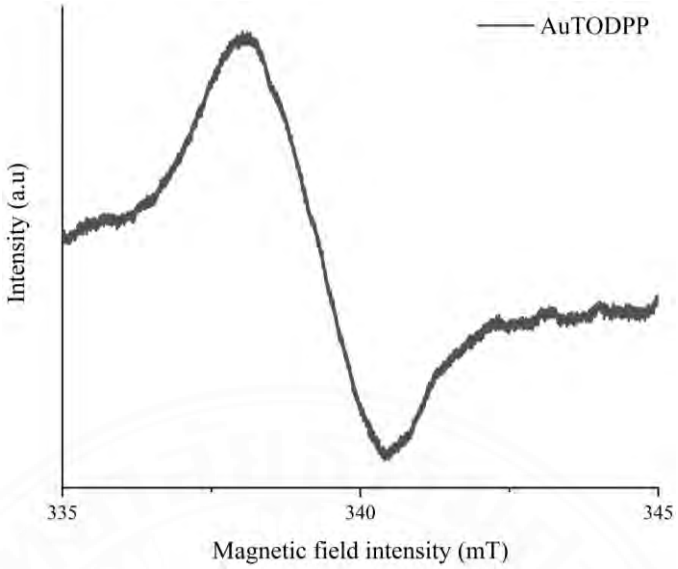

Figure F15 EPR spectrum of AuTODPP 23

APPENDIX G

CYCLICVOLTAMMETRY

The cyclicvoltammogram of free-base porphyrin compounds

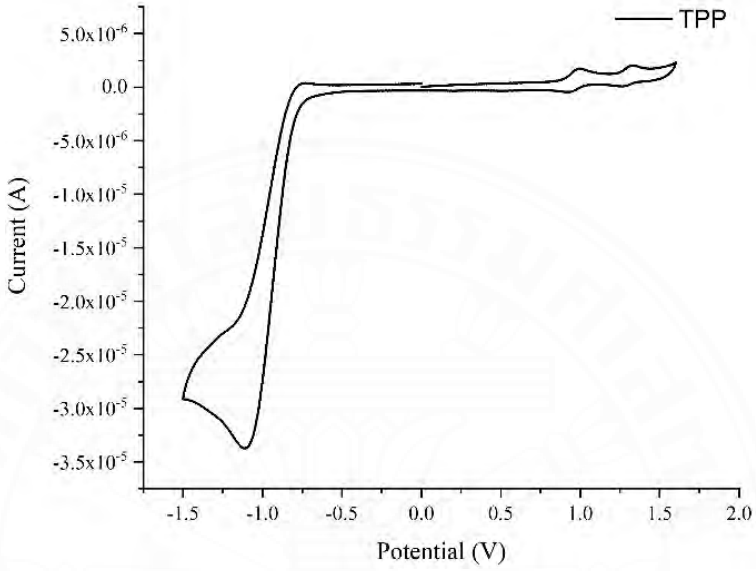

Figure G1 cyclicvoltammogram of TPP 4

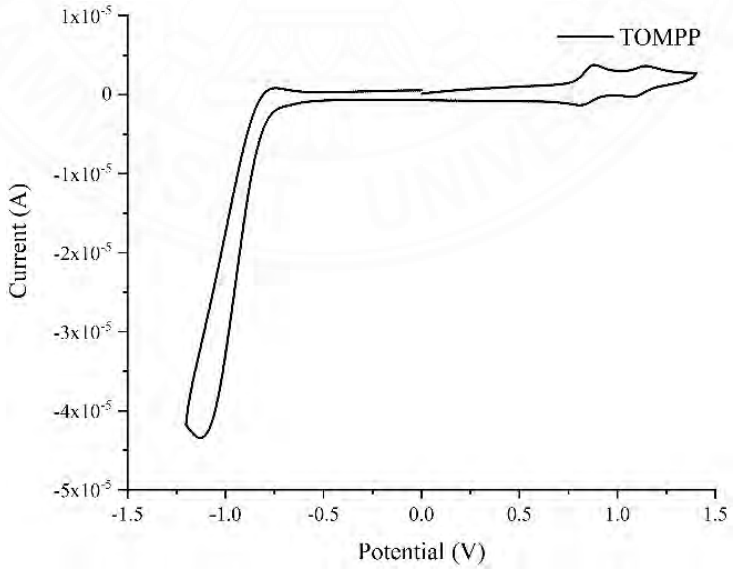

Figure G2 cyclicvoltammogram of TOMPP 5

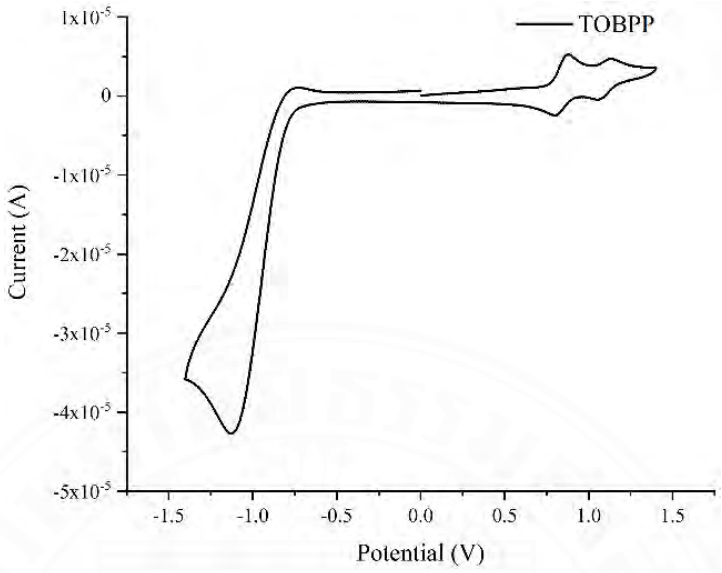

Figure G3 cyclicvoltammogram of TOBPP 6

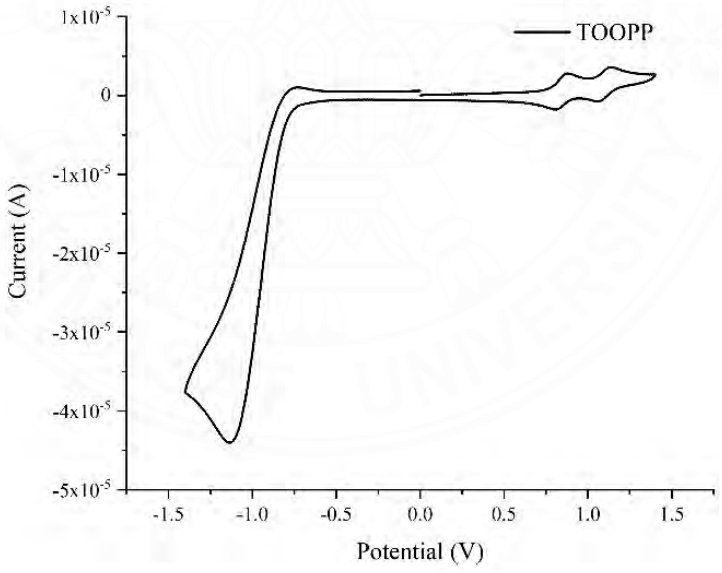

Figure G4 cyclicvoltammogram of TOOPP 7

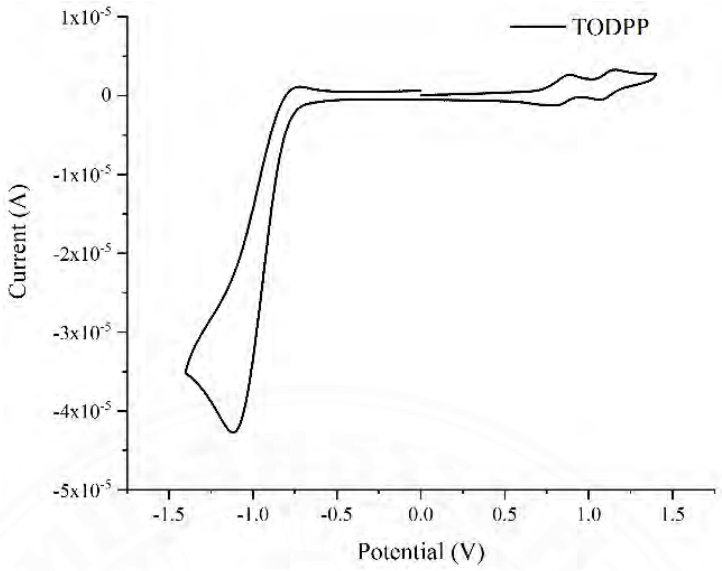

Figure G5 cyclicvoltammogram of TODPP 8

The cyclicvoltammogram of copper(II) porphyrin complexes

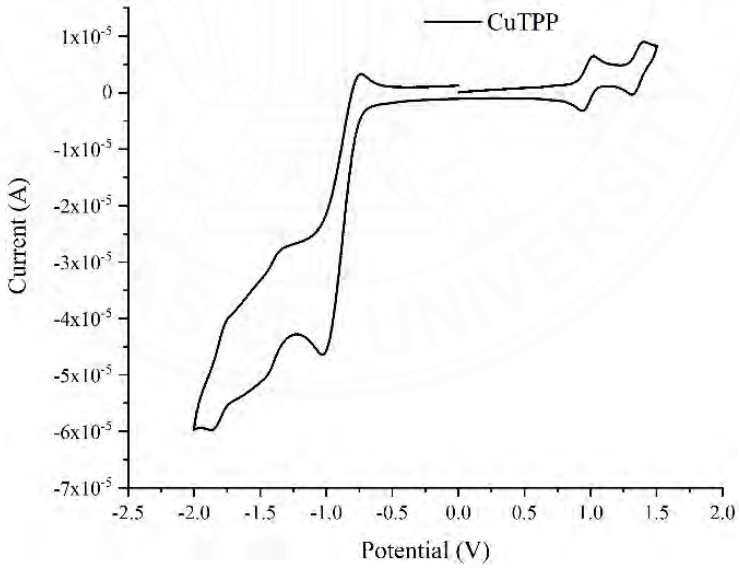

Figure G6 cyclicvoltammogram of CuTPP 9

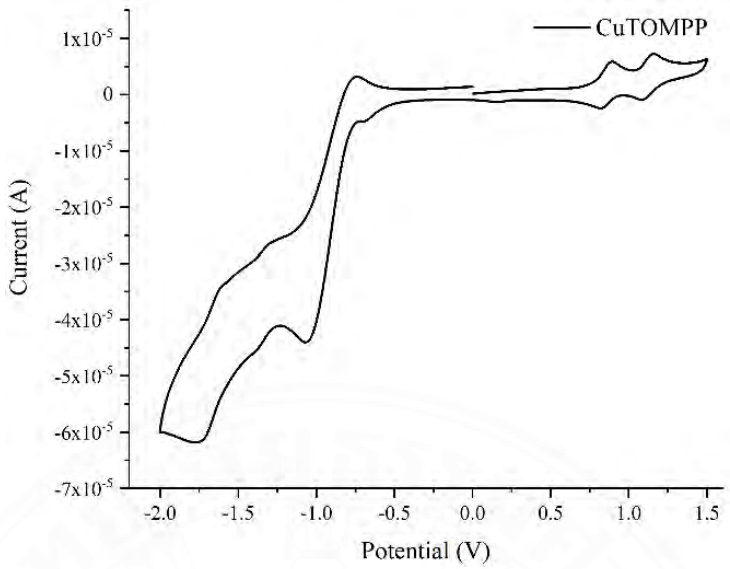

Figure G7 cyclicvoltammogram of CuTOMPP 10

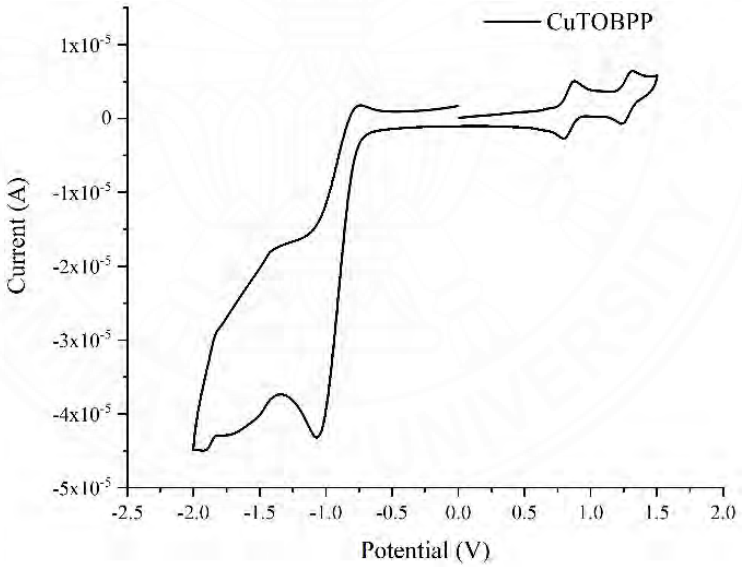

Figure G8 cyclicvoltammogram of CuTOBPP 11

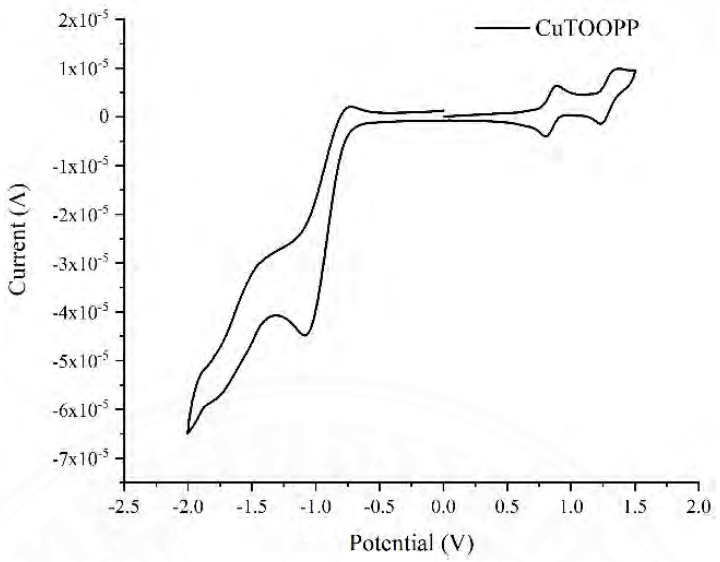

Figure G9 cyclicvoltammogram of CuTOOPP 12

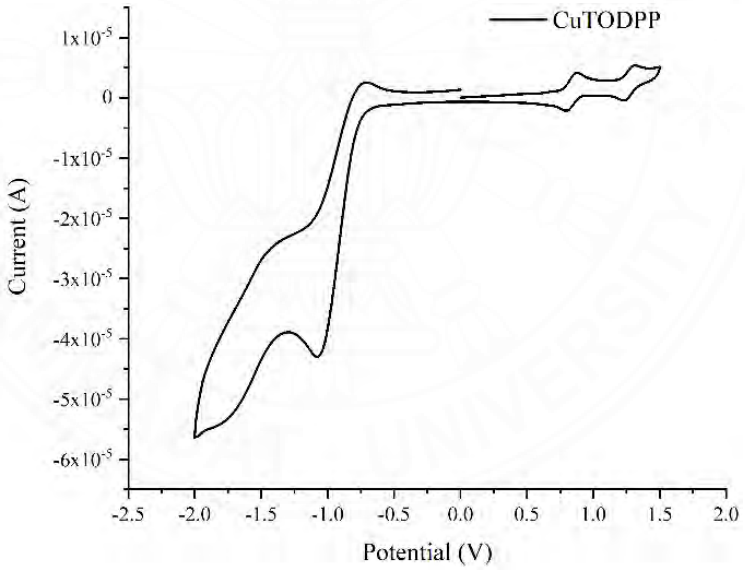

Figure G10 cyclicvoltammogram of CuTODPP 13

The cyclicvoltammogram of silver(II) porphyrin complexes

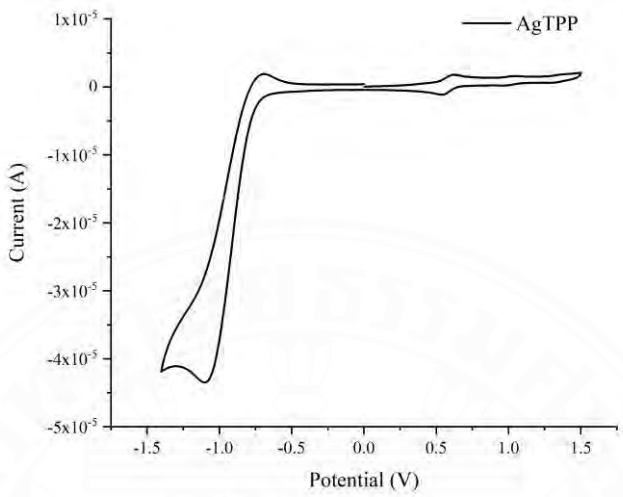

Figure G11 cyclicvoltammogram of AgTPP 14

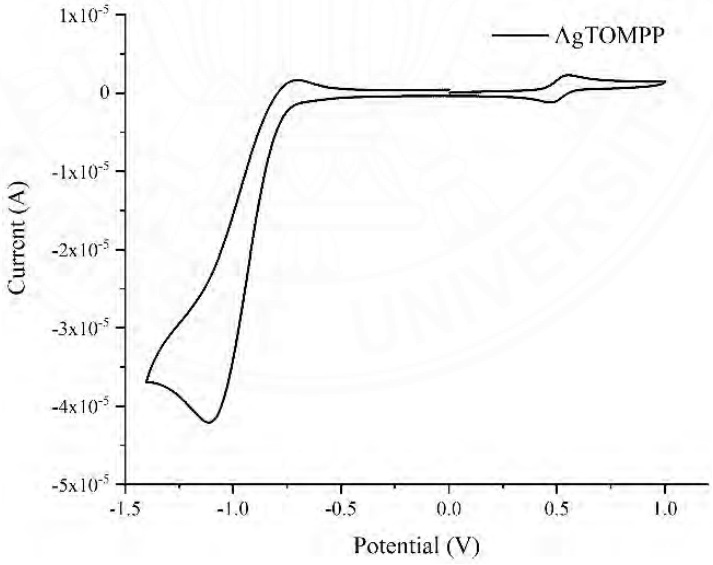

Figure G12 cyclicvoltammogram of AgTOMPP 15

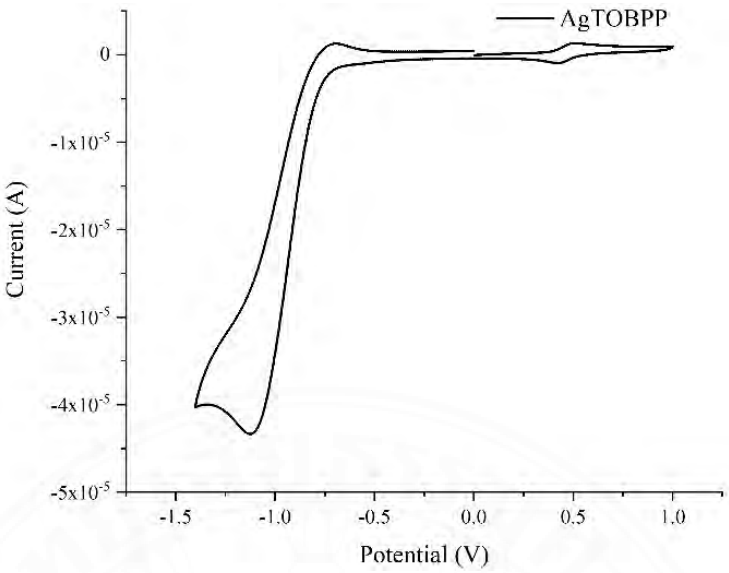

Figure G13 cyclicvoltammogram of AgTOBPP 16

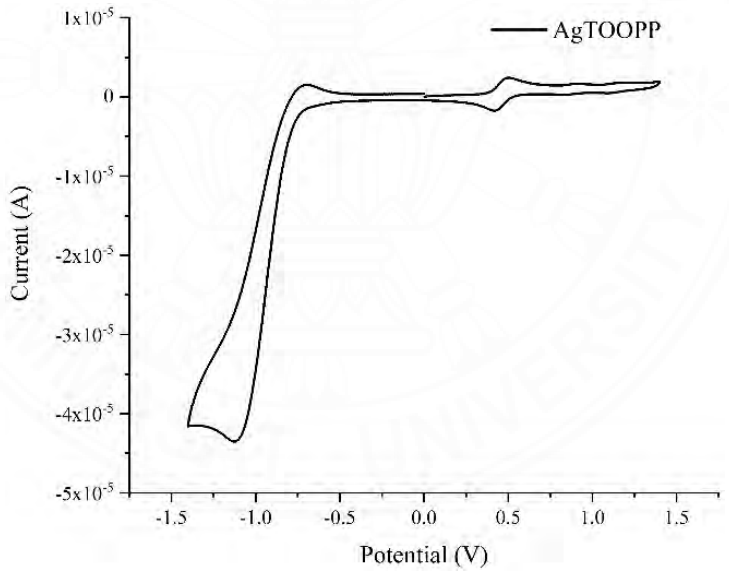

Figure G14 cyclicvoltammogram of AgTOOPP 17

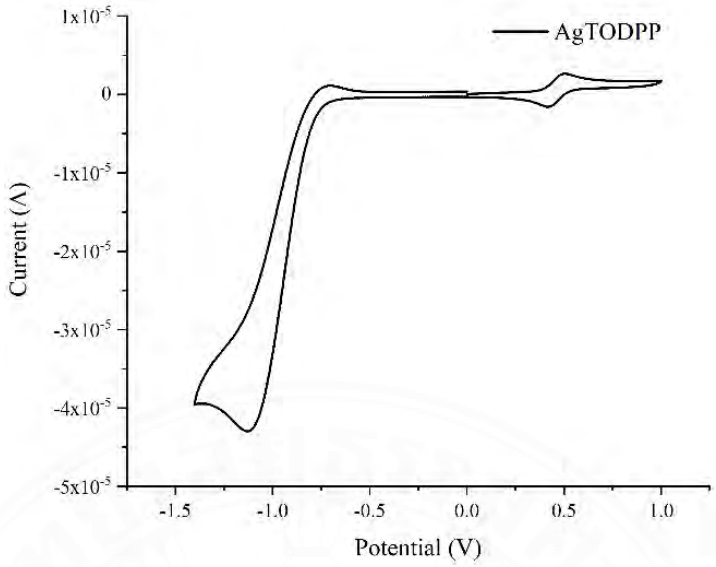

Figure G15 cyclicvoltammogram of AgTODPP 18

The cyclicvoltammogram of gold(III) porphyrin complexes

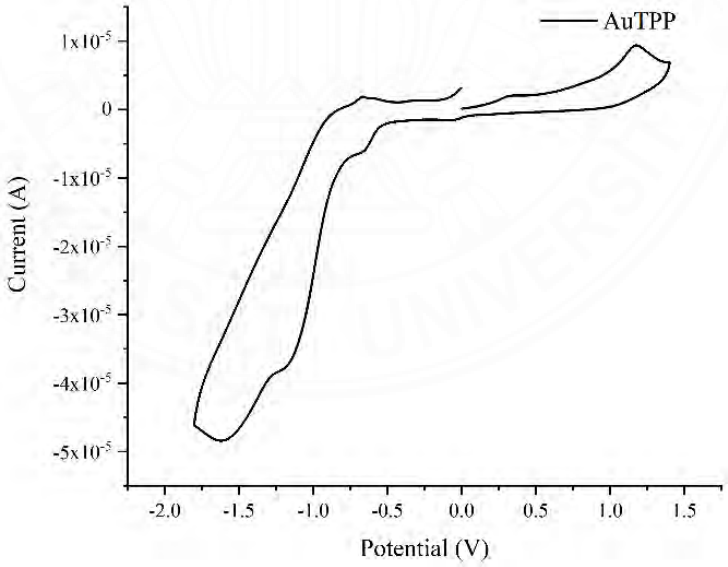

Figure G16 cyclicvoltammogram of AuTPP 19

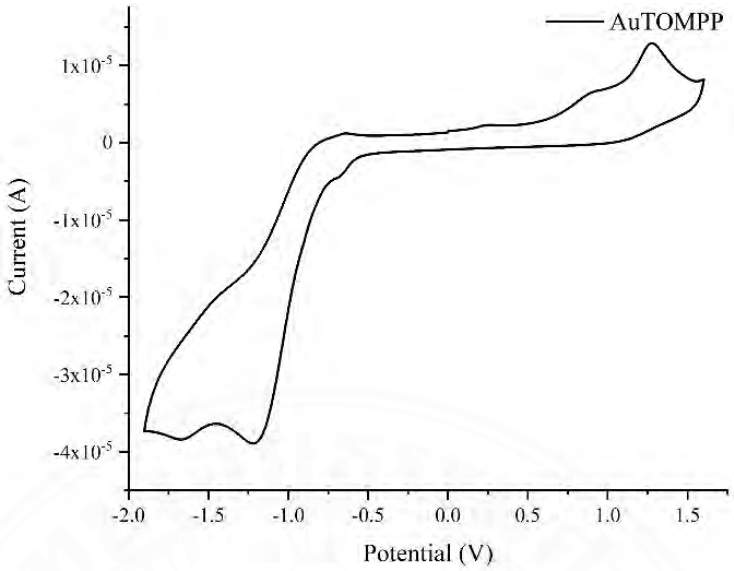

Figure G17 cyclicvoltammogram of AuTOMPP 20

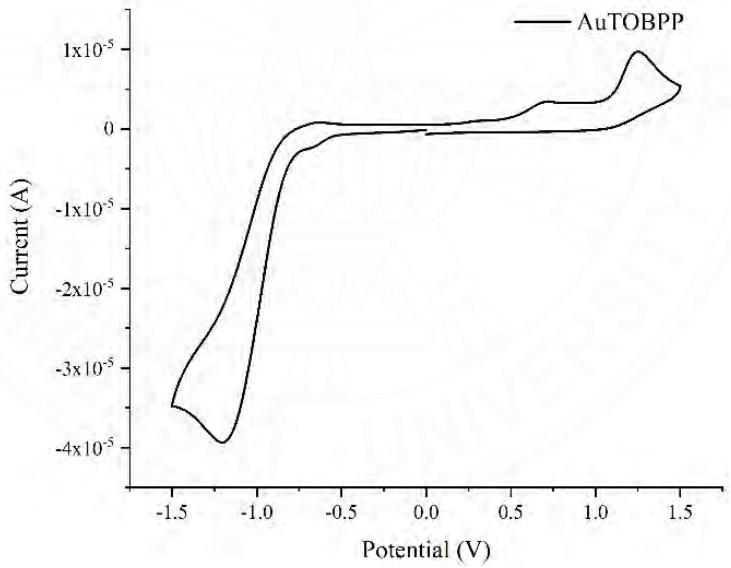

Figure G18 cyclicvoltammogram of AuTOBPP 21

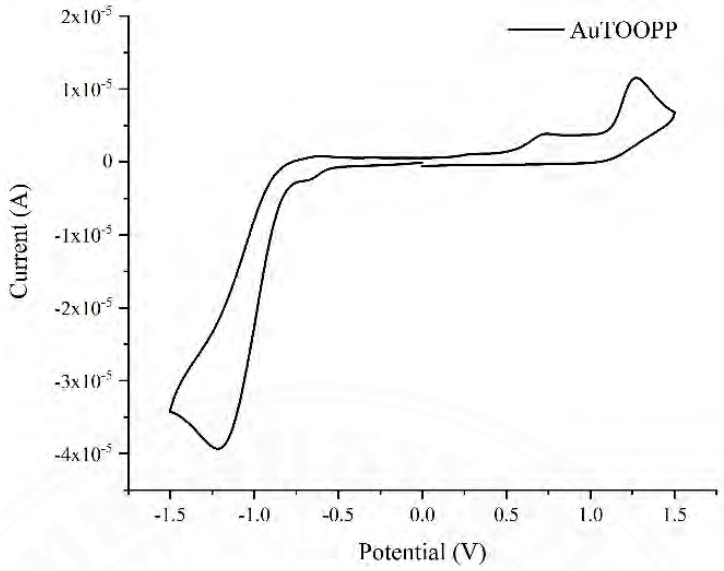

Figure G19 cyclicvoltammogram of AuTOOPP 22

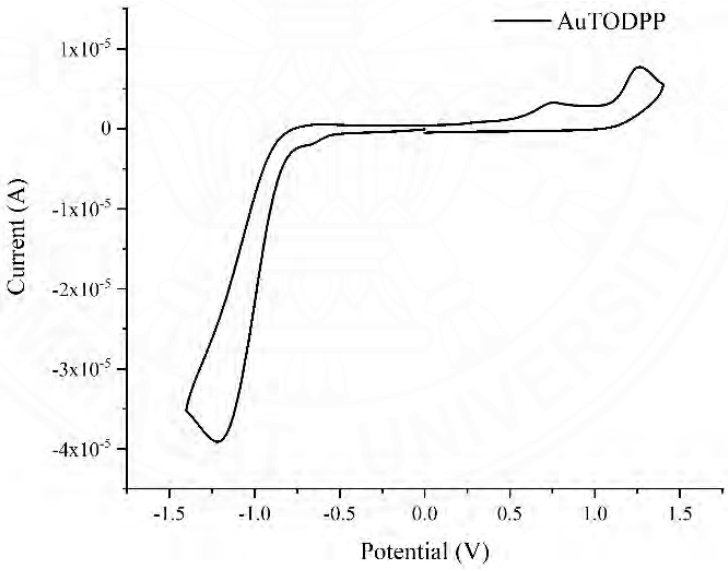

Figure G20 cyclicvoltammogram of AuTOMPP 23

APPENDIX H

THERMAL GRAVIMETRIC ANALYSIS (TGA)

Thermal gravimetric analysis (TGA) curves for free-base porphyrin

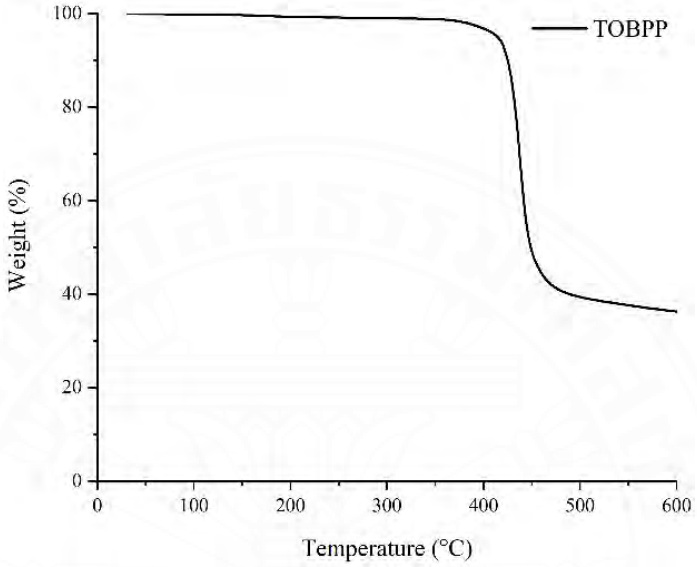

Figure F1 Thermal gravimetric analysis (TGA) curves of TOBPP 6

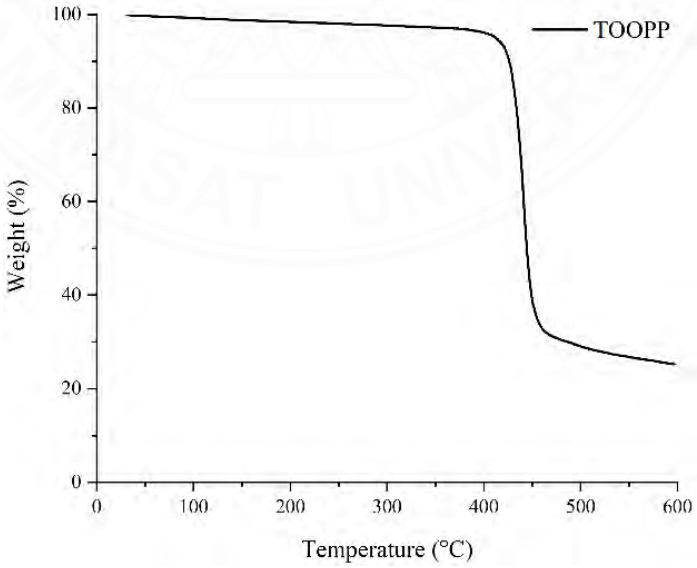

Figure F2 Thermal gravimetric analysis (TGA) curves of TOOPP 7

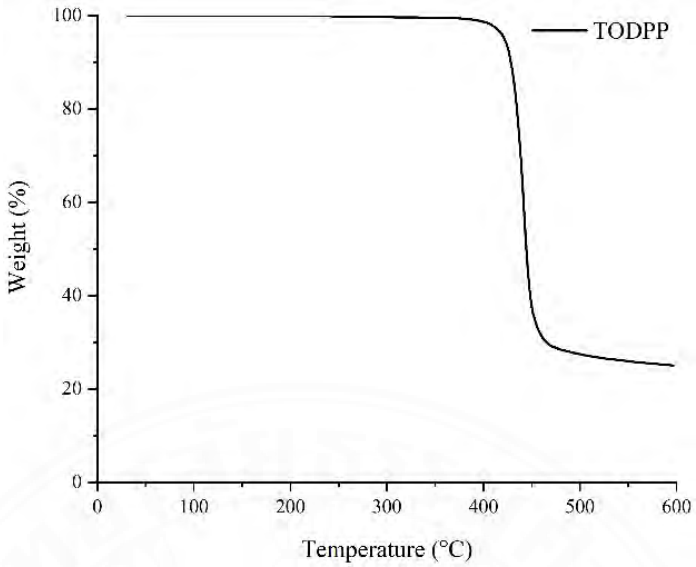

Figure F3 Thermal gravimetric analysis (TGA) curves of TODPP 8

Thermal gravimetric analysis (TGA) curves for copper(II) porphyrin complexes

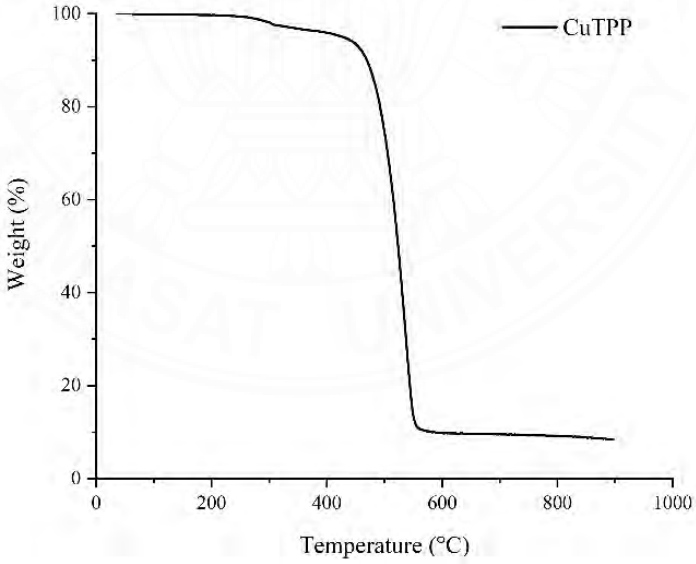

Figure F4 Thermal gravimetric analysis (TGA) curves of CuTPP 9

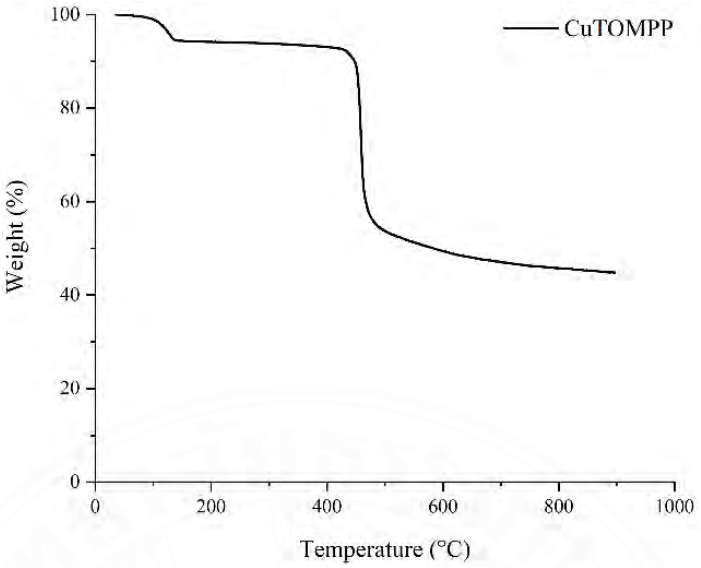

Figure F5 Thermal gravimetric analysis (TGA) curves of TOMPP 10

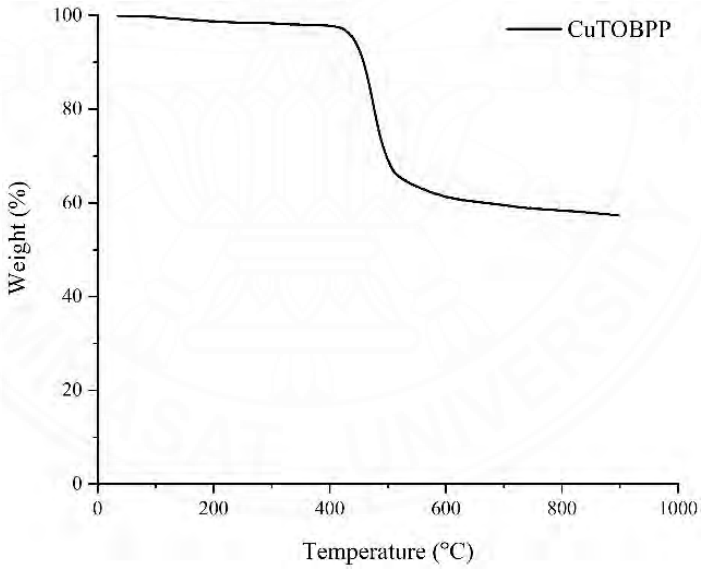

Figure F6 Thermal gravimetric analysis (TGA) curves of TOBPP 11

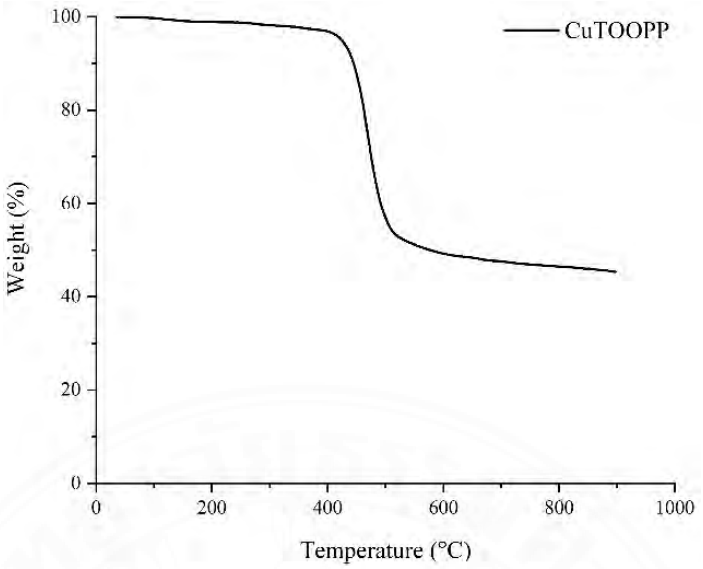

Figure F7 Thermal gravimetric analysis (TGA) curves of TOOPP 12

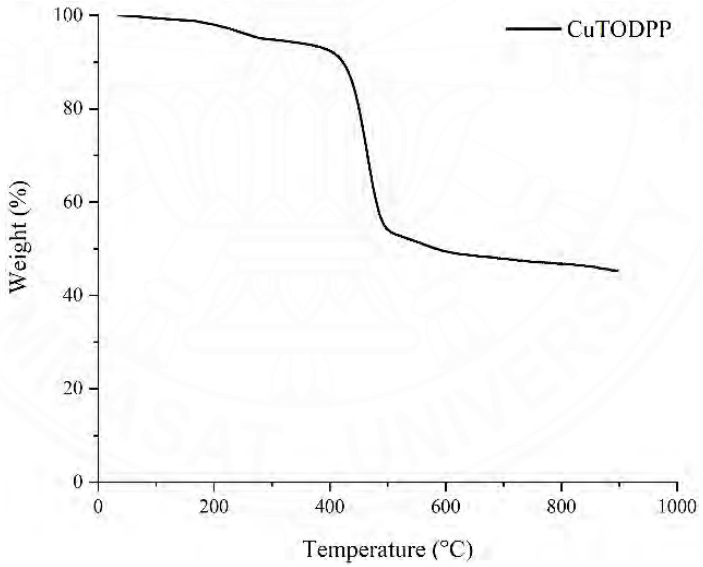

Figure F8 Thermal gravimetric analysis (TGA) curves of TODPP 13

Thermal gravimetric analysis (TGA) curves for silver(II) porphyrin complexes

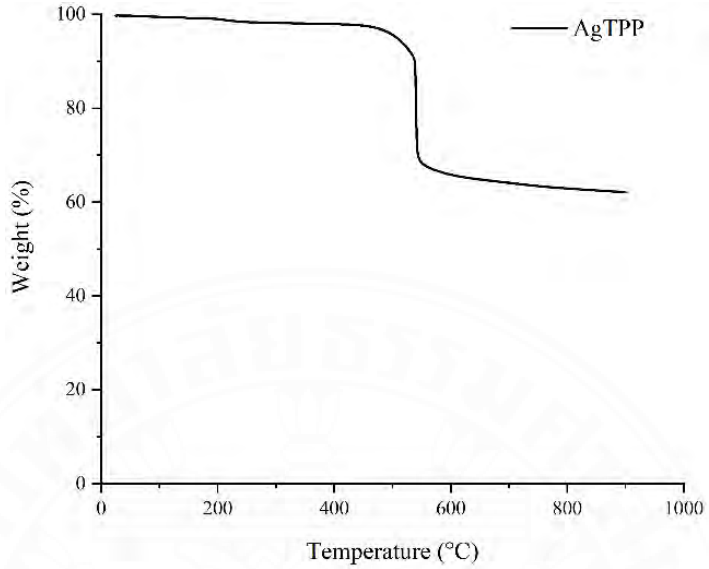

Figure F9 Thermal gravimetric analysis (TGA) curves of AgTPP 14

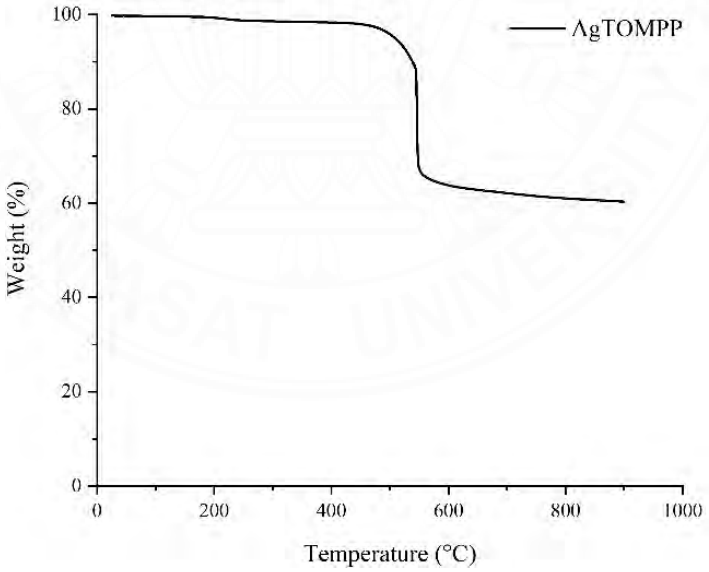

Figure F10 Thermal gravimetric analysis (TGA) curves of AgTOMPP 15

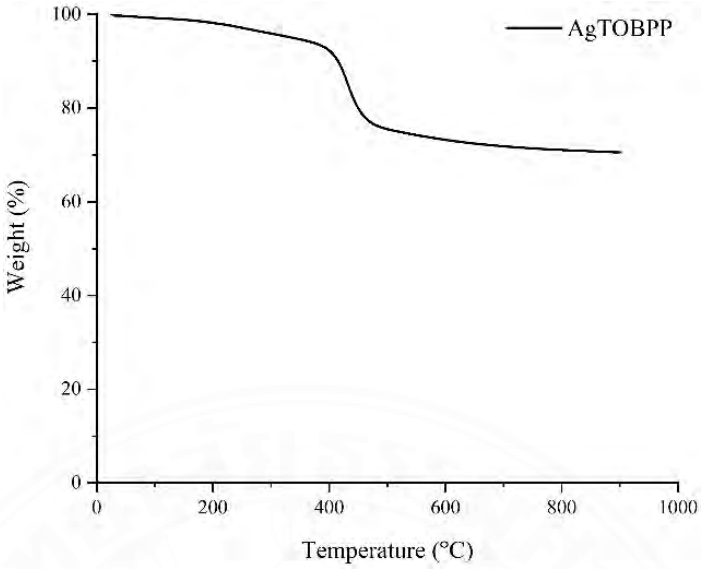

Figure F11 Thermal gravimetric analysis (TGA) curves of AgTOBPP 16

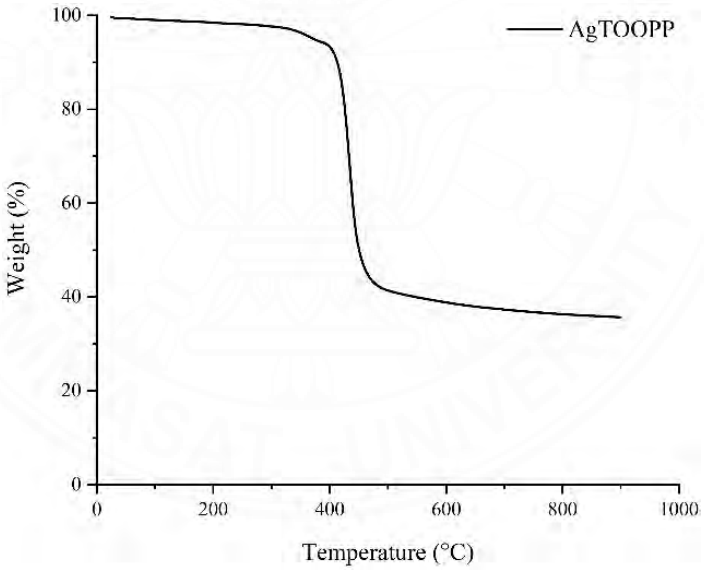

Figure F12 Thermal gravimetric analysis (TGA) curves of AgTOOPP 17

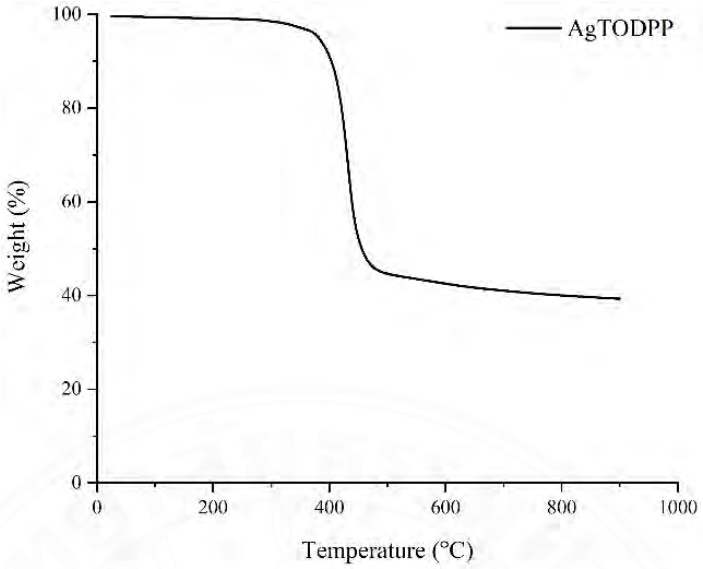

Figure F13 Thermal gravimetric analysis (TGA) curves of AgTODPP 18

Thermal gravimetric analysis (TGA) curves for gold(III) porphyrin complexes

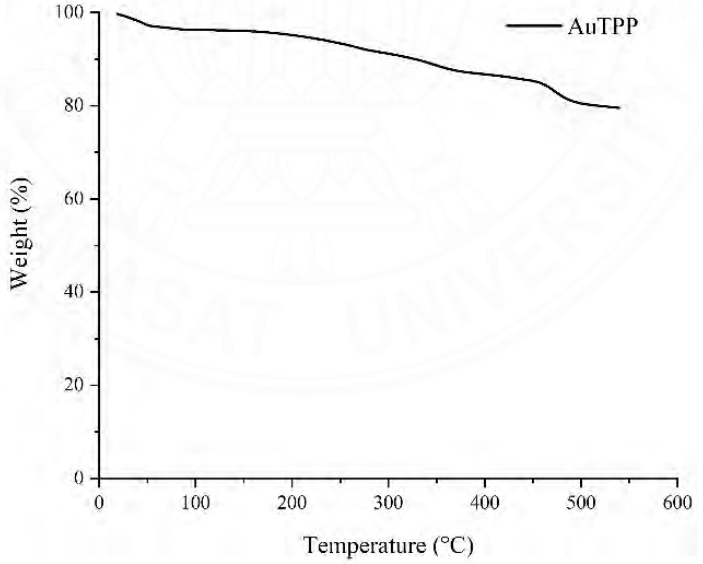

Figure F14 Thermal gravimetric analysis (TGA) curves of AuTPP 19

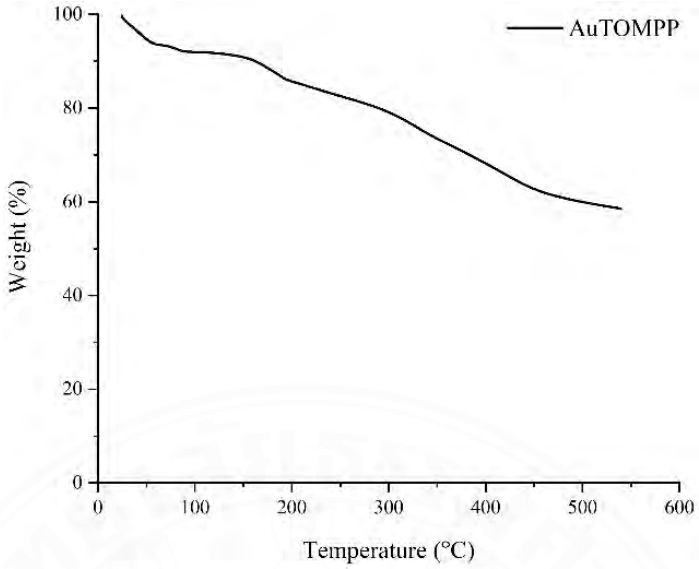

Figure F15 Thermal gravimetric analysis (TGA) curves of AuTOMPP 20

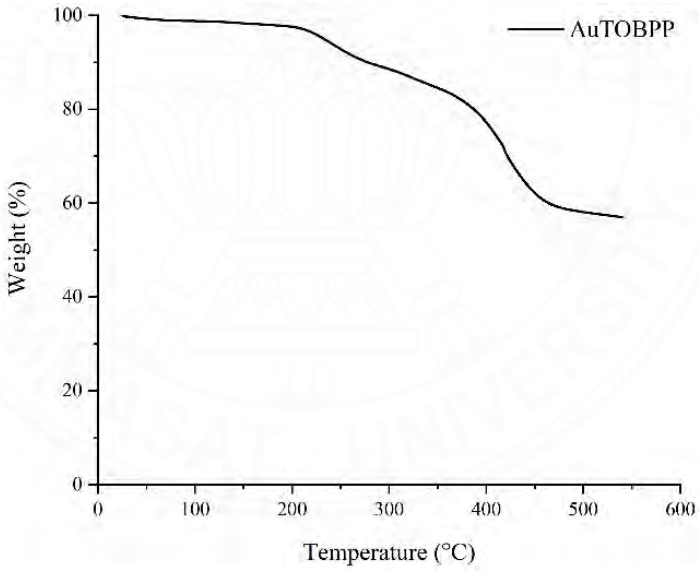

Figure F16 Thermal gravimetric analysis (TGA) curves of AuTOBPP 21

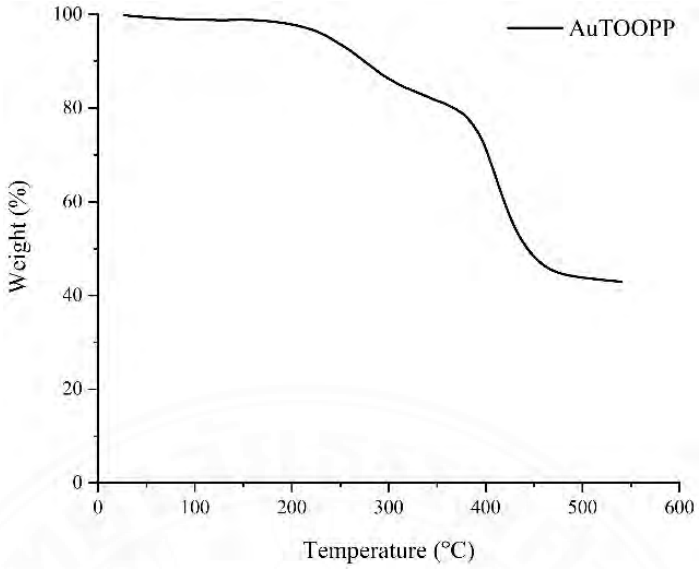

Figure F17 Thermal gravimetric analysis (TGA) curves of AuTOOPP 22

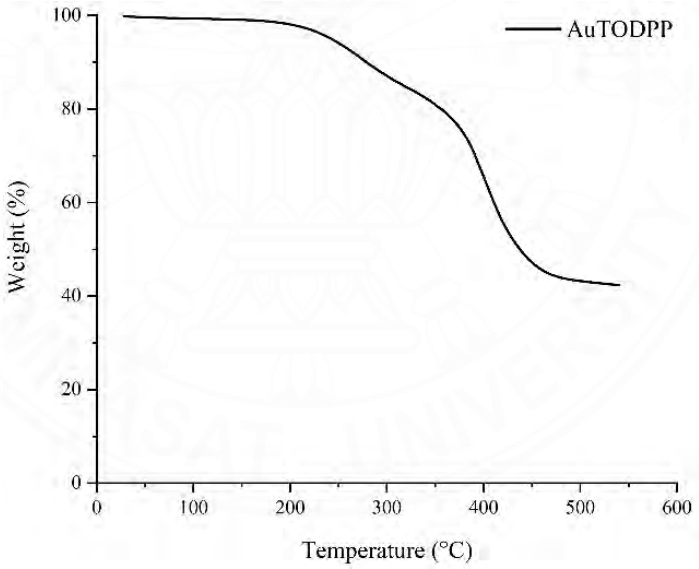

Figure F18 Thermal gravimetric analysis (TGA) curves of AuTODPP 23

APPENDIX I

DFT CALCULATION

Optimization structure and Frontier orbital of free-base porphyrin compounds

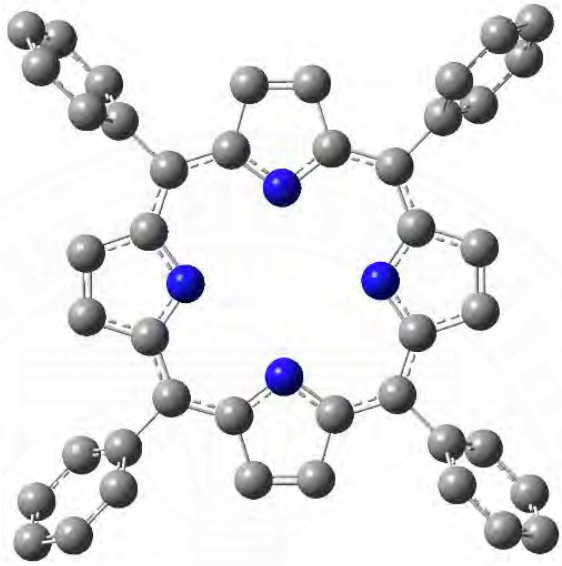

Figure I1 Optimization structure of TPP 4

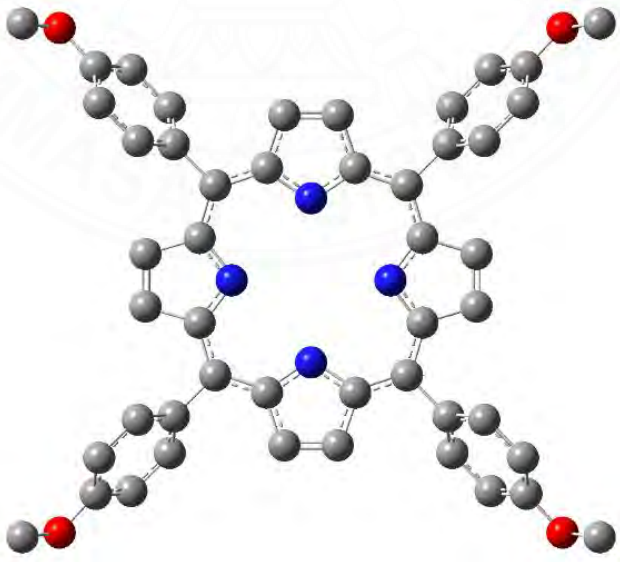

Figure I2 Optimization structure of TOMPP 5

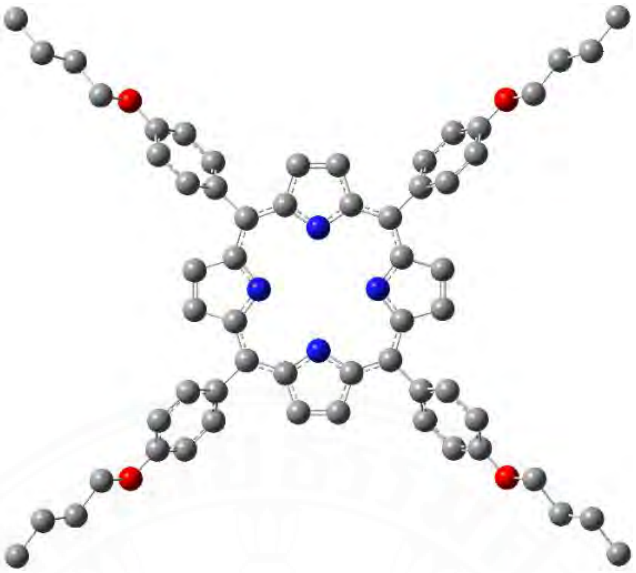

Figure I3 Optimization structure of TOBPP 6

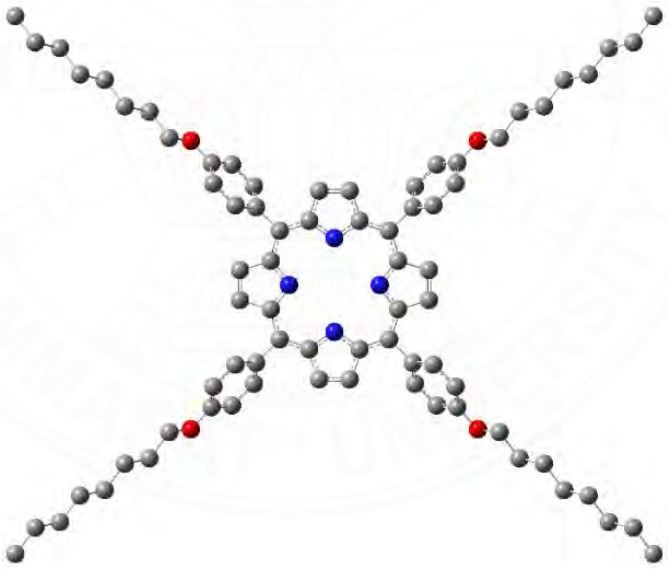

Figure I4 Optimization structure of TOOPP 7

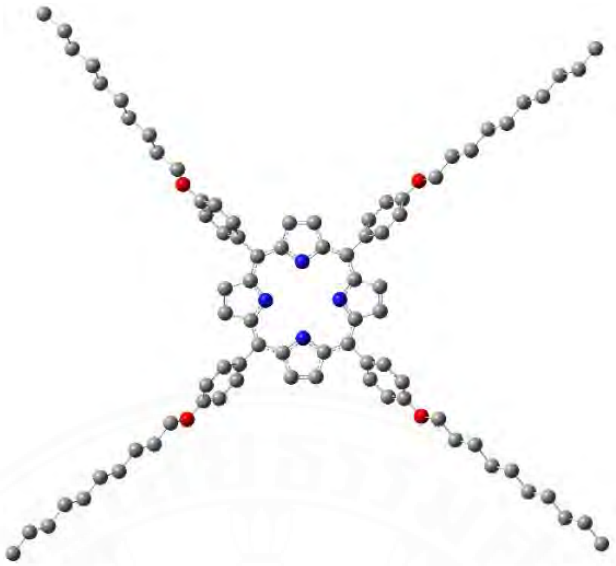

Figure I5 Optimization structure of TODPP 8

Optimization structure and Frontier orbital of copper(II) porphyrin complexes

Figure I6 Optimization structure of CuTPP 9

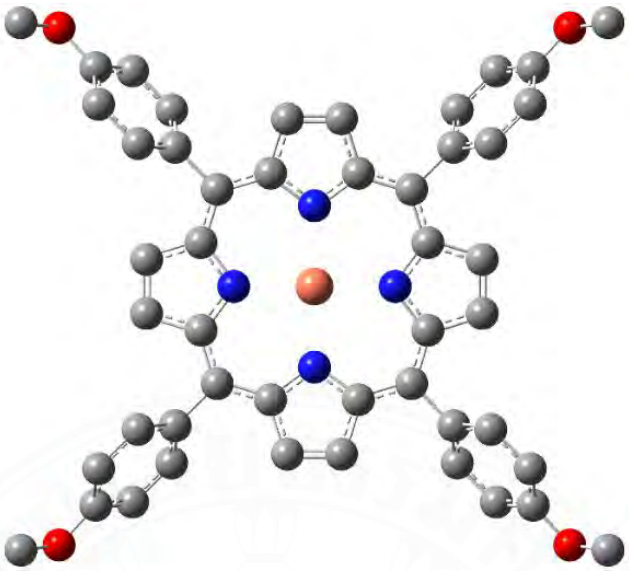

Figure I7 Optimization structure of CuTOMPP 10

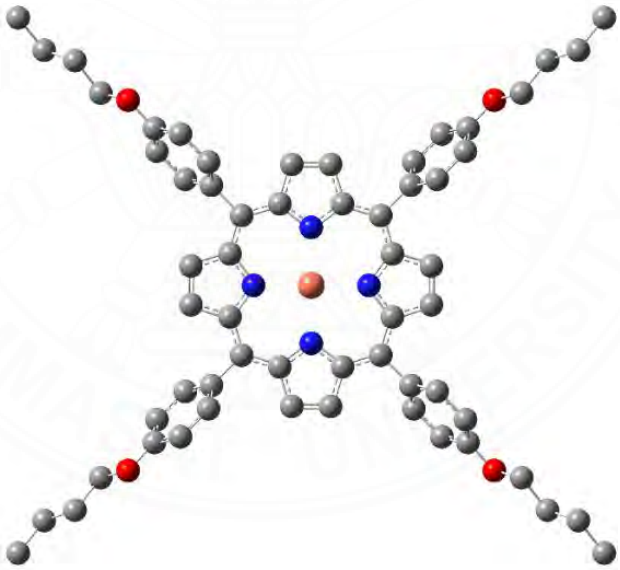

Figure I8 Optimization structure of CuTOBPP 11

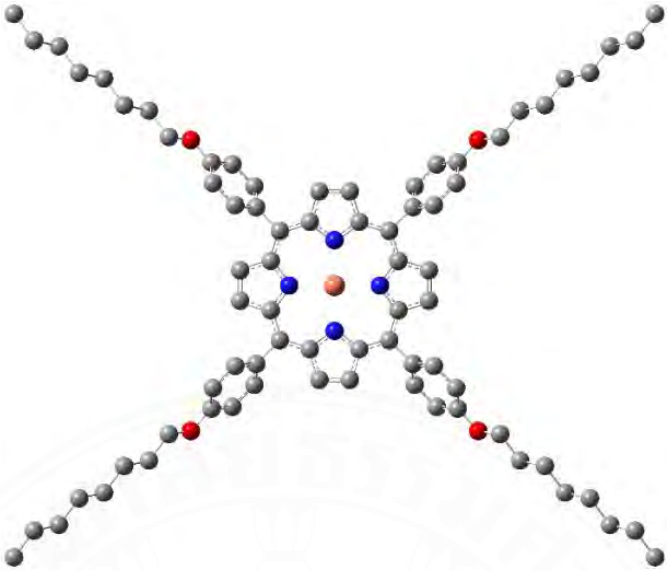

Figure I9 Optimization structure of CuTOOPP 12

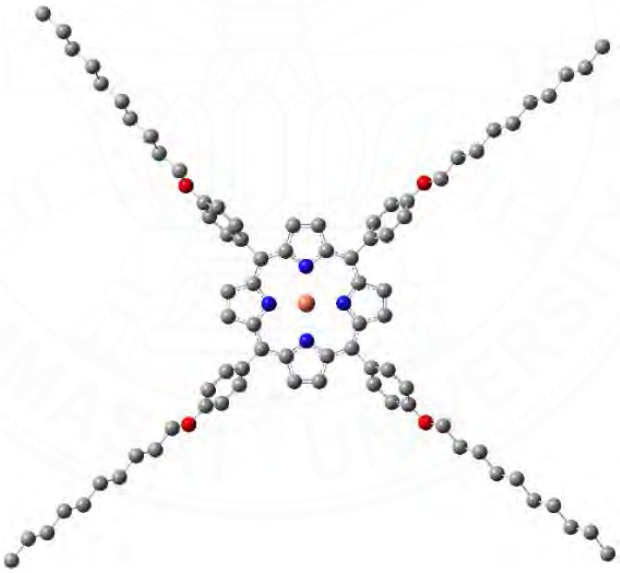

Figure I10 Optimization structure of CuTODPP 13

Optimization structure and Frontier orbital of silver(II) porphyrin complexes

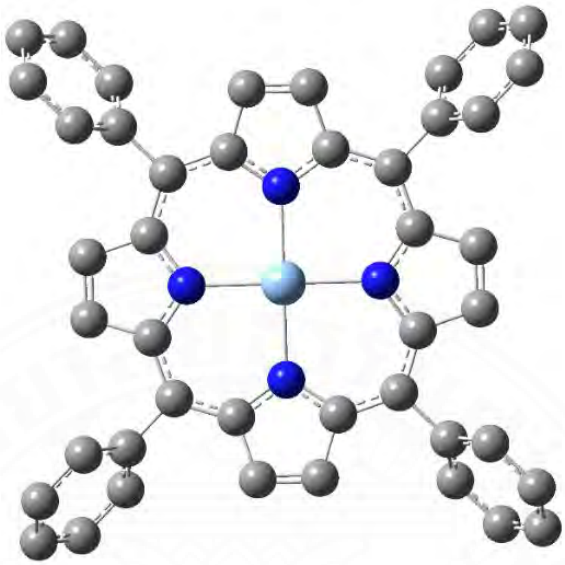

Figure I11 Optimization structure of AgTPP 14

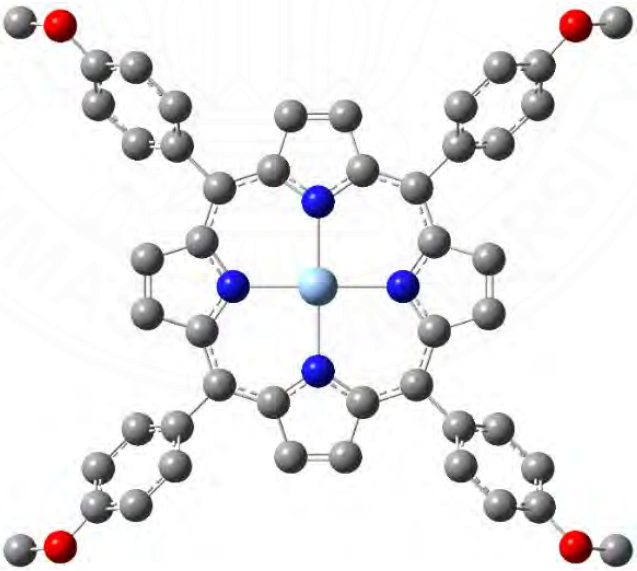

Figure I12 Optimization structure of AgTOMPP 15

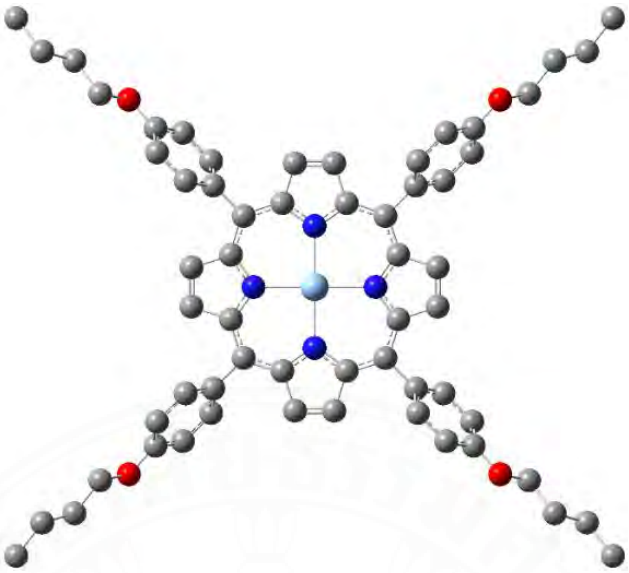

Figure I13 Optimization structure of AgTOBPP 16

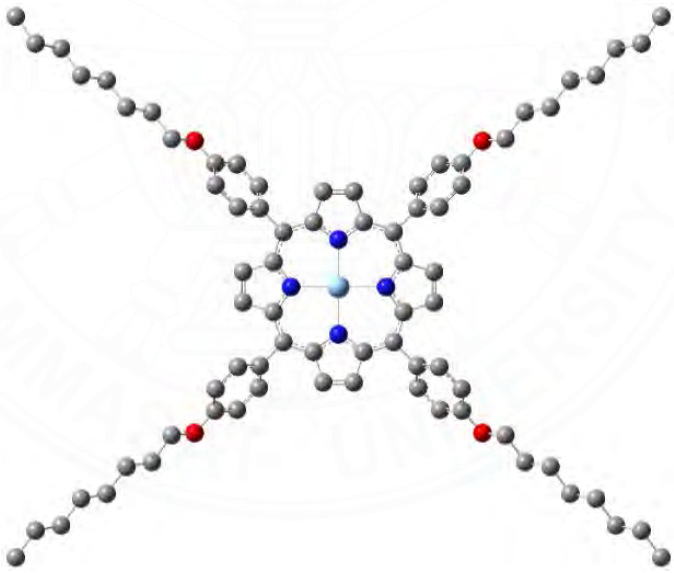

Figure I14 Optimization structure of AgTOOPP 17

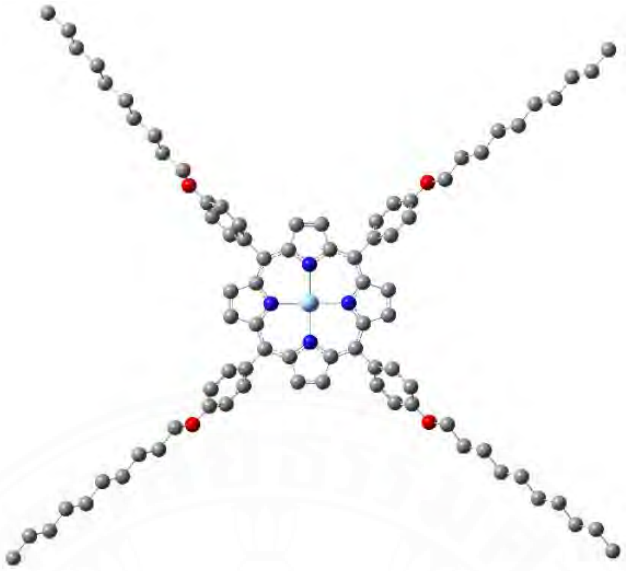

Figure I15 Optimization structure of AgTODPP 18

Optimization structure and Frontier orbital of gold(III) porphyrin complexes

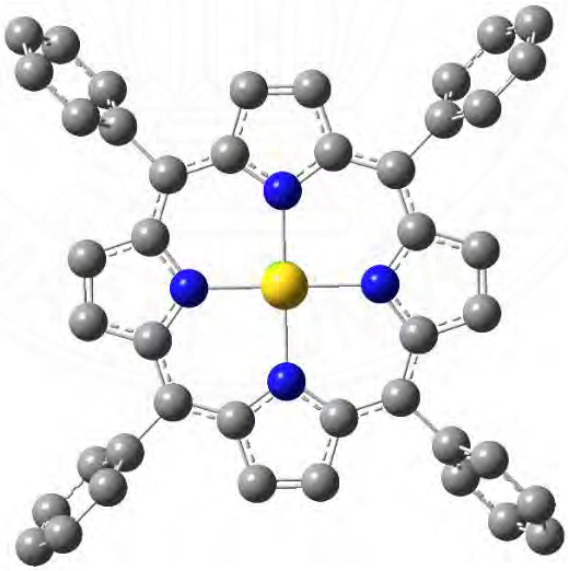

Figure I16 Optimization structure of AuTPP 19

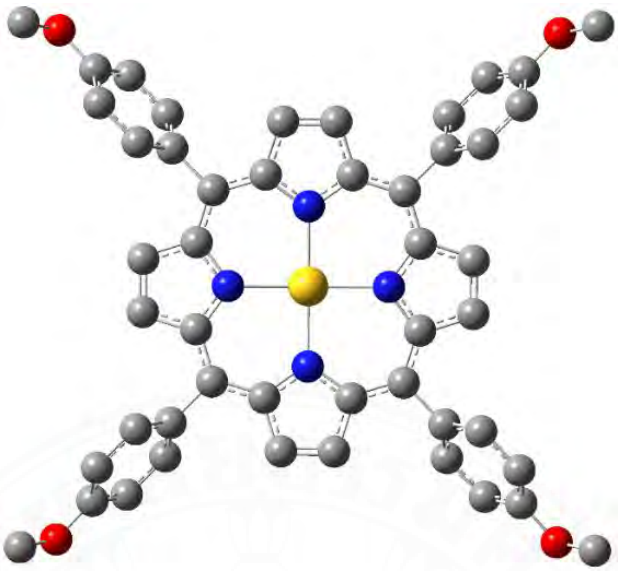

Figure I17 Optimization structure of AuTOMPP 20

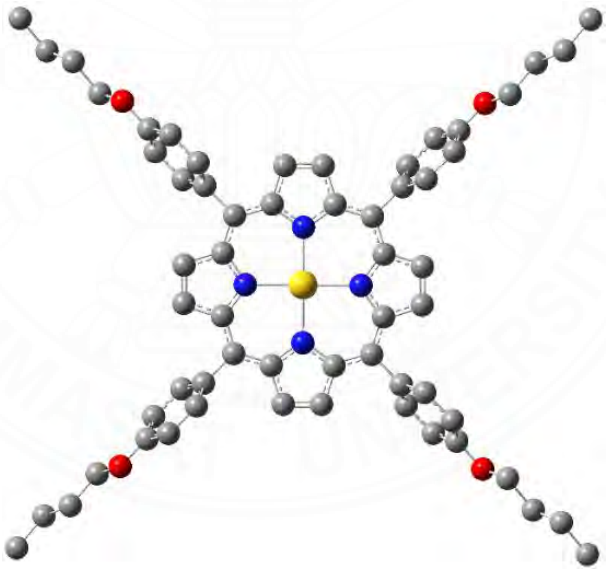

Figure I18 Optimization structure of AuTOBPP 21

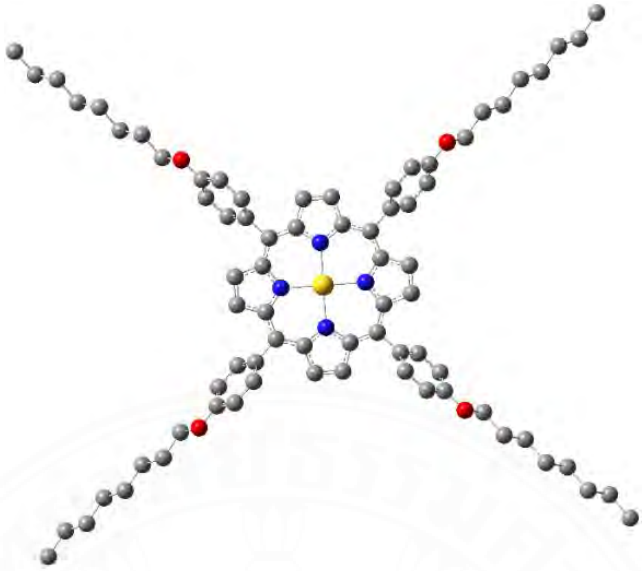

Figure I19 Optimization structure of AuTOOPP 22

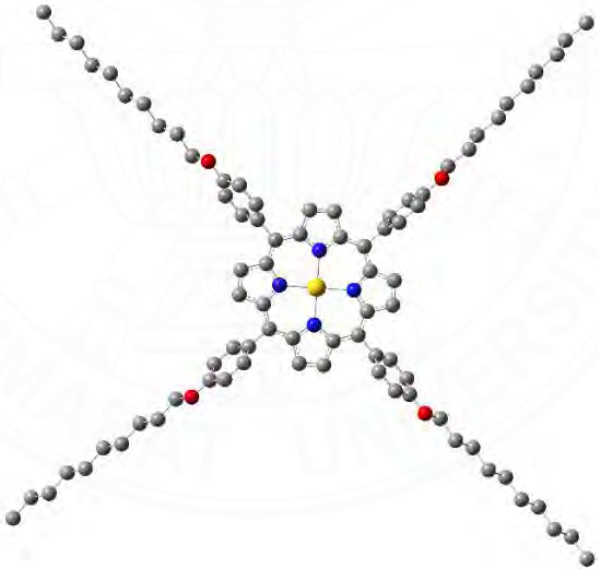

Figure I20 Optimization structure of AuTODPP 23

Frontier orbital of free-base porphyrin compounds

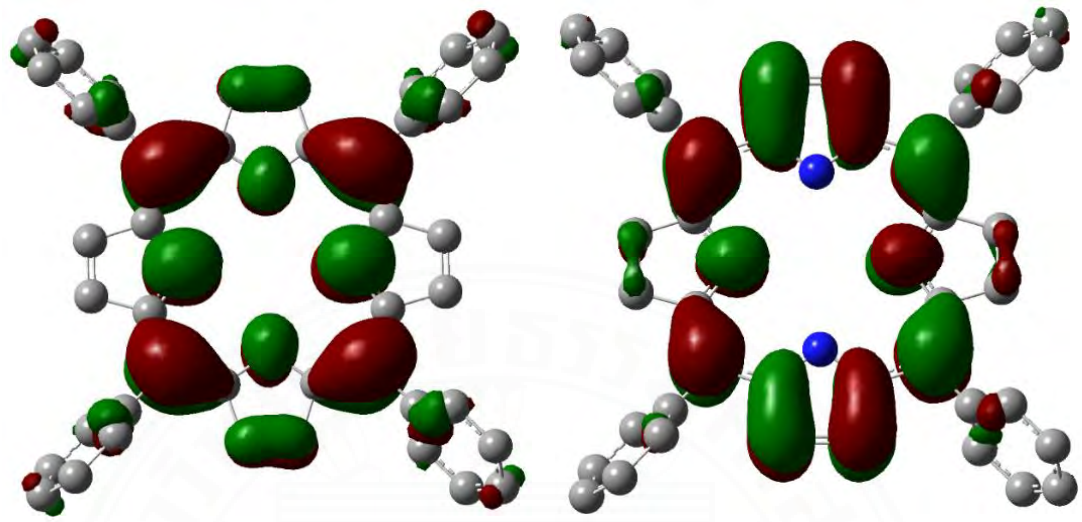

(a) (b)

Figure I21 Frontier orbital (a) HOMO, and (b) LUMO of TPP 4

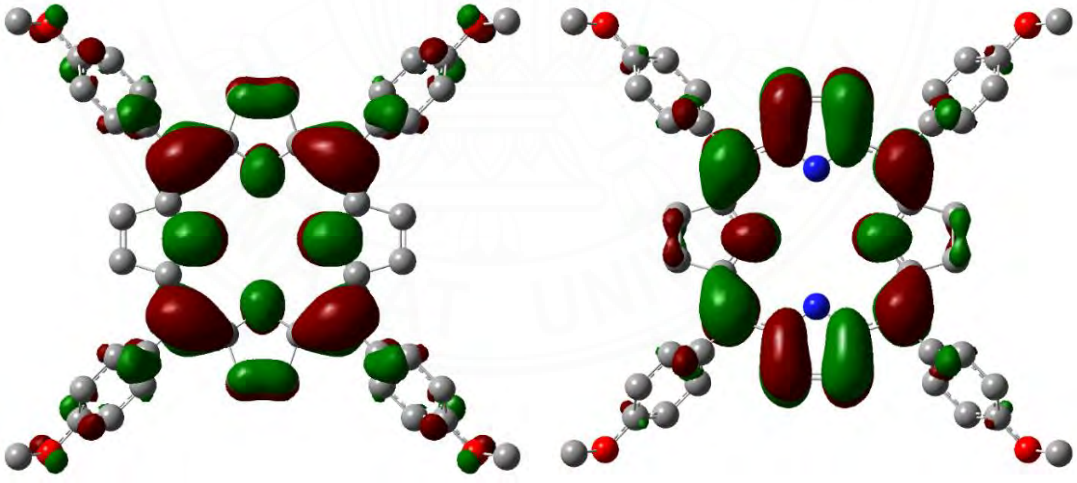

(a) (b)

Figure I22 Frontier orbital (a) HOMO, and (b) LUMO of TOMPP 5

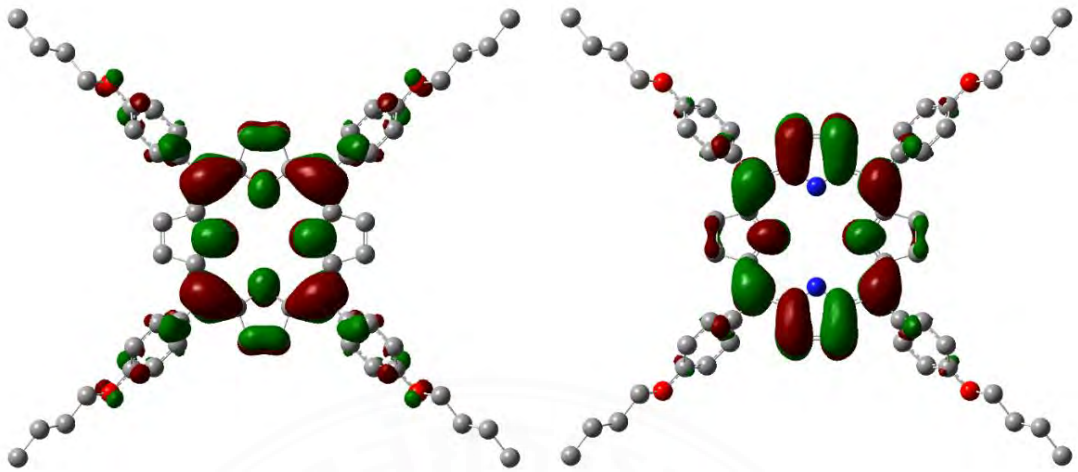

(a) (b)

Figure I23 Frontier orbital (a) HOMO, and (b) LUMO of TOBPP 6

5

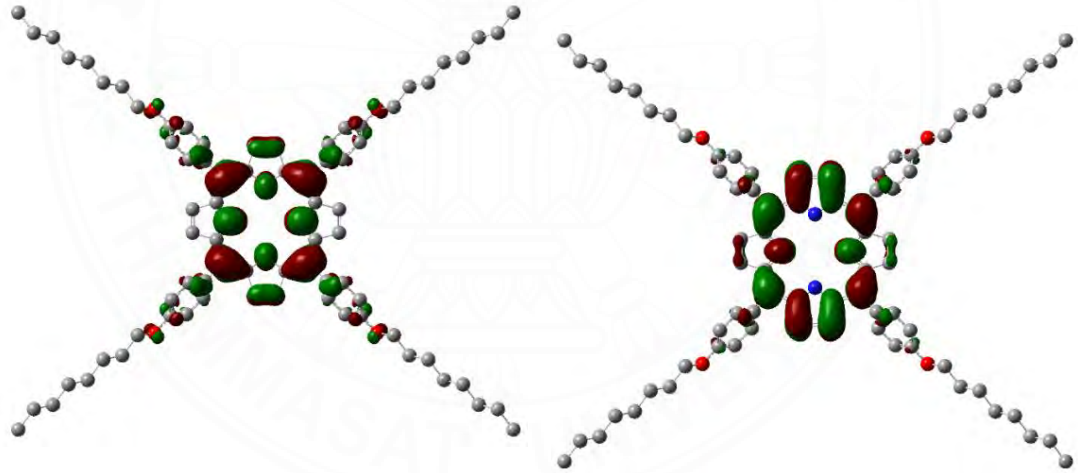

(a) (b)

Figure I24 Frontier orbital (a) HOMO, and (b) LUMO of TOOPP 7

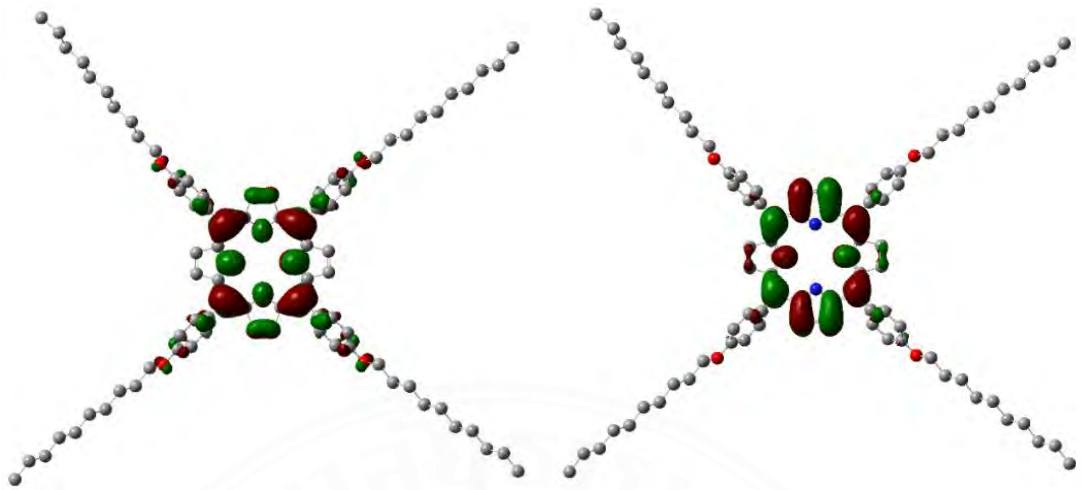

(a) (b)

Figure I25 Frontier orbital (a) HOMO, and (b) LUMO of TODPP 8

Frontier orbital of copper(II) porphyrin complexes

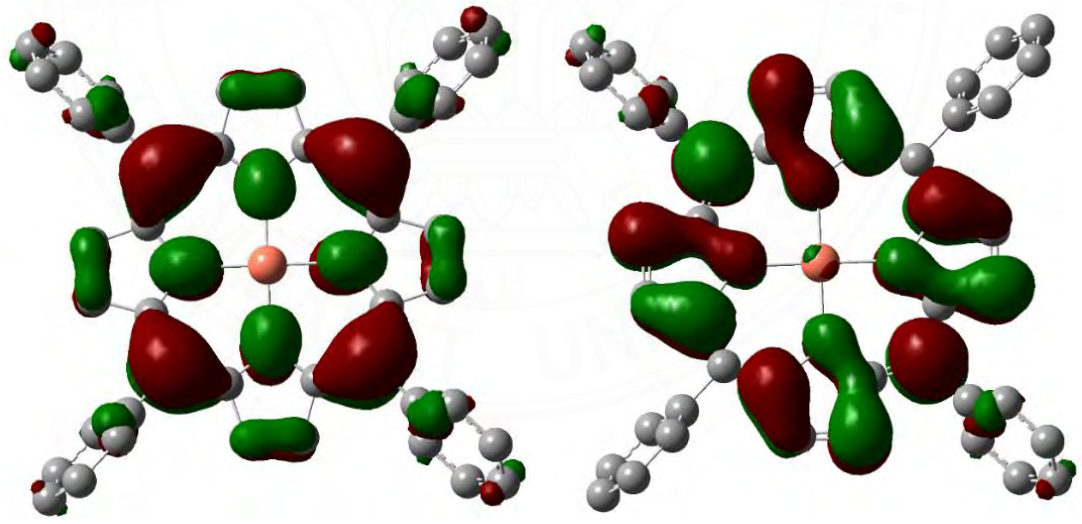

(a) (b)

Figure I26 Frontier orbital (a) HOMO, and (b) LUMO of CuTPP 9

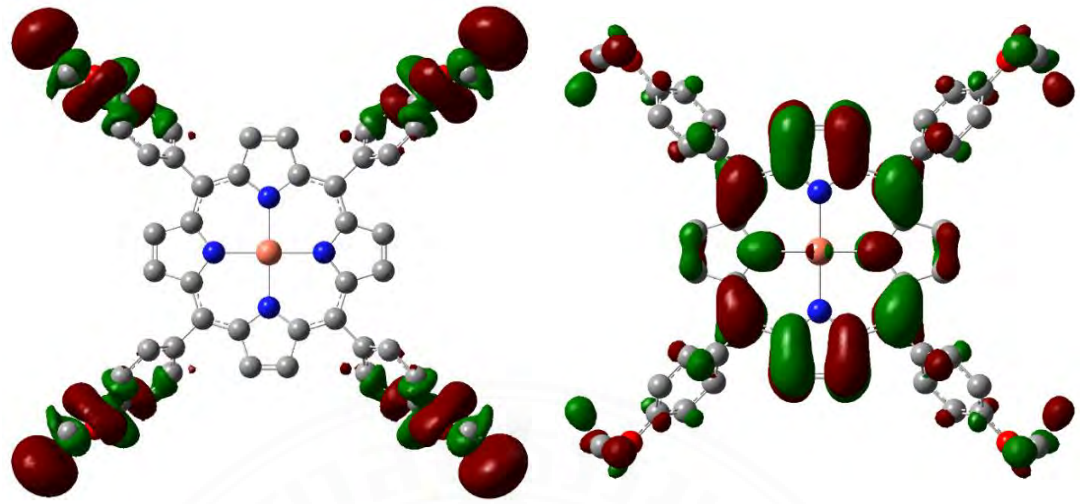

(a) (b)

Figure I27 Frontier orbital (a) HOMO, and (b) LUMO of CuTOMPP 10

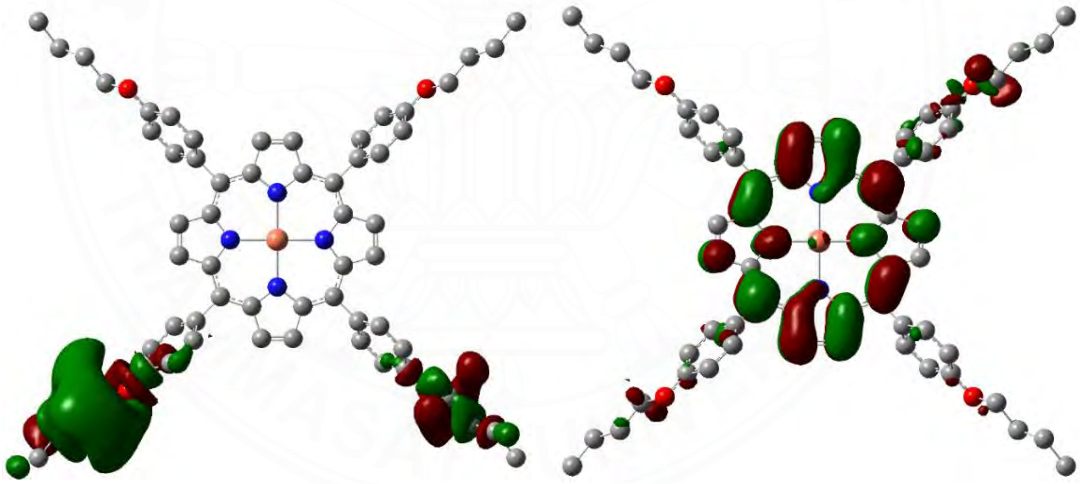

(a) (b)

Figure I28 Frontier orbital (a) HOMO, and (b) LUMO of CuTOBPP 11

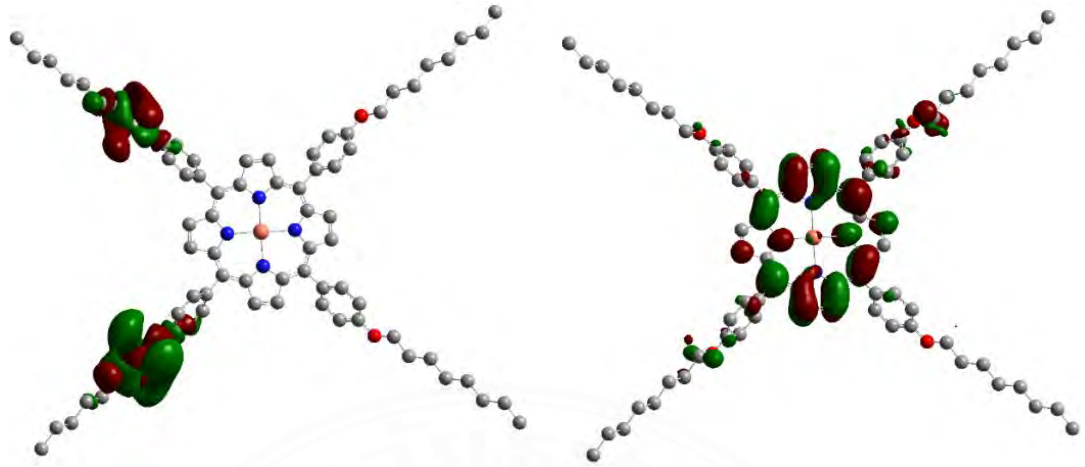

(a) (b)

Figure I29 Frontier orbital (a) HOMO, and (b) LUMO of CuTOOPP 12

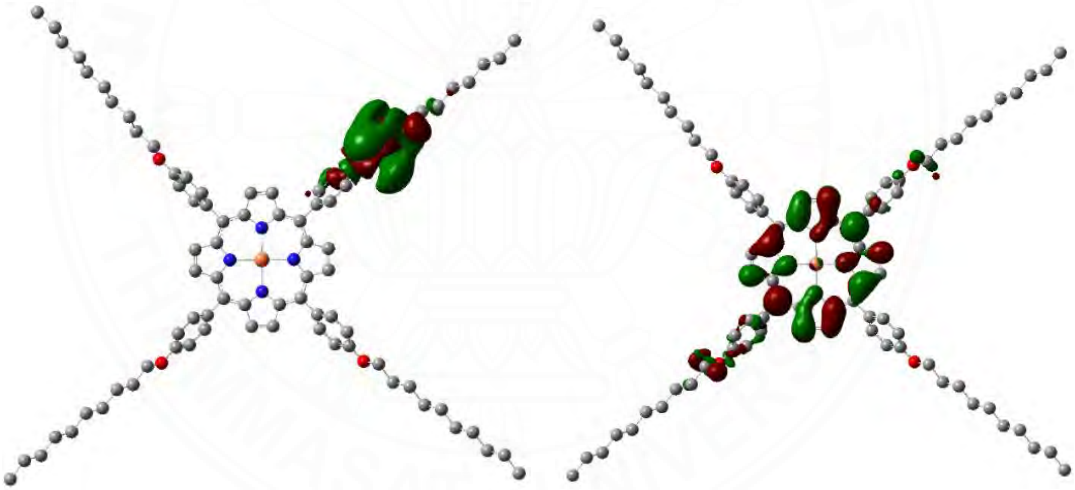

(a) (b)

Figure I30 Frontier orbital (a) HOMO, and (b) LUMO of CuTODPP 13

Frontier orbital of silver(II) porphyrin complexes

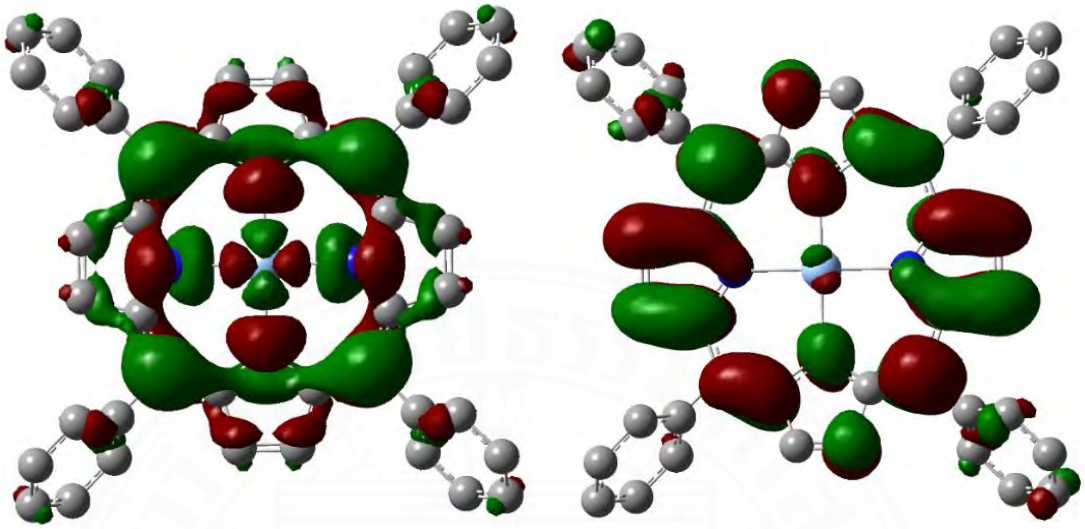

(a) (b)

Figure I31 Frontier orbital (a) HOMO, and (b) LUMO of AgTPP 14

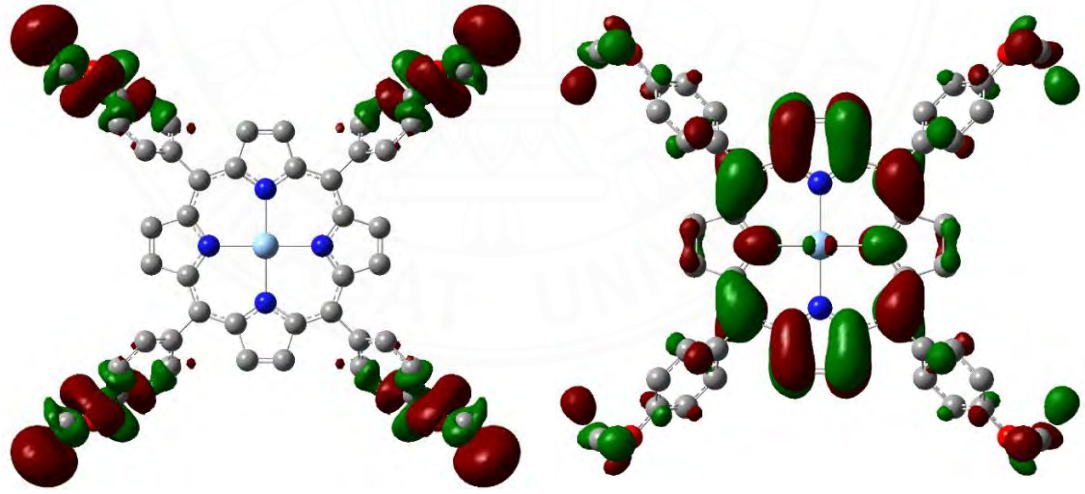

(a) (b)

Figure I32 Frontier orbital (a) HOMO, and (b) LUMO of AgTOMPP 15

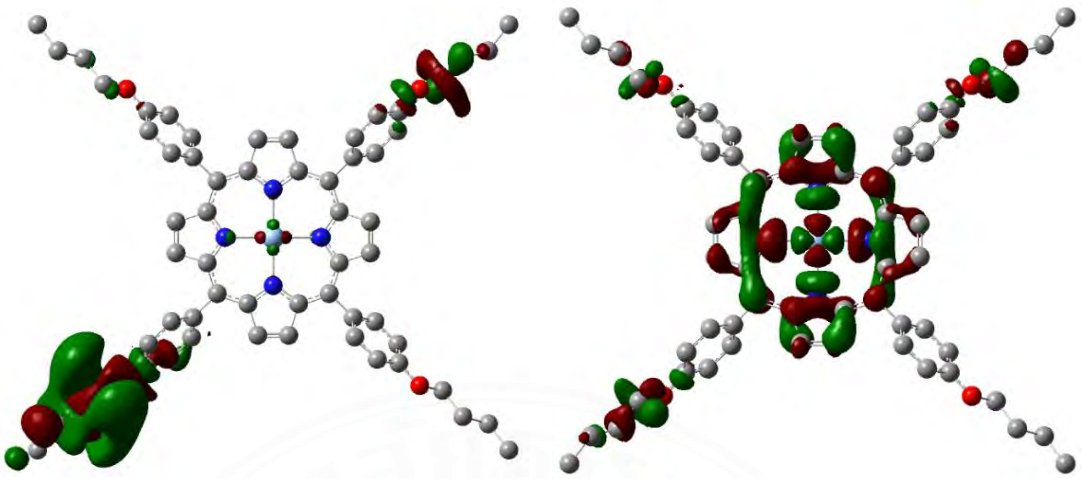

(a) (b)

Figure I33 Frontier orbital (a) HOMO, and (b) LUMO of AgTOBPP 16

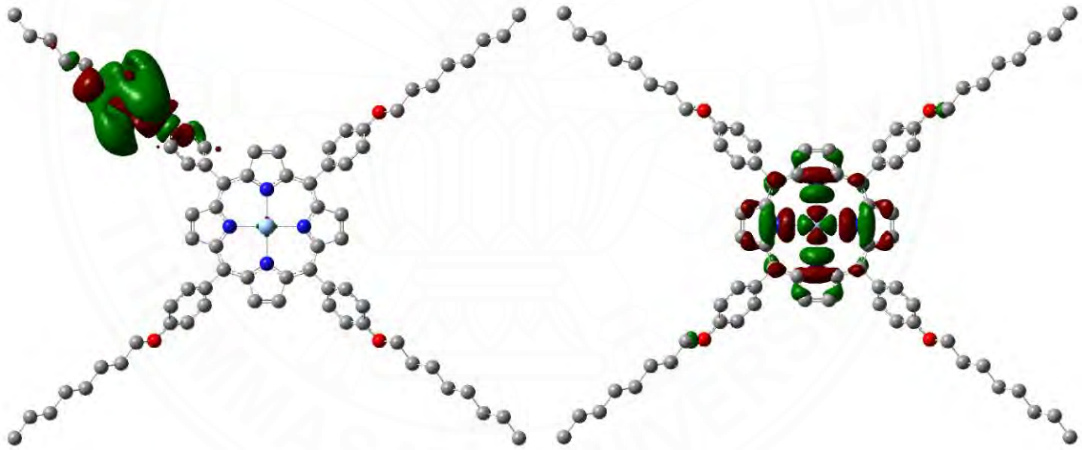

(a) (b)

Figure I34 Frontier orbital (a) HOMO, and (b) LUMO of AgTOOPP 17

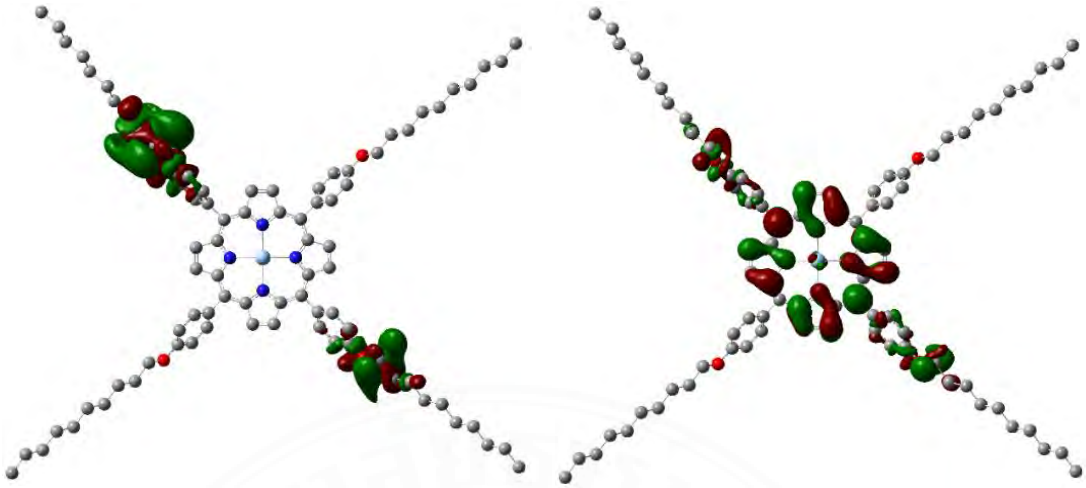

(a) (b)

Figure I35 Frontier orbital (a) HOMO, and (b) LUMO of AgTODPP 18

Frontier orbital of gold(III) porphyrin complexes

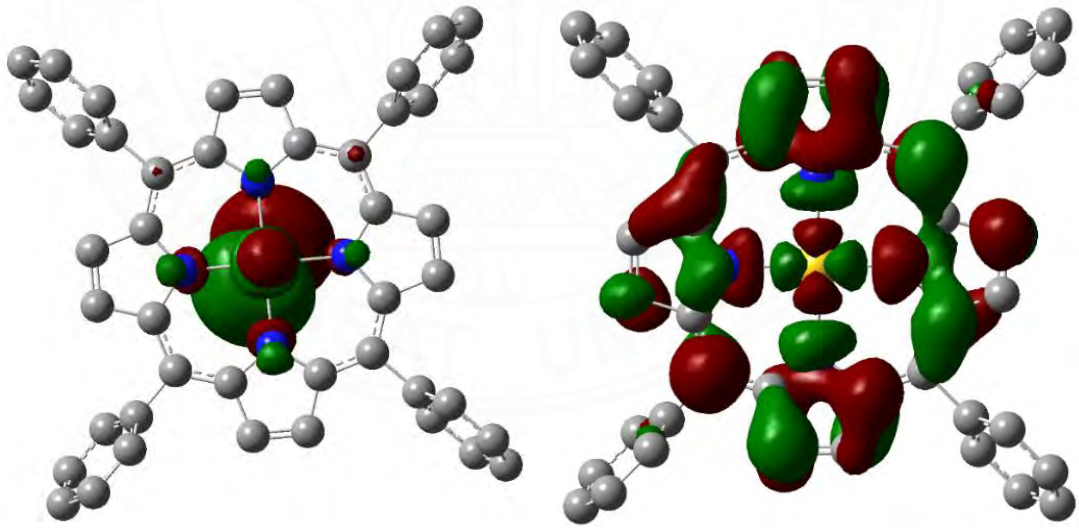

(a) (b)

Figure I36 Frontier orbital (a) HOMO, and (b) LUMO of AuTPP 19

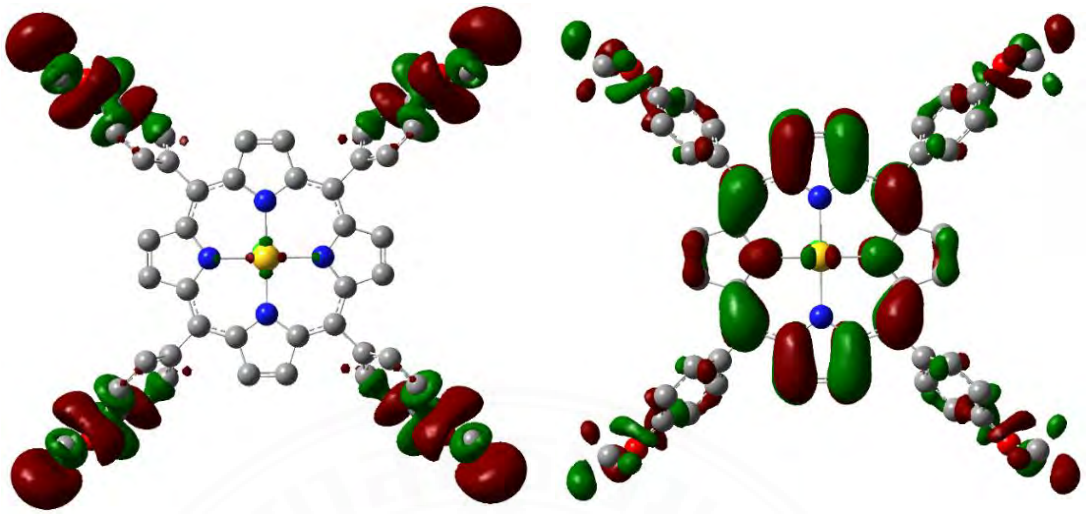

(a) (b)

Figure I37 Frontier orbital (a) HOMO, and (b) LUMO of AuOMPP 20

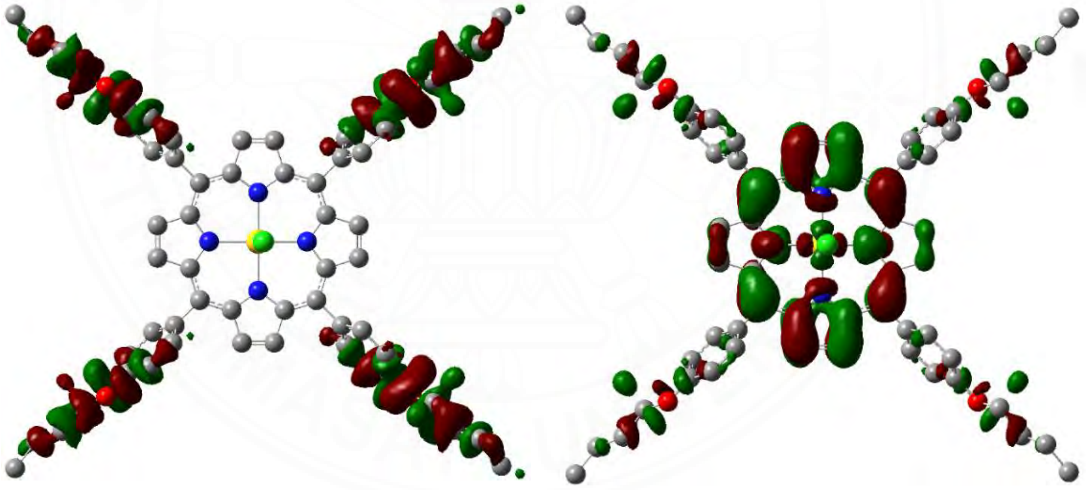

(a) (b)

Figure I38 Frontier orbital (a) HOMO, and (b) LUMO of AuOBPP 21

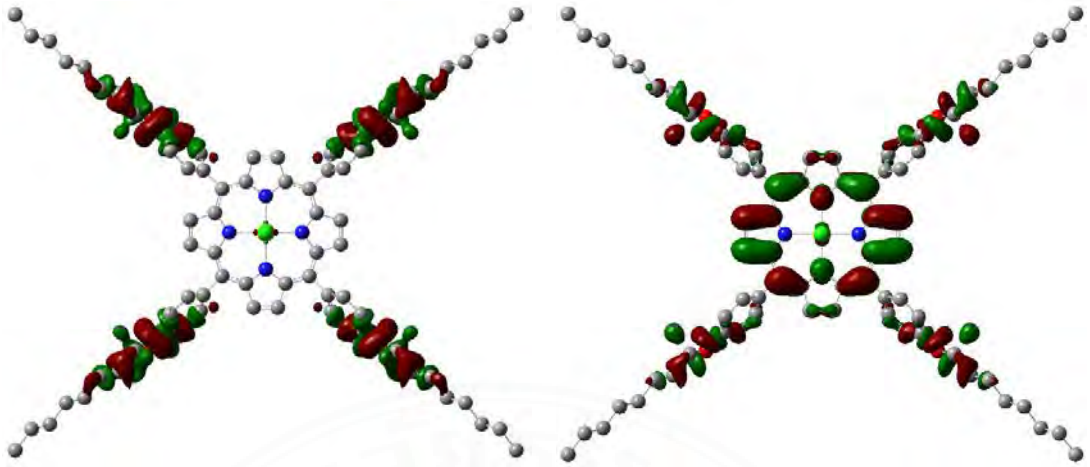

(a) (b)

Figure I39 Frontier orbital (a) HOMO, and (b) LUMO of AuOOPP 22

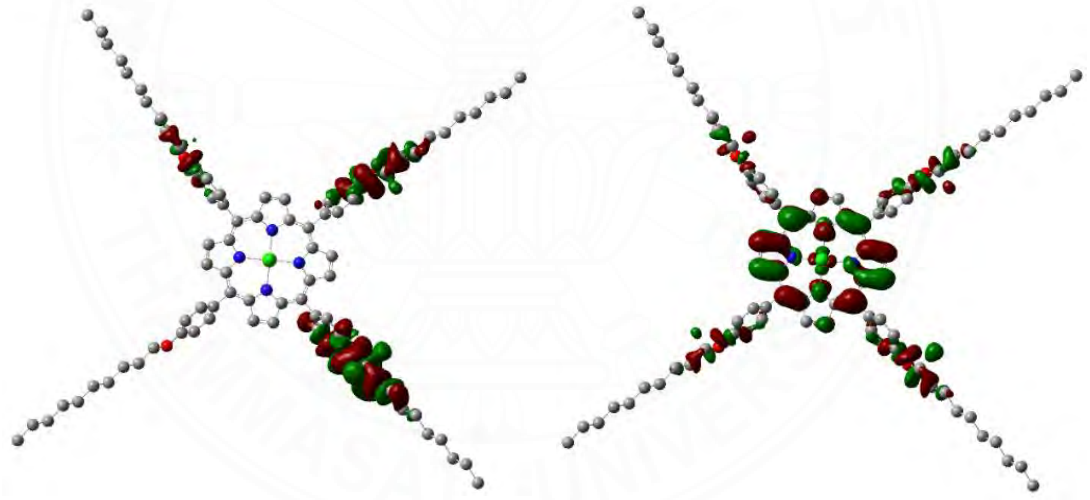

(a) (b)

Figure I40 Frontier orbital (a) HOMO, and (b) LUMO of AuODPP 23

APPENDIX J
ANTICANCER ACTIVITY

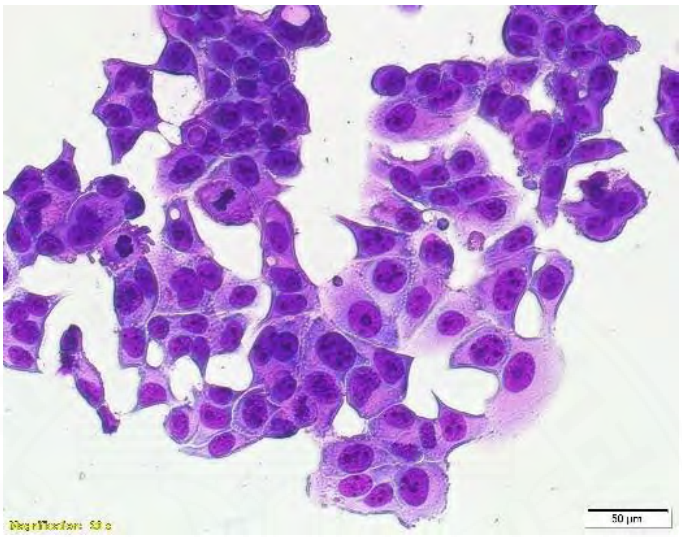

Figure J1 Diff-Quik stain image of MCF7 cell (Control)

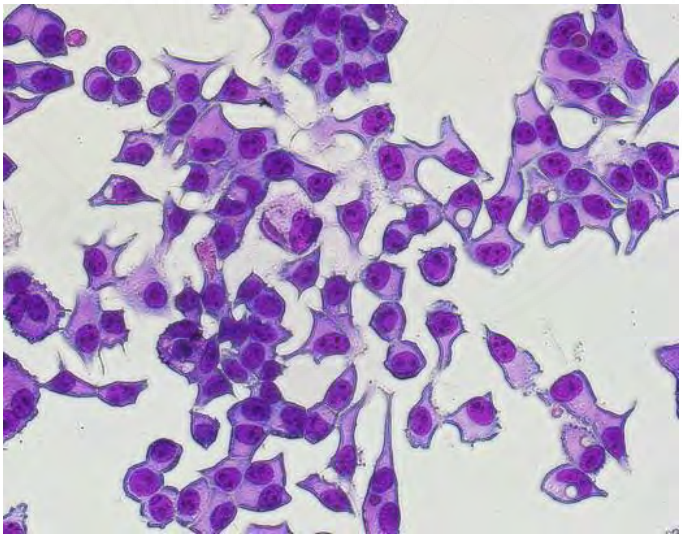

Figure J2 Diff-Quik stain image of MCF7 cell after treated with 1%DMSO for 24 Hours

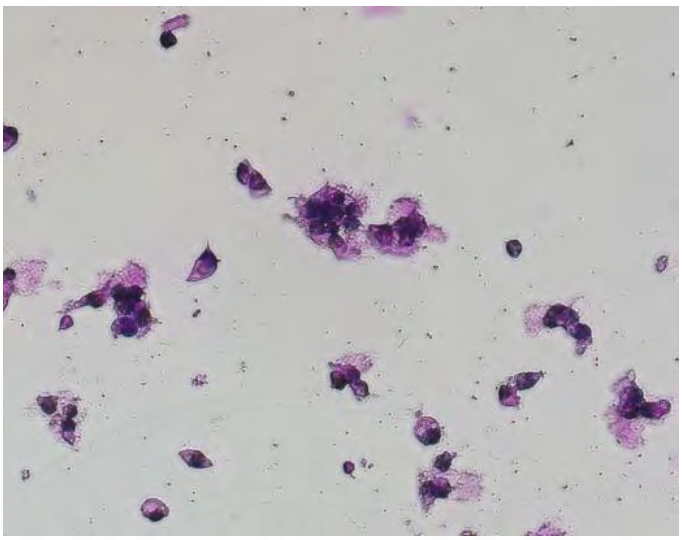

Figure J3 Diff-Quik stain image of MCF7 cell after treated with AuTPP 150 µM for 24 hours

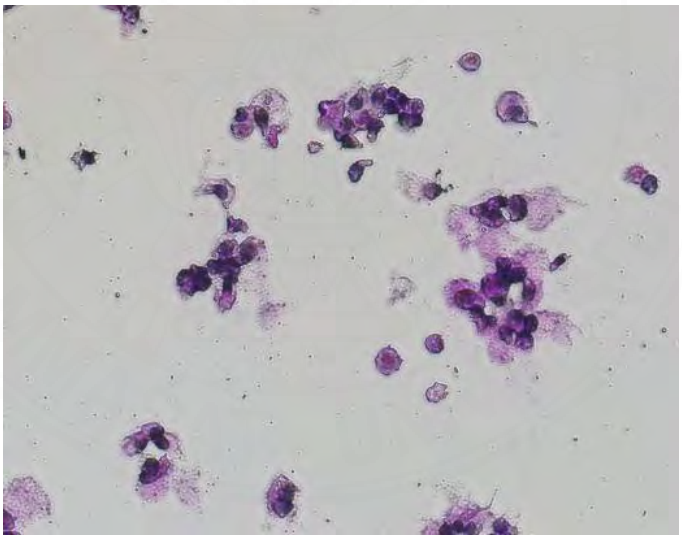

Figure J4 Diff-Quik stain image of MCF7 cell after treated with AuTPP 100 µM for 24 hours

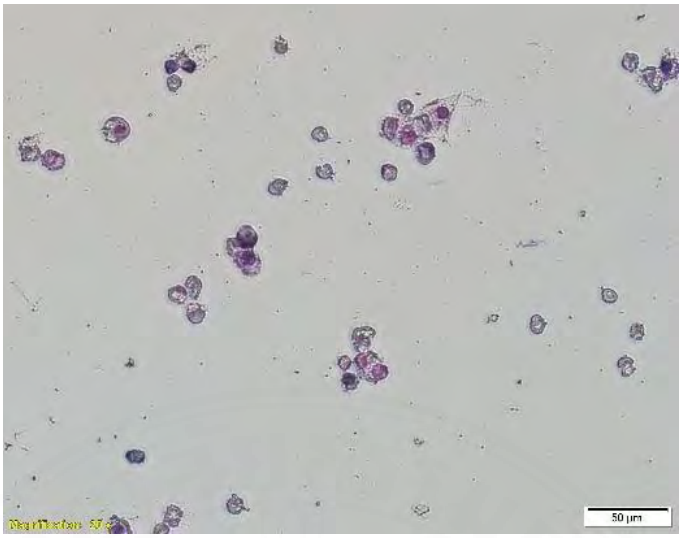

Figure J5 Diff-Quik stain image of MCF7 cell after treated with AuTPP 50 µM for 24 hours

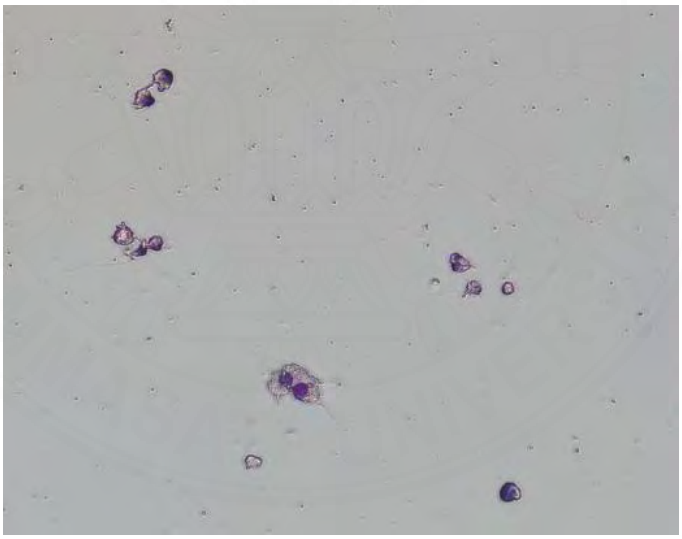

Figure J6 Diff-Quik stain image of MCF7 cell after treated with AuTPP 25 µM for 24 hours

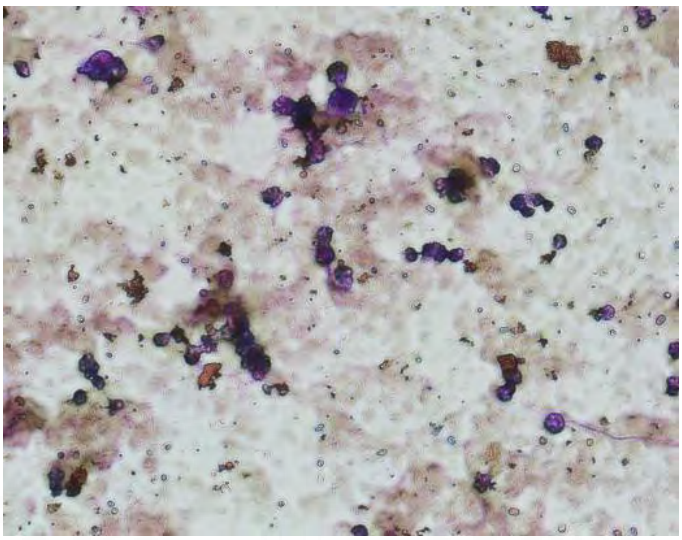

Figure J7 Diff-Quik stain image of MCF7 cell after treated with AuTOMPP 150 μM for 24 hours

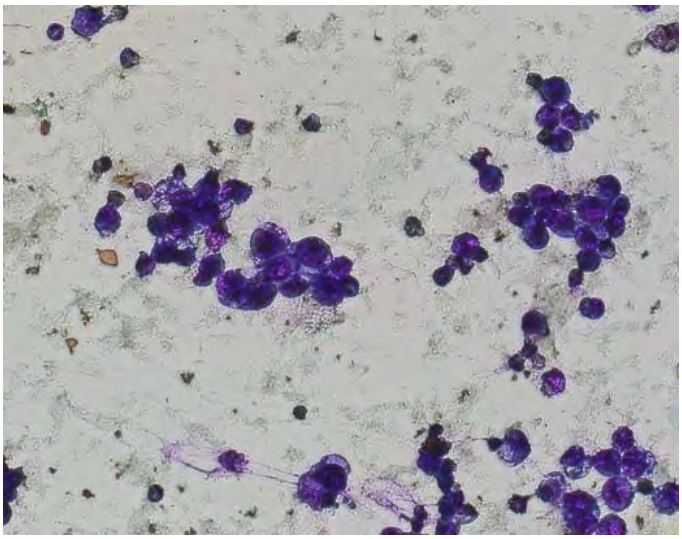

Figure J8 Diff-Quik stain image of MCF7 cell after treated with AuTOMPP 100 μM for 24 hours

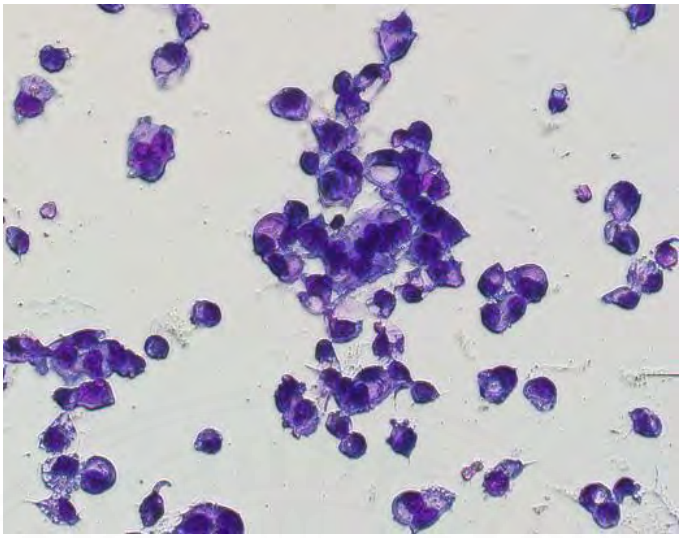

Figure J9 Diff-Quik stain image of MCF7 cell after treated with AuTOMPP 50 μM for 24 hours

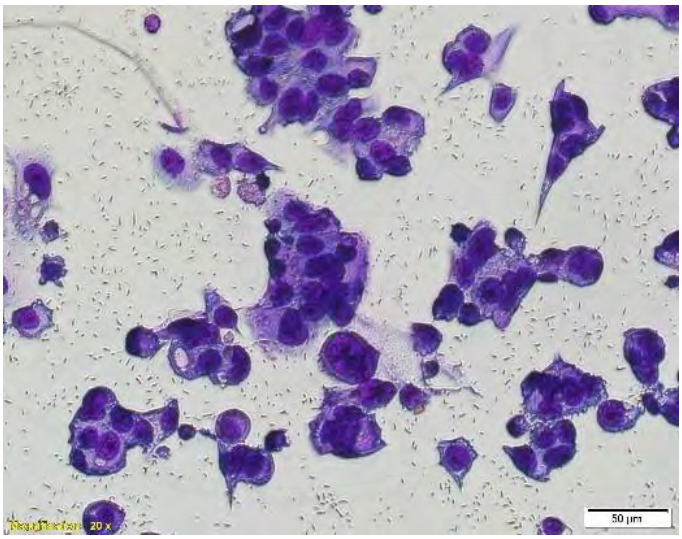

Figure J10 Diff-Quik stain image of MCF7 cell after treated with AuTOMPP 25 μM for 24 hours

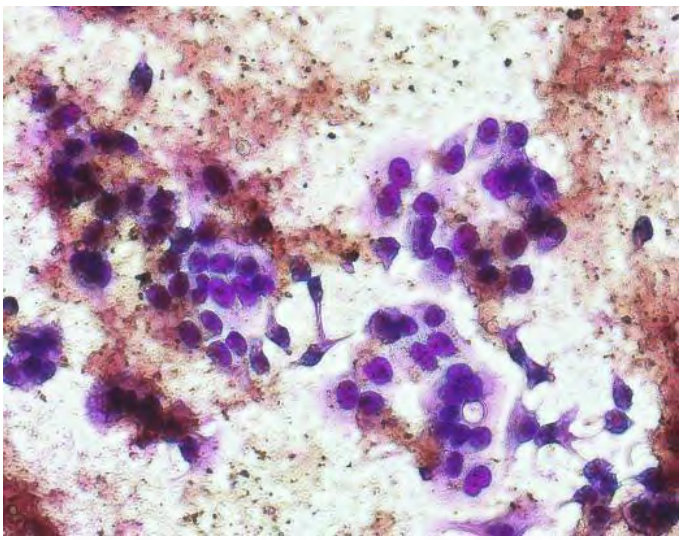

Figure J11 Diff-Quik stain image of MCF7 cell after treated with AuTOBPP 150 μM for 24 hours

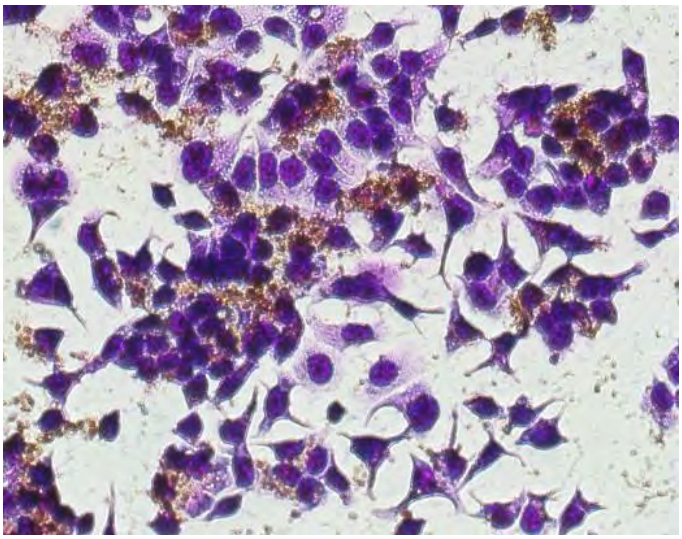

Figure J12 Diff-Quik stain image of MCF7 cell after treated with AuTOBPP 100 μM for 24 hours

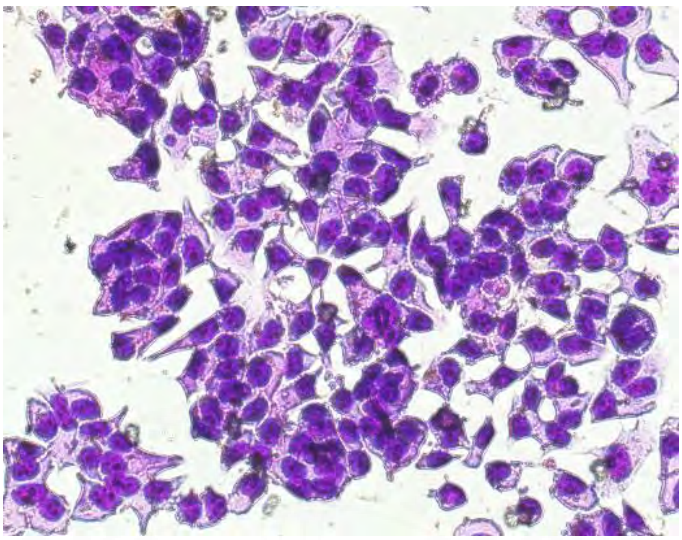

Figure J13 Diff-Quik stain image of MCF7 cell after treated with AuTOBPP 50 μM for 24 hours

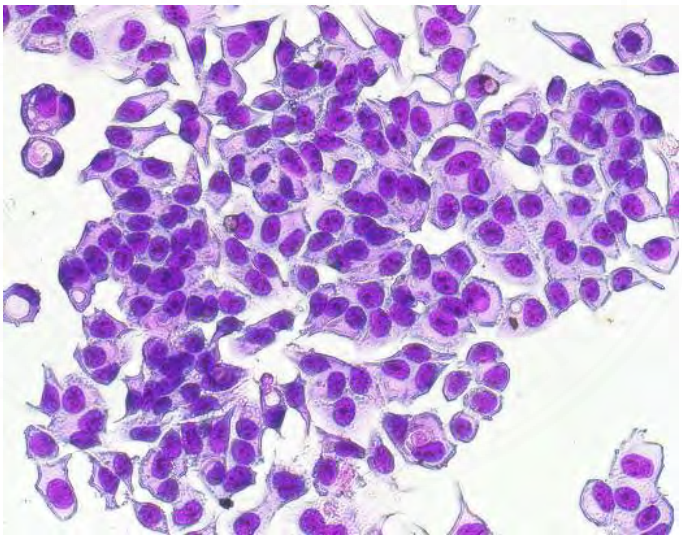

Figure J14 Diff-Quik stain image of MCF7 cell after treated with AuTOBPP 25 μM for 24 hours

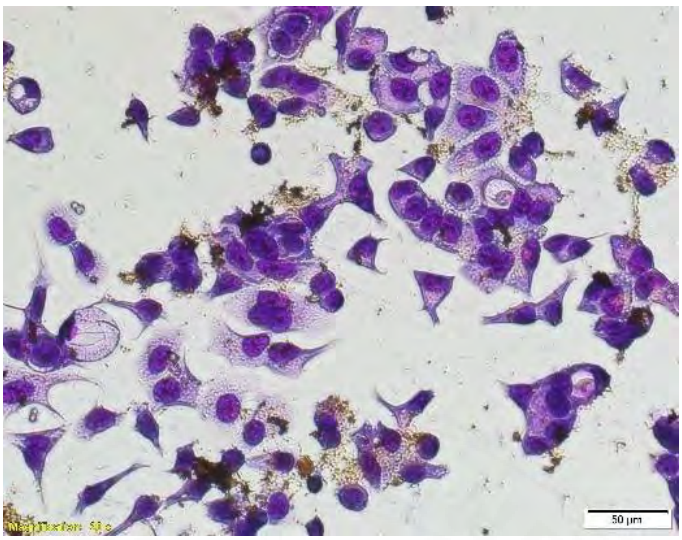

Figure J15 Diff-Quik stain image of MCF7 cell after treated with AuTOOPP 150 µM for 24 hours

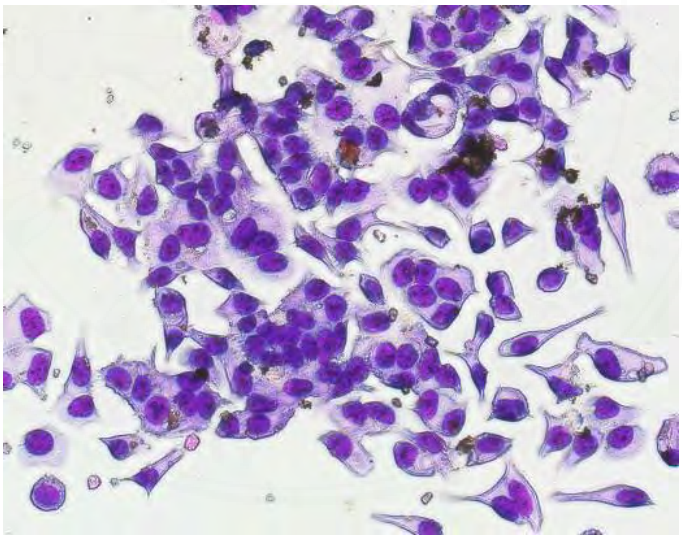

Figure J16 Diff-Quik stain image of MCF7 cell after treated with AuTOOPP 100 µM for 24 hours

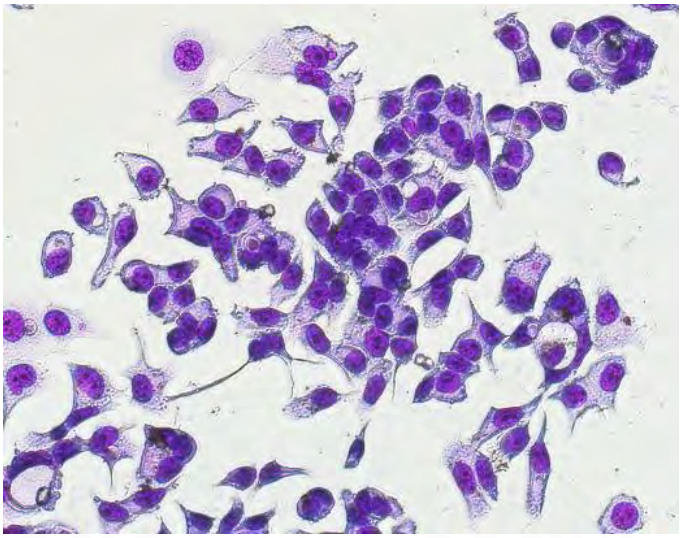

Figure J17 Diff-Quik stain image of MCF7 cell after treated with AuTOOPP 50 μM for 24 hours

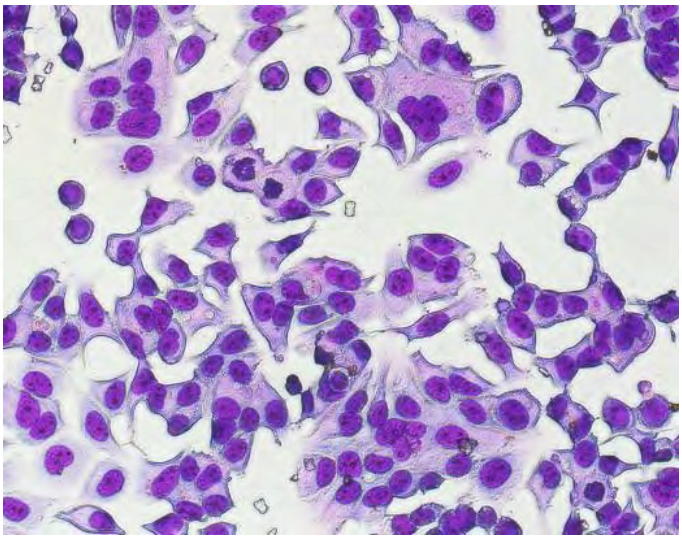

Figure J18 Diff-Quik stain image of MCF7 cell after treated with AuTOOPP 25 μM for 24 hours

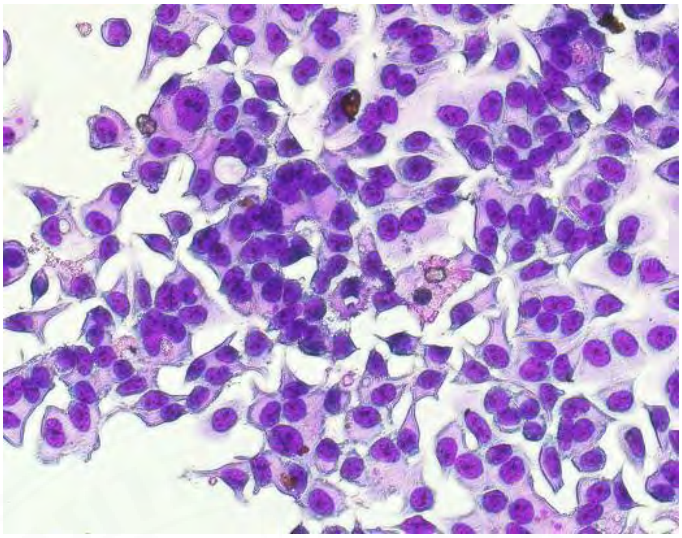

Figure J19 Diff-Quik stain image of MCF7 cell after treated with AuTODPP 150 µM for 24 hours

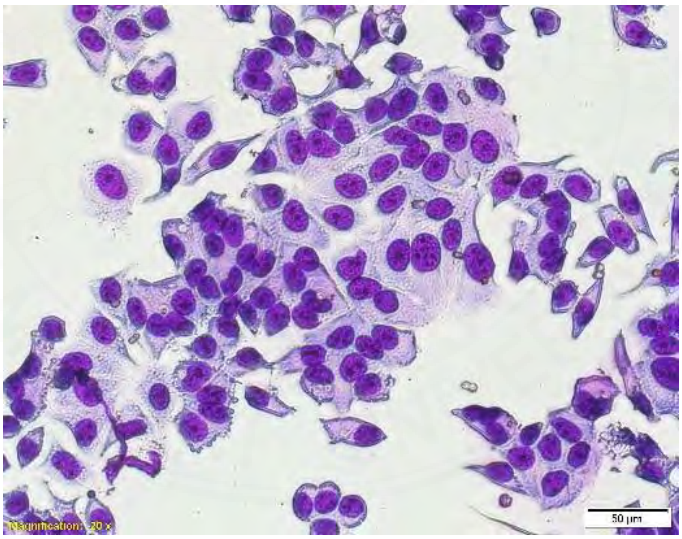

Figure J20 Diff-Quik stain image of MCF7 cell after treated with AuTODPP 100 µM for 24 hours

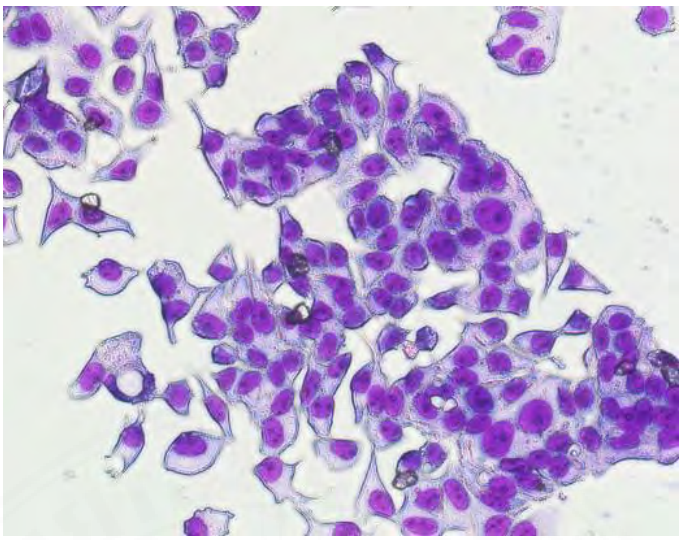

Figure J21 Diff-Quik stain image of MCF7 cell after treated with AuTODPP 50 μM for 24 hours

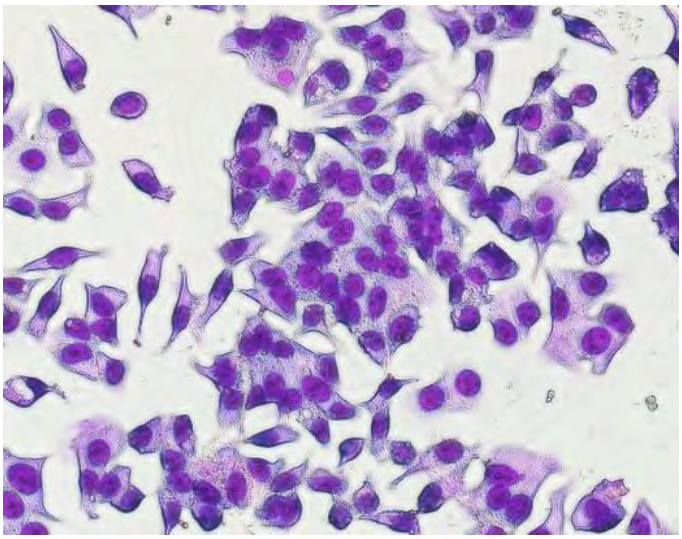

Figure J22 Diff-Quik stain image of MCF7 cell after treated with AuTODPP 25 μM for 24 hours

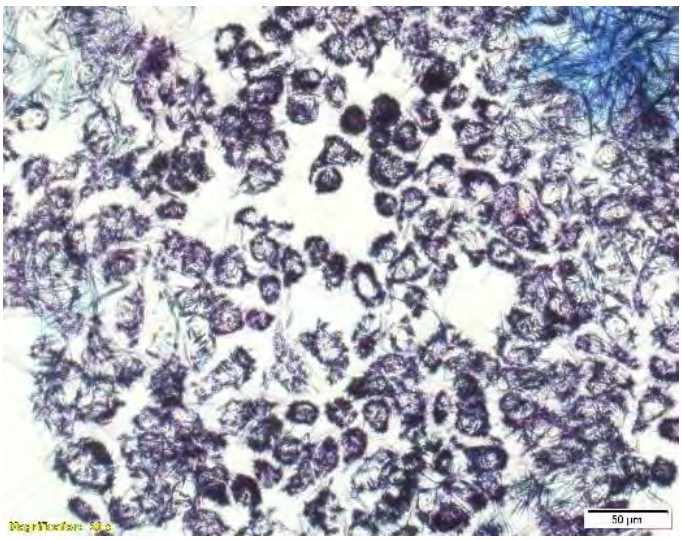

Figure J23 MCF7 cell image (Control) after 24 hours

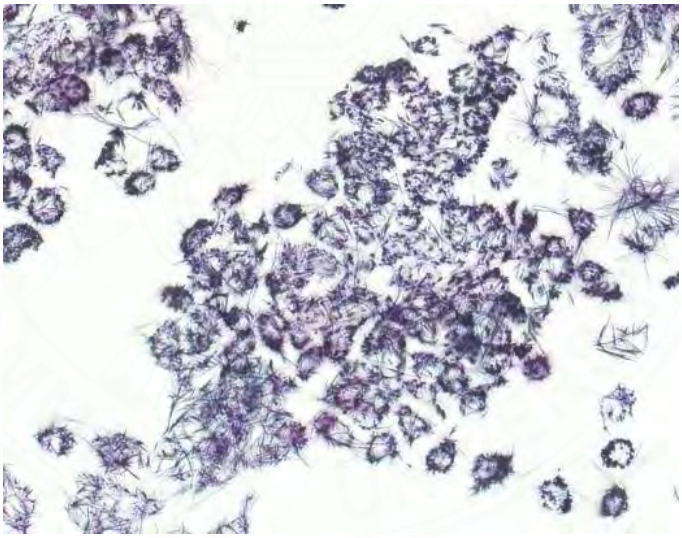

Figure J24 MCF7 cell image after treated with 1%DMSO for 24 hours

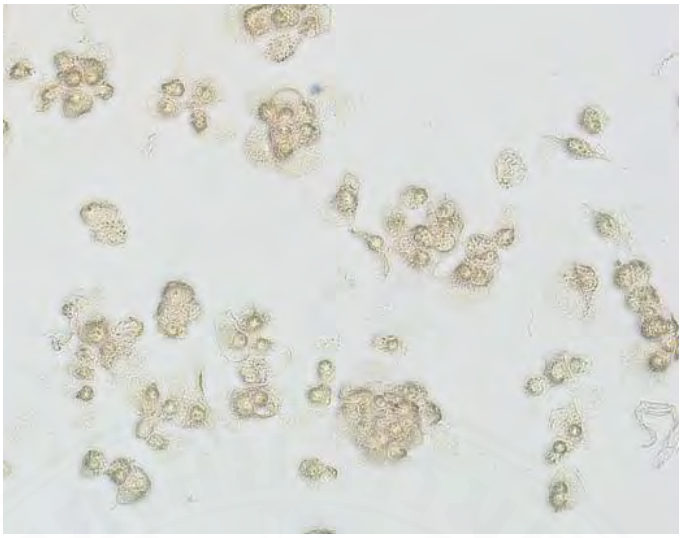

Figure J25 MCF7 cell image after treated with AuTPP 150 μM for 24 hours

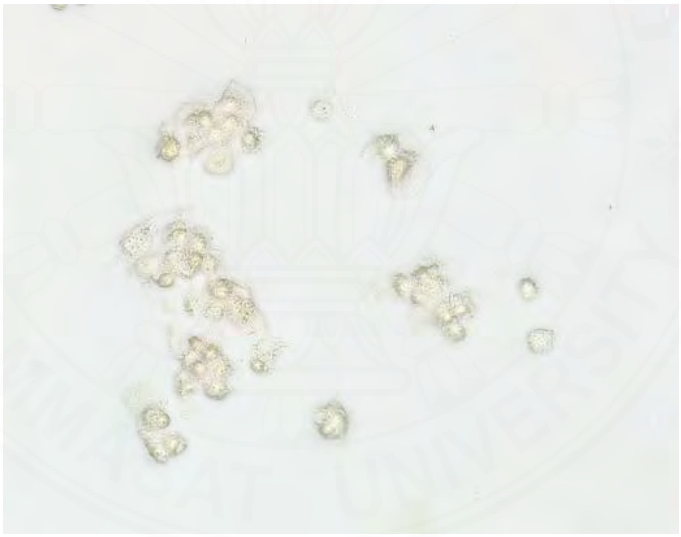

Figure J26 MCF7 cell image after treated with AuTPP 100 μM for 24 hours

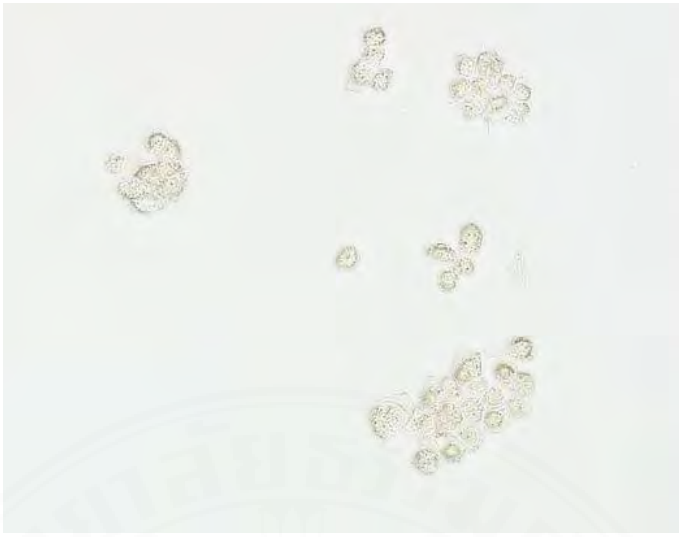

Figure J27 MCF7 cell image after treated with AuTPP 50 μM for 24 hours

Figure J28 MCF7 cell image after treated with AuTPP 25 μM for 24 hours

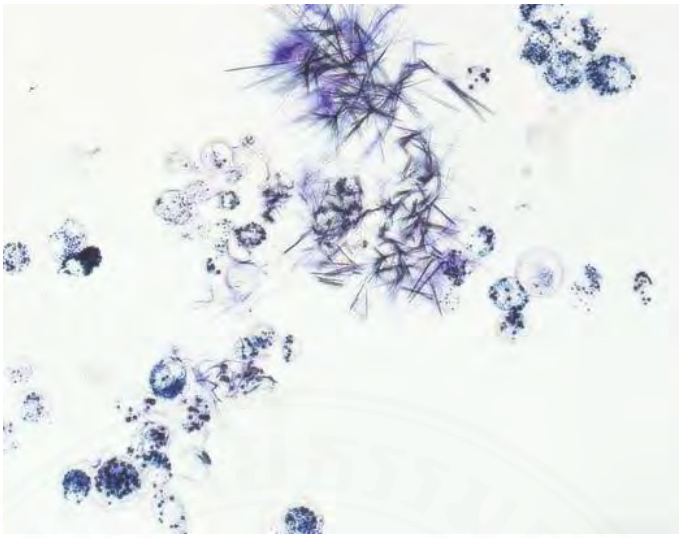

Figure J29 MCF7 cell image after treated with AuTPP 10 μM for 24 hours

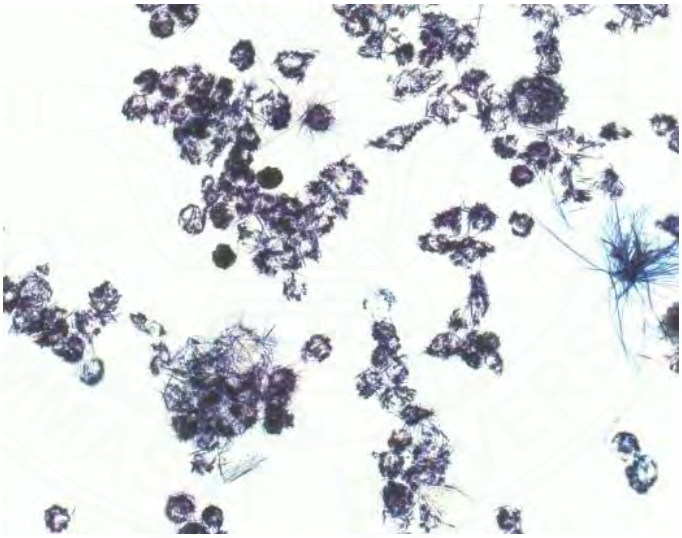

Figure J30 MCF7 cell image after treated with AuTPP 5 μM for 24 hours

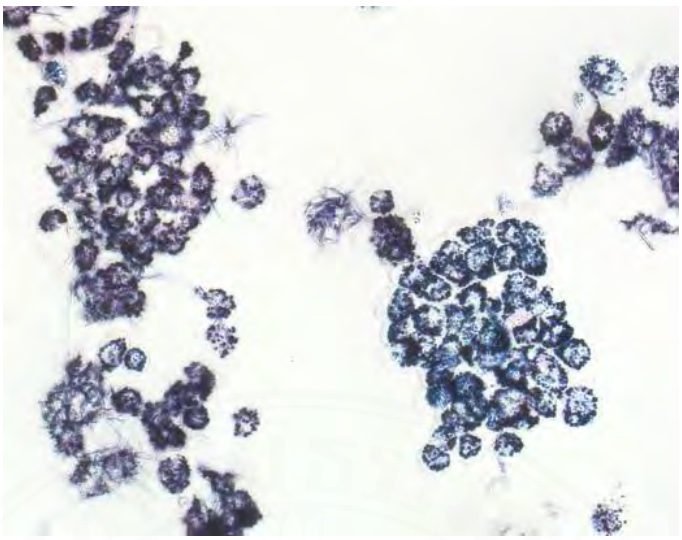

Figure J31 MCF7 cell image after treated with AuTPP 1 μM for 24 hours

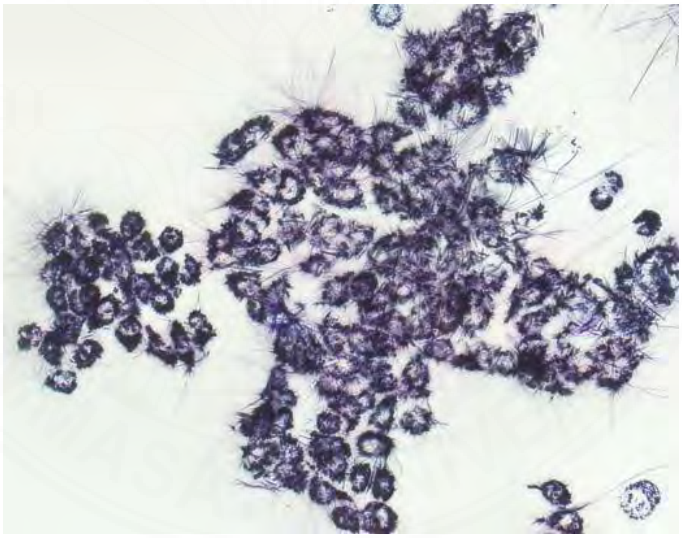

Figure J32 MCF7 cell image after treated with AuTPP 0.5 μM for 24 hours

BIOGRAPHY

Name	Tossapon Phromsatit
Educational Attainment	2013: Bachelor of Science in Chemistry
	2015: Master of Science in Chemistry
Scholarship	2016: Science Achievement Scholarship of Thailand

Publications

Proceeding PACCON 2017 “A new series of β-nitro substituted copper(II) porphyrin complexes and the alcohol sensing application”

Proceeding STT 43 “Synthesis and alcohol sensing activity of copper(II)poprhyrin and their alkyl long-chain derivative”

Proceeding ITIChE 2017 “Synthesis and it’s thermal stability of ρ-methoxytetra-phenyl porphyrin and their metal complexes”

Proceeding PACCON 2018 “Synthesis, ESR study and antibacterial activity of Cu(II) and Ag(II) tetrakis(4-alkyloxyphenyl)porphyrin complexes”

Proceeding PACCON 2018 “Synthesis and cytotoxicity study of Cu(II) tetrakis(4 alkyloxy)phenyl porphyrin complexes”

Proceeding STT 45 “Cytotoxicity of gold(III) porphyrin complexes and their derivative on MCF7 cell lines”

Lim Teik Zheng A, Phromsatit T, Boonyuen S, Andou Y. Synthesis of silver nanoparticles/porphyrin/reduced graphene oxide hydrogel as dye adsorbent for wastewater treatment. FlatChem. 2020;23.

Phromsatit T, Arpornmaeklong P, Shirosaki Y, Teerawatananond T, Rabablert J, Boonyuen S. Synthesis and cytotoxicity study of gold(III) porphyrin complexes and their derivative in breast cancer cells. Journal of Saudi Chemical Society. 2021;25(12).